A Photophysical Study of Electropolymerised Indoles

Peter Jennings

Degree of Doctor of Philosophy

The University of Edinburgh

1999

Abstract

It is known that the electropolymerisation of a range of 5-substituted indoles involves the formation of a cyclic trimer, which is then deposited onto the electrode surface and linked to form a redox active polymer of linked trimers. Previous studies have been concerned with the potential of such films as fast response potentiometric sensors and for the direct oxidation and reduction of biomolecules. We have found that these systems have intense photoluminescence, both in the solution and solid phase, presenting a novel example of a photoluminescent conjugated polymer system. Such polymers have potential applications as electroluminescent materials for thin-film light emitting diode structures and in the development of large-area light-emitting displays. This thesis presents a comprehensive photophysical study of the electropolymerised products of 5-cyanoindole, Indole-5-carboxylic acid, 5-bromoindole, 5-chloroindole, 5-methoxyindole, 5-aminoindole, 5-hydroxyindole, 5-nitroindole and indole using steady-state and time-resolved luminescence spectroscopic techniques.

Steady-state fluorescence spectroscopy in solution at room temperature has shown the monomer, trimer and polymer species to be highly fluorescent. The excitation and emission spectra of the trimer species show a significant shift to longer wavelength compared to the monomer, which emits in the near ultraviolet region, consistent with a greater extent of electron delocalisation. The emission properties of monomers are very dependent upon solvent polarity and the nature of the 5-substituent; in contrast the trimer species show little dependence. Controlling the electrochemical conditions allows variation of the relative proportions of trimer and polymer species. The excitation and emission spectra of the polymer species are shifted to longer

wavelength, are broader and are of lower intensity than those of the trimer. Spectroscopic measurements at 77K have shown that the systems are phosphorescent, allowing the position of the triplet excited state to be located as well as the measurement of phosphorescence lifetimes to be made. The phosphorescence lifetimes were found to be in the region of several seconds. Solid state electropolymerised films of 5-cyanoindole and Indole-5-carboxylic acid are fluorescent in the reduced state but not fluorescent in the oxidised state.

The technique of time-correlated single photon counting was used to measure fluorescence lifetimes and time resolved emission spectra of the monomer, trimer and polymer species of 5-cyanoindole, Indole-5-carboxylic acid and 5-bromoindole. This has provided a much more detailed insight into the characteristics of these materials. Lifetimes of the electropolymerised samples were found to possess multi-exponential decays, indicative of a multiplicity of emitting species. Lifetime components ranged from hundreds of picoseconds to several nanoseconds. There is evidence for emission from at least three classes of excited species: the free trimer (observed only in solution phase); excitation localised on trimer-like species in the polymer chain; excitation delocalised over polymer segments with a distribution of conjugation lengths.

A novel experimental method was used to measure the in-situ change in emission intensity as films of 5-cyanoindole and Indole-5-carboxylic acid were electrochemically cycled between a fluorescent reduced state and a non-fluorescent oxidised state. This has allowed a direct comparison of the electrochemical and photophysical properties of the films, with the emission response being measured as a function of sweep rate, film composition and wavelength of emission.

Declaration

I hereby declare the work presented in this thesis is my own unless otherwise stated by reference.

Acknowledgements

I would like to express thanks to the following people, for their help and encouragement during the course of my PhD.

Firstly I must thank my supervisors, Dr Anita Jones and Dr Andy Mount, whose enthusiasm and endless optimism made the whole process a great deal of fun. Anita in particular put a great deal of time and effort into proof reading the thesis.

In my lab group Ally Thomson, Mark Robertson and Lorna Kettle for their great help with the electrochemistry and making the lab a fun place to work. Also Fi Wild, Fiona Plows and Tricia Richardson, who rarely gave me a hard time for leaving the lab in a mess. Must not forget all those in room 252, including Mark, Ian and Ron, who introduced me to long lunchtimes and the Scotsman crossword.

A great deal of work was carried out at the Central Laser Facility of the Rutherford Appleton Laboratories, with invaluable help from Kevin Henbest, Mike Towry, Pavel Matousek and Tony Parker. None of the data would have meant anything without the assistance of Gary Rumbles and Paul Miller at Imperial College London.

Funding was gratefully received from the EPSRC.

Finally I would like to thank my friends and family for their support throughout. Stevie and John who were great fun to live with and Mullion and Dave who have put up with me for the last year. Everybody at Frbush, where I seem to have spent a great deal of my time and all those who I have climbed or kayaked with, especially Jamie Fisher, who was always looking for an adventure. That only leaves Juliette, with whom I have been the luckiest person to spend the last four years.

Publications

"Electrooxidation of 5-substituted indoles", P. Jennings, A. C. Jones, A. R. Mount, A. D. Thomson, *J. Chem. Soc., Faraday Trans.*, 1997, **93**, 3791.

"Fluorescence properties of electropolymerised 5-substituted indoles in solution", P. Jennings, A. C. Jones, A. R. Mount, *J. Chem. Soc., Faraday Trans.*, 1998, **94**, 3619.

"Photoluminescence of electropolymerised 5-substituted indoles in solution at 77K", P. Jennings, A. C. Jones, A. R. Mount, manuscript in preparation.

"Time-resolved fluorescence studies of electropolymerised 5-substituted indoles", P. Jennings, A. C. Jones, A. R. Mount, manuscript in preparation.

"In-situ investigation of the photoluminescence of 5-substituted indole electropolymers on the working electrode", P. Jennings, A. C. Jones, A. R. Mount, manuscript in preparation.

"Luminescence of electrochemically generated indole polymers", P. Jennings, A. C. Jones, A. R. Mount, conference proceedings of The 193rd meeting of The Electrochemical Society, May 1998, San Diego, California.

"Photophysics of novel electropolymerised indoles", P. Jennings, A. C. Jones, A. R. Mount, Annual report of the Central Laser Facility, Rutherford Appleton Laboratory, 1997-98.

Contents

Chapter 1 - Introduction

1.1 Introduction

With the rapid development in recent years of communications technology, demand for colourful, lightweight and effective display formats has been considerable. The traditional format of the cathode ray tube gives a high quality output, but is too bulky and heavy to be portable. There has been a concerted effort to develop new forms of display that perform equally well over large areas but remain thin and light. The market for flat panel displays is growing rapidly and is presently dominated by liquid crystal display (LCD) technologies, which have the disadvantage of a limited angle of viewing, poor contrast and delicate structure. Inorganic electroluminescent materials have been commercially available since the early 1960's and have recently shown considerable improvements over the LCD type displays. However, they have to be deposited as thin films using the relatively expensive techniques of sublimation or vapour deposition, which does not suit the fabrication of large area devices.

Materials that require simpler processing would be very attractive and a major advance towards this end was the development by Friend *et al* in 1990 of an electroluminescent light emitting diode, based upon the organic conjugated polymer poly(*p*-phenylene vinylene)[1]. This material has been studied in depth and is showing considerable potential for a range of electro-optical applications. This thesis is concerned with the photophysical investigation of a similar polymer system, consisting of electropolymerised indole, with potential applications as an electroluminescent material in the development of large area light emitting displays.

Electropolymerised indoles were first produced by Tourillon et al[2] in 1982. It was found that electropolymerisation of indole resulted in the deposition of a semi-conducting film onto the electrode surface, giving an example of a conjugated organic semiconductor. Considerable work has since focused on characterising the electrochemical properties of electropolymerised indole. Indole and its derivatives are known to be highly photoluminescent and are of particular interest since they are the fluorescent chromophore of the amino-acid tryptophan. The observation of fluorescence emission from an electropolymerised indole was first made by Mackintosh et al[3] in 1994. Comparatively little attention has been given to the luminescence properties of conjugated polymers, with electropolymerised indoles providing a new and previously uninvestigated example of a photoluminescent conjugated polymer system.

1.2 The indole chromophore

Indole, whose structure is shown in Figure 1.1, has a high fluorescence quantum yield which has been attributed to the promotion of an electron from a π to a π^* orbital on exposure to electromagnetic radiation and its subsequent return to the ground state. The assignment of this transition is discussed in detail in section 2.2. There have been extensive studies into the photophysics of indole and its derivatives. It is the fluorescent chromophore of the amino acid tryptophan and has great potential for probing the structure and dynamics of proteins and peptides [4-6], however, an understanding of the structural and chemical basis of its photophysics is necessary to interpret any further studies.

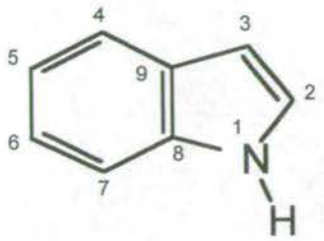

Figure 1.1 Structure and numbering system for indole.

1.2.1 The photophysics of indoles

Much of the work to date has been directed at understanding the unusually large fluorescence Stokes shift observed in polar media. This shift arises from a bathochromic shift in the emission wavelength with increasing solvent polarity; the energy of the absorption band displays much lower solvent dependence. Various mechanisms have been proposed to account for this shift and there has been considerable discussion in the literature, with some aspects still not fully resolved. These mechanisms include ^1L_a-^1L_b level inversion [7-12], exciplex formation [13-15], solvent reorientation [16], emission from a solvated Rydberg state [17], dual fluorescence[18] and emission from a solvent stabilised state with partial charge transfer character of ^1L_a origin [19, 20].

The majority of these theories are based upon the presence of two low-lying excited states labelled ^1L_a and ^1L_b (the origin of the labels is explained in section 2.2). In free molecules the ^1L_a state lies above the ^1L_b state, but they are very close in energy, molecular orbital calculations have been carried out to theoretically characterise these states [21, 22]. In solution, the solvent molecules will have time to reorient around the excited state molecule, before light emission occurs, to a configuration of lower energy (referred to as solvent relaxation).

The theory of ^1L_a-^1L_b level inversion, first suggested by Mataga et al in1964 [7], states that in non-polar solvents, the ^1L_b state lies below the ^1L_a state even after solvent relaxation, and is therefore the emitting state. It is thought that the ^1L_a state has a greater dipole moment than the ^1L_b state, therefore in polar solvents it undergoes a greater stabilisation due to solvent relaxation and drops below the energy of the ^1L_b state. It then becomes the emitting state, causing the observed bathochromic shift of the emission in polar solvents. A number of experiments have been carried out to support this theory, involving the use of solvents of different polarity along with theoretical solvatochromism models [7, 9, 11]. Experiments have also used temperature [8, 10, 11, 23], viscosity [24] and pressure[25] to alter the effect of polar solvents on the excited states.

Work presented by Lumry et al in 1966[13, 14] disagreed with the ^1L_a-^1L_b level inversion, suggesting that a specific solvent-solute excited state complex (termed an exciplex) was responsible for the bathochromic shift in the emission in polar solvents. They discounted an interaction due to specific molecular dipole-dipole attractions because they found no correlation between fluorescence shift and solvent dipole moment. This theory was discounted by Lami et al[11] who re-examined the ^1L_a-^1L_b level inversion using a different theoretical model of solvent polarity, developed by Amos and Burrows [26] and reasserted the inversion theory. Lami had previously attempted to explain the fluorescence anomalies of indole in terms of solvated Rydberg states [17], however, this model was not pursued much further. Experiments carried out by Eisinger et al in 1968 [16] on tryptophan over a range of temperatures agreed with the work of Mataga et al. They preferred the view that the bathochromic shift in a polar solvent arises from the reorientation of several solvent molecules rather than from the formation of stoichiometric exciplexes.

Meech at al presented a slightly different approach in 1983 [19, 20]. They examined the solvent, temperature, time and substituent dependence of the luminescence of indoles, and proposed the presence of a new state in polar media, stabilised by the process of solvent-solute relaxation, with partial charge transfer character of ^1L_a parentage. They classified the indole derivatives in terms of ΔE (where $\Delta E = [E\ (^1L_a) - E\ (^1L_b)]$), finding that where ΔE is large ($\Delta E > 1200\ cm^{-1}$) such as for 5-methoxyindole, there is no red shift and a decrease in the radiative lifetime in polar media. Where ΔE is small ($\Delta E < 600\ cm^{-1}$) they found the radiative lifetime to increase in polar media and for there to be a bathochromic shift in the emission wavelength. This is summarised in Figure 1.2, assigning the "exciplex" emitting state in polar solvents as ^1L_a /CT, indicating that the solvent stabilised state has a greater degree of charge transfer character and hence a higher dipole moment than the initially excited state.

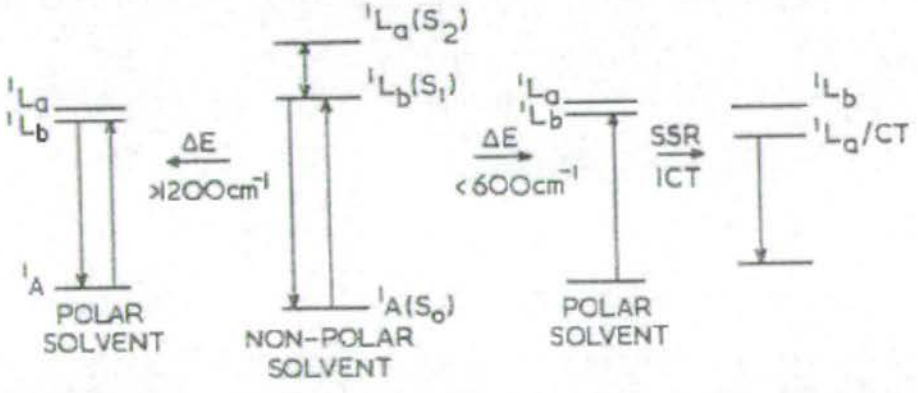

Figure 1.2 Schematic representation of two extreme cases of the solvent effect on the fluorescence of substituted indoles, taken from reference 19. Where SSR is solvent-solute relaxation and ICT is internal charge transfer.

From the preceding discussion, it can be seen that the emission properties of indoles are very complicated, with no single model giving a satisfactory explanation for all the observed anomalies. More recent studies have concentrated on understanding the response of the ^1L_a and ^1L_b states to specific environmental conditions. Callis et al have carried out considerable theoretical and high resolution experimental studies, using jet cooled spectroscopic techniques to obtain a more detailed picture of the ^1L_a and ^1L_b states [27-30]. Sulkes et al have also used high resolution spectroscopic techniques to obtain fluorescence lifetimes and emission details for a variety of indoles [31-35]. There is now considerable information available concerning the fluorescence properties of indole and its derivatives and the location of the two low lying excited states ^1L_a and ^1L_b, however, the exact mechanisms that cause such a large Stokes shift in polar media is still an area of debate.

1.3 Conducting polymers.

This thesis is concerned with the photophysical properties of electrochemically polymerised indoles, which belong to a unique group of materials known as conducting polymers. The traditional view of organic polymers is as an insulating material, however, a report published in 1977 by Chiang et al [36] illustrated how chemical oxidation of acetylene, C_2H_2, forms polyacetylene, shown in Figure 1.3, which was found to be electrically conducting in the semi-conducting range. Oxidative doping of the polymer allowed conductivities comparable to those of a metal to be achieved. This discovery was the beginning of significant research activity, as it became apparent that materials, with the desirable physical properties of synthetic organic polymers and with the conductivity of metals, were feasible. However, polyacetylene was found to be very sensitive to both moisture and air, resulting in an

irreversible drop in conductivity. This sensitivity along with processing difficulties made it unsuitable for most practical applications.

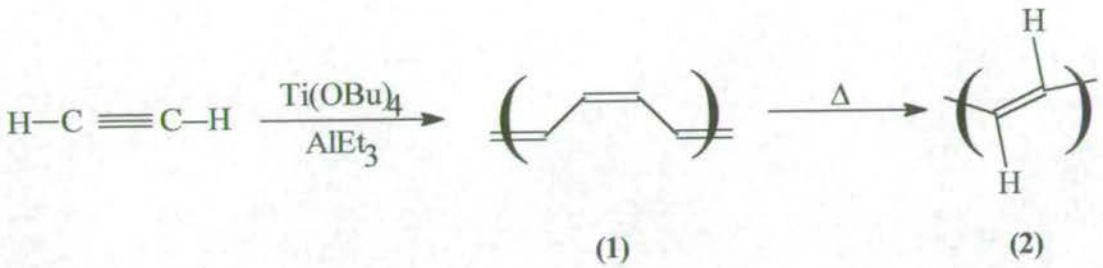

(1) (2)

Figure 1.3 Polyacetylene produced via the Ziegler-Natta polymerisation, showing the cis (1) and trans (2) isomers, taken from reference 37.

1.3.1 Advances in conducting polymers

For a conducting polymer to have any practical application it must fulfil certain criteria including good solution or melt processability, environmental stability, mechanical integrity and controllable conductivity. In a search for suitable materials, conducting polymers have been produced from a wide range of organic molecules. The most widely studied area is that of conducting polymers produced from heterocyclic monomers, since high conductivities and good environmental stability can be achieved. There is also the possibility of tailoring the properties of the material because of the existence of numerous derivatives.

Most work in this area has concentrated on polypyrrole, first polymerised in 1979 [38, 39, 40], shown in Figure 1.4 and polythiophene, first polymerised in 1981 [40], shown in Figure 1.5. Although the actual mechanism of charge conduction is of considerable debate, these

polymers exhibit the essential characteristic where the monomers link to form a conjugated π-electron system along which the charge can conduct.

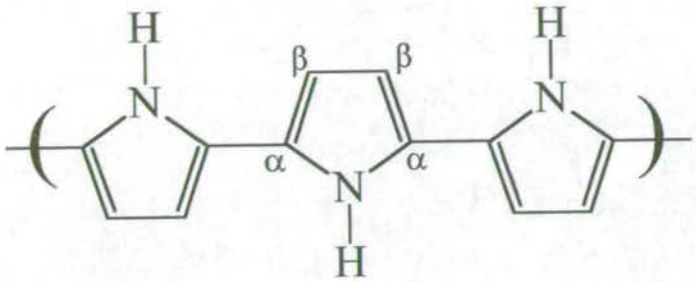

Figure 1.4 The structure of polypyrrole. α and β denote the sites of possible functionalisation.

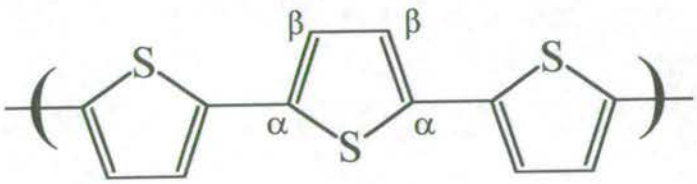

Figure 1.5 The structure of polythiophene. α and β denote the sites of possible functionalisation.

Pyrrole and thiophene undergo polymerisation by similar mechanisms to give the linear polymers illustrated above, if a substituent is present in the α position the polymerisation is inhibited. Substituents in the β position can affect the polymerisation mechanism and alter the conducting properties of the polymer [42, 43]. Electron donating groups have been found to increase the conductivity of the polymer, whereas large bulky groups cause the polymer to twist into different conformations and result in a loss of conductivity.

Work has also been carried out into the polymerisation of other aromatic and heterocyclic molecules [45] with larger ring systems to give conducting polymers, these include fluorene [43, 44], fluoranthene [43, 44], azulene [43, 44, 1], pyrene [43, 44], triphenylene [43, 44], carbazole [43], furan [1] and indole [1]. There is less information in the literature on these other polymers, except for indole, which is discussed in greater detail in section 1.4. There is also a considerable body of work on the conjugated polymers of poly(p-phenylene vinylene) (PPV) due to their light emitting properties, these are also discussed in greater detail in section 1.5.

1.3.2 Synthesis of conducting polymers

Conducting polymers are usually produced using one of two methods, either chemical or electrochemical oxidation. Both routes have their respective merits.

1.3.2.1 Chemical oxidation.

Chemical oxidation has the advantage that it can be carried out on a large scale and the resulting polymer can be fabricated into the desired form. However, it has been found that the polymers produced using chemical methods often have a lower conductivity than those produced using alternative methods. This has been attributed to a lack of control over the polymerisation conditions, resulting in polymers of varied conjugation length and random structure. There has been a considerable advancement in chemical methods with the research into PPV, which is synthesised via a solution processable precursor that can be spin coated onto a suitable substrate then thermally converted to PPV. The reaction scheme in Figure 1.6 [46] shows the first reported method for synthesising PPV for electroluminescent studies.

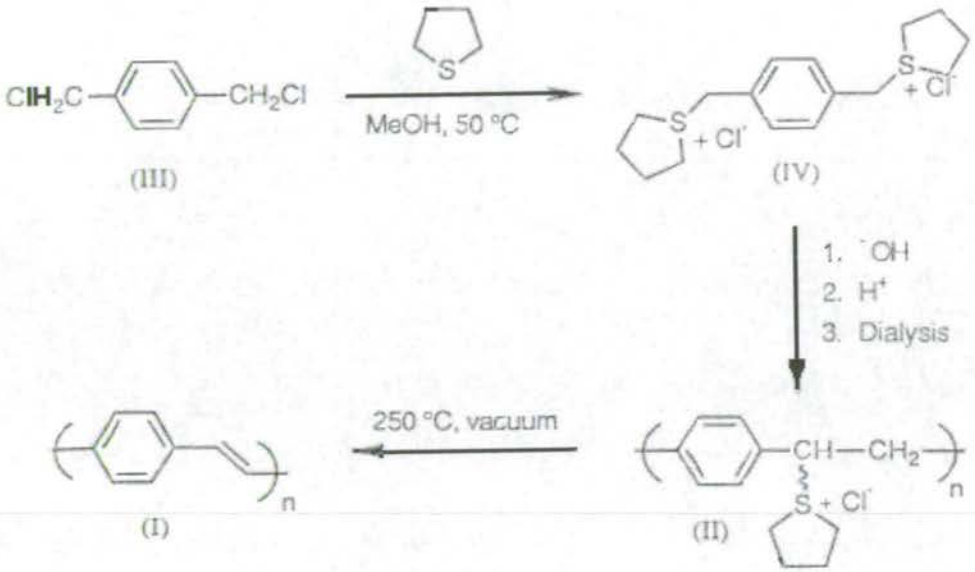

Figure 1.6 Reaction scheme for the synthesis of PPV (I), via a solution processable sulphonium polyelectrolyte precursor (II). The precursor polymer is fabricated, then converted to the conjugated PPV by thermal treatment.

1.3.2.2 Electrochemical oxidation.

For many studies electrochemical oxidation techniques have been used, since they offer a much greater degree of control over the reaction conditions and allow in-situ analysis of the polymerisation process. The monomer is dissolved in a solution containing a supporting electrolyte and is directly oxidised at an electrode, resulting in a film in which charge compensating anions are incorporated. These anions act as the dopant ions, with the resulting oxidised film being conducting. The adsorbed polymer film can be reversibly cycled between the conducting oxidised (doped) state, where counterions from the electrolyte are present in the film and a neutral reduced state, where the counterions are expelled back into solution. This process is summarised in Figure 1.7.

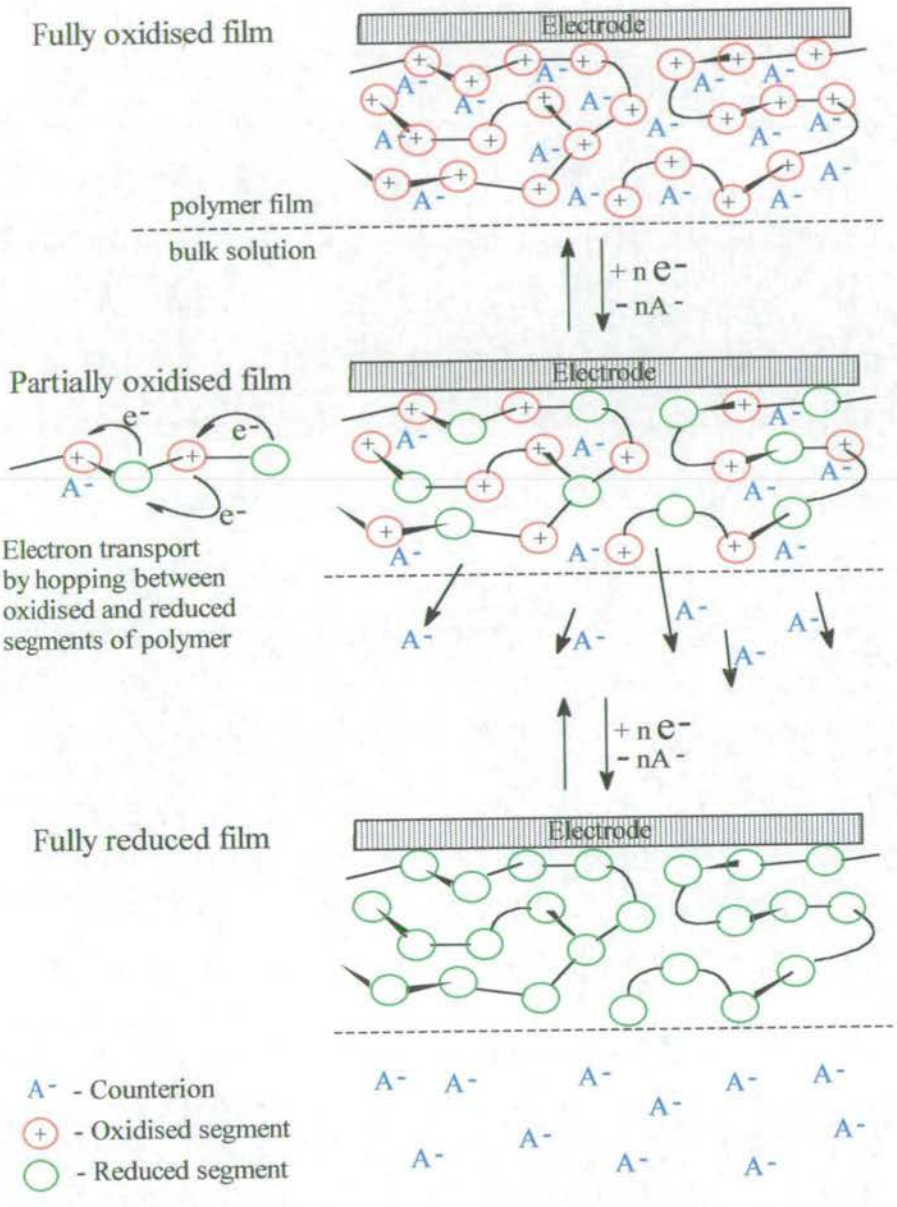

Figure 1.7 Reversible uptake of counterions by conducting polymer film, reproduced from reference 79.

The advantage over most chemical methods is that the polymers produced in this fashion are more homogeneous and regular, giving greater conjugation lengths, which allow easier charge transport. Hence the observation that electrochemically oxidised conducting polymers usually have greater conductivities than equivalent chemically oxidised conducting polymers. The morphology of the film produced on the electrode can be controlled by altering the polymerisation rate, achieved by controlling the concentration of monomer in solution and the hydrodynamic flow at the electrode. It is also possible to precisely control the duration of polymerisation and hence the film thickness, as oxidation of the monomer will only continue for as long as the oxidation potential is maintained at the electrode. Once formed, the conducting film can be studied on the electrode using electrochemical methods.

The majority of the work in this thesis is based upon polymers produced using electrochemical oxidation techniques. However, there is a major drawback in that the yields are always very low. Polymerisation using larger electrodes to give higher yields results in a loss of control over the polymerisation condition, therefore losing the advantage over chemical methods. To provide a comparison, some samples investigated in the following work were produced using chemical oxidation, to see if there was any great variation in their photophysical properties.

1.3.3 The potential uses of conducting polymers

Since the discovery of polyacetylene, the field of conducting polymer research has expanded greatly due to the possibility of a wide range of technological applications. The initial difficulties with environmental stability and problems with processing have resulted in only a few commercially available devices. However, with recent developments improving these

aspects there is now considerable progress towards multiple new technologies. The following discussion presents a selection of the main areas of interest.

1.3.3.1 Sensor technology

The development of sensor technologies is an area in which conducting polymers have been used with commercial success, an example being that of an "electronic nose" [47]. The basic concept is that either gas or solution species interact with the conducting polymer film and cause a change in its conductivity which is easily detected. The sensor is fabricated with an array of different polymers, each of which interacts with a different species, producing a fingerprint of the sample. The brewing industry has utilised this to monitor the build up of the unwanted side product diacetyl, using a sensor developed by a company called Neotronics at a lower cost than traditional techniques such as gas chromatography.

Electrochemically polymerised films of Indole-5-carboxylic acid have been proposed as potential pH sensors [48], since the presence of the carboxylate group makes the electrochemistry of the polymer pH sensitive over a range of pH 1-7. Such a film has an advantage over traditional pH sensors due to the ability to tailor the chemistry of the film to a particular need and the ease of deposition of the film in a controlled and reproducible manner. This allows individual electrodes to be coated on a micron scale to produce microelectrochemical sensors.

1.3.3.2 Applications in biotechnology.

There has been considerable interest in the use of conducting polymers as sensors in biological systems, using the conducting polymer to modify an electrode. Metallic electrodes

are not always suitable for use in a biological system, therefore the conducting polymer acts as a mediator [49, 50, 51, 52], as illustrated in Figure 1.8. The role of the mediator is to shuttle electrons efficiently between the electrode and the enzyme. It has been shown that enzymes can be entrapped or covalently bound to the functional groups of a conducting polymer such as polypyrrole [53]. This allows the production of a stable sensor based around the immobile enzyme, with the ability to deposit the film onto a microelectrode. Another example [54] is the incorporation of dithiocarbamate or anti-human serum albumin into polypyrrole, giving a sensor capable of responding selectively to Cu^{2+} or human serum albumin respectively. Polyindole has been proposed as an intermediate in the direct oxidation and reduction of cyctochrome c and related redox proteins [55].

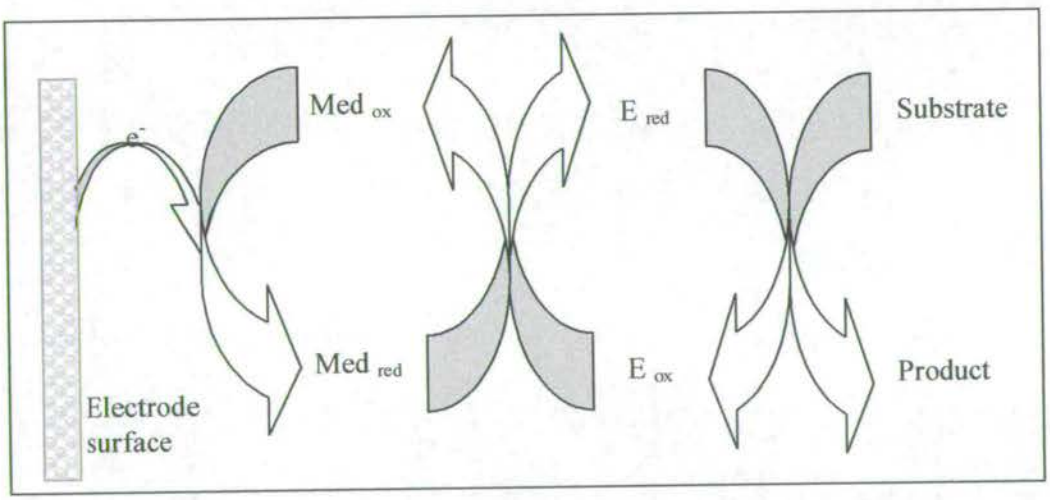

Figure 1.8 Schematic diagram of a mediated electrode system. Med_{ox} and Med_{red} are the redox forms of the mediating conducting polymer. E_{ox} and E_{red} are the redox forms of an enzyme.

1.3.3.3 Batteries

Development of batteries is of significant commercial importance and the reversible doping-undoping, behaviour of conducting polymers, with efficient storage and discharge currents has made them a possible candidate in battery applications [56, 57]. Chemically polymerised polyacetylene was the first material used successfully to fabricate batteries, subsequently it has been demonstrated that solid state batteries consisting of electrochemically produced polythiophene and polyazulene are feasible.

1.3.3.4 Electro-optical devices

The discovery that electroluminescence could be generated from the conducting polymer PPV [1] has generated considerable interest in the area of light emitting displays. The details of this work are given in section 1.5. Many conducting polymers also display a colour change when electrochemically cycled between the oxidised and reduced state, known as electrochromic behaviour. This property suggests possible uses in the development of passive display devices, replacing existing liquid crystal type displays. They have a number of advantages including low power usage, since power is only required to switch between redox states, not hold the final state. There is also the possibility of large-scale displays that can be viewed from any angle. Embedding a thin layer of a suitable conducting polymer in a transparent conducting material such as indium tin oxide produces a "smart window", with the ability to alter the tint of the window by applying a potential. Linking the charge passed to a light sensor has been utilised to produce windows that react to the intensity of sunlight.

1.4 The electropolymerisation of indoles

Since the first observation that indole can be electropolymerised to form a conducting polymer film [2], there has been considerable debate concerning the mechanism of polymerisation and the molecular structure of the film. It was initially assumed that indole would polymerise in the same way as other heterocycles such as pyrrole and thiophene, to give a linear polymer. This led to a number of conflicting theories in an effort to explain behaviour inconsistent with the other heterocycles. Tourillon et al [2] proposed the linear, N-N bonded structure shown in Figure 1.9, since they found that the oxidation of N-methyl indole did not give a conducting film and the N-H band in the IR spectrum disappears in the conducting polyindole. However, the second linking site was not defined.

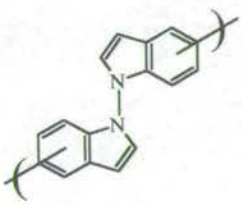

Figure 1.9 N-N bonded structure of polyindole as proposed by Tourillon et al [2].

A number of other possible structures have since been proposed and these are shown in Figure 1.10 [54-66]. In all cases it has been assumed that a linear chain of monomers, linked through two sites, forms the polymer and this has led to a diverse range of proposed structures and mechanisms.

The 1-3 linked polymer proposed by Waltman et al [54] was the result of studying the substitution effects of derivatised indoles and finding that polymerisation will not occur with substituents in the 1,2 or 3 position. They also found from molecular orbital calculations that

the greatest electron density was in the 1 and 3 positions. More recently Kong et al [69] and Bartlett et al [70] have agreed with these findings utilising a number of spectroscopic techniques, including Fourier transform infra red (FTIR), electron spin resonance (ESR), FT-NMR, and scanning electron microscopy (SEM). Jackowska et al used in situ Raman and infrared spectroscopy of polyindole films on a platinum film [60], finding the results to be consistent with a 1-6 bonding mechanism.

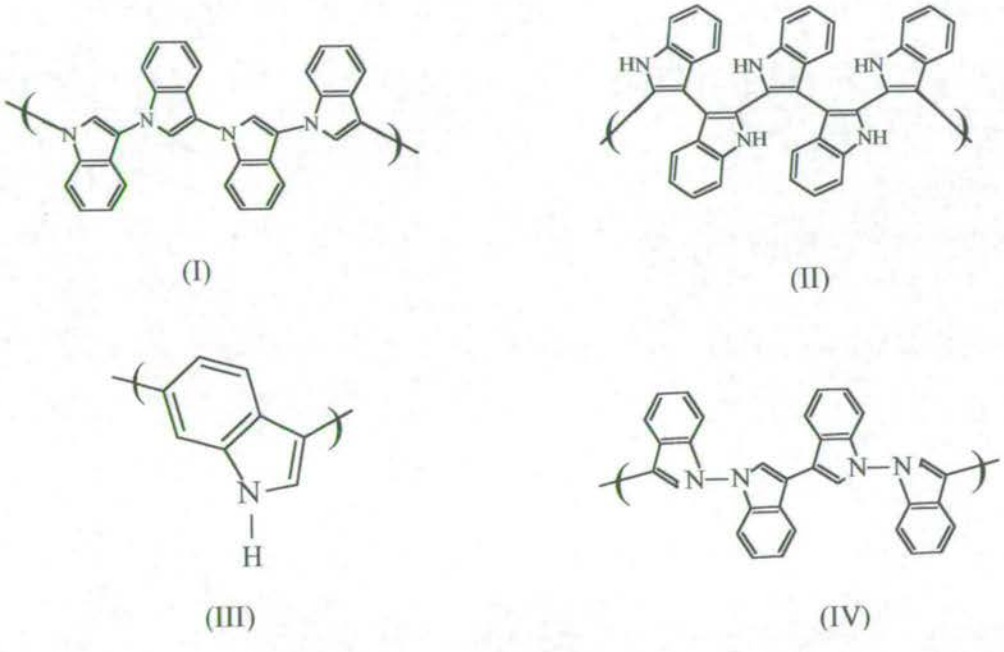

(I) (II)

(III) (IV)

Figure 1.10 Proposed structures of polyindole, (I) 1-3 bonded by Waltman et al [56], (II) 2,2-3,3 bonded by Zotti et al [58,59], (III) 1-6 bonded by Jackowska et al [60, 61] and (IV) 1,1-3,3 bonded by Talbi et al [62-68].

This is challenged by work from Zotti et al who utilised electrochemical methods, (FTIR) and uv-vis spectroscopy and in-situ conductivity measurements to probe the structure of

polyindole [58]. They concluded that "the shape and the pH dependence of the CV response, the potential window of conductivity, the disappearance of the NH band upon oxidation and the pH-dependent electrochromism are due to a regular alternance of 2,2 and 3,3-couplings". Over the past 5 years, Talbi et al have carried out a range of investigations on polyindole using parallel detection electron energy loss spectroscopy (PEELS), X-ray photoelectron spectroscopy (XPS), FTIR spectroscopy and Raman spectroscopy [65, 66] along with electrochemical methods [62, 63]. They concluded that the structure consists of a regular alternation of 1,1-3,3 couplings. Recently they have published results on the electrochemical oxidation of 5-cyanoindole [66] and 5-nitroindole [67] along with a theoretical study of indole polymerisation [68] based upon Hartree-Fock calculations. Once again they cite the 1,1-3,3 bonding mechanism; this is in direct disagreement with the work previously published by Mount et al [74, 75] on the 5-substituted indoles (presented in section 1.4.1) to which they make no reference.

1.4.1 Recent studies on the electropolymerisation of 5-substituted indoles.

An initial study by Waltman et al [56] on the electropolymerisation of 5-substituted indoles suggested that the capacity to form a conducting film was a function of electronic effects and not due to steric effects. This was proposed since the presence of a bulky substituent such as bromine does not inhibit film formation, whereas a smaller substituent such as hydroxy does. The plot shown in Figure 1.11 gives the oxidation peak potential versus the Hammett substituent constant, a measure of the relative electron withdrawing power of the substituent, for a range of 5-substituted indole monomers. The 5-substituted monomers indicated within the smaller green box indicate those that Waltman et al found would polymerise to form a film. They found that the best quality films were achieved from indole monomers substituted

with electron withdrawing groups. It was suggested that polymer formation depends upon the stability of the monomer radical cation that is formed upon oxidation. An electron withdrawing group destabilises this cation, encouraging linking to form a polymer, whereas a strongly electron donating group stabilises the cation, allowing them to diffuse away from the electrode before linking can occur.

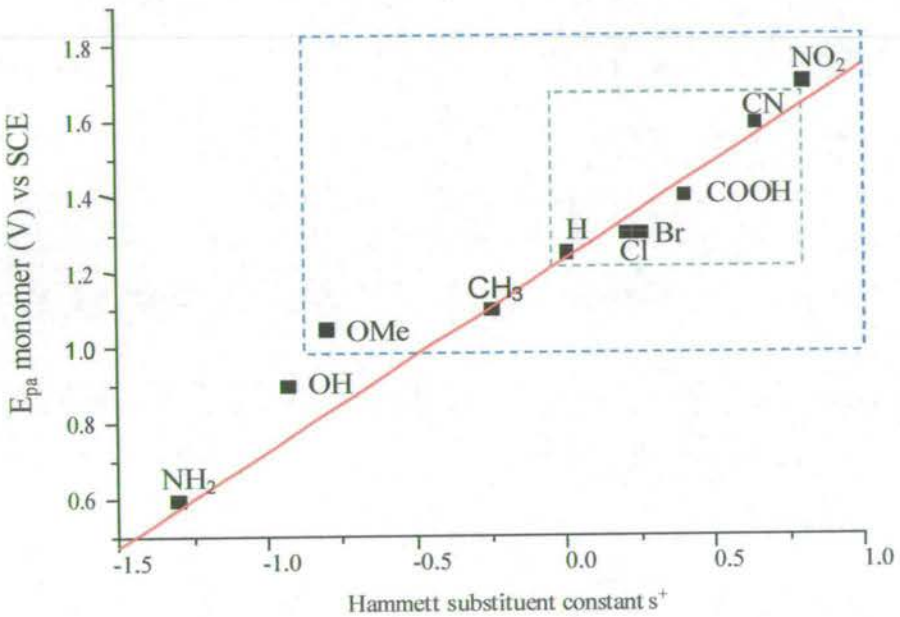

Figure 1.11 Plot of oxidation peak potential (relative to an $Ag/AgClO_4$ reference electrode) against Hammett substituent constant for a range of 5-substituted indoles. Those marked within the smaller green box were found to form a film by Waltman et al, those marked within the larger blue box were found by Mount et al to form a film.

1.4.1.1 Electropolymerisation studies on 5-substituted indoles by Mount et al

With a view to resolving the conflicting theories presented above, a substantial area of work has been carried out, since 1991, in Edinburgh by Mount et al [71-80]. They have shown that the 5-substituted indoles: 5-cyanoindole, 5-bromoindole, 5-chloroindole, 5methylindole and 5-methoxyindole (illustrated within the larger blue box in Figure 1.11) form conducting polymer films. Initially work was centred on Indole-5-carboxylic acid and 5-cyanoindole, since they presented immediate potential as fast response pH sensors [70]. For both indole derivatives it was found that electropolymerisation formed a film that consisted of two different chemical species that could be separated by their differential solubility in dimethylformamide. Characterisation of these products was carried out using mass spectroscopy, uv-visible spectroscopy, fluorescence spectroscopy, IR spectroscopy and NMR spectroscopy [72]. It was proposed that the DMF-soluble product had an asymmetric trimer structure, as shown in Figure 1.12, and that the DMF-insoluble product was a polymer consisting of linked trimers.

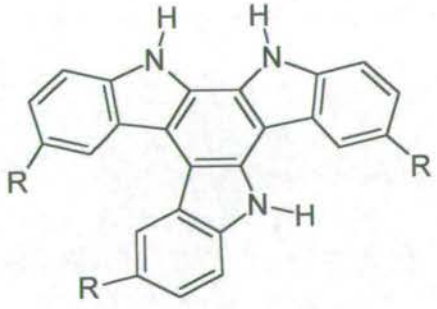

Figure 1.12 Structure of the electrochemically oxidised, 5-substituted indole trimer, as proposed by Mount et al[72].

The trimer consists of three monomers, linked through their 2 and 3 positions, corresponding with the findings of Zotti et al [58, 59] and Tabli et al [62-69] who also proposed binding via the 2 and three positions. The evidence also suggests that the trimers link via two of the 1 positions on each trimer, thus accounting for the observed decrease in intensity of the N-H stretch in the infra red spectrum upon polymerisation reported by Waltman et al [56] and Tourillon et al [2]. The proposed mechanism of trimer and polymer formation is given in Figure 1.13, with the polymerisation occurring in two steps. Step one is the initial monomer oxidation and occurs in the diffusion layer near the electrode, which results in the deposition of a film of an asymmetric cyclic trimer onto the electrode surface. This film then acts as a surface on which further adsorption and oxidation of monomer can occur, followed by radical cation linkage to form more cyclic trimer, which is the mechanism by which the film grows. Once deposited, step two can occur where the trimers can undergo further oxidation and react with a neighbouring trimer unit to form a conductive polymer chain. Step one is kinetically favoured over step two, hence controlling the supply of monomer to the electrode surface affects the composition of the film with respect to polymer and trimer content

$$3n\ \mathrm{In} \rightarrow n(\mathrm{In})^{+}_{3(s)} + 7\mathrm{e}^{-} + 6\mathrm{H}^{+} \qquad \text{Step one}$$

$$\mathrm{n(In)}^{+}_{3(s)} \rightarrow -\left[(\mathrm{In})^{+}_{3}\right]_{\mathrm{n}} + 2\mathrm{ne}^{-} + 2\mathrm{nH}^{+} \qquad \text{Step two}$$

Figure 1.13 The electropolymerisation mechanism for 5-substituted indoles as proposed by Mount et al [68]. In, In_3^+ and $-(In_3^+)-_n$ represent the indoles monomer, oxidised trimer and oxidised polymer species respectively.

Further work on a wider range of 5-substituted indoles [75] has confirmed this proposed mechanism and shown it to be consistent for all the monomers that form a redox active film. Although 5-aminoindole and 5-hydroxyindole form soluble products upon polymerisation, it has been shown through rotating ring disc electrode studies and the use of 5-cyanoindole films as a template [79], that polymerisation probably occurs via the same mechanism to form an asymmetric trimer. The use of a pre-formed polymer layer as a template was an important advance, since it opened up the possibility of incorporating a greater variety of substituents into indole polymer films.

1.4.1.2 Other relevant work on the polymerisation of indoles.

As previously mentioned, recent work by Talbi et al is contrary to that presented by Mount et al, however, other workers have agreed with the proposed trimer structure shown in Figure 1.12. Kokkinidis et al [81] recently examined the electrochemical behaviour of 4-nitro and 5-nitroindole, concluding that their results were consistent with the formation of a conducting film consisting of asymmetric trimer units linked to form a polymer. Independently, in 1996, Bocchi et al [82] polymerised indole, using iodine as the supporting electrolyte to obtain a crystalline product. From partial X-ray diffraction data they proposed the same asymmetric trimer structure as Mount et al, claiming to have made a charge transfer complex of iodine and an indole trimer.

Chemical methods have also been used to polymerise indoles [63, 83-86] with a wide range of results, and the presence of an asymmetric trimer species has been suggested by some workers [83, 86]. In general, the chemical polymerisation methods were found to produce less conductive and less homogeneous polymers, with complex synthesis and low yields.

1.5 Photophysics of conducting polymers.

Until recently, comparatively little attention has been given to the luminescence properties of conjugated polymers, probably because polyacetylene, one of the most widely studied materials of this type, shows only weak photoluminescence. But the development of conjugated polymers that exhibit high photoluminescence quantum yields has generated considerable interest, the most notable and only such system to have been studied in detail being poly(p-phenylene vinylene) (PPV) and its derivatives. These systems have been studied in depth, particularly after it was discovered that they were electroluminescent and therefore potential materials for the development of light emitting devices. Although PPV is produced using chemical methods, it has similarities to the electropolymerised indoles, being an organic conjugated polymer system with conducting properties and a high photoluminescence quantum yield. Due to the extensive nature of the work on PPV, it provides a useful model with which to compare the results from this study, although there is still considerable debate concerning the mechanisms of photo- and electro-luminescence. Much of this debate arises from the very different approaches of researchers from physical and chemical backgrounds with the associated difference in terminology used to describe similar phenomena. The following discussion gives a review of some of the work carried out on PPV and its derivatives, with particular attention being given to the model developed by Samuel et al[131] to describe the luminescence properties.

1.5.1 Photoluminescence and electroluminescence.

Much of the work on PPV has involved studies of the photo-excited luminescence, using the results to build a model for the mechanisms of electroluminescence. The scheme shown in Figure 1.14 [87, 88] is a representation that has been used for the photoluminescence of a

conjugated polymer. Photo-excitation of an electron from the highest occupied molecular orbital (HOMO) to the lowest unoccupied molecular orbital (LUMO) generates a singlet excited state, which is often referred to as a singlet exciton. The polymer may then relax to the ground state, with the emission of light at a longer wavelength than that absorbed (the Stokes shift). The magnitude of this Stokes shift, the quantum yield of the fluorescence and measurements of fluorescence lifetimes have been used to gain a greater understanding of the mechanisms of photo-excitation.

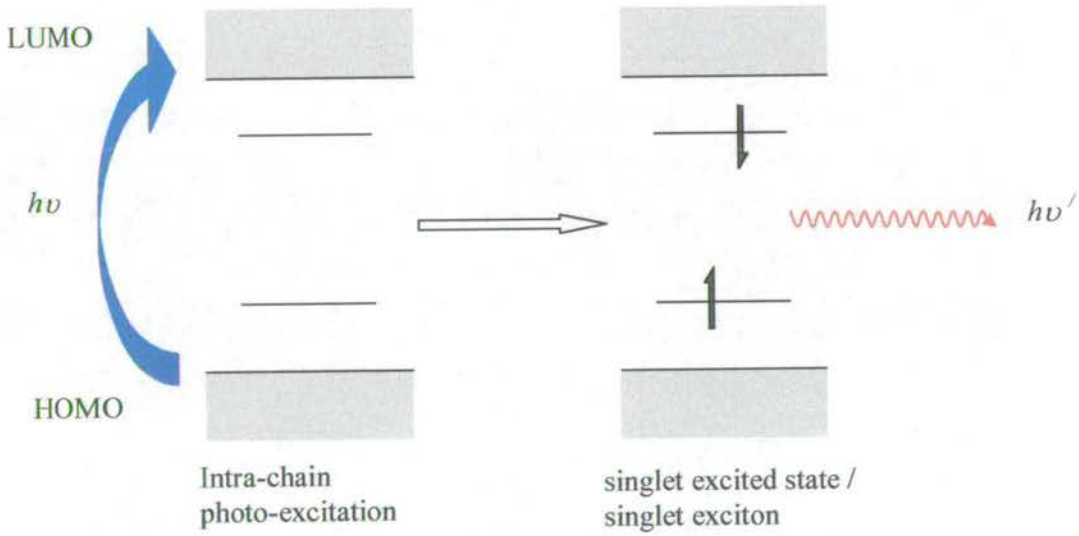

Figure 1.14 Photoluminescence from a conjugated polymer, reproduced from reference 87.

The process of electroluminescence is somewhat more complex as can be seen from the scheme in Figure 1.15 [87, 88]. The HOMO and LUMO states are often described as the valence and conduction bands respectively and the properties of the polymer described in terms of a

semi-conducting band model [89, 90]. To generate electroluminescence an electron is injected into the LUMO or conduction band, forming a radical anion, often referred to as a negatively charged polaron. Injection of a hole into the HOMO or valence band forms a radical cation, or positively charged polaron. These charges then migrate under the influence of the applied electric field and if they combine on a single conjugated segment of the polymer, a singlet excited state, or singlet exciton is formed, equivalent to that produced from photoluminescence, which can then decay radiatively to the ground state. An important feature is that the light emitted due to electrical-excitation also exhibits a Stokes shift as seen for photo-excitation, therefore there is no self-absorption of the emitted light by the polymer.

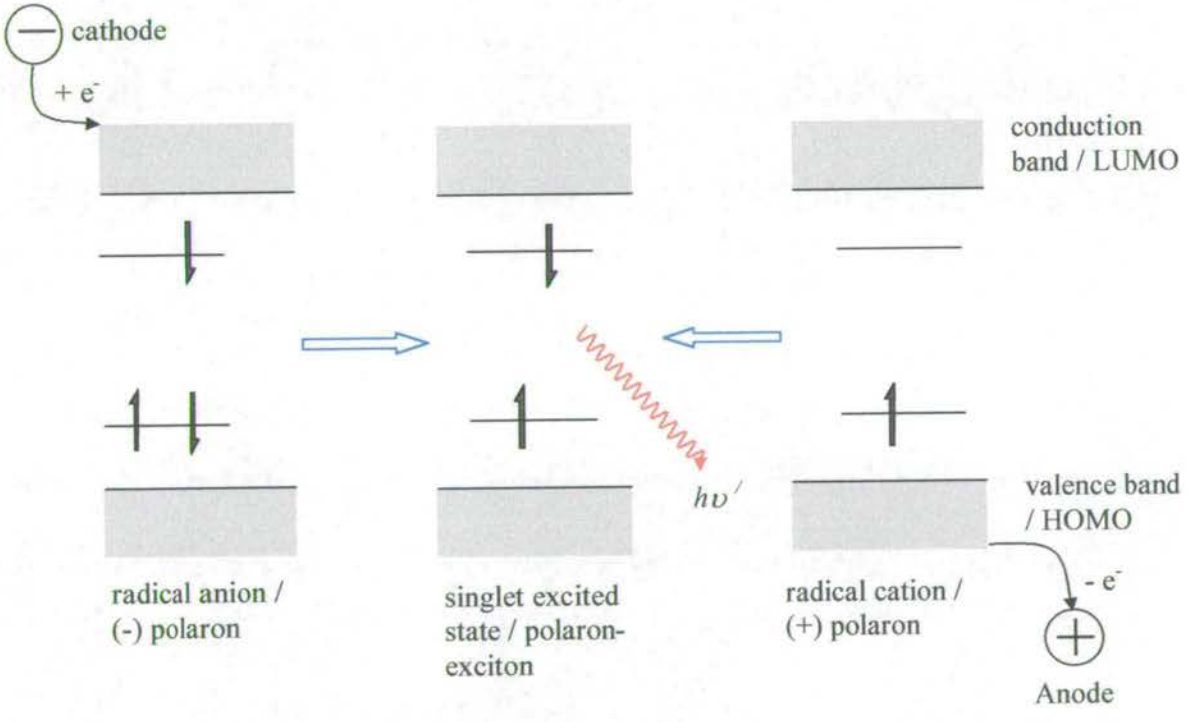

Figure 1.15 Electroluminescence from a conjugated polymer, reproduced from reference 87.

1.5.2 Fabrication of electroluminescent devices.

PPV is produced chemically using a pre-cursor route synthesis [91, 92] that allows thin layers of the precursor material to be laid down using spin-coating techniques, before thermal conversion to the fully conjugated polymer. Work by Heeger et al [93-95] showed that the derivative poly(2-methoxy, 5-(2'-ethyl-hexoxy)-p-phenylene vinylene) (MEH-PPV), is soluble in the conjugated form and therefore a conjugated polymer film can be cast with no subsequent processing or heat treatment.

1.5.2.1 Single layer devices

The earliest and simplest from of electroluminescent device is composed of a single layer of polymer as shown in Figure 1.16 [88].

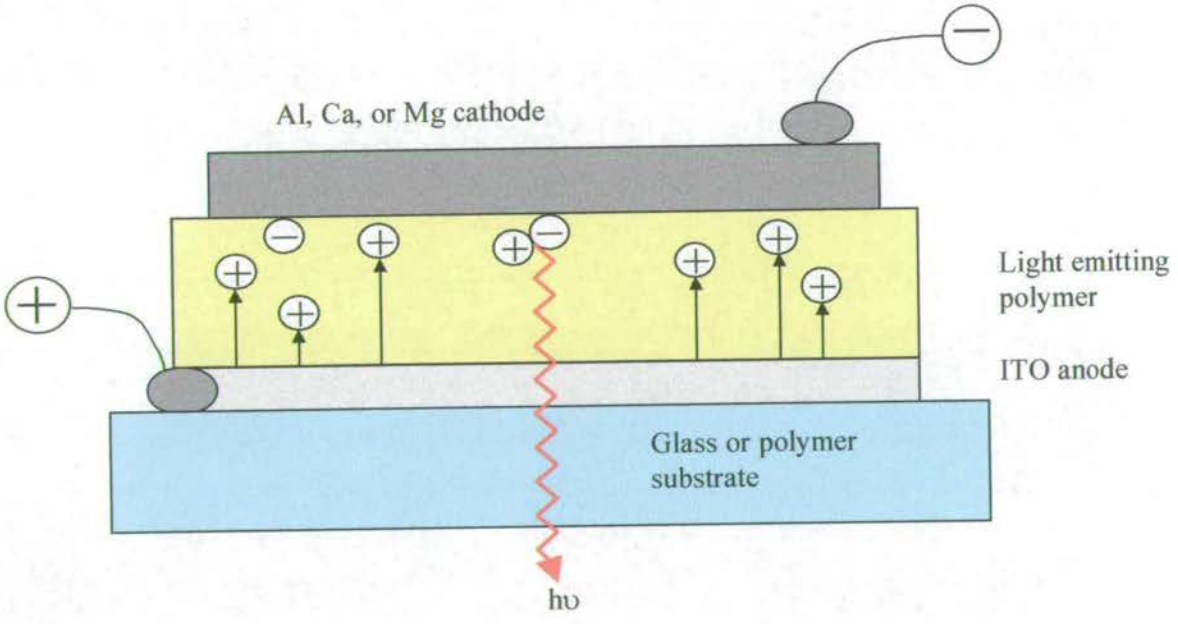

Figure 1.16 Single layer electroluminescent device, reproduced from reference 88.

Application of an electric field results in the injection of electrons and holes into the polymer film from the two electrode contacts, one of which is the transparent conducting material ITO. The electrons and holes can then migrate as described in Figure 1.15 and combine to form a singlet excited state, which may decay radiatively. It has been found that the migration of holes in PPV is more facile than for electrons, therefore recombination occurs close to the metal polymer interface.

1.5.2.2 Multi-layer devices

The metal polymer interface is known to act as a quenching site, therefore the efficiency of the single layer device is low, due to the difficulty in injecting electrons. This was overcome by the use of an electron conducting/hole blocking (ECHB) layer [96, 97], such as oxadiazole containing materials, illustrated for the bilayer device shown in Figure 1.17.

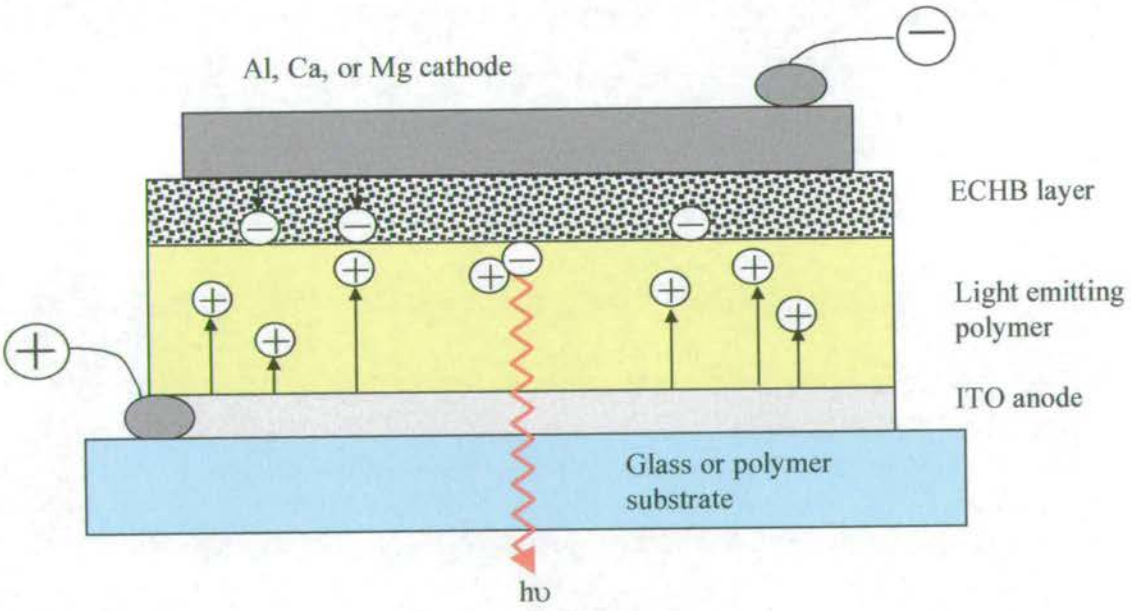

Figure 1.17 Bilayer electroluminescent device, containing an electron conducting/hole blocking (ECHB) layer, reproduced from reference 88.

This layer promotes the passage of electrons and provides a barrier to the passage of holes, therefore confining the site of charge recombination and photon generation to the PPV layer and away from the cathode. The use of such layers has resulted in considerably better device efficiencies.

The multi-layer construction was extended to include further polymer layers with differing band gaps [98], these provide a range of different colour light-emitting layers and can be used to control charge injection and transport. Devices were fabricated that used a variety of copolymers and different polymer blends with the aim of achieving light emitting diodes with variable colours and multicolour displays.

1.5.2.3 Blue-light emitting diodes.

Blue light emission is essential for applications involving multicolour displays, however it has proved to be difficult to achieve with inorganic devices and as yet, a bright blue emitting, stable, efficient polymer has not been found, although considerable advances have been made [101-103]. To achieve blue emission, a large HOMO-LUMO or band gap is required, however due to the feature of Stokes shifting, the emission is usually to longer wavelengths than desired. One way of getting a blue-shift in the emission is to interrupt the conjugation of the polymer at short intervals with non-conjugated segments. This prevents the migration of the excitation energy to longer conjugation lengths, therefore minimising the Stokes shift.

1.5.2.4 Lasers based upon conjugated polymers

Recently work has been published in which PPV-based conjugated polymers have been used in the fabrication of lasing devices [104-110]. One method uses a microcavity structure in which

PPV is sandwiched between two highly reflecting mirrors. If the thickness of the PPV is of the order of the wavelength of the emitted light, then the cavity acts as a resonator for a standing electromagnetic wave and creates a narrowing in the emission spectrum. This has been successfully demonstrated when the cavity is optically pumped. There would be considerable interest if lasing could be generated from an electrically pumped device, although it has been questioned whether the conjugated polymers could withstand the high current densities required. Work by Bradley et al [106] has demonstrated luminescence induced by injecting charge at high current densities using a scanning tunnelling microscope, suggesting that a polymer laser diode is an attainable target.

1.5.3 Photoluminescence mechanisms in conjugated polymers.

The initial studies on the photoluminescence of PPV and its derivatives was aimed at gaining an understanding of their fundamental optical properties and to locate suitable materials for electroluminescence applications [89, 111-114]. Since recombination of electrons and holes produces the equivalent of a singlet (S_1) excited state, the emission properties of the polymer can be studied using photo-excitation and there has been much debate concerning the nature of this S_1 state. A number of theoretical studies have examined the nature of the excited states [115-118] providing useful comparisons with experimental data. However it has become apparent that the emission characteristics of the polymers are complex with both intra- and inter-chain interactions being important, making theoretical calculations difficult.

Work by Samuel et al using a combination of fluorescence lifetime and quantum yield measurements has provided considerable insight into the nature of photo-excitations in conjugated polymers [119-131]. The results are interpreted in terms of the widely held belief that

the generation of singlet intra-chain excited states is the dominant product of photo-excitation. However, this is disputed by Rothberg et al [131] who have suggested that photo-excitation predominantly leads to non-emissive inter-chain polaron pairs. The evidence presented by Samuel et al strongly supports the former view and this is discussed below.

1.5.3.1 Evidence for a distribution of conjugation lengths

Since PPV is produced from a non-conjugated precursor, the degree of conjugation can be controlled by the conversion conditions and by using different leaving groups on the precursor. It has been shown that as the conjugation length is increased there is an increase in the wavelength of emission and a decrease in the fluorescence lifetime [119]. It was also found [120] that when the polymer was excited at short wavelengths (300nm) the fluorescence decay was complicated and a maximum entropy method (MEM) analysis gave a broad distribution of lifetimes. When excited at longer wavelengths (560nm), the decay was approximately mono exponential with only a narrow distribution of lifetimes. The results from the MEM analysis for MEH-PPV are shown in Figure 1.18.

These results were explained in terms of a distribution of conjugation lengths being present on the polymer chains. Excitation at shorter wavelengths generates excitons on segments of the polymer chain with a wide range of conjugation lengths. These excitons are mobile and can migrate to longer, lower energy segments. By exciting at a longer wavelength, excitons will only be generated on the segments with longest conjugation lengths, from which migration is unlikely since any neighbouring segments will be of higher energy. This explains the simpler behaviour when exciting at longer wavelength, since excitation and emission is limited to only the longest segments.

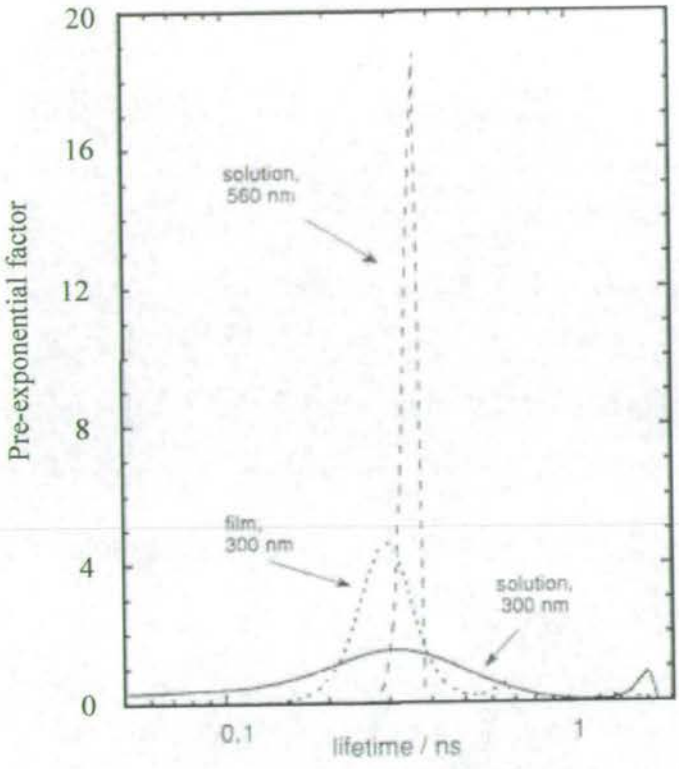

Figure 1.18 MEM distribution analyses for transient luminescence in MEH-PPV, reproduced from reference 120.

This view is supported by time-resolved emission experiments [119, 121] where it has been observed that there is a red shift in the emission spectrum with time. Therefore, absorption of the sample is due to chains of many different conjugation lengths, whereas emission only occurs from the longest conjugated segments, which are acting as traps for the excitation energy. This model accounts for the observation of a much broader spectrum for absorption than emission.

1.5.3.2 Evidence for an intra-chain photo-excitation in PPV

A number of different values for the fluorescence lifetime of PPV have been given, ranging from 50 picoseconds to 1.2ns, with the variation being attributed to differences in the sample preparation. Due to this variation, it is important for comparisons of photophysical properties to be made on the same sample. Measurements of quantum yields are difficult to make on solid state samples, however the use of an integrating sphere as shown in Figure 1.19 [123] allowed measurements with a good degree of accuracy to be made. The quantum yield of PPV and a number of derivatives have been reported, with values ranging from 0.1 for MEH-PPV to 0.48 for MEH-CN-PPV.

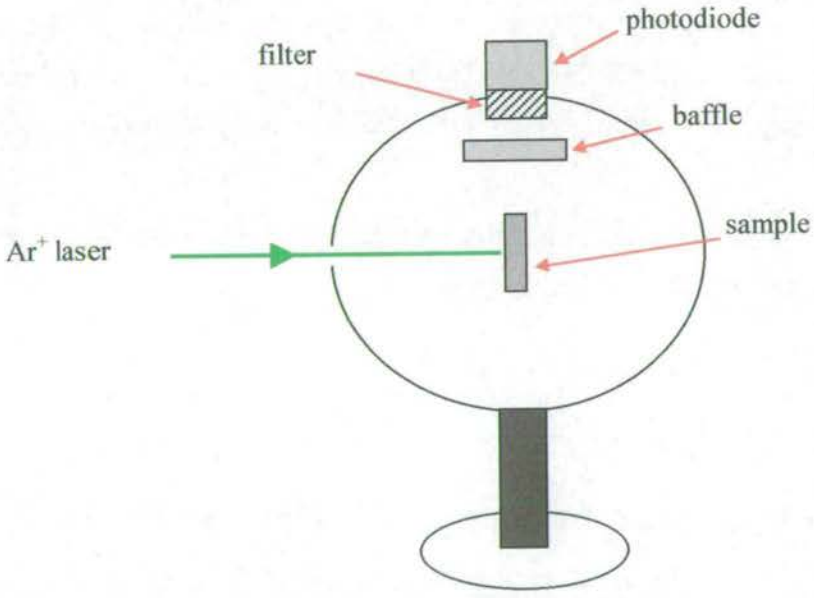

Figure 1.19 Experimental arrangement for quantum yield measurements using an integrating sphere, reproduced from reference 123.

The theory of luminescence decay kinetics is described in detail in section 2.4.5; however an important feature is that for a single excited species decaying via a unimolecular decay process, the rates of radiative and non-radiative decay can be described by the rate constants k_R and k_{NR}. These constants are related to the measurable luminescence lifetime τ by:

$$\tau = \frac{1}{k_R + k_{NR}} \qquad (1.1)$$

and to the quantum yield Φ by:

$$\Phi = \frac{k_R}{k_R + k_{NR}} = \frac{\tau}{\tau_R} \qquad (1.2)$$

where τ_R is the natural radiative lifetime, which would be identical to the luminescence lifetime if there were no non-radiative decay processes. From the above equations it can be seen that both the quantum yield and the lifetime need to be measured to obtain both rate constants. If it is possible, as suggested by Rothberg et al, that photo-excitation may lead to species other than the singlet excited state, then equation 1.2 must be modified to show that the quantum yield is the fraction of absorbed photons that generate an excited singlet state, multiplied by the rate of radiative decay:

$$\Phi = \frac{bk_R}{k_R + k_{NR}} = \frac{b\tau}{\tau_R} \qquad (1.3)$$

where b is the fraction of absorbed photons generating the singlet excited state and $0 \leq b \leq 1$.

By combining the results of lifetime and quantum yield measurements for PPV it was found that $\Phi = 0.27$, the value of $\tau_R \geq 1.2$ns and the value of b is in the range of 0.9 to 1. This implies that the dominant product of photo excitation in PPV is an emissive species, with singlet excitons being produced with close to unit quantum yield and a fraction, 0.27, of them decaying radiatively. These results are consistent with photo-excitation of PPV giving an intra-chain singlet exciton.

1.5.3.3 Evidence for inter-chain excitations.

Studies of the cyano substituted derivative of PPV (CN-PPV) produced anomalous results compared with those of PPV. This derivative was developed to increase the efficiency of electron injection, a limiting factor to the efficacy of LED's. The fluorescence lifetime of the solid film, 5.6ns, was found to be much longer than that of the solution, 900ps [122, 124-126]. These lifetimes were obtained using a long wavelength excitation to give mono-exponential decay kinetics. This result is the opposite of unsubstituted PPV and is unexpected, since more rapid migration of excitons to quenching sites in the film should result in a shorter lifetime. The similarity of the solution phase results suggests that emission is from an intra-chain exciton, however, in the film the nature of the emitting species must be different.

It has been suggested that the emission from the film is from an inter-chain excitation such as a physical dimer or excimer. Initial excitation is thought to form an intra-chain singlet exciton, which then rapidly migrates to pre-existing dimers or a region where excimers can form. The quantum yield for the film was found to be in the region of 0.35 to 0.46, higher than for PPV films which, when combined with the much longer-lived emission, implies that the rate of non-radiative decay is much smaller. A possible explanation for the decrease in

non-radiative processes is that inter-chain excitations are less mobile than intra-chain excitations, therefore migration to quenching sites is slower. The inter-chain model is consistent with steady state fluorescence, where the emission is broad and structureless. The presence of excitation features due to inter-chain interactions no longer allows these materials to be considered as one-dimensional systems, making theoretical calculations more complex.

These conclusions have been supported by studies of some other conjugated polymers such as poly(3-alkyl thiophenes) (P3ATs) [128] in good and bad solvents and MEH-PPV films [126]. It has also been shown [131] that PPV, which only exhibits intra-chain excitation characteristics under normal conditions, begins to show characteristics of an inter-chain excitation at high pressure, possibly due to the high pressure forcing chains to interact and allowing the excitation to delocalise between adjacent chains.

1.5.3.4 The relationship between inter- and intra-chain interactions

The model suggested by Samuel et al to describe the excited state kinetics in conjugated polymers can be summarised in a simple kinetic scheme [129] as shown in Figure 1.20. X^* represents the excited state initially formed over a short conjugation sequence. A^* and B^* are the intra-chain and inter-chain excitation species respectively. The rate of relaxation of X^* into the longer conjugation sequences A^* is given by k_{XA} which competes with population of the inter-chain B^* state, given by k_{XB}. If k_{XB} is greater than k_{XA} then it will appear as if the inter-chain B^* state has been directly excited. Both the intra- and inter-chain state can decay via radiative and non-radiative processes back to the ground state, with the rate constants k_{rA}, k_{nrA} and k_{rB} and k_{nrB} respectively. The states A^* and B^* may interconvert, but it has been

assumed that the rate of dissociation of the inter-chain excitation back to the intra-chain species, described by k_{BA}, is small enough to be negligible.

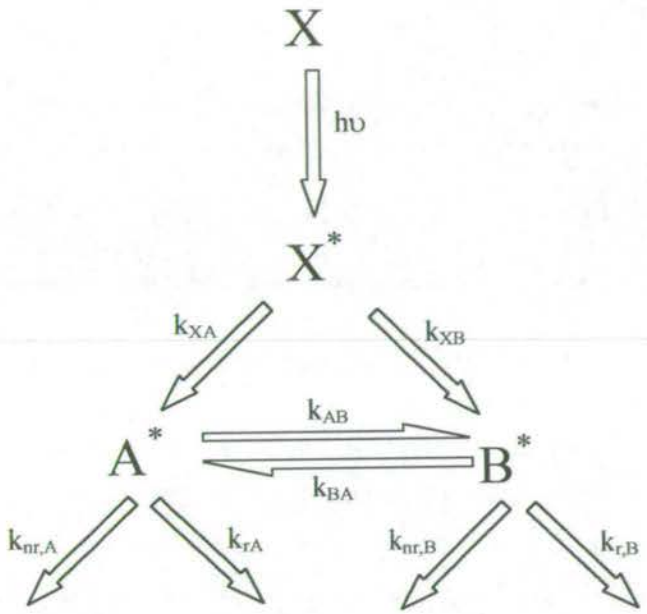

Figure 1.20 Kinetic scheme for general model representing the rate processes between an initially excited state X*, an intra chain excitation A* and an inter-chain excitation B*. Reproduced from reference 129.

1.5.4 Other organic materials with electroluminescence potential.

Although the most widely studied material with potential for electroluminescence applications is PPV, a number of other organic materials have been examined with the same goals in mind. Electroluminescence has been reported from devices containing non-polymeric material with an aromatic amine being used as the hole transporting material and the emitting electron transporting layer being a perylene tetracarboxylic acid derivative [132, 133] or a fluorescent metal chelate complex [134]. A number of photophysical studies have been

carried out on polythiophenes [135-139] and electroluminescence has been demonstrated from poly(3-alkylthiophene) [140]. Fullerene has also been suggested [136] as a potential electroluminescent material.

1.5.5 Electrogenerated chemiluminescence (ECL).

In the preceding discussion, the potential of materials for electroluminescent devices has been explored, however, it is also possible to generate emission via electrogenerated chemiluminescence (ECL). ECL involves the emission of light due to the electron transfer reactions between electrogenerated species. An electron transfer reaction between an oxidised species (the radical cation) and a reduced species (the radical anion) produces the excited state. The redox species are generated at an electrode by alternate pulsing of the electrode potential [141, 142]. Studies have been carried out on a wide range of materials [143-146] and ECL has been reported for films of MEH-PPV [147] with a view to probing the properties of the polymer and investigating potential applications in display devices.

Very recently, investigations by Mount et al have used the technique of ECL to assess the potential of electropolymerised indoles as electroluminescent materials. Preliminary results are very encouraging, with emission being observed for films of 5-cyanoindole.

1.6 Aim of this work

The aim of this work was to carry out a comprehensive photophysical characterisation of a range of 5-substituted indole electropolymers. The primary aim of the project was to use time-resolved fluorescence to explore the photophysical properties of these systems in detail and gain an understanding of the excitonic properties of the monomer, trimer and polymer

species. As a basis to this time-resolved work, steady-state fluorescence studies, at room and low temperature, were carried out to characterise the monomer and trimer species in solution and to attempt to spectroscopically isolate the polymer species. With potential uses as electroluminescent materials in mind, solid state polymer films were examined to determine their photoluminescence properties. In studying the polymer systems (in solution and the solid state), specific objectives were to investigate the effects of intra-chain and inter-chain interactions and oxidation state on photoluminescence properties, particularly photoluminescence efficiency.

In carrying out this investigation, steady state and time-resolved fluorescence spectroscopic techniques have been employed, along with electrochemical preparation and characterisation methods. This chapter gives an overview of the techniques used and a literature review of the electrochemical and luminescent research concerning indole and other conducting polymer systems. Chapter Two provides a summary of the theoretical aspects related to this work. Chapter Three gives the experimental details for this thesis. Chapters Four and Five present the results from steady state luminescence investigations at room temperature and low temperature, respectively. Chapters Six and Seven are concerned with time-resolved fluorescence studies, using the technique of picosecond time-correlated single photon counting, and the associated time-resolved emission spectroscopy. Chapter Seven also reports on a new experimental technique; this technique allows the measurement of the in situ fluorescence response of an indole polymer film with respect to electrochemical conditions, allowing a correlation between the film's redox and fluorescence properties.

1.7 References

1. J. H. Burroughes, D. D. C. Bradley, A. R. Brown, R. N. Marks, K. Mackay, R. H. Friend, P. L. Burns and A. B. Holmes, *Nature.*, 1990, **347**, 539.
2. G. Tourillon, F. Garnier, *J. Electroanal. Chem.*, 1982, **135**, 173.
3. J. G. Mackintosh, C. R. Redpath, A C. Jones, P. R .R. Langridge-Smith, D. R. Reed, A.R. Mount, *J. Electroanal. Chem.*, 1994, **375**, 163
4. L. Tilstra, M. C. Sattler, W. R. Cherry, M. D. Barkley, *J. Am. Chem. Soc.*, 1990, **112**, 9176.
5. S. V. Konev, *fluorescence and Phosphorescence of Proteins and Nucleic Acids.*, Plenum: New York, 1967.
6. Y. Chen, R. L. Rich, F. Gai, J. W. Petrich, *J. Phys. Chem.*, 1993, **97**, 1770.
7. N. Mataga, Y. Torihashi, K. Ezumi, *Theoret. Chim. Acta (Ber).*, 1964, **2**, 158.
8. S. Suzuki, T. Fujii, A. Imai, H. Akahorl, *J. Phys. Chem.*, 1977, 81, **16**, 1592
9. M. Martinaud, A. Kadiri, *Chem. Phys.*, 1978, **28**, 473.
10. N. Glasser, H. L. Lami, *J. Chem. Phys.*, 1978, **68(7)**, 3317.
11. H. L. Lami and N. Glasser, *J. Chem. Phys.*, 1986, **84**, 597.
12. N. Glasser, H. L. Lami, *J. Chem. Phys.*, 1981, **74(11)**, 6526.
13. M. S. Walker, T. W. Bednar, R. L. Lumry, *J. Chem. Phys.*, 1966, **45**, 3455.
14. M. S. Walker, T. W. Bednar, R. L. Lumry, *J. Chem. Phys.*, 1966, **45**, 3455
15. I. Tatischeff, R. Klein, T. Zemb, M. Duquesne, *Chem. Phys. Letts.*, 1978, **54(2)**, 394.
16. J. Eisinger, G. Navon, *J. Chem. Phys.*, 1969, **50(5)**, 2069.
17. H. L. Lami, *J. Chem. Phys.*, 1977, **67(7)**, 3274.
18. P. S. Song, W. E. Kurtin, *J. Am. Chem. Soc.*, 1969, 4892.
19. S. R. Meech, D. Phillips, A.G. Lee, *Chem. Phys.*, 1983, **80**, 317.
20. S. R. Meech, D. Phillips, A.G. Lee, *Chem. Phys. Letts*, 1982, **92(5)**, 523.

21. P. R. Callis, *J. Chem. Phys.*, 1991, **95**, 4230.

22. J. T. Vivian, P. R. Callis, *Chem. Phys. Letts.*, 1994, **229**, *153.*

23. E. P. Kirby, R. F. Steiner, *J. Phys. Chem.*, 1970, **74(26)**, 4480.

24. G. J. Smith, W. H. Melhuish, Y. Huang, M. Sulkes,

25. T. G. Poliitis, H. G. Drickamer, *J. Chem. Phys.*, 1981, **75(7)**, 3203.

26. A. T. Amos, B. L. Burrows, *Adv. Quantum. Chem.*, 1973, **7**, 289.

27. M. R. Eftink, L. A. Selvidge, P. R. Callis, A. A. Rehms, *J. Phys. Chem.*, 1990, **94**, 3469.

28. D. M. Sammeth, S. S. Siewert, L. H. Spangler, P. R. Callis, *Chem. Phys. Letts.*, 1992, **193(6)**, 532.

29. P. L. Muino, P. R. Callis, *Chem. Phys. Letts.*, 1994, **222**, 156.

30. B. J. Fender, D. M. Sammeth, P. R. Callis, *Chem. Phys. Letts.*, 1995, **239**, 31.

31. Y. Huang, M. Sulkes, *Chem. Phys. Letts.*, 1996, **254**, 242.

32. Y. Huang, M. Sulkes, *J. Chem. Phys.*, 1996, **100**, 16479.

33. S. Arnold, M. Sulkes, *J. Phys. Chem.* 1992, **96**, 4768.

34. S. Arnold, M. Sulkes, *Chem. Phys. Letts.*, 1992, **200(1,2)**, 125.

35. S. Arnold, L. Tong, M. Sulkes, *J. Phys. Chem.* 1994, **98**, 2325.

36. C. K. Chiang, C. R. Fincher, Y. W. Park, H. Shirakawa, E. J. Louis, S. C. Gau, A. G. MacDiarmid, *Phys. Rev. Lett.*, 1977, **39**, 1098.

37. J. R. Reynolds, C. K. Baker, C. A. Jolly, P. A. Poropatic, J. P. Ruiz, *Conductive Polymers and Plastics*, chapter 1.

38. A. F. Diaz, K. Kanazawa, G. P. Gardini, *J. Chem. Soc. Chem. Comm.*, 1979, 635.

39. K. Kanazawa, A. F. Diaz, W. D. Gill, P. M. Grant, G. B. Street, G. P. Gardini, J. F. Kwak, *Synth. Met.*, 1979/80, **1**, 329.

40. K. Kanazawa, A. F. Diaz, R. H. Geiss, W. D. Gill, J. F. Kwak, J. A. Logan, J. F. Rabolt, G. B. Street, *J. Chem. Soc. Chem. Comm.*, 1979, 854.

41. A. F. Diaz, J. Crowley, J. Bargon, G. P. Gardini, J. B. Torrance, *J. Electroanal. Chem.*, 1981, **121**, 355.

42. R.J. Waltman, A.F. Diaz, J. Bargon, *J. Phys. Chem.* 1984, **88**, 4343.

43. R.J. Waltman, J. Bargon, *Can. J. Chem.*, 1986, **64**, 76.

44. R.J. Waltman, A.F. Diaz, J. Bargon, *J. Electrochem. Soc. Electrochem. Sci.and Tech.*, 1985, **123(3)**, 631.

45. R. L. Greene, G. B. Street, *Science*, 1984. **226**, 651.

46. N. F. Colaneri, D. D. C. Bradley, , R. H. Friend, P. L. Burns, A. B. Holmes, C. W. Spangler, *Am. Phys. Soc. Phys. Rev. B.*, 1990, **42(18)**, 11670.

47. A. Coghlan, *New Scientist*, 1994, **2**, 20.

48. P.N. Bartlett, J. Farington, *Bull. Electrochem.*, 1992, **8(5)**, 208.

49. J. E. Frew, H. A. O. Hill, *Anal. Chem.* 1987, **59(15)**, 933.

50. R. W. Murray, A. G. Ewing, R. A. Durst, *Anal. Chem.*, 1987, **59(5)**, 379.

51. A. Riklin, E. Katz, I. Willner, A. Stocker, A. Buckmann, *Nature*, 1995, **376**, 672.

52. C. A. Marsden, *Chem & Ind.*, 1993, 324.

53. W. Schumann, *Mikrochimica. Acta.*, 1995, **121**, 1.

54. T. W. Lewis, G. G. Wallace, *J. Chem. Ed.*, 1997, **74(6)**, 703.

55. P. N. Bartlett, J. Farrington, *J. Electroanal. Chem.*, 1989, **261**, 471.

56. R.J. Waltman, A.F. Diaz, J. Bargon, *J. Phys. Chem.* 1984, **88**, 4343.

57. J. P. Nigrey, A. G. Macdirmid, A. J. Heeger, *J. Chem. Soc. Chem. Comm.*, 1979, 594.

58. G. Zotti, S. Zecchin, G. Schiavon, R. Seraglia, A. Berlin, A. Canavesi, *J. Am. Chem. Soc. Chem. Mater.*, 1994, **6**, 1742.

59. A. Berlin, A. Canavesi, G. Schiavon, S. Zecchin, G. Zotti, *Tetrahedron*, 1996, **52(23)**, 7947.

60. K. Jackowska, A. Kudelski, J. Bukowska, *Electrochimica Acta.*, 1994, **39(10)**, 1365.

61. K. Jackowska, J. Bukowska, *Polish. J. Chem.* 1992, **66**, 1477.

62. E.B. Maarouf, D. Billaud, E. Hannecart, *Materials. Research. Bull.* 1994, **29 (12)**, 637.

63. D. Billaud, E.B. Maarouf, E. Hannecart, *Materials. Research. Bull.* 1994, **29 (12)**, 1239.

64. H. Talbi, E.B. Maarouf, B. Humbert, M. Alnot, J. J. Ehrhardt, J. Ghanbaja, D. Billaud, *J. Phys. Chem. Solids.*, 1996, **57(6-8)**, 1145.

65. H. Talbi, J. Ghanbaja, D. Billaud, B. Humbert, *Polymer.*, 1997, **38(9)**, 2099.

66. H. Talbi, B. Humbert, D. Billaud, *Synth. Met.*, 1997, **84**, 875.

67. H. Talbi, D. Billaud, *Synth. Met.*, 1998, **97**, 239.

68. H. Talbi, G. Monard, M. Loos, D. Billaud, *J. Mol. Struc. (Theochem.)*, 1998, **434**, 129.

69. S. W. Kong, K. M. Choi, K. H. Kim, *J. Phys. Chem. Solids.*, 1992, **53(5)**, 657.

70. P.N. Bartlett, D.H. Dawson, J. Farrington, *J. Chem. Soc. Faraday. Trans.* 1992, **88 (18)**, 2685.

71. . J. G. Mackintosh, A.R. Mount, *J. Chem. Soc., Faraday Trans.*, 1994, **90**, 1121.

72. J. G. Mackintosh, C. R. Redpath, A C. Jones, P. R .R. Langridge-Smith, D. R. Reed, A.R. Mount, *J. Electroanal. Chem.*, 1994, **375**, 163.

73. J. G. Mackintosh, A.R. Mount, D. Reed, *Magn. Reson. Chem.*, 1994, **32**, 559.

74. J. G. Mackintosh, C. R. Redapth, A. C. Jones, P. R. R. Langridge-Smith, A. R. Mount, *J. Electroanal. Chem.*, 1995, **388**, 179.

75. P. Jennings, A. C. Jones, A. R. Mount, A. D. Thomson, *J. Chem. Soc., Faraday Trans.*, 1997, **93**, 3791.

76. A. R. Mount, A. D. Thomson, *J. Chem. Soc., Faraday Trans.*, 1998, **94(4)**, 553.

77. J. G. Mackintosh, S. J. Wright, P. R .R. Langridge-Smith, A.R. Mount, *J. Chem. Soc., Faraday Trans.*, 1996, **92(20)**, 4109.

78. J.G. Mackintosh, *PhD Thesis*, The University of Edinburgh 1996.

79. A. D. Thomson, *PhD Thesis*, The University of Edinburgh 1996.

80. M. Robertson, *PhD Thesis*, The University of Edinburgh 1996.

81. G. Kokkinidis, A. Kelaidopoulou, *J. Electroanal. Chem.*, 1996, **414**, 197.

82. V. Bocchi, A. Colombo, W. Porzio, *Synth. Met.*, 1996, **80**, 309.

83. T. Kaneko, M. Matsuo, Y. Iitaka, *Heterocycles*, 1979, **12(4)**, 471.

84. H. Ishii, K. Murakami, E. Sakurada, K. Hosoya, Y. Murakami, *J. Chem. Soc. Perkin. Trans.*, 1988, 2377.

85. H. Ishii, E. Sakurada, K. Murakami, S. Takase, H. Tanaka, *Chem. Soc. Perkin. Trans.*, 1988, 2387.

86. V. Bocchi, G. Palla, *Tetrahedron*, 1986, **42(18)**, 5019.

87. A. B. Holmes, D. D. C. Bradley, A. R. Brown, P. L. Burn, J. H. Burroughes, R. H. Friend, N. C. Greenham, R. W. Gymer, D. A. Halliday, R. W. Jackson, A. Kraft, J. H. F. Martens, K. Pichler, I. D. W. Samuel, *Synth Met.*, 1993, **55-57**, 4031.

88. A. Kraft, A. C. Grimsdale, A. B. Holmes, *Angew. Chem. Int. Ed.*, 1998, **37**, 402.

89. R. H. Friend, D. D. C. Bradley, P.D. Townsend, *J. Phys. D. Appl. Phys.*, 1987, **20**, 1367.

90. R. H. Friend, D. D. C. Bradley, *Fraday Diss. Chem. Soc.*, 1989, **88**, 213.

91. D. D. C. Bradley, *J. Phys. D. Appl. Phys.*, 1987, **20**, 1389.

92. P. L. Burn, D. D. C. Bradley, R. H. Friend, D. A. Halliday, A. B. Holmes, R. W. Jackson, A. Kraft, *J. Chem. Soc. Perkin. Trans.*, 1992, 3225.

93. D. Braun, A. J. Heeger, ?

94. D. Braun, A. J. Heeger, H. Kroemer, *J. Elec. Mat.*, 1991, **20(11)**, 945.

95. G. Gustafsson, Y. Cao, G. M. Treacy, F. Klavetter, N. Colaneri, A. J. Heeger, , *Nature.*, 1992, **357**, 477.

96. A. R. Brown, D. D. C. Bradley, J. H. Burroughes, R. H. Friend, N. C. Greenham, P. L. Burn, A. B. Holmes, A. Kraft. *Appl. Phys Lett.*, 1992, **61(23)**, 2793.

97. D. D. C. Bradley, A. R. Brown, P. L. Burn, J. H. Burroughes, R. H. Friend, N. C. Greenham, R. W. Gymer, A. B. Holmes, A. M. Kraft, R. N. Marks, *Photochemistry and Polymeric systems – Conjugated Polymer Electro Optic Devices.*

98. A. R. Brown, N. C. Greenham, J. H. Burroughes, D. D. C. Bradley, R. H. Friend, P. L. Burn, A. Kraft, A. B. Holmes, *Chem. Phys. Letts.*, 1992, **200(1,2)**, 46.

99. P. L. Burn, A. B. Holmes, A. Kraft, D. D. C. Bradley, A. R. Brown, R. H. Friend, R. W. Gymer, *Nature.*, 1992, **356**, 47.

100. M. Berggren, O. Inganas, G. Gustafsson, J. Rassmusson, M. R. Andersson, T. Hjertberg, O. Wennerstrom, *Nature.*, 1994, **372**, 444.

101. C. Adachi, T. Tsutsui, S. Saito, *Appl. Phys Lett.*, 1990, **56(9)**, 799.

102. Y. Yang, Q. Pei, A. J. Heeger, *J. Appl. Phys*, 1996, **79(2)**, 934.

103. P. L. Burn, A. B. Holmes, A. Kraft, D. D. C. Bradley, A. R. Brown, R. H. Friend, *J. Chem. Soc. Chem. Comm.*, 1992, 32.

104. N. Tessler, G. J. Denton, R. H. Friend, *Nature.*, 1996, **382**, 695.

105. F. Hide, M. A. Diaz-Garcia, B. J. Schwartz, M. R. Andersson, Q. Pei, A. J. Heeger, *Science*, 1996, **273**, 1833.

106. D. G. Lidzey, D. D. C. Bradley, S. F. Alvarado, P. F. Seidlerm, *Nature.*, 1997, **386**, 135.

107. B. J. Schwartz, F. Hide, M. R. Andersson, A. J. Heeger, *Chem. Phys. Letts.*, 1997, **265**, 327.

108. G. H. Gelinck, J. M. Warman, M. Remmers, D. Neher, *Chem. Phys. Letts.*, 1997, **265**, 320.

109. X. Long, A. Malinowski, D. D. C. Bradley, M. Inbasekaran, E. P. Woo, *Chem. Phys. Letts.*, 1997, **272**, 6.

110. R. H. Friend, R. W. Gymer, A. B. Holmes, J. H. Burroughes, R. N. Marks, C. Taliani, D. D. C. Bradley, D. Santos, J. L. Bredas, M. Logdlund, W. R. Salaneck, *Nature.*, 1999, **397**, 121.

111. K. S. Wong, D. D. C. Bradley, W. Hayes, J. F. Ryan, R. H. Friend, H. Lindenberger, S. Roth, *J. Phys. C: Slid State Phys.*, 1987, **20**, L187.

112. D. D. C. Bradley, R. H. Friend, *J. Phys. Condens. Matter.*, 1989, **1**, 3671.

113. M. Furukawa, K. Mizuno, A. Matdui, S. D. D. V. Rughooputh, W. C. Walker, *J. Phys. Soc. Jap.*, 1989, **8**, 2976.

114. S. Heun, R. F. Mahrt, A. Greiner, U. Lemmer, H. Bassler, D. A. Halliday, D. D. C. Bradley, P. L. Burn, A. B. Holmes, *J. Phys. Condens. Matter.*, 1993, **5**, 247.

115. J. Cornil, D. Beljonne, D. A. dos Santos, Z. Shuai, J. L. Bredas, *Synth Met.*, 1996, **78**, 209.

116. J. Cornil, D, Beljonne, C. M. Heller, I. H. Cambell, B. K. Laurich, D. L. Smith, D. D. C. Bradley, K. Mullen, J. L. Bredas, *Chem. Phys. Letts.*, 1997, **278**, 139.

117. D. A. dos Santos, D. Beljonne, J. Cornil , J. L. Bredas, *Chem. Phys.*, 1998, **227**, 1.

118. J. Cornil , A, J, Heeger, J. L. Bredas, *Chem. Phys. Letts.*, 1997, **272**, 463.

119. I. D. W. Samuel, B. Crystall, G. Rumbles, P. L. Burn, A. B. Holmes, R. H. Friend, *Synth Met.*, 1993, **54**, 281.

120. I. D. W. Samuel, B. Crystall, G. Rumbles, P. L. Burn, A. B. Holmes, R. H. Friend, *Chem. Phys. Letts.*, 1993, **213(5, 6)**, 472.

121. G. R. Hayes, I. D. W. Samuel, R. T. Phillips, *Phys. Rev. B.*, 1995-II, **52(16)**, 569.

122. N. C, Greenham, I. D. W. Samuel, G. R. Hayes, R. T. Phillips, Y. A. R. R. Kessener, S. C. Moratti, , B. Crystall, R. H. Friend, *Chem. Phys. Letts.*, 1995, **241**, 89.

123. I. D. W. Samuel, G. Rumbles, C. J. Collison, *Phys. Rev. B.*, 1995-II, **52(16)**, 573.

124. G. R. Hayes, I. D. W. Samuel, R. T. Phillips, *Phys. Rev. B.*, 1996-II, **54(12)**, 8301.

125. I. D. W. Samuel, G. Rumbles, C. J. Collison, B. Crystall, S. C. Moratti, A. B. Holmes, *Synth Met.*, 1996, **76**, 15.

126. G. R. Hayes, I. D. W. Samuel, R. T. Phillips, *Synth Met.*, 1997, **84**, 889.

127. M. Halim, I. D. W. Samuel, E. Rebourt, A. P. Monkman, *Synth Met.*, 1997, **84**, 951.

128. L. Magnani, G. Rumbles, I. D. W. Samuel, K. Murray, S. C. Moratti, A. B. Holmes, R. H. Friend, *Synth Met.*, 1997, **84**, 899.

129. I. D. W. Samuel, G. Rumbles, C. J. Collison, R. H. Friend, S. C. Moratti, A. B. Holmes, *Synth Met.*, 1997, **84**, 497.

130. I. D. W. Samuel, G. Rumbles, C. J. Collison, S. C. Moratti, A. B. Holmes, *Chem. Phys.*, 1998, **227**, 75.

131. I. D. W. Samuel, G. Rumbles, R. H. Friend, in: *N. S. Sariciftci (Ed.), Primary Photoexcitations in Conjugated Polymers: Molcecular Exciton Versus Semiconductor Band Model, World Scientific, Singapore*, 1997.

132. C. Adachi, T. Tsutsui, S. Saito, *Appl. Phys. Lett.*, 1989, **55(15)**, 1489.

133. C. Adachi, S. Tokito, T. Tsutsui, S. Saito, *Jap. J. Appl. Phys.*, 1988, **27(2)**, L269.

134. C. W. Tang, S. A. VanSlyke, *Appl. Phys. Lett.*, 1987, **51(12)**, 913.

135. K. E. Ziemelis, A. T. Hussain, D.D. C. Bradley, R. H. Friend, J. Ruhe, G. Wegner, *Phys. Rev. Lett.*, 1991, **66(17)**, 2231.

136. A. T. Werner, G. Grem, H. J. Byrne, G. Leising, S. Roth, *Mat. Sci. Forum*, 1995, **191**, 195.

137. S, V. Frolov, X. Wei, W. Gellermann, Z, V. Vardney, E. Ehrenfreund, *Chem. Phys.*, 1998, **227**, 125.

138. W. Gebauer, M. Sokolowski, E. Umbach, *Chem. Phys.*, 1998, **227**, 33.

139. I. D. W. Samuel, L. Magnani, G. Rumbles, B. M. Stone, S. C. Moratti, A. B. Holmes,

140. Y Ohmori, M. Uchida, K. Muro, K. Yoshino, *Jap. J. Appl. Phys.*, 1991, **30(11B)**, L1938.

141. A. J. Bard, L. R. Faulkner, in, *Electrochemical methods, J. Wiley & Sons*, 1980.

142. L. R. Faulkner, A. J. Bard, in, *Electroanal. Chem. Vol 10, Marcel Decker Inc*, New York 1977.

143. R. Bexman, L. R. Faulkner, *J. Am. Chem. Soc.*, 1972, 6317.

144. F. R. F. Fan, A. Mau, A. J. Bard, *Chem. Phys. Letts.*, 1985, **116(5)**, 400.

145. M. Hamaguchi, H. Nambu, K. Yoshino, *Jap. J. Appl. Phys.*, 1997, **36**, L124.

146. H. Nambu, M. Hamaguchi, K. Yoshino, *J. Appl. Phys.*, 1997, **82**, 1847.

147. M. M. Richter, F. R. F. Fan, F. Klavatter, A. J. Heeger, A. J. Bard, *Chem. Phys Lett.*, 1994, **226**, 115.

Chapter Two - Theory

2.1 Introduction

The work presented in this thesis utilises a wide range of experimental and analytical techniques for which there exists a sizeable background of theoretical literature. This chapter is a summary of the most important theoretical aspects and introduces the concepts on which the work has been based.

2.2 The electronic structure of aromatic molecules

Indole is one of a vast range of aromatic molecules which, due to their molecular structure, posses particular photophysical properties. These properties arise from the delocalised nature of the bonding between sp^2 hybridised carbon atoms in a six membered carbon ring. The σ sp^2 hybrid orbitals interact with each other and with the 1s orbitals of hydrogen forming localised σ bonds. The remaining six π atomic orbitals interact to give C-C π-bonds where the electrons are delocalised forming a cloud of π-electrons above and below the carbon ring. The resulting benzenoid structure is well characterised and provides the basis for photophysical studies of aromatic compounds.

The accepted nomenclature for the electronic states of aromatic compounds is based upon the perimeter free electron orbital model developed by Platt to explain the types of absorption band which appear in the spectra of the benzenoid hydrocarbons. In a molecule with *n* benzene rings,

there will be $2(2n+1)$ π-electrons due to each C atom possessing one π-electron. In an n-ringed molecule in the ground state, the highest filled energy level is found when $q = n$, where q is the orbital ring quantum number, and the letters *e, f, g* and *h* are assigned to energy levels where $q = n-1, n, n+1, n+2$ respectively. The algebraic sum of the values of q for each individual electron gives the value of Q, the total ring quantum number and the letters *A, B, C* are assigned to states where $Q = 0, 1, 2$ and *K, L, M* where $Q = 2n, 2n+1, 2n+2$ respectively. Using the constant potential approximation, all the states except *A* are doubly degenerate; however, this degeneracy is removed by including the periodic potential due to the nuclei, causing each state to be split into two components represented by the subscripts a and b. Singlet and triplet excited states exist dependent upon maintaining or reversing the electron spin during an electronic transition. These are labelled with the superscripts 1 and 3 respectively. In the case of this study on indoles, the electronic states of interest are the ground singlet state ^1A, and the two low lying excited singlet states ^1L_a and ^1L_b along with the lowest triplet state ^3L_a.

2.2.1 Singlet and triplet states

The labels singlet and triplet state refer to the total electron spin of that state, known as the spin multiplicity and defined as $2S+1$ where S is the total spin quantum number, calculated as the vector sum of the individual contributions of all electrons. Each individual electron possesses spin angular momentum which is quantified by the spin quantum number and has the value $s = ½$. In the presence of a magnetic field the electron may be in one of two possible spin states, which are defined by the magnetic spin quantum number m_s where $m_s = \pm ½$. Two electrons each with $m_s = \pm ½$ can either have their spins parallel or opposed. If the spins are opposed then

S= ½-½ = 0, thus $2S+1$ = 1 and such an electronic state is a singlet state. If the spins are parallel then S= ½ + ½ and $2S+1$ = 3, resulting in a triplet state. Molecules in the ground state are in a singlet state, labelled S_0. Promotion of an electron to a higher energy level can either result in a singlet excited state S_n (n= 1, 2, 3...) where the electron spin remains unchanged, or a triplet excited state T_n where the spin multiplicity alters. In the process of electron excitation there is a preference for preservation of spin multiplicity and singlet to triplet transitions are spin forbidden.

The energy of a triplet state is lower than the corresponding singlet state due to the operation of the Pauli exclusion principle and summarised by Hund's rule of maximum multiplicity. With electron spins parallel the state possesses an antisymmetric spatial wavefunction for which there is zero probability of finding both electrons in the same location. The electrons avoid each other so minimising the energy of repulsion between them and consequently lowering the energy of that state.

2.2.2 Vibronic states

So far only the electronic energy levels of the molecules have been considered, however, molecules undergo vibrational and rotational motion and associated with each electronic energy level are vibrational and rotational energy levels. The energy associated with rotational motion is two orders of magnitude lower than vibrational energies. Rotational transitions are not resolved in luminescence spectra in the condensed phase, although population of rotational levels contributes to the broadening of spectra. A state involving electronic and vibrational energy is a

vibronic state, with a transition between two such states being referred to as a vibronic transition. Aromatic hydrocarbons possess many vibrational modes which results in an overlap of the vibronic transitions and a further broadening of the luminescence spectra. Under certain conditions, such as at low temperature, vibronic structure can be resolved.

2.3 Excitation processes

The separation between molecular electronic energy levels corresponds to the energy of photons in the ultraviolet, visible and infrared regions of the electromagnetic spectrum. Absorption of a photon of equivalent energy to this separation will excite an electron from a lower to a higher energy level, producing an excited state of the molecule.

$$\mathbf{M} + h\nu \rightarrow \mathbf{M}^* \tag{2.1}$$

2.3.1 The Einstein coefficients

The probability that the absorption transition will occur is defined by the *Einstein B coefficient*. The rate of transition of molecules from a ground state m to an excited state n due to the absorption of radiation is given by:

$$-\frac{\mathbf{d}}{\mathbf{dt}}\mathbf{N}_m = \mathbf{N}_m \mathbf{B}_{m\rightarrow n}\rho(\nu_{m\rightarrow n}) \tag{2.2}$$

where N_m is the number of molecules in state *m*, $\nu_{m\to n}$ is the frequency of the radiation and ρ is the radiation energy density. The probability of spontaneous emission is defined by the Einstein A coefficient, with the rate of transition of molecules from state *n* to *m* given by:

$$-\frac{d}{dt}N_n = N_n\{A_{n\to m} + B_{n\to m}\rho(\nu_{n\to m})\} \tag{2.3}$$

where N_n is the number of molecules in state n and:

$$B_{n\to m} = B_{m\to n} \tag{2.4}$$

$$\nu_{n\to m} = \nu_{m\to n} \tag{2.5}$$

$A_{n\to m}$ is related to the radiative lifetime τ_r^0 by:

$$\frac{1}{A_{nm}} = \tau_r^0 \tag{2.6}$$

2.3.2 Transition moments

The excitation of an electron from a lower to a higher energy state results in the separation of electronic charge within the molecule, with the development of a radiation-induced dipole moment, known as the transition dipole moment μ_{nm}. For an absorption transition to be allowed there must be a specific interaction between the electric component of the incident radiation and

the molecule, resulting in a change in the dipole moment of the molecule during the transition. For this to occur the transition dipole moment integral must be non-zero and is defined as:

$$\mu_{nm} = \langle \psi_n | \mu | \psi_m \rangle \tag{2.7}$$

where ψ_n and ψ_m are the wavefunctions for the states n and m respectively.

2.3.3 The Beer-Lambert Law

When experimental measurements of absorption of radiation are made, they are presented in terms of the Beer-Lambert absorption law, which relates the intensity of radiation transmitted through the sample to the path length and sample concentration. There are a number of ways of expressing this law, the most common is to use the decadic molar absorption or extinction coefficient ε:

$$\mathbf{I = I_0 10^{-\varepsilon c l}} \tag{2.8}$$

where I is the intensity of radiation transmitted through the sample, I_0 the intensity of incident radiation, c the concentration and l the path length. Rearrangement of (2.8) gives:

$$\mathbf{\log\left(\frac{I_0}{I}\right) = \varepsilon c l = D} \tag{2.9}$$

where D is the decadic absorbance.

2.3.4 Oscillator strengths

The extinction coefficient ε is a function of the radiation frequency and a measure of the transition intensity can be obtained by integrating ε over the whole absorption band to give the integrated absorption coefficient *A* where:

$$\mathbf{A} = \int_{\text{band}} \varepsilon(\bar{\nu})\, d\bar{\nu} \qquad \textbf{(2.10)}$$

which is related to the Einstein B coefficient since:

$$\int \varepsilon(\bar{\nu})\, d\bar{\nu} = \frac{\mathbf{N_A h \upsilon_{nm} B_{nm}}}{\mathbf{\ln 10}} \qquad \textbf{(2.11)}$$

1.

The experimental value *A* can be connected to the theoretical value of the oscillator strength f_{nm} for the absorption transition. The oscillator strength f_{nm} is a measure of the strength of an electric dipole transition compared to that of a free electron oscillating in three dimensions and is related to *A* by:

$$\mathbf{f_{nm}} = \left[\frac{\mathbf{4\varepsilon_0 m_e c^2 \ln(10)}}{\mathbf{N_A e^2}} \right] \mathbf{A} \qquad \textbf{(2.12)}$$

Electric dipole allowed transitions have oscillator strengths close to one whereas spin forbidden transitions have oscillator strengths close to zero. The oscillator strength can also be related to the transition dipole moment μ_{nm} by the equation:

$$f_{nm} = \left[\frac{8\pi^2 m_e c}{3e^2 h}\right] \bar{\nu}_{nm} \left|\mu_{nm}\right|^2 \qquad (2.13)$$

where $\bar{\nu}$ is the wavenumber of the transition.

2.3.5 The Franck Condon principle

The time scale of an electronic transition (promotion of an electron) due to excitation by electromagnetic radiation is negligible compared with that of nuclear motion. Thus it can be assumed that the nuclei remain frozen at the equilibrium configuration of the ground state molecule during the transition. Therefore, a vibronic transition involves no change in the nuclear co-ordinates and is represented as a vertical transition on a potential energy diagram as shown in Figure 2.1. This is known as the Franck Condon principle. Since an electron is being excited into some antibonding orbital, there is likely to be a weakening of the bond strength, so the potential energy curve of the excited state is shown displaced to larger equilibrium internuclear separations with respect to the ground state. Due to the vertical nature of the transition, the excited state will be produced with some additional vibrational excitation. The vibrational level of the excited state most likely to be populated in the transition is dependent upon the vibrational overlap integral, defined as:

$$\int \psi_v'^{*} \psi_v'' \, dr \qquad (2.14)$$

where ψ_v' and ψ_v'' are the vibrational wavefunctions for the ground and excited states respectively and r is the vibrational co-ordinate. If the $v'' = 0$ vibrational wavefunction were to be projected on top of the excited state wavefunctions, then the area underneath the overlapped functions would represent the vibrational overlap integral. The square of the overlap integral is known as the Franck Condon factor.

Figure 2.1 represents a molecule with different equilibrium geometries in the ground and excited states. In this example, the largest overlap integral occurs between the vibrational levels $v'' = 0$ and $v' = m$ in absorption. The other v' vibrational levels will have overlap integrals with $v'' = 0$ that may be non-zero and will therefore be present as transitions in the absorption spectrum, but with lower intensity than the transition with the largest overlap integral. This manifests itself in the absorption spectrum where there is a vibronic progression dependent upon the nuclear geometries of the ground and excited states. In the case of aromatic hydrocarbons, as for other polyatomic molecules, the potential energy surfaces of the ground and excited states are more complicated and there are many vibronic transitions that overlap to produce a broader absorption profile. The shape of the absorption profile is referred to as the Franck Condon envelope.

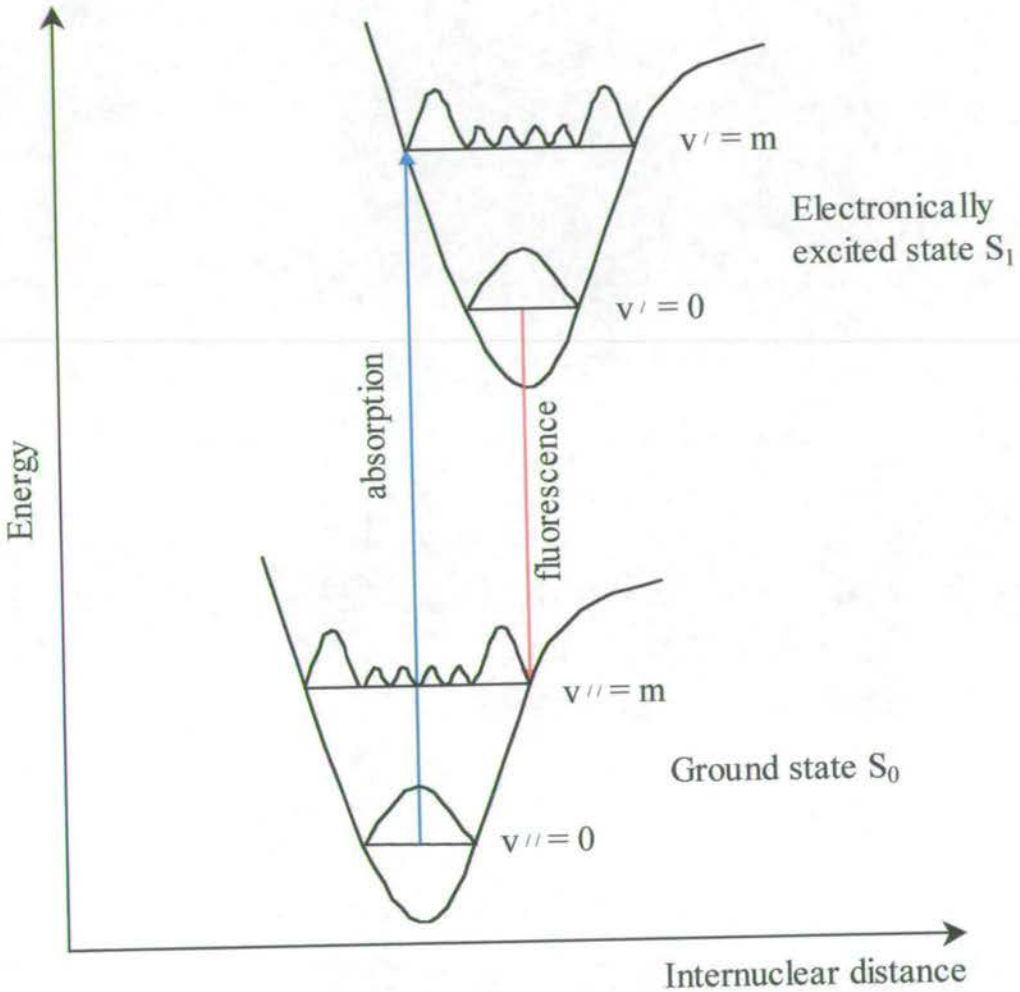

Figure 2.1 Potential energy curves for a diatomic molecule illustrating the vertical transitions as described in the Franck Condon Principle.

2.3.6 Transition types

The ground state of organic molecules consists of σ, π or nonbonding molecular orbitals. Excitation promotes an electron from the highest occupied molecular orbital to the lowest unoccupied molecular orbital, usually a σ^* or π^* antibonding orbital. A number of different types of transition are possible, we are most interested in $\pi \rightarrow \pi^*$ transitions exhibited by aromatic molecules which result in intense radiative de-excitation transitions and account for the highly fluorescent nature of aromatic molecules. Also of note are $n \rightarrow \pi^*$ transitions, observed in compounds containing carbonyl, thiocarbonyl, nitro, azo and imine groups, since they are associated with very weak radiative decay with little or no fluorescence activity, explained in further detail in section 2.2.2. The term chromophore is used in discussions of photophysical properties and refers to the part of an organic molecule responsible for the transitions that occur upon interaction with light. The chromophore can be thought of as the functional group of organic photochemistry. Chromophores that exhibit fluorescence properties are referred to as fluorophores.

2.4 De-excitation processes

An electronically excited molecule is in an energetically unstable state and will find some way of losing its excess energy. This may occur by chemical means, rearrangement or fragmentation of the molecule, or by a de-excitation mechanism to return the molecule to its ground state. De-excitation may occur via a number of pathways, broadly split into unimolecular and multimolecular processes. Unimolecular processes include:

1. *Radiative decay (luminescence)*, transitions where the molecule returns to the ground state accompanied by the emission of electromagnetic radiation:

$$\mathbf{M^* \rightarrow M} + h\nu \tag{2.15}$$

2. *Non-radiative decay*, transitions from an excited state to a lower electronic state without any accompanying emission.

In multimolecular processes, de-excitation occurs by the transfer of energy from the excited molecule to other molecules:

$$\mathbf{M^* + Q \rightarrow M + Q} \tag{2.16}$$

This is known as quenching. Radiative and non-radiative decay mechanisms are displayed concisely on a Jablonski diagram (Figure 2.2). Vertical (as according to the Franck-Condon principle) solid lines denote a radiative transition, wavy lines show non-radiative transitions. Absorption of electromagnetic radiation usually excites a molecule to some vibrational level of an excited singlet state. For a molecule excited into the second excited state S_2 the total energy E''_t of the molecule is given by:

$$\mathbf{E''_t = E''_e + \frac{1}{2}E''_{uv} + n''E''_{uv}} \tag{2.17}$$

where E''_e is the electronic energy, $\frac{1}{2} E''_{uv}$ is the zero point vibrational energy and $n''E''_{uv}$ is the vibrational excitation energy. The excess vibrational energy is rapidly lost through collisions with surrounding molecules and the total energy becomes:

$$\left(\mathbf{E}_t''\right)_0 = \mathbf{E}_e'' + \frac{1}{2}\mathbf{E}_{uv}'' \tag{2.18}$$

A radiationless intramolecular transition, termed internal conversion, can then occur to an isoenergetic level of the S_1 state, displayed as a horizontal transition on the Jablonski diagram. The energy of the new state is given by:

$$\left(\mathbf{E}_t''\right)_0 = \mathbf{E}_t' = \mathbf{E}_e' + \frac{1}{2}\mathbf{E}_{uv}' + \mathbf{n}'\mathbf{E}_{uv}' \tag{2.19}$$

Further vibrational relaxation rapidly lowers the energy of the molecule to a thermal population of the lowest vibrational levels of the S_1 state:

$$\left(\mathbf{E}_t'\right)_0 = \mathbf{E}_e' + \frac{1}{2}\mathbf{E}_{uv}' \tag{2.20}$$

The mechanism of non-radiative internal conversion is very fast, occurring on a picosecond time scale. This is faster than any radiative transitions, which therefore occur predominantly from the first exited state.

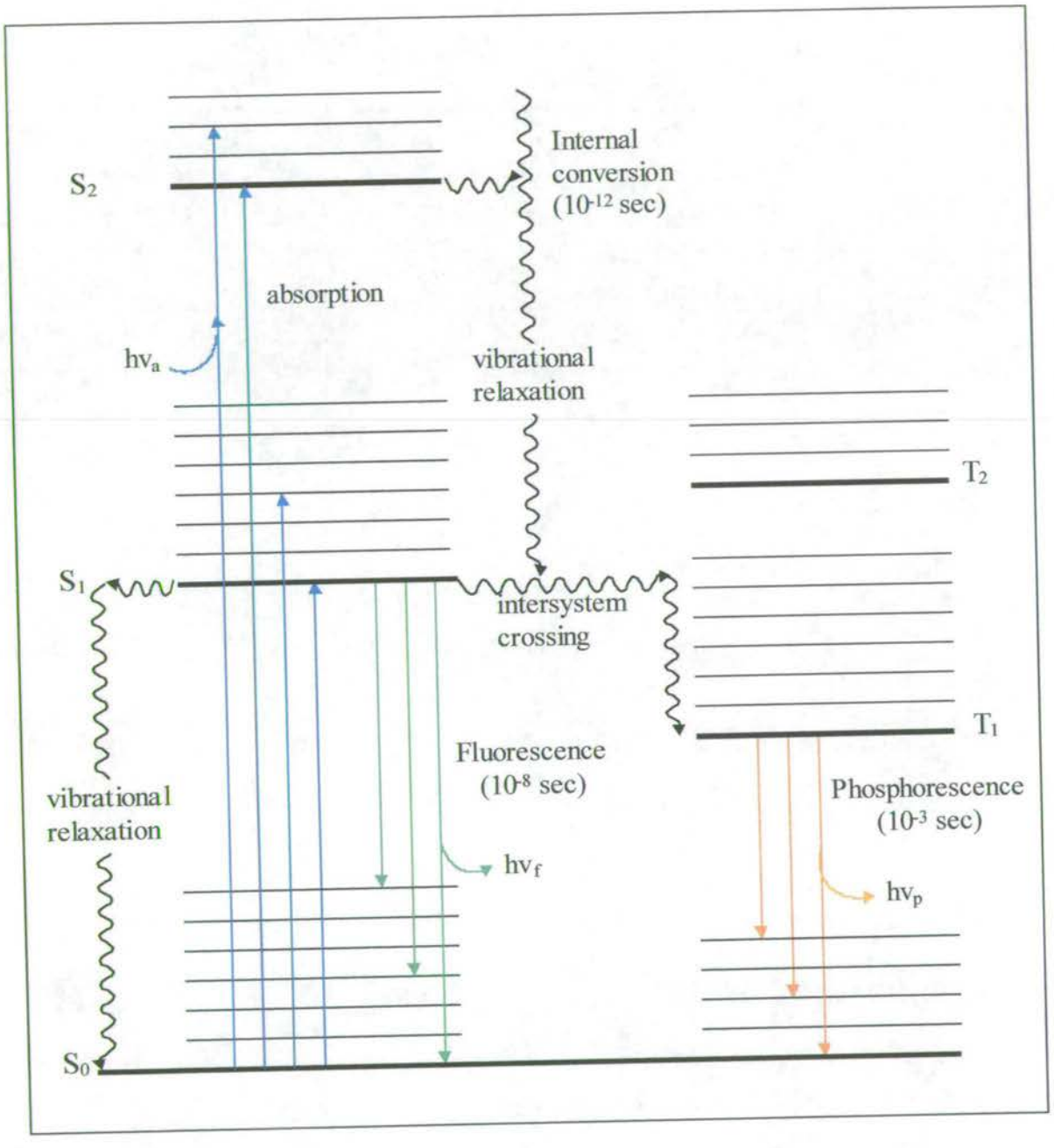

Figure 2.2 A Jablonski diagram showing the transitions between ground and excited states for absorption and emission processes.

2.4.1 Fluorescence

Fluorescence is the radiative de-excitation transition from the first singlet excited state S_1 to the ground state S_0. Since the spin multiplicity of each state is the same, the transition is strongly allowed occurring on a fast time scale, typically in the nanosecond (10^{-9}sec) range. This is in general slower than internal conversion from higher excited states to the S_1 state, with rapid vibrational relaxation ensuring that emission occurs predominantly from the $v' = 0$ level of the S_1 excited state. Because of this effect, the emission spectrum is independent of excitation wavelength.

Referring back to the Franck-Condon principle, the transitions back to the ground state are vertical, therefore the emission intensity will be greatest for the equivalent transition that displayed the most intense absorption. This is illustrated in Figure 2.3 for a molecule where the 0-0 transition is dominant in absorption and therefore also in emission. If the vibrational spacing of the ground and excited states are similar, then this leads to a phenomenon known as mirror symmetry, where the emission spectrum closely resembles the absorption spectrum as shown in the lower half of Figure 2.3.

For molecules in solution the 0-0 transitions in absorption and emission are generally not coincident, as a result of a difference in the interaction of solvent molecules between the ground and excited states. The difference in energy between the 0-0 transition in absorption and emission is called the Stokes shift and the magnitude of this shift is seen to be dependent upon the solvent. The position and structure of the emission spectrum is sensitive to the solvating medium: the Stokes shift is seen to increase with increasing solvent polarity along with a

bathochromic shift in the emission spectrum and a broadening of the structure. The absorption spectrum is relatively unaffected by solvent. This implies that the solvent is affecting the excited state of the molecule, via a number of possible mechanisms, including hydrogen bonding with protic solvents, electrostatic interaction between the dipole moment of the excited state and the solvent and reorientation of the solvent molecules. The generation of a greater dipole moment upon excitation of an organic molecule means that there is a perturbation of the environment surrounding the fluorophore in the presence of a polar solvent, resulting in reorganisation of the solvent cage. This is known as solvent relaxation and results in the loss of energy from the excited state, with emission occurring at longer wavelength. The more polar the solvent, the greater the interaction between solvent and excited state, causing a greater shift in the spectrum. If the solvent is protic then hydrogen bonding may also occur, increasing the effect. Solvent relaxation occurs over about 10^{-11} seconds and is therefore complete before radiative emission takes place.

By cooling the sample down to 77K the solvent freezes into a solid glass, preventing the reorganisation of the solvent cage upon excitation as well as preventing any collisional quenching processes. The resulting fluorescence spectra are more intense than at room temperature, are seen at shorter wavelength and posses greater vibrational structure.

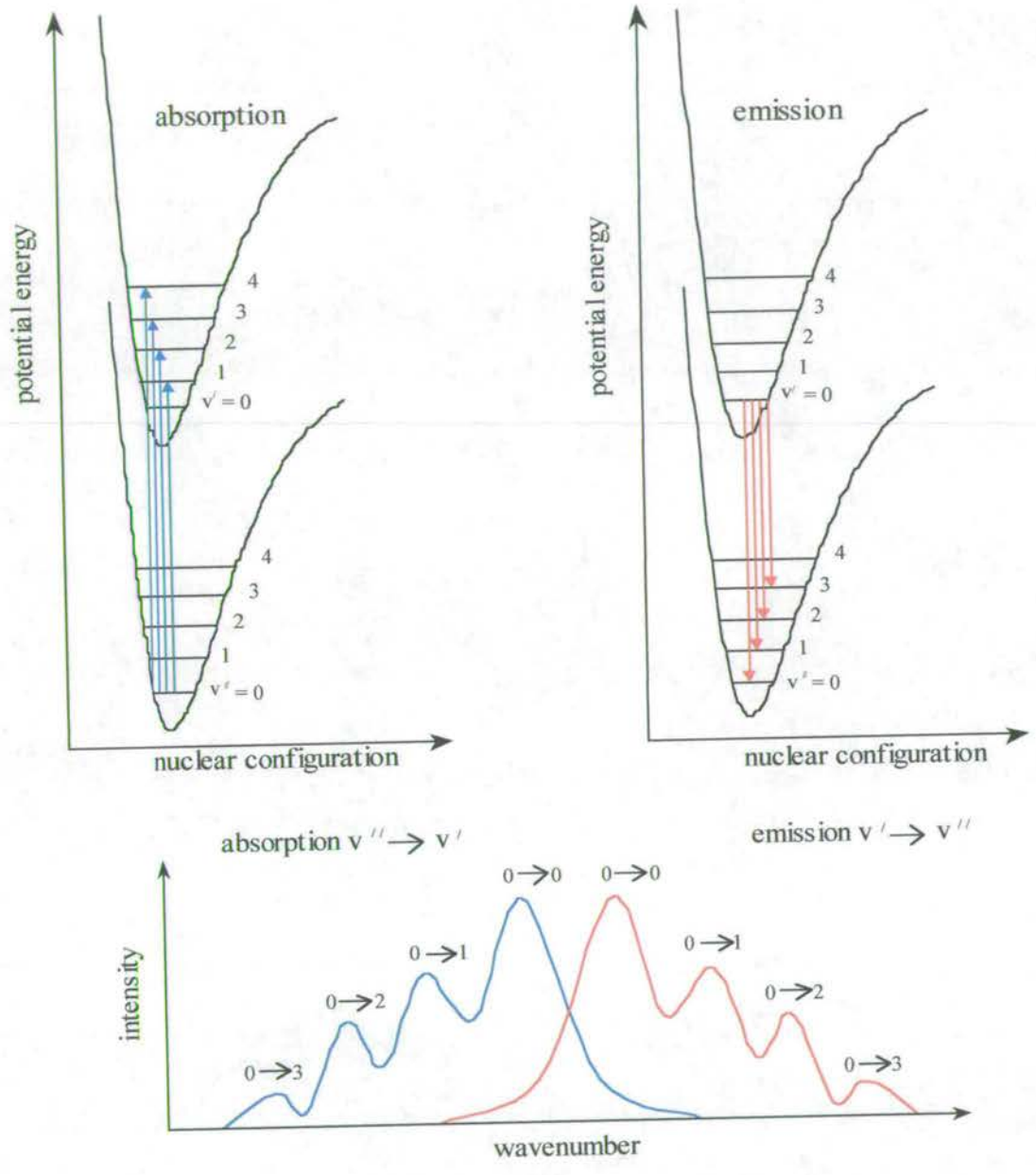

Figure 2.3 Potential energy curves, absorption and emission spectra for a molecule where the 0-0 transition is dominant, illustrating the mirror image phenomena.

2.4.2 Non-radiative decay of the S_1 state

As well as internal conversion from higher excited states to the S_1 state, it is also possible for non-radiative transitions via internal conversion to occur from the S_1 state to the ground state. The mechanism is the same as before, however, the surrounding molecules may not be able to accept the large amount of energy needed to lower the molecule to the ground state, allowing the excited state to survive long enough for radiative emission to occur.

There is another non-radiative mechanism competing with radiative emission, that of intersystem crossing to the triplet manifold. This will occur if there is a mechanism for unpairing the electron spins of the singlet ground and excited states, creating a vibrationally excited triplet excited state. The excess vibrational energy is rapidly lost, relaxing the molecule to the lower vibrational levels of the T_1 state. This singlet to triplet transition is spin forbidden but it is enhanced by the presence of spin orbit coupling. An electron has two sources of angular momentum deriving from its intrinsic spin and orbital motion and in certain circumstances it is possible for angular momentum to be exchanged between them. This results in spin-orbit coupling and blurs the distinction between states of different multiplicity, allowing mixing of singlet and triplet states. The magnitude of this interaction is related to the size of the spin-orbit coupling constant, which is dependent upon the values of the n and l quantum numbers and on the fourth power of the atomic number Z. Therefore spin-orbit coupling becomes more significant in heavier atoms and intersystem crossing is enhanced in molecules possessing a heavy atom (the internal heavy atom effect).

Intersystem crossing is also enhanced in molecules where excitation promotes an electron from an n to a π^* orbital ($n \rightarrow \pi^*$) rather than the previously discussed $\pi \rightarrow \pi^*$ transition. The n, π^* configuration may be present on the S_1 state, T_1 state or both. According to El-Sayed's selection rules, intersystem crossing is allowed to occur by spin-orbit coupling between an n,π^* state and a π-π^* state. Because of this molecules that exhibit the $n \rightarrow \pi^*$ transition such as compounds containing carbonyl, thiocarbonyl, nitro, azo and imine groups have very weak, fluorescence properties.

2.4.3 Phosphorescence

After intersystem crossing, the triplet state is generated with excess vibrational energy that is lost via vibrational relaxation, however the solvent can not extract the final large quantum of energy required to lower the molecule to the ground state, so it is trapped. A radiative transition to the ground state is spin forbidden, but the presence of spin orbit coupling allows the forbidden singlet-triplet transitions to become weakly allowed. Hence radiative transitions do occur from the triplet state but are much less intense and occur less rapidly than fluorescence transitions from the singlet state, generally on a microsecond to second time scale. As previously discussed, the triplet states lie at lower energy than their corresponding singlet states, therefore emission from the triplet state is seen at longer wavelength than emission from the singlet state.

2.4.4 Energy transfer mechanisms

So far only the mechanisms of internal conversion and intersystem crossing have been discussed as means of non-radiatively removing excitation energy, with the transitions being associated with a single molecule or functional group. However, it is possible for the energy to be transferred from an aromatic molecule or group to another molecule or group of a different species, this being known as energy transfer, or to an aromatic molecule or group of the same species, known as energy migration. Where there is no resulting radiative emission then the process is termed a quenching mechanism. Energy transfer may occur with other molecules via a radiationless process where there is an interaction with the donor and acceptor molecules during the excitation lifetime of the donor molecule. For a donor D and acceptor A this is simply:

$$\mathbf{D^* + A \rightarrow D + A^*} \qquad \textbf{(2.21)}$$

This interaction may occur via two different mechanisms, Coulombic and electron-exchange energy transfer. Coulombic energy transfer (known as the Förster mechanism) is dominated by long range dipole-dipole interactions, which cause perturbations of the electronic structures of the energy donor and acceptor, with no transfer of electrons. Electron –exchange energy transfer requires much closer contact between the donor and acceptor molecules, with the excited electron from the donor molecule transferring to the lowest unoccupied orbital of the acceptor molecule. This requires the donor and acceptor molecules to be sufficiently close together to allow overlap of the electron orbitals involved.

Energy transfer may also occur via a radiative process, where a photon emitted by the donor is subsequently absorbed by the acceptor, which is a non-collisional mechanism:

$$\mathbf{D}^* \rightarrow \mathbf{D} + h\nu \tag{2.22}$$

$$h\nu + \mathbf{A} \rightarrow \mathbf{A}^* \tag{2.23}$$

An example of a collisional mechanism and one of the most significant quenching processes in solution phase work is collisional deactivation of the excited state by oxygen molecules. This competes with the emission process, with the presence of oxygen reducing the emission intensity. Because fluorescence emission occurs on a very rapid time scale, it is not strongly affected by these mechanisms. However, since the triplet state is longer lived, it is far more susceptible to being quenched, therefore phosphorescence emission is rarely seen in solutions at room temperature or with oxygen present. Cooling the sample so that the solvent freezes into a glass reduces the rate of oxygen diffusion, therefore inhibiting collisional quenching and increasing the intensity of fluorescence emission and allowing phosphorescence emission to be observed.

Energy transfer is commonly an intermolecular phenomenon, however it is also possible for intramolecular processes to occur between different aromatic groups in the same molecule. This is of particular importance when studying polymeric samples where excitation migration can occur between different segments of an aromatic polymer. An aromatic polymer will have sequences of conjugated units, however, in solution the polymer will rotate and kink, creating regions of different conjugation length. The absorption and emission characteristics are

dependent upon this conjugation length, with the effect of a wide range of conjugation lengths being equivalent to a mixture of chromophores, resulting in broad absorption and emission features. Excitation usually occurs to the shorter, higher energy segments, with energy migrating to lower energy, longer segments The mobile excitation energy is often referred to as an exciton. Therefore, in solution, emission will usually occur from the longer conjugated sequences.

2.4.5 Decay Kinetics

If the radiative decay process is considered in isolation, then it is seen that a concentration of excited molecules **[M*]** decays to its thermal population as a function of time due the spontaneous emission of radiation:

$$\mathbf{M^* \rightarrow M} + h\nu \tag{2.24}$$

Such a random process follows first-order kinetics so that:

$$-\frac{\mathbf{d}}{\mathbf{dt}}[\mathbf{M^*}] = \mathbf{k}_r[\mathbf{M^*}] \tag{2.25}$$

where $\mathbf{k}_r$ is the rate coefficient for the spontaneous emission process, determined by the nature and properties of the emitting state. Integration of 2.25 gives:

$$[\mathbf{M^*}] = [\mathbf{M^*}]_0 \mathbf{e}^{-\mathbf{k}_r \mathbf{t}} \tag{2.26}$$

Therefore M^* decays exponentially to zero from an initial concentration of $[M^*]_0$ at t = 0. The rate of radiative decay is characterised by its lifetime, with the natural lifetime of a radiative process defined as the reciprocal of the radiative rate coefficient:

$$\tau_r^0 = \frac{1}{k_r} \tag{2.27}$$

In a time $t = \tau_r^0$, the concentration of excited molecules will fall to 1/e of its initial value. Because k_r is a first order rate constant with units of s^{-1} the value of the lifetime will have units of s. The exponential decay of emission intensity, I(t), is given by:

$$\begin{aligned} I_{(t)} = k_r [M^*] &= k_r [M^*]_0 e^{k_r t} \\ &= I_{(0)} e^{-k_r t} \end{aligned} \tag{2.28}$$

However, it has been shown that de-excitation is the result of several processes, each of which can be defined in terms of a first order rate constant:

$^1M^* \rightarrow M + h\nu$	k_r **(fluorescence)**	**(2.29**
$^1M^* \rightarrow {}^3M$	k_{ISC} **(intersystem crossing)**	**(2.30)**
$^1M^* \rightarrow M$	k_{IC} **(internal conversion)**	**(2.31)**
$^1M^* \rightarrow$ **products**	k_D **(dissociation)**	**(2.32)**
$^1M^* + Q \rightarrow {}^1M + Q$	$k_q[Q]$ **(quenching)**	**(2.33)**

Therefore the fluorescence decay time can be expressed as:

$$\tau_f = (k_r + k_{ISC} + k_{IC} + k_D + k_q[Q])^{-1} \qquad (2.34)$$

and $I_{(t)}$ can be expressed in terms of τ_f:

$$I_{(t)} = k_r\left[M^*\right]_0 e^{-\frac{t}{\tau_f}} = I_{(0)} e^{-\frac{t}{\tau_f}} \qquad (2.35)$$

The intensity of emission from a molecule will depend upon the magnitude of the sum of the rate constants k_{ISC}, k_{IC}, and k_D (Σk), relative to k_r. The intensity of emission is expressed as the quantum yield of fluorescence Φ_f and is defined as:

$$\Phi_f = \frac{\textbf{number of photons emitted}}{\textbf{number of photons absorbed}} \qquad (2.36)$$

In terms of the above rate constants this is expressed as:

$$\Phi_f = \frac{k_r}{k_r + k_{ISC} + k_{IC} + k_D + k_q[Q]} \qquad (2.37)$$

The fluorescence decay rate, quantum yield and lifetime are related by:

$$\tau_f = \frac{\Phi_f}{k_r} \tag{2.38}$$

and:

$$\Phi_f = \frac{k_r}{k_f} \tag{2.39}$$

The fluorescence quantum yield can also be described in terms of the fluorescence lifetime τ_f and the natural radiative lifetime τ_r^0:

$$\Phi_f = \frac{\tau_f}{\tau_r^0} \tag{2.40}$$

Molecules of similar structure will have similar radiative decay rates; therefore a measure of the fluorescence lifetime will provide information on comparative quantum yields. This is very useful, as it is possible to obtain very accurate lifetime measurements, whereas the quantum yield is much more difficult to measure experimentally, especially with solid samples.

2.5 Time-resolved fluorescence techniques

A number of experimental methods have been developed to measure fluorescence lifetimes. In this work, the technique of time-correlated single photon counting has been used which allows measurement of changes of light intensity as a function of time on a sub-nanosecond time scale.

2.5.1 Principles of time-correlated single photon counting

The single photon counting experiment utilises a very fast repetition rate, low intensity, short pulse excitation source. It is set up so that at most one photon is detected for each excitation pulse, with the time of arrival of this photon relative to the excitation pulse being determined. The probability of detecting a single emitted photon after an excitation event is directly proportional to the emission intensity. Sampling the single photon emission following a large number of excitation flashes yields a probability distribution function corresponding to emission intensity versus time. A simplified block diagram for the single photon counting experiment is shown in Figure 2.4, specific experimental details are given in section **3.5.2**.

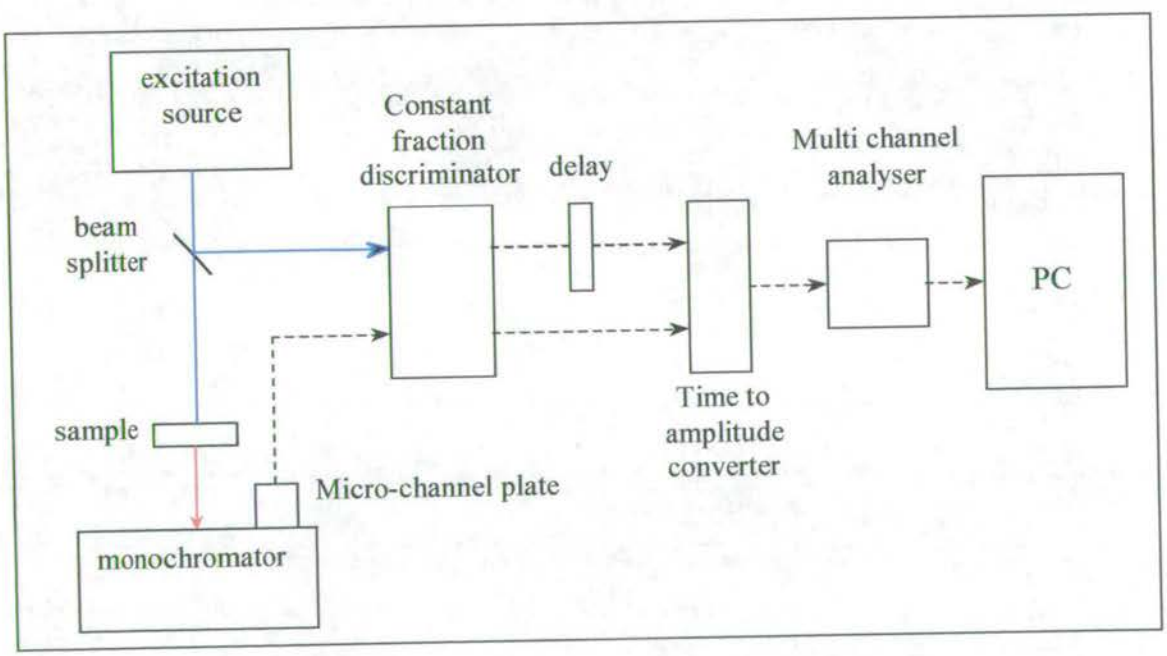

Figure 2.4 Simplified block diagram for the time-correlated single photon counting experiment

The main feature of this technique is the ability to accurately time the arrival of a photon relative to an excitation event. This is achieved with the use of a time to amplitude converter (TAC). The excitation source emits pulses of 10 ps duration at a repetition rate of 4MHz. The sample is excited and then radiatively decays emitting photons, an aperture is set so that the probability of detecting more than one photon per pulse is very small. The signal resulting from this photon hitting the microchannel plate (the START signal), is routed through a constant fraction discriminator (CFD) and initiates the charging of a capacitor in the TAC, which has a linear voltage ramp. A beam splitter diverts part of the excitation beam to a photodiode, the signal from which passes through a CFD and is delayed using variable lengths of cable. The arrival of the delayed signal from the photodiode (the STOP signal) halts charging of the TAC, which generates an output voltage. This output voltage is directly proportional to the elapsed time between START and STOP signals. The output pulse from the TAC is given a numerical value in an analogue to digital converter (ADC) and a count is stored in the appropriate channel of a multi-channel analyser (MCA), the data being stored on a PC. Repetition of this process builds up a histogram of number of counts against time of arrival, which represents the fluorescence decay curve of the sample.

2.5.1.1 The time to amplitude converter and 'pulse pile-up'

The TAC is responsible for time correlation between excitation and emission signals and operates as shown in Figure 2.5. A START signal initiates linear charging of a capacitor after a fixed delay, this charging halts upon receipt of a STOP signal ($STOP_1$) and an output pulse is released with an amplitude proportional to the time elapsed between START and STOP signals.

If no STOP signal is received, then charging of the TAC is discontinued after a set period, called the TAC range ($STOP_2$).

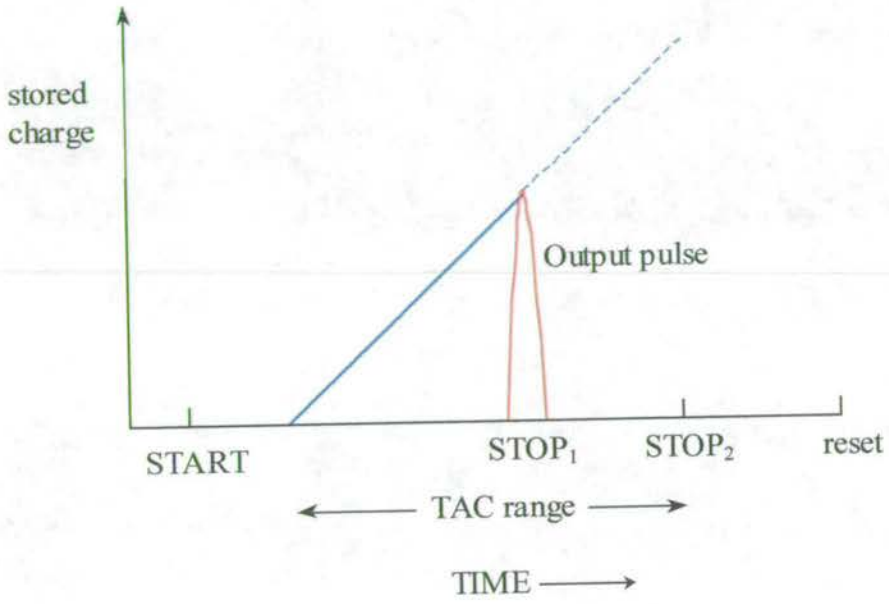

Figure 2.5 Operation of the time to amplitude converter

A fixed time then elapses called the dead time, before the capacitor is reset and another START pulse can be accepted. The phenomenon known as pulse pile-up occurs when more than one photon is detected per excitation pulse. The microchannel plate will generate a signal, but the TAC will not record it, as it will arrive during the 'dead time'. If this occurs repeatedly then a pile-up of unrecorded pulses occurs that biases detection towards early arriving photons.

To avoid pulse pile up, the intensity of emission from the sample is attenuated so that the probability of detecting more than one photon per excitation event is very small. It has been found that operating with $N_D/N_E < 0.005$ presents negligible pulse pile up effects (where N_D = number of detected photons; N_E = number of excitation pulses). In practice, with a 4MHz repetition rate, the photon counting rate was always kept below 20 000 counts per second.

Operating the TAC with the sample emission as the START signal and the excitation pulse as the STOP signal is called the reverse mode. It allows the fast repetition rate of the laser to be utilised since the TAC voltage ramp is only initiated when an excitation event results in the detection of a photon. If operated with the excitation pulse as the START signal, then a large portion of the excitation pulses will arrive during the dead time of the TAC and be wasted, along with any photons emitted during those pulses. Since to avoid pulse pile-up, only 0.05% of the excitation pulses result in emission of a photon, the detection rate of the system is greatly reduced. Operating in the reverse mode allows many more of the fluorescence signals to be processed by the TAC. Data is stored with time increasing from higher to lower channel numbers as illustrated in Figure 2.6. Before analysis the data is reversed so that time increases from lower to higher channel numbers.

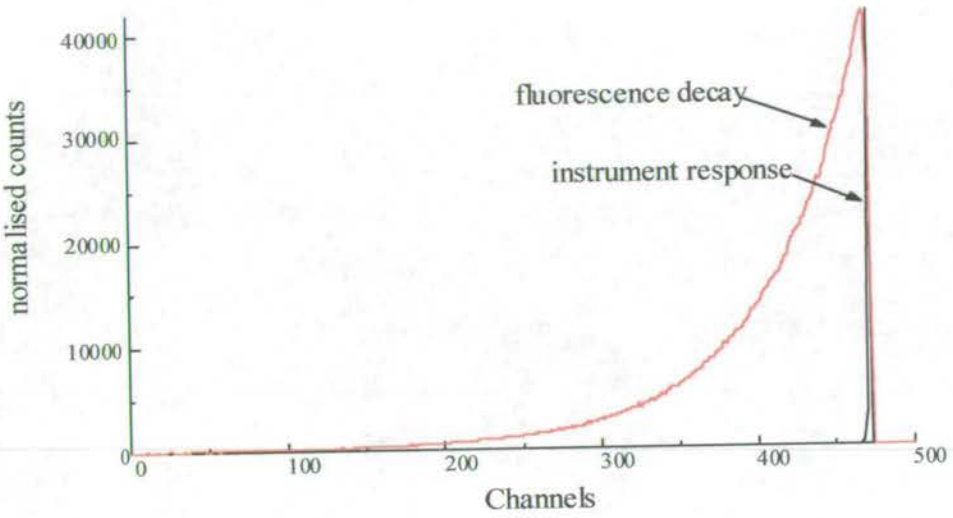

Figure 2.6 Fluorescence decay curve for a 5-cyanoindole trimer sample, illustrating the reverse mode of operation of the TAC.

2.5.1.2 The constant fraction discriminator

The signals from both the photodiode and the microchannel plate are routed through a constant fraction discriminator before entering the TAC. These signals will consist of a broad distribution of pulse heights, originating from dark noise, single and multi photon events. Routing through a discriminator will increase the signal to noise ratio and provide constant amplitude pulses for the TAC, independent of pulse shape. Due to the range of pulse heights a constant fraction discriminator was used where the pulses are timed from a point on the leading edge that is a fixed fraction of the pulse height. For pulses of similar shape but differing amplitudes this timing point is constant. Only those pulses above a set threshold are timed, this threshold being optimised to provide the most accurate fitting for the decay of a known standard.

2.5.1.3 The detector

In these experiments a microchannel plate photomultiplier tube was used for single photon detection. It is much faster than traditional photomultiplier tubes and has very good single photon resolution, with minimal wavelength dependence. The speed of the PM tube has a large effect on the instrument response time and the use of a MCP helps to cut it down. The MCP is a secondary electron multiplier that consists of millions of 10-20μm glass capillaries coated with a secondary electron emissive material, the electron amplification effect of a single channel is shown in Figure 2.7.

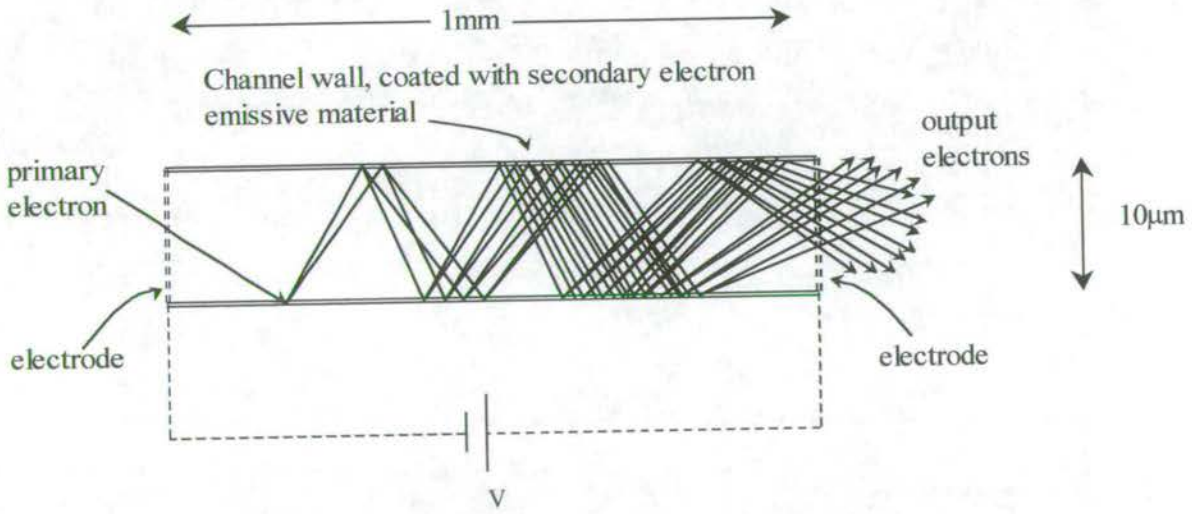

Figure 2.7 Electron amplification in a single glass capillary of a microchannel plate.

The use of a MCP along with optimisation of the CFD settings and laser pulse shape allowed an instrument response with a full width half max (FWHM) of lower than 100ps to be achieved.

Figure 2.8 shows a typical instrument response for the system, using a Ludox solution as a light scatterer, the FWHM is 70ps, with deconvolution this allows lifetimes of around 50ps to be measured accurately. A low intensity after pulse is always seen at a fixed time after the laser pulse. This is attributed to some process within the photomultiplier tube, but is of low enough intensity not to affect fitting of lifetimes.

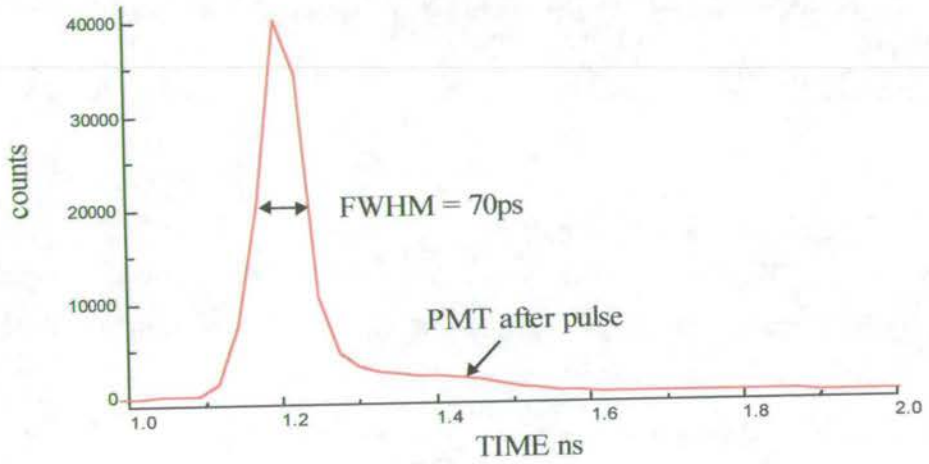

Figure 2.8 Instrument response function with FWHM = 70ps.

2.5.2 The excitation source

Excitation was provided by a picosecond pulsed laser system consisting of a mode-locked Nd-YAG laser synchronously pumping a cavity dumped tuneable dye laser (details are given in 3.5.2.1). Mode locking of the Nd-YAG laser produces a train of high power, short duration pulses, at a repetition rate of 82MHz and a typical average power of 1W. This is achieved by modulating the gain of the laser cavity using an acousto-optic cell, which effectively acts as a

shutter, opening every 2L/c seconds where L = cavity length and c = speed of light. Only light, which is travelling back and forth in phase with the modulation of the shutter, will experience amplification, resulting in a single pulse within the cavity.

To optimise the lasing efficiency of the dye laser it was synchronously pumped. This is achieved by setting the optical cavity length of the dye laser to match that of the pump laser. The frequency-converted pulses propagating within the dye laser cavity arrive at the dye jet at the same time as the pump pulses, maximising the lasing efficiency. In order to achieve effective synchronous pumping, the cavity length of the dye laser has to be kept constant to within several microns and was set by examining the output pulse shape on an autocorrelator.

The dye laser has an integral cavity dumper that stores energy within the cavity and releases a single high-energy pulse when switched on. The repetition rate of this pulse can be varied from kHz to MHz and a longer inter-pulse separation is achieved than for the mode locked output. Modulation of the cavity dumper is carried out using an acousto optic Bragg cell (Figure 2.9) that works on the same principles as the mode locker.

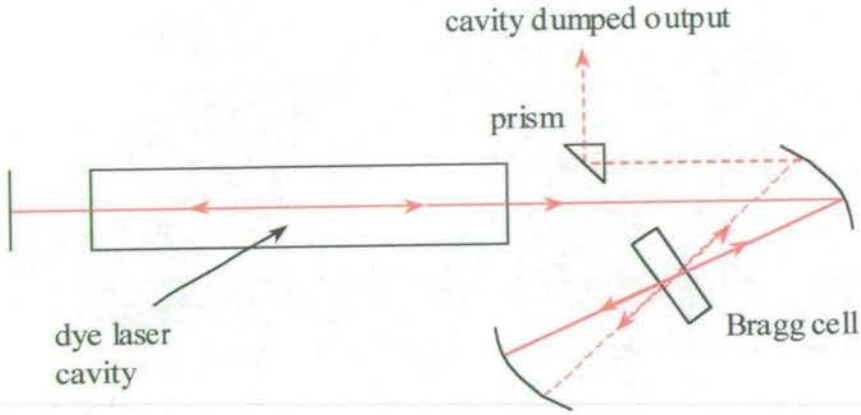

Figure 2.9 Schematic diagram of the cavity dumper.

A piezoelectric transducer generates an acoustic wave in the Bragg cell altering its refractive index and producing off axis diffraction of part of the light in the cavity. The diffracted beam is then diverted out of the cavity dumper by a prism. Pulses of 10 ps duration are produced with a variable repetition rate from 4kHz to 4MHz and a sinusoidal temporal profile.

Rhodamine 6G was used as the dye and in conjunction with a birefringent filter allowed tuning of the dye laser output from 580nm to 630nm. The output from the dye laser was frequency doubled by passing through a correctly aligned crystal of β-barium borate (BBO). This is an example of a non-linear optical process where the efficiency of second harmonic generation is non-linearly dependent upon laser intensity. The mechanism of second harmonic generation is a concerted process where the crystal absorbs two photons of light from the input beam and a

single photon is emitted with half the wavelength, with the output beam remaining coherent Using this method excitation wavelengths from 290nm to 310nm were obtained.

2.5.3 Data analysis

Once a fluorescence decay function has been obtained experimentally it must be quantified in terms of an analytical function. In doing this, distortions due to the experimental technique must be considered and the results presented within acceptable error limits.

2.5.3.1 Convolution

Because excitation of the sample does not occur on an infinitely small time scale, molecules excited at the start of the pulse are decaying while others are being excited by photons in the tail of the pulse. This leads to a phenomenon known as convolution. The experimentally observed decay function $I_{(t)}$ is composed of the true decay function $G_{(t)}$ convoluted with the measured instrument response function $P_{(t)}$:

$$\mathbf{I_{(t)} = G_{(t)} \otimes P_{(t)}} \qquad \textbf{(2.41)}$$

Where $\otimes$ represents the convolution operation and $P_{(t)}$ is in fact a convolution of the true δ-pulse of the pump $E_{(t)}$ and the δ-pulse response of the detection system $H_{(t)}$:

$$\mathbf{P_{(t)} = E_{(t)} \otimes H_{(t)}} \qquad \textbf{(2.42)}$$

To ensure that shorter lifetimes are accurately calculated, the distortion of $I_{(t)}$ by $P_{(t)}$ must be taken into account in any fitting procedures.

Inherent in the detection system is a constant low level of background noise, this must also be taken into account before running any data analysis. To calculate the background noise level, the first 20 channels of the MCA were used to store background counts from which an average noise level was calculated. This was then subtracted channel by channel from the remaining data.

$$\mathbf{I_0(t_i) = I(t_i) - B} \tag{2.43}$$

$$\mathbf{P_0(t_i) = P(t_i) - B} \tag{2.44}$$

Where B is variable and represents the mean background level. The convolution of the instrument response and true decay functions can now be expressed in terms of a convolution integral, corrected for constant background:

$$\mathbf{I_0(t) = \int_0^t P_0(t')G(t-t')dt'} \tag{2.45}$$

However, each channel of data represents not the decay at an instantaneous time t_i, but an integrated decay across the channel width Δt. The decay curve is a histogram, not a continuous distribution, therefore the number of counts in channel i is represented by:

$$C(t_i) = \int_{t_i}^{t_i+1} I_0(t)dt \qquad (2.46)$$

To solve the convolution integral, a true fluorescence response function is postulated and convoluted with the observed instrument response function to give an estimate of the observed fluorescence function. The parameters of the theoretical function are varied to achieve the best fit to the experimental data. This is carried out using a software program that runs a non-linear least squares curve fitting routine.

2.5.3.2 Least squares fitting

An optimum fit is achieved when the weighted sum of the squares of the deviations of the experimental points $I_0(t_i)$ from the theoretical function $Y(t_i)$ is at a minimum. This quantity is expressed as:

$$R(i)^2 = \sum_{i=1}^{n} W_i[I_0(t_i) - Y(t_i)]^2 \qquad (2.47)$$

Where W_i is the weighting factor for the *i*th data point and is equal to the reciprocal standard deviation in $I_0(t_i)$ and n is the total number of data points. Since the decay curve is a histogram, each channel represents an estimate of the mean of a Poisson distribution of counts in that channel. In a Poisson distribution the mean is equal to the variance, therefore W_i can be shown to be:

$$\frac{1}{\sqrt{I_0(t_i)}} \tag{2.48}$$

and the sum of squares becomes:

$$\sum_{i=1}^{n} R(i)^2 = \sum_{i=1}^{n} \left\{ \frac{[I_0(t_i) - Y(t_i)]^2}{I(t_i)} \right\} \tag{2.49}$$

2.5.3.3 *Assessing the quality of a fit*

Once a theoretical function has been fitted to the experimental data, the quality of the fit must be assessed to ensure it falls within an acceptable level of error and that the simplest explanation of results has been obtained. Four criteria were used to assess the fit quality in this work: the reduced chi squared value χ^2_v, a plot of the weighted residuals, the autocorrelation function of the weighted residuals and the Durbin-Watson parameter *DW*. The reduced chi-squared statistic χ^2_v is the ratio of the sum of squares of Poisson error to the sum of squares of weighted residuals and is calculated from:

$$\chi^2_v = \frac{1}{v} \sum_{i=1}^{n} \left\{ \frac{[I_0(t_i) - Y(t_i)]}{I_0(t_i)} \right\} \tag{2.51}$$

$$\textbf{and: } v = n\text{-}m\text{-}1 \tag{2.50}$$

where: n = number of data points, m = number of parameters

For a perfect statistical fit, this ratio equals 1, however, there are range of acceptable values. Ideally, the χ^2_v value should be no lower than 0.8 and no higher than 1.2, but values from 0.75 to 1.5 can be accepted. It is possible for a 'good' χ^2_v to be associated with a poor fit, which is why the other criteria are necessary.

Plots of weighted residuals and the autocorrelation function of weighted residuals are both visual tests and must be evaluated with care. The plot of weighted residuals $r(t_i)$ is calculated from:

$$\mathbf{r(t_i) = \frac{I_0(t_i) - Y(t_i)}{\sqrt{I(t_i)}}} \qquad \textbf{(2.52)}$$

The residuals are plotted against channel number and for a good fit they should be randomly distributed about zero with no correlation between residuals. This method will illustrate any large degree of non-randomness, however small variations are harder to see. It is more rigorous to quantify the correlation between residuals using the autocorrelation function Cr(j) expressed as the correlation between the residual in channel i and the residual in channel i + j summed over a selected number of i channels:

$$\mathbf{Cr(j) = \frac{\frac{1}{m}\sum_{i=n_1}^{n_1=m-1} r(t_i)\, r(t_{i+j})}{\frac{1}{n_3}\sum_{i=n_1}^{n_2} [r(t_i)]^2}} \qquad \textbf{(2.53)}$$

$$\mathbf{n_3 = n_2 - n_1 + 1} \qquad \textbf{(2.54)}$$

m is defined as $n_3 - j$ and varies for each sum. For a set of random residuals, a plot of Cr(j) versus correlation channel will consist of a set of points close to and random about zero.

The final criterion is the numerical value of the Durbin-Watson parameter *DW* that does not require a subjective visual interpretation. *DW* is calculated from:

$$\mathbf{DW} = \frac{\sum_{i=n_1+1}^{n_2} \left[r(t_i) - r(t_{i-1})\right]^2}{\sum_{i=n_1}^{n_2} \left[r(t_i)\right]^2} \qquad \textbf{(2.55)}$$

The *DW* statistic is similar to the autocorrelation function, but gives a single numerical value which for a perfect fit would equal 2. As for the χ^2_v value, there are acceptable values of *DW*, for single exponential fits, values below 1.75 imply a poor fit. For double and triple exponential fits the value should be greater than 1.75 and 1.8 respectively for a good fit.

2.5.3.4 Fitting multiexponential decays

From a study of the fluorescence decay kinetics, it is expected that a single emitting species will result in a single exponential decay, with the resulting fitted function yielding a single lifetime. However, when there is more than one emitting species, as for example in a polymeric material with distributions of chain lengths or chain conformations, then fitting the experimental data to a single exponential fit will be unsatisfactory. The number of parameters in the theoretical function can be increased to give a sum of two or more exponentials such as:

$$\mathbf{I_t = A_1\ exp\left(\frac{-t}{\tau_1}\right) + A_2\ exp\left(\frac{-t}{\tau_2}\right)} \qquad \textbf{(2.57)}$$

where A_1 and A_2 are constants representing the relative intensities of each component and τ_1 and τ_2 are the lifetimes of each component. Increasing the number of exponentials in a fit will always result in a better fit, however there must be some justification in doing this and when fitting, the simplest starting point must be used. If the data will not fit, within the stated criteria, to three exponentials or less then the results must be interpreted with some caution.

2.5.4 Time-resolved emission spectroscopy

To examine the emission spectra of individual components in a multi-component system, the technique of time-resolved emission spectroscopy was used. For lifetime measurements, the emission wavelength is set at a single value. By scanning the emission monochromator and operating the MCA in multi-channel scaling mode, with the dwell time in each channel synchronised with the monochromator scan, a steady state fluorescence spectrum is obtained. If the output from the TAC is routed through an upper and lower level discriminator, then a time gate can be introduced, so that an emission spectrum within a chosen time window can be recorded. This is illustrated in Figure 2.10.

If a three dimensional surface is imagined that covers the intensity at all wavelengths and times during the fluorescence decay then any point on this surface can be represented by:

$$\mathbf{I_n(\lambda_j , t_k)} \qquad \textbf{(2.58)}$$

The total fluorescence spectrum can therefore be represented by:

$$\mathbf{F(\lambda) = \int_0^\infty I_n(\lambda_1 , t)dt, \int_0^\infty I_n(\lambda_2 , t)dt, ... \int_0^\infty I_n(\lambda_j , t)dt} \qquad \textbf{(2.59)}$$

The decay function at a wavelength λ_j $G(\lambda_e,t)$ will be made up of the points:

$$\mathbf{G(\lambda_j,t) = I_n(\lambda_j , t_1), I_n(\lambda_j , t_2), ...I_n(\lambda_j , t_k)} \qquad \textbf{(2.60)}$$

and the time resolved emission spectrum $S(\lambda,t_k)$ is made up of the points:

$$\mathbf{S(\lambda,t_k) = I_n(\lambda_1,t_k), I_n(\lambda_2, t_k), ...I_n(\lambda_j, t_k)} \qquad \textbf{(2.61)}$$

By using TRES techniques we are able to spectroscopically isolate the short and long lifetime components in our multicomponent samples and obtain a visual spectroscopic representation of the lifetime data.

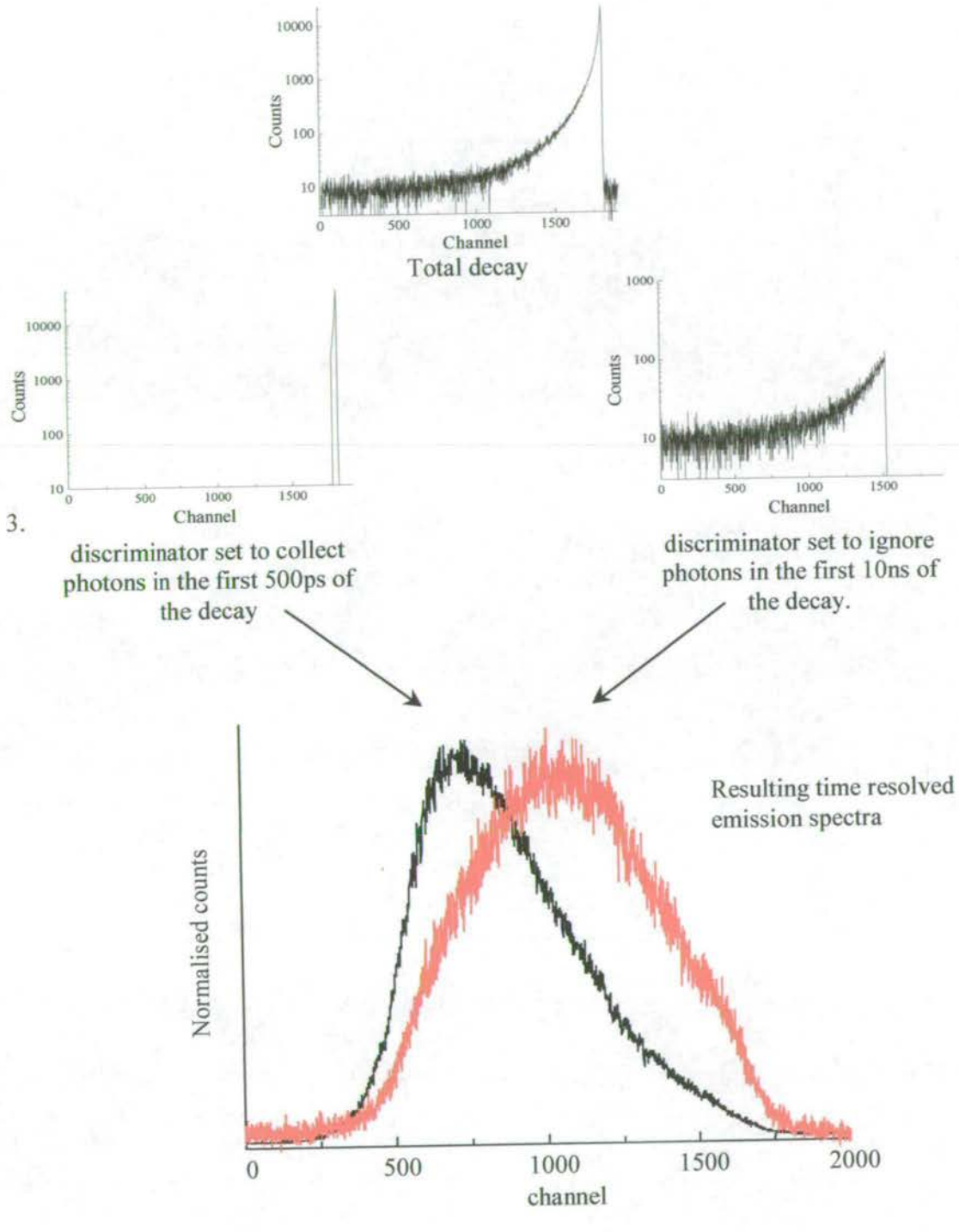

Figure 2.10 Selecting a time window for a TRES experiment, illustrated for a 5-cyanoindole film

2.6 Electrochemistry

The bulk of the samples produced for these studies were synthesised and characterised using electrochemical techniques. The following sections are a brief summary of the corresponding theory.

2.6.1 Electrochemical synthesis

Electrooxidation of the indole monomers was carried out at a platinum rotating disc electrode (Pt RDE). The RDE was used to provide a forced convection-diffusion method controlling mass transport of the electroactive species to the electrode surface. At a stationary electrode, before a potential is applied, the concentration of electroactive species [O] in the solution will be constant and uniform. When an oxidising potential is applied, there will be depletion in [O] at the electrode surface as it is oxidised to $[O^{n+}]$ and a boundary layer is formed near the electrode, with a concentration profile as illustrated in Figure 2.11. The rate of electrochemical reaction at the electrode surface is limited by how quickly material can be transported to the electrode and the current passed at this point is called the diffusion limited current. As shown in Figure 2.11 the concentration profile is a curve, whose behaviour can be mathematically modelled with diffusion across a diffusion layer of thickness δ, usually between 0.5-1mm in a stagnant solution. This is termed the Nernst diffusion layer. The limiting current density I_L can be calculated by:

$$\mathbf{I_L = - \mathit{n}\, F\, D\, \mathit{c}_\infty / \delta} \qquad \textbf{(2.62)}$$

where: n = number of electrons, F= The Faraday constant, D = diffusion coefficient ($cm^2\ s^{-1}$), c_∞ = bulk concentration (mol cm^{-3}).

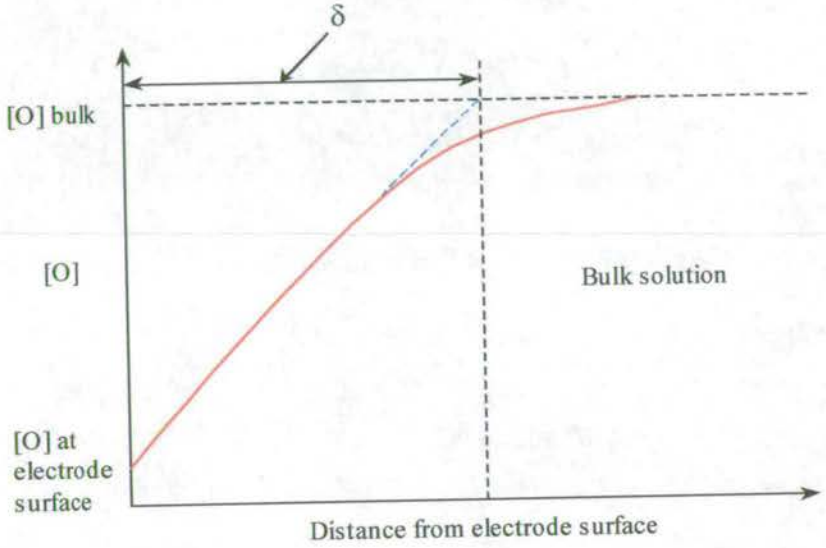

Figure 2.11 Relationship between concentration of electroactive species and distance from the electrode surface under stagnant conditions.

The RDE allows precise control of the flow of solution to the electrode surface and therefore allows variation in the rate of mass transport. If this is varied at a given potential, the current data obtained will relate to the kinetic parameters of the system. The RDE consists of a platinum disc within a cylindrical Teflon housing, with the surface of the electrode polished flush with the housing. Figure 2.12 illustrates the hydrodynamics of the RDE. Rotation of the electrode acts as a hydrodynamic pump, pulling solution up to the electrode surface then throwing it out radially across it.

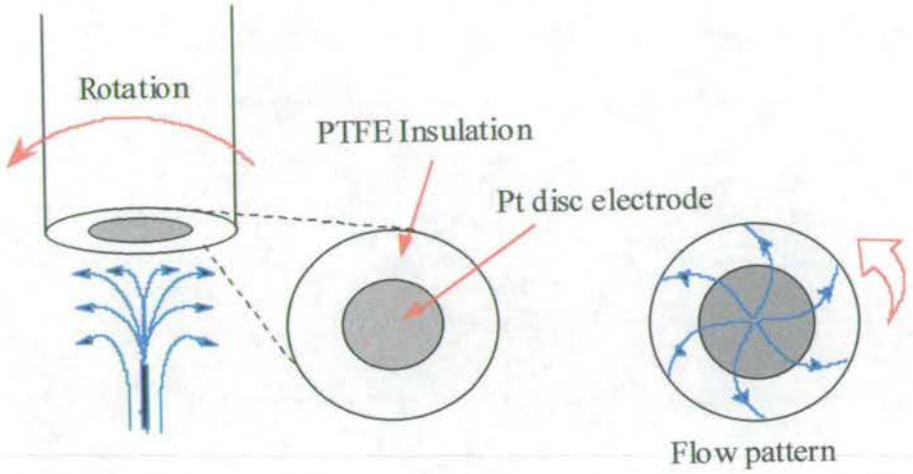

Figure 2.12 Hydrodynamics of the rotating disc electrode.

The limiting current density I_L can now be related to the rotation rate W (in Hz), which is directly controlling the rate of mass transport, using the Levich equation:

$$\mathbf{I_L = 1.554\, n\, F\, A\, D^{2/3}\, \upsilon^{-1/6}\, C_\infty W^{1/2}} \qquad \textbf{(2.63)}$$

Where: υ = Kinematic viscosity ($cm^2\ s^{-1}$), A = Area of electrode (cm^2)

If the current density is entirely mass transport controlled, then a plot of I_L against $W^{1/2}$ should be linear and pass through the origin. The gradient will provide an estimate of the number of electrons transferred in the reaction.

If there is a mass transport independent step at the electrode then the reaction mechanism can be described as:

$$C_{bulk} \xrightarrow[\text{mass transport}]{k_d} C_0 \xrightarrow[-ne^-]{k_{ox}} C \qquad (2.64)$$

where C_{bulk} is the bulk concentration, C_0 is the surface concentration, C is the product concentration, k_d is the rate constant for mass transport and k_{ox} the rate constant for electrode reaction. The kinetics of the reaction can now be described as:

$$\frac{1}{I_{obs}} = \left(\frac{1}{nFAC_\infty}\right)\left[\frac{0.643\nu^{1/6}}{D^{2/3}W^{1/2}} + \frac{1}{k_d}\right] \qquad (2.65)$$

where I_{obs} is the observed current. If the number of electrons passed n, is invariant then a plot of $1/I_{obs}$ versus $1/W^{1/2}$ will be linear and is termed a Koutecky-Levich plot. The gradient gives a measure of the mass transport and can be used to calculate the number of electrons passed if the diffusion coefficient is known. The intercept is the point at which $I = \infty$ and provides a measure of the electron transfer, at a given potential the value of k_{ox} can be calculated.

Samples were produced using the technique of potential step voltammetry along with mass transport control with the RDE. The potential at the electrode is instantaneously stepped from a potential of no reaction (E_1) to the peak oxidation potential of the reactant. In a stagnant solution

the initial current will be large, as the diffusion layer thickness increases, due to depletion of reactant, the current will fall. This is shown in Figure 2.13.

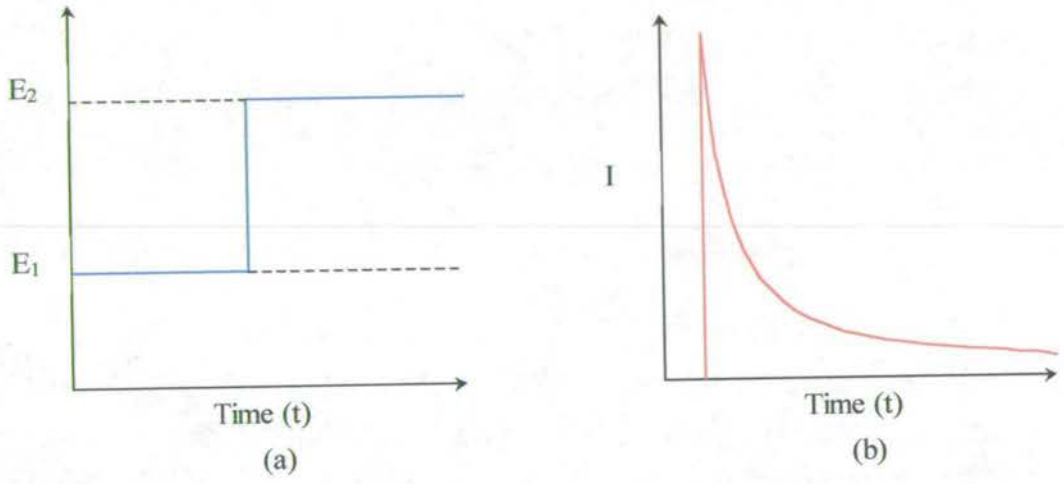

Figure 2.13 The variation of applied potential (a) and the current response (b) in a stagnant solution in a potential step experiment.

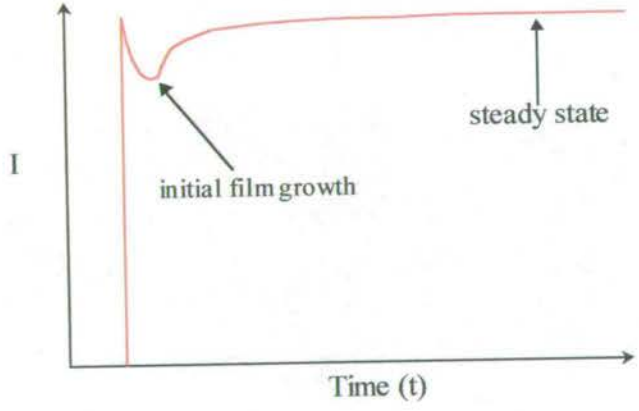

Figure 2.14 The current response for a potential step experiment with a rotating electrode.

The introduction of a rotating electrode removes the time dependency of the depletion of reactant at the electrode and after the initial growth of a layer on the electrode a steady state current can be achieved as shown in Figure 2.14. This provides a far more reproducible method for the electropolymerisation reaction.

2.6.2 Electrochemical characterisation – Voltammetry

The technique of potential sweep voltammetry was used to characterise the films formed by potential step methods. The simplest experiment is linear sweep voltammetry (LSV) carried out in a stagnant solution. The potential of the working electrode is swept linearly at a fixed rate from a value E_1 to E_2, it is then reversed and swept back at the same rate to E_1. The applied potential E is a function of the sweep rate (v_s) and the time of the sweep (t). Therefore for the forward sweep:

$$\mathbf{E(t_1) = E_1 + v_s t} \qquad \textbf{(2.66)}$$

And for the reverse sweep:

$$\mathbf{E(t_1) = E_2 - v_s t} \qquad \textbf{(2.67)}$$

A plot of E against the current produced by electroactive species in solution will give a linear sweep voltammogram. If this technique is expanded and the linear sweep repeated a number of times (Figure 2.15), then it becomes cyclic voltammetry and the changes in the current response upon successive cycles can be monitored.

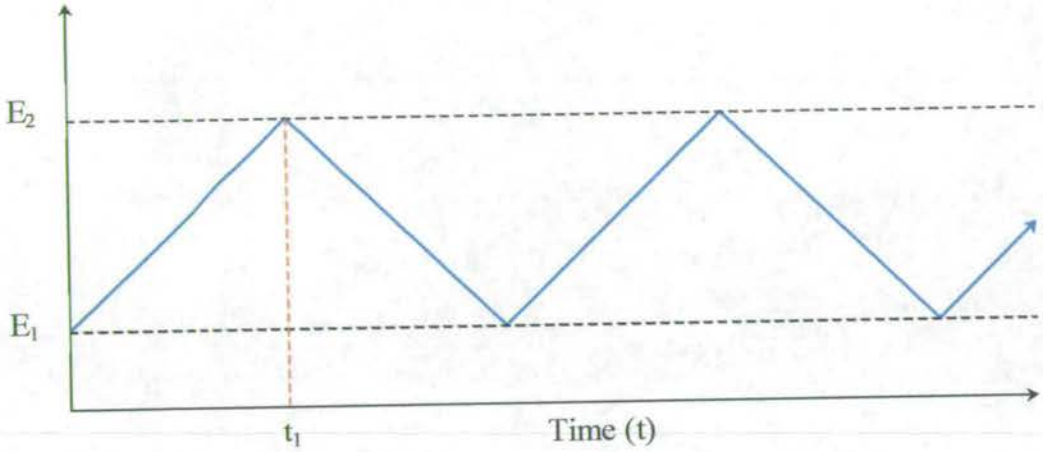

Figure 2.15 Potential time profile for a cyclic voltammetry experiment.

The sweep rate has a significant effect on the appearance of a cyclic voltammogram. In a solution where the availability of reacting species at the electrode surface is diffusion controlled, the peak current I_p is seen to vary as the square root of the sweep rate, whereas the peak potential is independent of sweep rate. For a surface-adsorbed species the kinetics are much faster and at slow sweep rates the charge passed is for the complete oxidation and reduction of the film. Therefore, if the sweep rate is doubled, the time for oxidation or reduction is halved and therefore the current passed will double. This leads to the relationship at slow sweep rates of:

$$\mathbf{I_p \propto v} \qquad \textbf{(2.68)}$$

At fast sweep rates there may be incomplete oxidation and reduction. The kinetics become diffusion limited as for a solution and:

$$\mathbf{I_p \propto v^{1/2}} \tag{2.69}$$

At intermediate sweep rates then:

$$\mathbf{v > I_p > v^{1/2}} \tag{2.70}$$

The relationship of the sweep rate to the peak current provides useful information regarding the kinetic response of a film.

2.7 Bibliography

The following texts were used in the writing of this chapter:

J. B. Birk, *The Photophysics of Aromatic Molecules, Wiley-Interscience*, 1969.

A.J. Gilbert, J. Baggott, *Essentials of Molecular Photochemistry, Blackwell Scientific*, 1991.

N. J. Turro, *Modern Molecular Photochemistry, University Science Books*, 1991.

J. N. Murrell, *The theory of the Electronic Spectra of Organic Molecules, John Wiley and Sons Inc*, 1963.

J. R. Lakowicz, *Principles of Fluorescence Spectroscopy, Plenum Press*, 1983.

J. Guillet, *Polymer Photophysics and Photochemistry, Cambridge University Press*, 1985.

P. W. Atkins, *Physical Chemistry fifth ed., Oxford University Press*, 1994.

D. V. O'Connor, D. Phillips, *Time-Correlated Single Photon Counting, Academic Press*, London 1984.

A. C. Fisher, *Electrode Dynamics, Oxford University Press*, 1996.

Chapter Three Experimental

3.1 Introduction

In this chapter the experimental methods used during the course of study are outlined. These include electrochemical and chemical preparation of samples, steady state luminescence spectroscopy at room and low temperature and time resolved fluorescence techniques. There are also details concerning the set-up of an in-situ experiment for measuring fluorescence emission intensity synchronously with electrochemical data.

3.2 Chemicals

3.2.1 Purification

Indole-5-carboxylic acid (Aldrich, 99%), 5-cyanoindole (Aldrich 99%) 5-bromoindole (Aldrich 99%) and 5-nitroindole (Aldrich 99%) were recrystalised from deionised water and dried in a vacuum oven at 70°C for two days prior to use.

3.2.2 Other chemicals

5-methoxyindole (Aldrich 99%), 5-chloroindole (Aldrich 98%), 5-aminoindole (Aldrich 97%), 5-hydroxyindole (Aldrich 97%), indole (Aldrich 99%), 2,5-diphenyloxazole (Aldrich 97%), 1-cyanonaphthalene (Aldrich 98%) and silver perchlorate (Aldrich 99%) were all used as received. Lithium perchlorate ($LiClO_4$ Acros 99%) was dried in a vacuum oven at 100°C for two days prior to use.

3.3 Solvents

Acetonitrile (MeCN, Fisons, dried doubly distilled), ethanol (EtOH Acros spectrophotometric grade), methanol (MeOH Fisons spectrophotometric grade) diethyl ether (Prolabo, AnalR grade), isopentane (Aldrich, spectrophotometric grade), acetone (Prolabo, AnalR grade), N,N-dimethylformamide (DMF, Aldrich, spectrophotometric grade), Dimethylsulfoxide (DMSO, Aldrich 99+% anhydrous), tetrahydrofuran (THF, Labscan, AnalR grade), Hexane (Aldrich, spectrophotometric grade), cyclohexane (Aldrich, spectrophotometric grade), and ethyl acetate (Prolabo, AnalR grade) were all used as received

3.4 Electrochemistry

3.4.1 Circuitry

Electrochemical synthesis and studies were carried out using a modular potentiostat/galvanostat with combined waveform generator and voltage sources (Oxford Electrodes Ltd). Data was collected on a *x-y-t* chart recorder (Bryans instruments 6000).

3.4.2 Electrodes

The working electrode was a Pt-Pt rotating disc electrode (Oxford Electrodes Ltd) disc area 0.387 cm^2 and collection efficiency, $N_0 = 0.21$, as measured by the ferrocene/ferrocinium couple. The working electrode was polished by hand using a 3 μm alpha-alumina polish (Buehler Ltd) in a water slurry, then washed in doubly deionised water. A $2cm^2$ platinum gauze was used as the counter-electrode which was cleaned by rinsing in acetone then flaming over a micro Bunsen burner. The reference electrode was made in house and

consisted of a silver wire dipping into a solution of silver perchlorate (0.01 mol dm^{-3}) in background electrolyte solution of anhydrous lithium perchlorate in acetonitrile. This electrode has a potential of +0.437V with respect to a saturated calomel reference electrode and a potential of +0.681V with respect to a normal hydrogen electrode.

3.4.3 Rotating system

The rotating disc electrode was controlled using a rotator and motor controller (Oxford Electrodes Ltd); the system has been described elsewhere[1].

3.4.4 Polymerisation procedure

Polymer films were produced at the rotating disc electrode using the technique of potential step chronoamperometry as described in section 2.6 The background electrolyte was $LiClO_4$ in MeCN (0.1 mol dm^{-3}). For trimer-rich films the monomer concentration was between 50–200 mmol in 20ml electrolyte, for polymer-rich films concentrations of 10-20 mmol were used. The rotation speed was set to between 0 and 20 Hz. The peak oxidation potentials utilised to polymerise the monomers are shown in Table 3.1.

MONOMER	POLYMERISATION POTENTIAL E_{pa}/V
Indole	+ 1.1
Indole-5-carboxylic acid	+ 1.46
5-cyanoindole	+ 1.64
5-bromoindole	+ 1.1
5-chloroindole	+ 1.3
5-methoxyindole	+ 0.83
5-nitroindole	+ 1.70
5-hydroxyindole	+ 0.93
5-aminoindole	+ 0.93

Table 3.1 Peak oxidation potentials for the 5-substituted indole monomers.

For experiments where a film of 5-nitroindole was used as the template for the polymerisation of 5-aminoindole and 5-hydroxyindole, the 5-nitroindole film was initially formed from a 50 mmol solution of monomer. Any monomer solution remaining on the electrode was removed by spinning the electrode in background electrolyte. The reference and counter electrodes were thoroughly washed in acetonitrile. The coated electrode was then placed in the new monomer solution and further polymerisation carried out at the corresponding potential.

To remove films from the electrode, they were either scraped off using a scalpel, or dissolved off in ethanol, DMF or DMSO.

3.5 Chemical polymerisation

Electropolymerisation produces samples on a very small scale, therefore samples were prepared using chemical polymerisation methods on a larger scale. This allowed a comparison of the photophysical properties of the chemically produced polymers to the electrochemically-produced polymers.

3.5.1 5-cyanoindole

5-cyanoindole was chemically polymerised using $FeCl_3$ as the oxidising agent at two different ratios of 5-CI to $FeCl_3$; 2.3:1 to favour trimer formation and 4:1 to favour polymer formation. At 2.3:1 $FeCl_3$ (0.5g) in MeCN (25ml) was slowly added to 5-CI (0.19g) in MeCN (25ml) the solution immediately darkened and a brown precipitate formed. The solution was stirred for 12 hours, then doubly deionised water was added. The resulting precipitate was filtered under gravity and repeatedly washed in water to remove any traces of $FeCl_3$ and then dried in and oven at 100^0C for 24 hours. The same procedure was used for the 4:1 reaction but with $FeCl_3$ (0.45g) in MeCN (25ml) and 5-CI (0.1g) in MeCN (25ml).

3.5.2 5-aminoindole

$FeCl_3$ was used as the oxidising agent with a ratio of 2.3:1 $FeCl_3$ to 5-AI. $FeCl_3$ (0.28gm) in MeCN (50ml) was slowly added to 5-AI (0.1g) in MeCN (50ml). The solution darkened but no precipitate was formed. The solution was stirred for 12 hours. Some of the solution was removed for immediate analysis; the rest was worked up by reducing the volume of MeCN under vacuum then adding doubly deionised water. A very small amount of precipitate formed which was filtered under gravity and washed in water.

3.5.3 5-bromoindole

Again $FeCl_3$ was used as the oxidising agent at a ratio of 2.3:1. $FeCl_3$ (0.9g) in MeCN (50ml) was slowly added to 5-BrI (0.39g) in MeCN (50ml). The solution immediately darkened and was stirred for 1 hour then doubly deionised water was added, forming a precipitate. This

was filtered under gravity and washed in water. The product was dried in an oven at 100^0C for 24hours.

3.6 Steady state fluorescence spectroscopy

3.6.1 Fluorescence spectrometer

All steady state fluorescence and phosphorescence measurements were carried out on a Jobin Yvon Spex Fluoromax spectrofluorimeter (Instruments S.A. group). The electronic and optical layouts are illustrated in Figure 3.1. Data was acquired using Instruments S.A. Datamax software. The excitation source is a 150W continuous ozone-free xenon lamp, with modified Czerny-Turner spectrometers in both the emission and excitation positions; gratings allow light dispersion from 200nm to 900nm. Gratings in both the excitation and emission positions allow two forms of experiments to be run. If the excitation wavelength is held constant and the emission spectrometer scanned, then the result is an emission spectrum. If the emission spectrometer is held at a constant wavelength and the excitation wavelength scanned, then an excitation spectrum results.

3.6.2 Room temperature experiments

All room temperature fluorescence measurements were carried out using disposable poly(methyl methacrylate) (PMMA) cuvettes (Fisons 4.5ml), which have 100% transmission above 280nm with a 1cm path length. All spectra presented with wavelengths below 280nm are corrected for the absorption of the PMMA cuvette. In June 1998 a red-sensitive photomultiplier tube was installed, all spectra run before this date are corrected for the reduced sensitivity at emission wavelengths above 550nm.

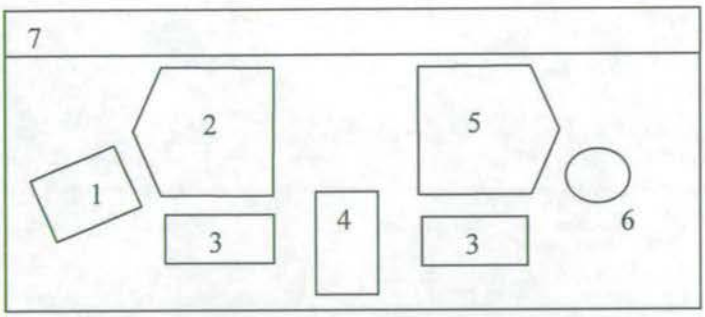

1. Illuminator
2. Excitation spectrometer
3. Sample compartment coupling optics
4. Sample compartment
5. Emission spectrometer
6. Emission detector
7. Electronic components

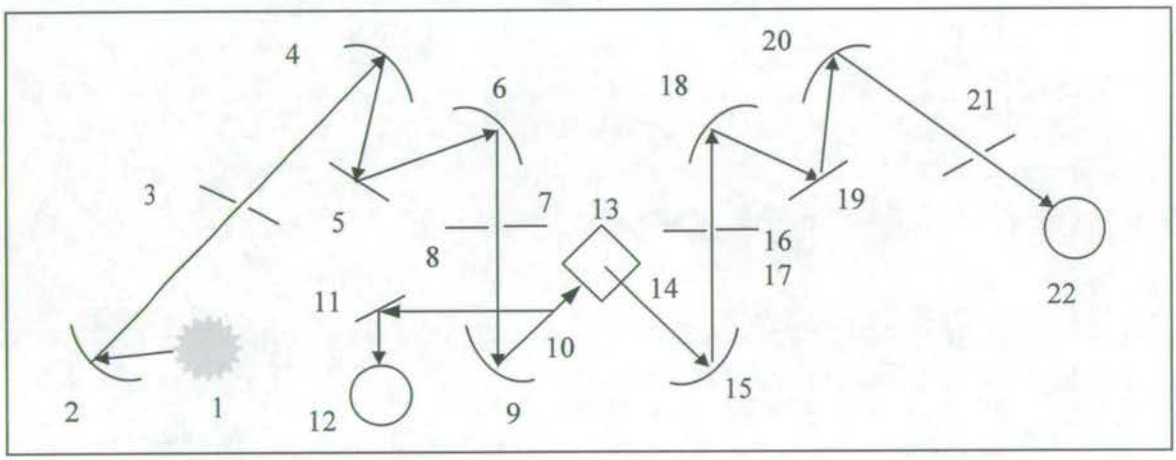

1. 150W ozone free lamp
2. Collection mirror (excitation spectrometer)
3. Entrance slit (excitation spectrometer)
4. Collection mirror (excitation spectrometer)
5. Grating
6. Focussing mirror (excitation spectrometer)
7. Excitation slit (emission spectrometer)
8. Excitation shutter
9. Collection mirror (excitation spectrometer)
10. Beam splitter
11. Deflection mirror
12. Photodiode reference collector
13. Sample position
14. Window
15. Sample collection mirror
16. Emission shutter
17. Entrance slit
18. Collection mirror
19. Grating (1200 gr./mm)
20. Focussing mirror.
21. Exit slit (emission spectrometer)
22. Emission detector

Figure 3.1 Schematic diagrams of the electronic and optical components of the fluorescence spectrometer.

3.6.3 Low temperature experiments.

All low temperature analysis was carried out using fused silica sample tubes, constructed in house. Samples were cooled to 77K with liquid nitrogen contained in a fused silica dewar (Instruments S.A.). The only suitable solvents for low temperature work were found to be Ethanol and EPA (an ether, isopentane, and ethanol mix at a ratio of 5:5:2). These were the only solvents that formed a clear glass without cracking, giving good transmission of the excitation light without excessive scattering.

3.6.4 Phosphorescence emission and lifetimes.

To differentiate between the fluorescence and phosphorescence emission at 77K, a shutter system was used to gate out the fluorescence emission as shown in Figure 3.2. This was based on the knowledge that the fluorescence lifetimes are on the nanosecond time scale whereas the phosphorescence lifetimes are on the millisecond or greater time scale. The shutters were supplied by Oriel instruments (model 76994) along with a controller (model 76995). Timing control was provided by a digital delay/ pulse generator (Stanford Research Systems model DG535). To collect phosphorescence spectra, the excitation shutter was opened for 15ms, followed by at least a 10 ms delay, gating out the fluorescence emission, before opening the emission shutter, which was left open for up to 100ms to collect the phosphorescence emission. The shutters were run at up to 40Hz repetition rate and the emission or excitation monochromators scanned to build up a phosphorescence emission or excitation spectrum, respectively. The operation of the shutters is summarised in Figure 3.3.

To determine phosphorescence lifetimes the spectrofluorimeter was run in a time acquisition mode with excitation and emission wavelengths remaining constant. The excitation shutter was opened for 15 ms, followed by a 10 ms delay to gate out the fluorescence emission, and then the emission shutter was opened for the duration of the phosphorescence decay. Resulting decay curves were fitted to a single exponential function to obtain the phosphorescence lifetime.

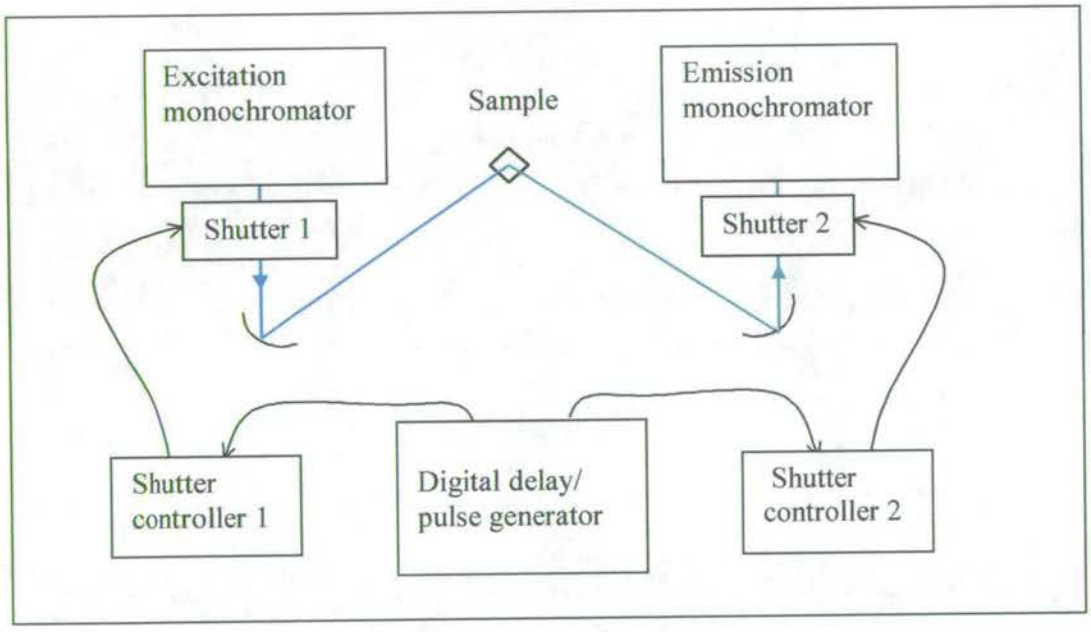

Figure 3.2 Set-up of fluorescence spectrometer to measure phosphorescence spectra and lifetimes.

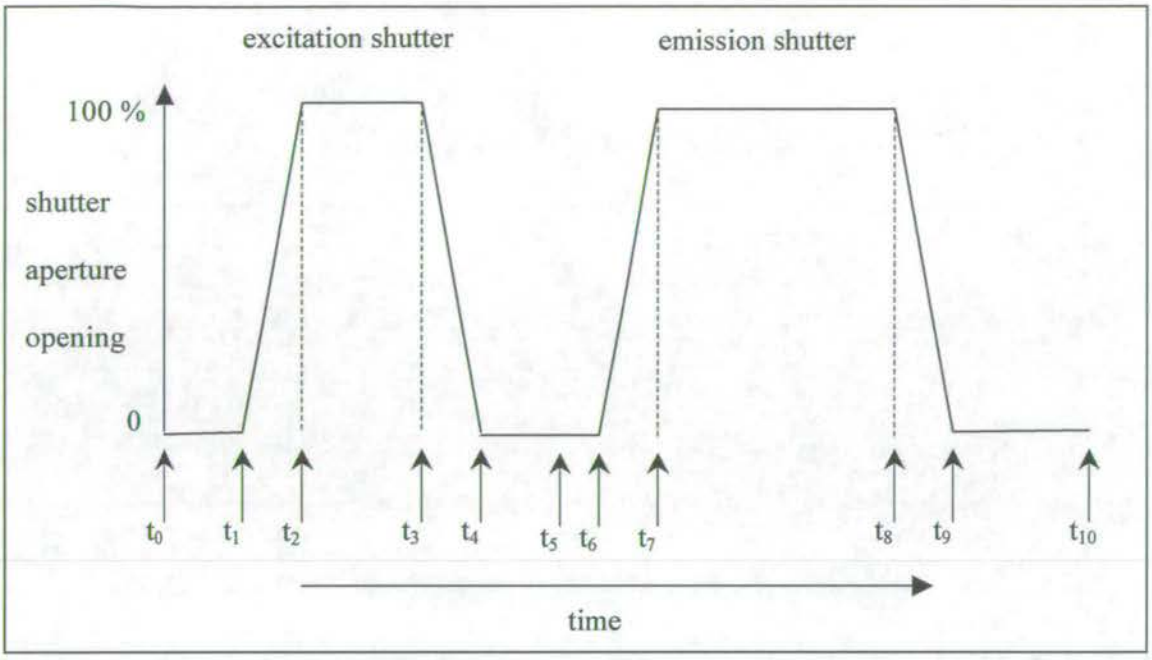

t_0	open signal from delay generator to excitation shutter
$t_1 = t_0 + 3$ ms	shutter starts to open
$t_2 = t_1 + 3$ ms	shutter fully open
$t_3 = t_2 + 9$ ms	close signal from delay generator to excitation shutter
$t_4 = t_3 + 4.2$ ms	shutter fully closed
$t_5 = t_4 + 15.8$ ms	open signal from delay generator to emission shutter
$t_6 = t_5 + 3$ ms	shutter starts to open
$t_7 = t_6 + 3$ ms	shutter fully open
$t_8 = t_7 + 94$ ms	close signal from delay generator to emission shutter
$t_9 = t_8 + 4.2$ ms	shutter fully closed
$t_{10} = t_9 + 60$ms	cycle starts again

Figure 3.3 A typical shutter sequence set-up to detect phosphorescence emission with a 15ms ($t_3 - t_0$) excitation pulse, 20ms ($t_5 - t_3$) delay and 100ms ($t_8 - t_5$) emission detection.

3.6.5 Solid state film experiments.

Fluorescence measurements on the electropolymerised films were carried out using a removable platinum-working electrode as shown in Figure 3.4. The film coated electrode tip was placed in a sample holder made in house and positioned at an angle, θ, less than 45^0 to the incident excitation light to minimise the scattered light entering the emission monochromator as shown in Figure 3.5. A Schott long pass filter was placed over the emission slits to further minimise any scattered light.

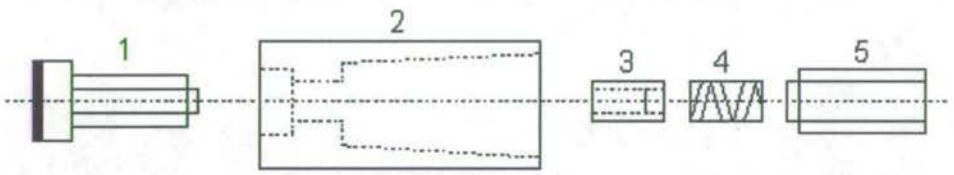

1. Platinum electrode and screw thread
2. Teflon body
3. holding screw
4. spring
5. screw thread

Figure 3.4 Exploded view of the removable rotating disc electrode.

3.6.6 Quantum yield measurements

An approximation of the quantum yield of chemically polymerised Indole-5-carboxylic acid was made using indole monomer as a standard. NMR analysis showed the Indole-5-carboxylic acid sample to contain approximately 80% trimer. It was assumed that the extinction coefficients of the trimer and monomer were similar, with the absorption of each being measured using a matched pair of 1cm quartz cuvettes with a uv/vis spectrometer (ATI Unicam Ltd, model UV2-200). Fluorescence emission intensities were measured using

excitation wavelengths of 280nm for the monomer and 320nm for the trimer to minimise emissions from impurities.

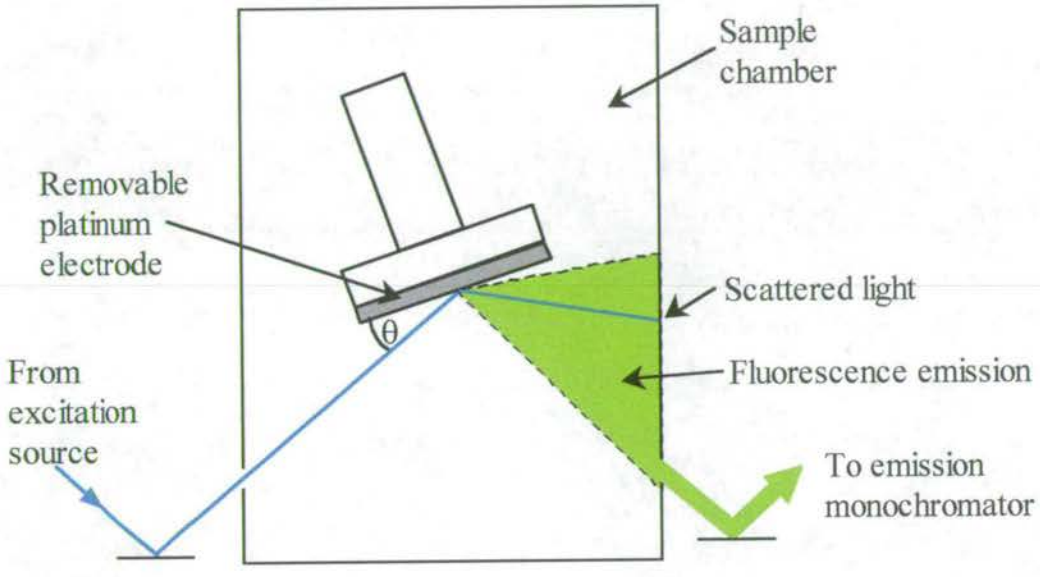

Figure 3.5 Positioning of electrode tip in fluorescence spectrometer sample chamber, maximising signal and minimising scattered light.

3.7 Measurements of Fluorescence lifetimes

3.7.1 Nanosecond laser set-up.

Initial fluorescence lifetime measurements were carried out using a nanosecond Nd-YAG laser (Continuum, Surelite II) as the excitation source. The experimental set-up is shown in Figure 3.6. The third harmonic output of the laser was used to excite at 355nm, with emission from the sample collected by a photomultiplier tube (Hamamatsu R928) via a PC controlled monochromator (SPEX 270M). The signal from the photomultiplier tube was

processed through a fast gated integrator and boxcar averager (Stanford Research Systems), triggered by the laser pulse. Data was collected on a PC. The sample was placed in a fused silica cuvette for room temperature analysis and in a fused silica tube and liquid nitrogen dewar for low temperature analysis, as detailed for the steady state measurements. This set-up was also used to collect initial steady state emission data for the solid films. Films on the electrode and drop coated onto glass slides were placed in the excitation beam. The monochromator was scanned across a wavelength range and the boxcar used to integrate the emission over time, giving an emission spectrum of the sample.

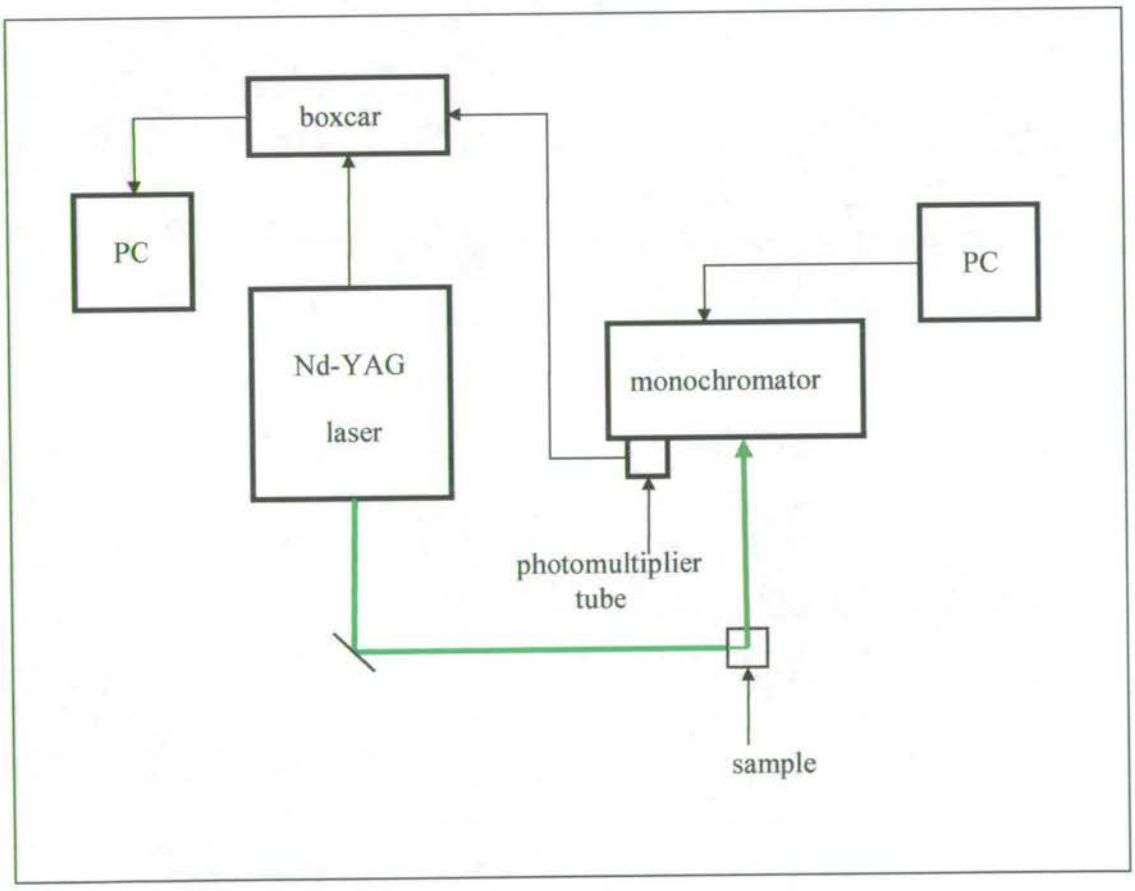

Figure 3.6 Set-up for lifetime measurements, using a nanosecond Nd-YAG laser.

3.7.2 Picosecond time correlated single photon counting.

The main set of fluorescence lifetime measurements was made using the technique of picosecond time-correlated single photon counting. A block diagram of the experimental set-up is shown in Figure 3.7. The experiment consists of three main components, a picosecond pulsed laser system, the sample, the time-correlated single photon counting system and data acquisition software installed on a PC. These are discussed below.

3.7.2.1 The laser system

The second harmonic output (532nm) of a mode locked Nd-YAG laser (Spectra Physics model SL 903) giving a train of pulses at 41.13 MHz was used to synchronously pump a dye laser (Spectra Physics model 3500) with integral cavity dumper (Spectra Physics model 3290). The frequency doubled YAG output was passed through a stabilisation unit (LiCONiX model 505A) to provide pulses of constant power to the dye laser. The cavity length of the dye laser was matched to that of the pump laser so that a jet of rhodamine 6G was synchronously pumped to maximise the pulsed lasing efficiency. The cavity dumper was controlled by an external cavity dumper driver (Spectra Physics model 454 and power supply model 451), giving an output of pulses with 10 ps duration and of variable repetition rate between 0.4kHz and 4MHz. A birefringent filter allowed tuning of the rhodamine 6G emission between 570nm and 650nm. This output was frequency double using a crystal of β-barium borate (BBO) to give an excitation wavelength between 285nm and 325nm. The quality of the output pulse was checked using an autocorrelator (Spectra Physics model 409) and average power output was measured using a power meter (Newport research corporation model 409).

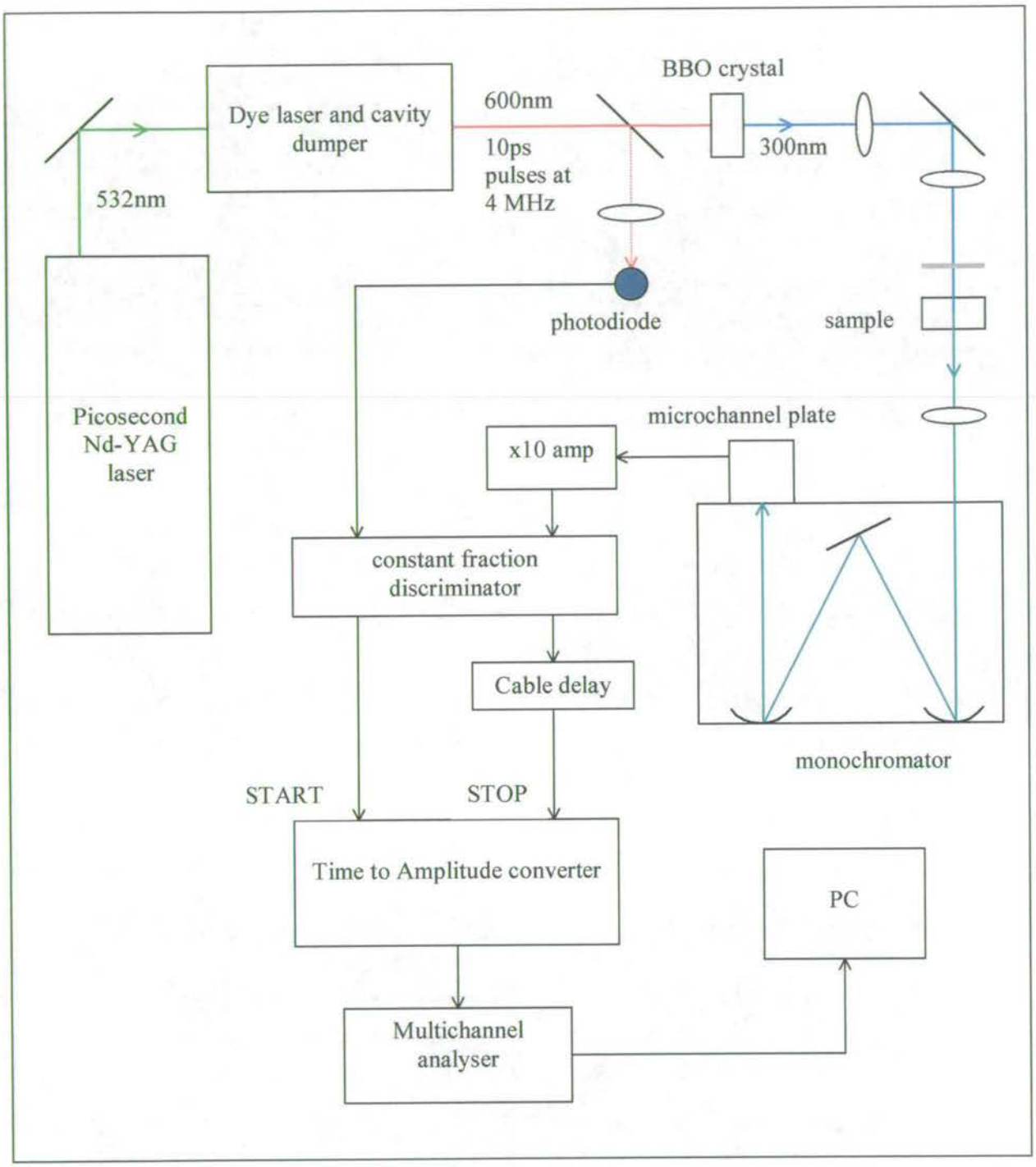

Figure 3.7 Picosecond time-resolved single photon counting experimental set-up.

3.7.2.2 The sample

For all solution phase experiments a 3.5ml, 1cm path length fused silica cuvette was used (Starna 3/Q/10). Prior to use, cuvettes were cleaned with detergent in a sonic bath for 12 hours, rinsed with doubly deionised water then dried in an oven. A UG9 filter was placed in front of the sample to cut out any fundamental light from the dye laser.

For measurements on polymer films, the removable working electrode was used, mounted at 45^0 to the excitation beam. Drop coated films were examined on a fused silica window (Spectroscopy Central) mounted in the same way. Band pass filters were placed in front of the monochromator to cut out any fundamental and second harmonic scattered light.

The samples were housed in a light-tight black anodised aluminium box, with slits for excitation and emission.

3.7.2.3 Time-correlated single photon counting

Emission from the sample was collected with a 10cm focal length lens and passed through a monochromator (SPEX 270M). The slits of the monochromator were set so that no more than one photon was detected for each excitation pulse. The emission signal was detected with a microchannel plate (Hamamatsu) and the resulting signal amplified (Ortec fast preamplifier model 9306), then routed through a constant fraction discriminator (Tenelec Quad CFD model TC 454) to the START input of a time to amplitude converter (TAC, Ortec/EG & G model 457), initiating charging of a capacitor. A beam splitter diverted part of the excitation pulse to a photodiode, the resulting signal was passed down a cable delay through a CFD to the STOP input of the TAC, halting the charging ramp. The TAC then

releases a signal proportional to the charge in the capacitor, and therefore to the time difference between START and STOP pulses. This pulse is passed through an analogue to digital converter that assigns it a numerical value and then a Multichannel analyser (Ortec ADCAM MCA model 918A) stores it as a count in a corresponding channel. As this process is repeated a histogram builds up of number of counts against time after excitation, giving the decay profile of the sample. Counts were collected until there were at least 20 000 counts in the peak channel. The data was written to and stored on a PC using LIFETIME software (developed in-house at the central laser facility).

The instrument response function was measured by collecting scattered excitation light using a solution of Ludox (Aldrich) in water as a light scatterer for solution phase experiments and a bare platinum electrode for solid samples. The monochromator was set at the excitation wavelength with slits at their minimum setting to prevent damage to the MCP.

The constant fraction discriminator levels were set to optimise the instrument response function and provide the best fit for a known standard. 2,5-diphenyloxazole (PPO) in cyclohexane and 1-cyanonaphthalene in hexane were used as standards, having lifetimes of 1.28ns (degassed) and 18.23ns (degassed) respectively.

A picture of the dye laser and cavity dumper unit along with the excitation optics in the single photon counting laboratory is shown in Figure 3.8. Shown in Figure 3.9 is a close up of the sample chamber, containing a degassing cell filled with a solution 5-cyanoindole trimer.

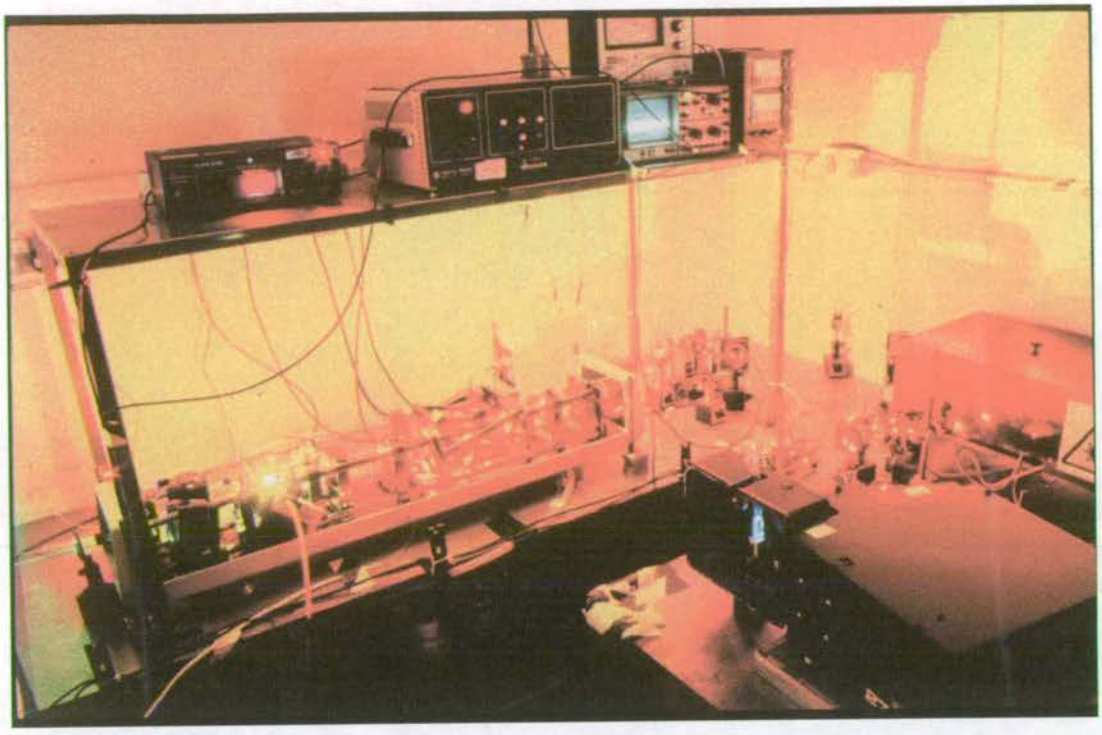

Figure 3.8 Dye laser, cavity dumper and optical setup in SPC laboratory.

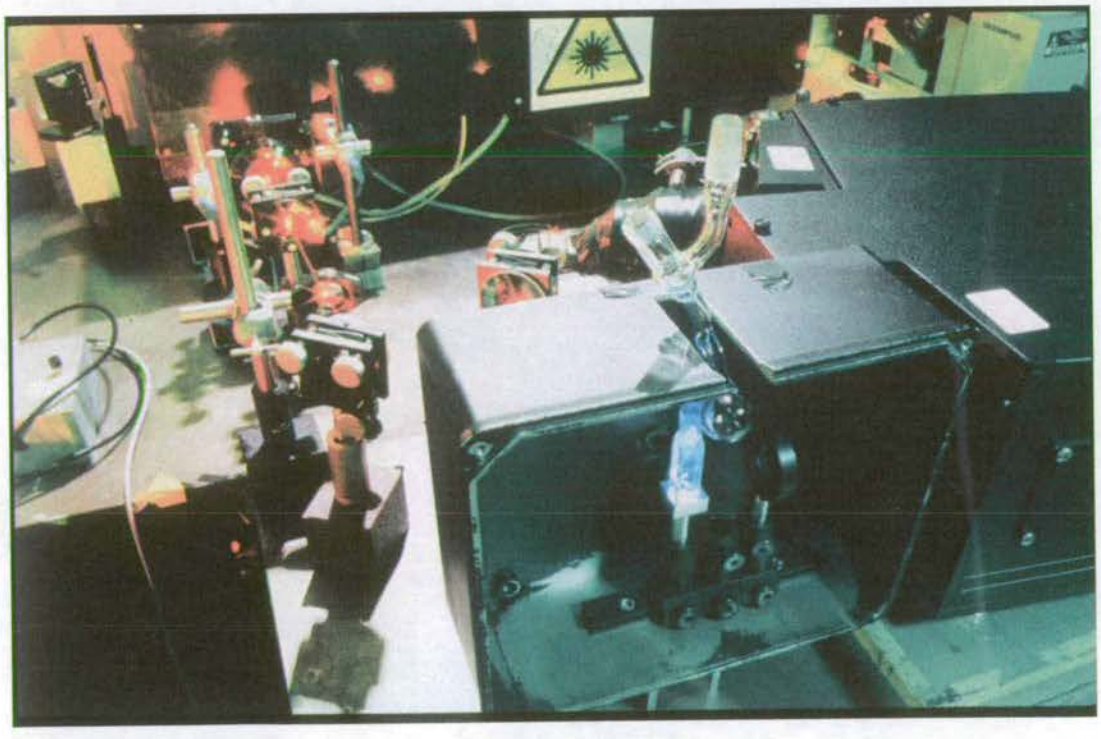

Figure 3.9 Close up of sample chamber in SPC laboratory.

3.7.3 Degassing technique.

To examine samples in an oxygen-free environment, they were degassed using a freeze, pump, thaw technique. Sample holders were made in house, consisting of a fused silica cuvette with an attached glass bulb reservoir and connector for a vacuum line. The sample solution was placed in the reservoir and frozen using liquid nitrogen. The sample container was then evacuated down to a pressure of 10^{-5}torr. The sample was then thawed, allowing dissolved gas to escape, and the process repeated at least four times to ensure complete degassing.

3.8 Time-resolved emission spectroscopy.

To measure time-resolved emission spectra the MCA and associated PC card were replaced with a new PC card (Oxford Instruments Inc, PCA3) with an internal analogue to digital converter and capable of running in a multichannel scaling mode as well as a multichannel analyser. To collect fluorescence decays the output from the TAC was fed to the card and it was run in pulse height analysis mode to give data as previously obtained. In this mode upper and lower level discriminators, operated from the rear panel of the card, were adjusted to select a time window in the decay. The system was then configured to run as a multichannel scaler by connecting the Single channel analyser output to the multichannel scaler input. The monochromator was set to scan across a wavelength range at a speed compatible with the dwell time of the MCS in each channel. As the monochromator is scanned a time-gated emission spectrum, corresponding to the time window set in the decay is obtained.

3.9 In-situ cyclic voltammetry/ fluorescence experiments

For steady state measurements of the emission response of a polymer film as a function of its oxidative state, an in-situ experiment was set up that allowed the emission intensity from the film to be measured as it was cycled in an electrochemical cell, between reduced and oxidised states. The in-situ cell consisted of a fused silica cuvette (2cm x 4cm x 4cm), with the removable tip of the working electrode housed in a PTFE block made in house. The electrode surface was placed almost flush with the front face of the cuvette and aligned at 45^0 to the excitation light with long and low pass filters in the emission output to cut out scattered light. The experimental set-up is shown in Figure 3.10. The excitation and detection set-up was the same as in the lifetime experiments (section 3.5.2, Figure 3.7) and electrochemical control was as for section 3.3. The digital signal from the constant fraction discriminator was converted to an analogue output by routing it through a dual gate generator (Ortec model) and then producing an averaged signal with a value from 1-10V using a boxcar (Stanford research systems model SR250).

The voltage and current outputs from the potentiostat and emission output from the boxcar were sent to the inputs of a data acquisition card (Intelligent Instruments) with data processing carried out by Visual Designer software (Intelligent Instruments). A virtual chart recorder was designed displaying current against voltage and emission against voltage.

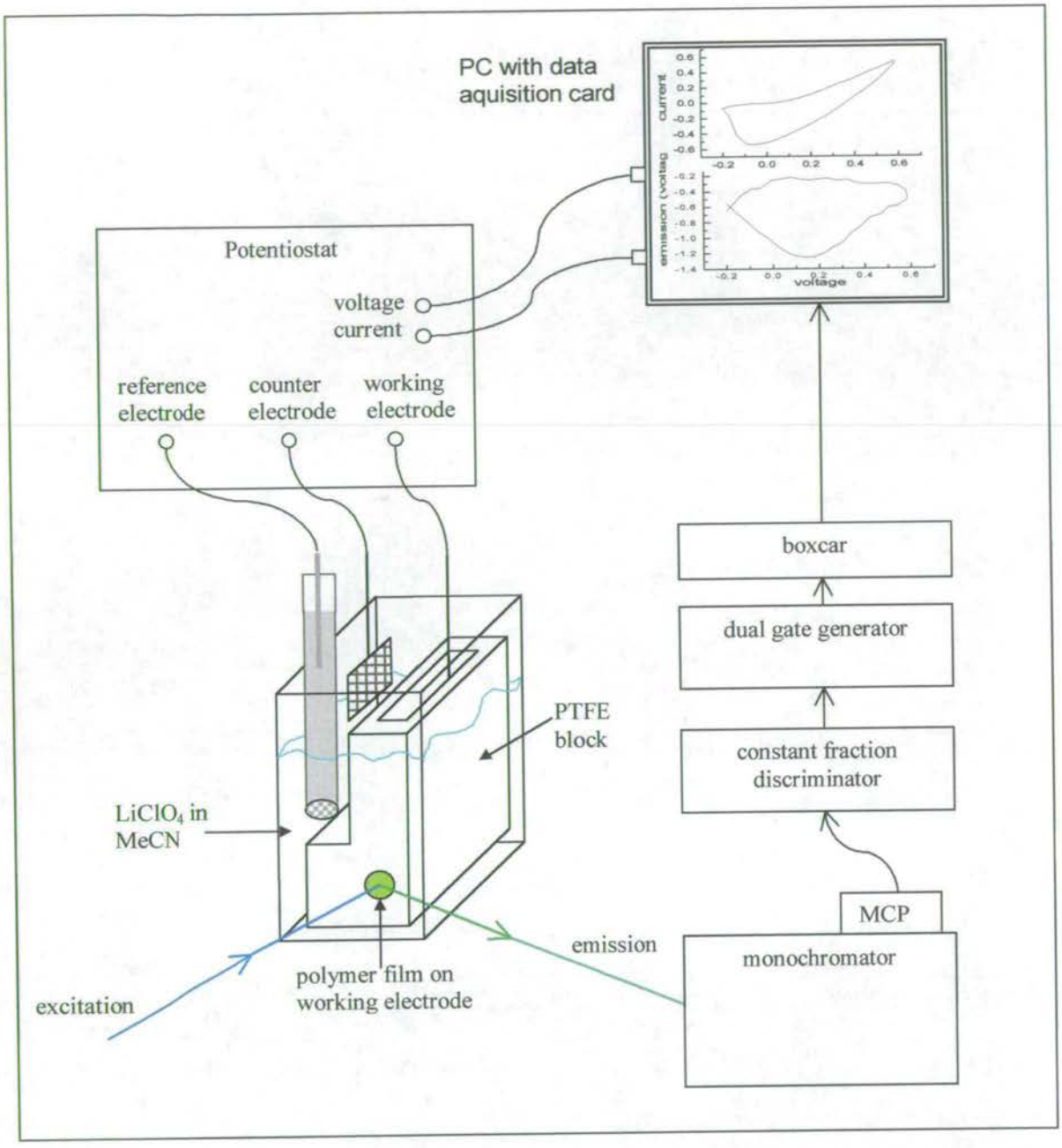

Figure 3.10 experimental set-up for in-situ current/fluorescence response measurements.

3.10 Thin Layer chromatography

In an attempt to separate the trimer and polymer species produced during electropolymerisation, the technique of thin layer chromatography was employed. Thin layer chromatography was carried out on non-fluorescent silica plates (Merck Polygram-Sil G) with a mixture of 1:1 ethyl acetate:diethyl ether was used as the mobile phase. Solutions of trimer and polymer in DMF, DMSO and EtOH were deposited on the silica plates using a glass dropper. Once dry the plates were examined under an UV lamp.

3.11 References

1. A. R. Mount, *PhD Thesis, Imperial College London*, 1987.

Chapter Four – Steady-state, room temperature fluorescence studies

4.1 Introduction

Indole and its 5-substituted derivatives have been the subject of extensive electrochemical investigation, with Mount and co workers [1-10] having made considerable progress in characterising the polymerisation mechanism. It has been found that some of the 5-substituted indoles produce high quality electroactive films, polymerising via an asymmetric trimer species that links to form a polymer consisting of linked trimer units. The structure of the trimer is shown in Figure 4.1. As previously discussed in chapter one, the polymerisation process is:

$$3n\,\mathbf{In} \rightarrow n(\mathbf{In})^{+}_{3\,(s)} + 7n\mathbf{e}^{-} + 6n\mathbf{H}^{+} \qquad (4.1)$$

$$n(\mathbf{In})^{+}_{3\,(s)} \rightarrow -\left[(\mathbf{In})^{+}_{3}\right]_{n} + 2n\mathbf{e}^{-} + 2n\mathbf{H}^{+} \qquad (4.2)$$

Equation (4.1) shows the oxidation of monomer to form trimer and equation (4.2) the subsequent linking of trimers to form polymer, where In is the 5-substituted indole monomer.

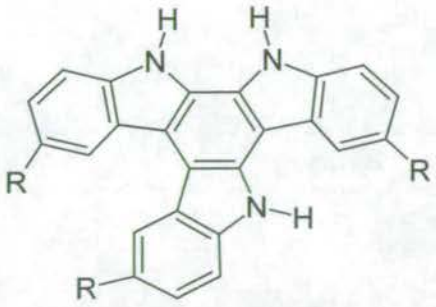

Figure 4.1 Structure of the electrochemically oxidised, 5-substituted indole trimer.

The initial trimer formation occurs in the diffusion layer near the electrode, which results in the deposition of a film of an asymmetric cyclic trimer onto the electrode surface. This film then acts as a surface on which further adsorption and oxidation of monomer can occur, followed by radical cation linkage to form more cyclic trimer, which is the mechanism by which the film grows.

The electropolymerised 5-substituted indoles have been found to be highly photoluminescent and this thesis is concerned with a photophysical characterisation of the electrochemically generated indole trimer and polymer species, comparing their properties to those of the monomer species. Steady state and time-resolved techniques have been employed for this study, with samples examined in solution phase and solid state, at room temperature and at low temperature.

This chapter details the results of the steady-state room temperature studies of the monomer, trimer and polymer species in solution, exploring substituent and solvent effects and examining how polymerisation conditions affect the luminescence properties.

4.2 Fluorescence properties of the monomer species

The first part of this chapter concerns the steady state fluorescence properties of the indole monomers in solution at room temperature, in order to provide a background for the study of the trimer and polymer species. The indoles examined are indole, 5-cyanoindole, indole-5-carboxylic acid, 5-bromoindole, 5-chloroindole, 5-methoxyindole, 5-hydroxyindole, 5-aminoindole and 5-nitroindole, with a systematic study of solvent effect carried out on 5-cyanoindole and indole-5-carboxylic acid. As previously discussed in chapter one (section 1.1) the fluorescence properties of indole and its derivatives are highly sensitive to their environmental conditions. In polar media, an unusually large Stokes shift is observed, arising from a bathochromic shift in the emission wavelength with increasing solvent polarity, whereas the absorption band is much less affected. The sensitivity of the emission to solvent polarity is linked to the near degeneracy of two low-lying excited states ^1L_a and ^1L_b.

4.2.1 Substituent effects

The excitation and emission spectra of all the indole monomers were collected using isopentane as a solvent. A selection of the excitation and emission spectra are shown in Figure 4.2 and the data are summarised in Table 4.1. Isopentane was chosen as it is the least polar and non-protic solvent in which all the indoles will dissolve, therefore minimising any solvent effects so that the effect of substituent variation could be examined. The solutions were made up at concentrations of 10^{-6} molar or less; so as to minimise any self-absorption, inner filter or aggregation effects [11].

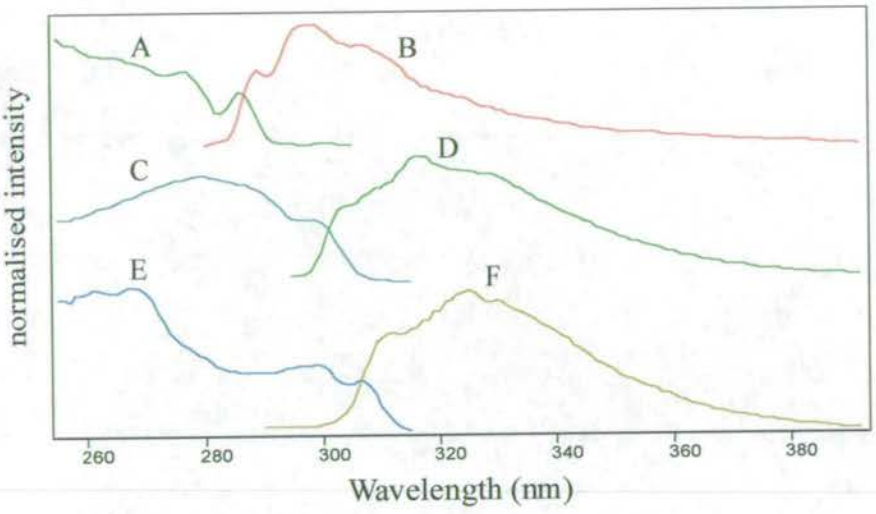

Figure 4.2 An illustration of the substituent effect on a range of indole monomers in isopentane. Excitation spectra for indole (A), 5-cyanoindole (C) and 5-hydroxyindole (E); emission spectra for indole (B), 5-cyanoindole (D) and 5-hydroxyindole (F).

Since the effect of solvent on the excited state is minimal, it is expected that the observed emission will be from the ^1L_b state, since there will be no solvent stabilisation of the ^1L_a state as described in section 1.1.1. There is a small degree of vibrational structure on some of the emission spectra, allowing the ^1L_b 0-0 emission transition to be located. Some of the excitation spectra also have a degree of vibrational structure allowing the ^1L_b 0-0 excitation transition to be located, as well as the onset of the ^1L_a state. From these transitions two Stokes shift values have been calculated, one for the 0-0 transitions of the ^1L_b state, the other for the separation of excitation and emission maxima.

monomer	Excitation maximum/nm	Emission maximum/nm	Stokes shift (^1L_bex-^1L_bem) $\Delta\bar{\nu}$/cm^{-1}	Stokes shift (λ_{max}ex-λ_{max} em) $\Delta\bar{\nu}$/cm^{-1}
Indole	278 / 286	289 / 298	400	2400
N-methylindole	279 / 286 / 292	298 / 308	700	3400
5-cyanoindole	280 / 299	304 / 317	600	4200
5-chloroindole	271 / 297	300 / 311	300	4700
5-hydroxyindole	269 / 299 / 306	312 / 325	600	6400
Indole-5-carboxylic acid	284	311 / 329		4800
5-methoxyindole	270 / 288	326		6400
5-aminoindole	270 / 315	326 / 339	1100	7500

Table 4.1 Excitation and emission data for indole and a selection of 5-substituted derivatives in isopentane. Values in red are the onset of the ^1L_a state, values underlined in blue are the 0-0 transitions of the ^1L_b state. Two Stokes shift values are given. ^1L_bex-^1L_bem is the difference between the values for the 0-0 transition of the ^1L_b state. λ_{max}ex-λ_{max}em is the difference between the maximum peaks in excitation and emission.

4.2.1.1 5-nitroindole

The first observation to note is the very weak fluorescence emission measured for 5-nitroindole compared to all the other indole monomers studied. This can be attributed to the influence of the nitro group and the presence of a low energy n-π^* state. Aromatic compounds with a nitro group present are known to show n-π^* transitions, from a non-bonding n orbital to an antibonding π^* orbital [12]. The presence of an n-π^* state enhances spin

orbit coupling as explained in chapter two (section 2.4.2), resulting in very efficient intersystem crossing to the triplet state. This provides an efficient non-radiative decay pathway; therefore the very low intensity of fluorescence emission from 5-nitroindole is to be expected. The nature of this n-π^* state is dealt with in greater detail in the discussion on low temperature fluorescence, where the effect of enhanced intersystem crossing is observed in phosphorescence measurements.

4.2.1.2 Correlation of emission characteristics with the Hammett substituent constant.

Changing the substituent predominantly affects the energy of the ^1L_b state, with relatively little effect on the ^1L_a state as shown in Figure 4.2 and Table 4.1. Notably all the substituted indoles have a greater Stokes shift between the excitation maximum (^1L_a) and emission maximum (^1L_b) than unsubstituted indole. Previous work by Aaron et al [13] has examined the substituent effect on several indoles including indole, 5-bromoindole and 5-cyanoindole. Their findings were very similar to those presented here, with bathochromic shifts in the emission wavelength being noted for the substituted indoles. This shift to longer wavelength implies that there is a lowering in energy of the S_1 ^1L_b state due to the presence of the substituent group. It was suggested that the magnitude of the substituent effect is related to the electron withdrawing or donating capacity of the functional group, quantified by the Hammett substituent constant σ^+. A list of the Hammett constant values is given in Table 4.2 [14], with increasing value of σ^+ corresponding to an increase in the electron withdrawing power of the group. To see if there is any correlation between the Hammett constant and the emission properties, a plot of emission wavenumber against the value of σ^+ is shown in Figure 4.3.

Substituent	NH_2	OH	OMe	H	Cl	COOH	CN
Hammet constant	-0.66	-0.37	-0.27	0	0.23	0.45	0.66

Table 4.2 Values of the Hammett substituent constant taken from reference 14.

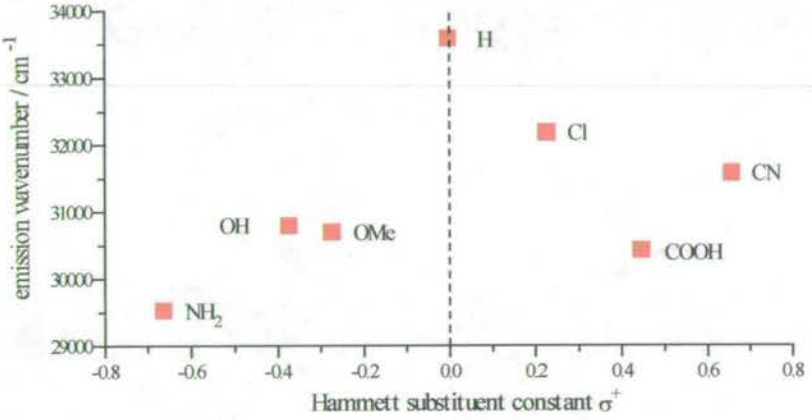

Figure 4.3 Plot of emission wavenumber against the Hammett Substituent constant for indole and a selection of 5-substituted derivatives.

From the plots in Figure 4.3 it can be seen that there is some correlation between the value of σ^+ and the emission properties, although the data for 5-cyanoindole is somewhat anomalous. In general there is an increasing bathochromic shift and increased Stokes shift as the value of σ^+ becomes more positive (more electron withdrawing) and more negative (more electron donating). The greatest effect is observed for the more negative value of σ^+, implying that the S_1 (^1L_b) excited state is stabilised more by the electron donating groups than the electron withdrawing groups. This is consistent with the findings of Aaron et al[13].

4.2.1.3 Substituent effect in Ethanol

To provide a comparison with low temperature studies and work on the trimer species, the effect of substituent on the monomer emission in ethanol solution is presented here, excitation, emission and Stokes shift values are shown in Table 4.3.

Monomer	Excitation Maximum / nm	Emission Maximum / nm	Stokes Shift, $\Delta\bar{\nu}$/ cm^{-1}
Indole-5-carboxylic acid	282	397	10300
5-cyanoindole	283	364	7800
5-bromoindole	275	338	6800
5-chloroindole	275	328	5900
5-methoxyindole	300	329	2900

Table 4.3 Excitation and emission data for 5-substituted indole monomers in ethanol solution at room temperature. The Stokes shift, $\Delta\bar{\nu}$, is calculated as the wavenumber difference between the excitation and emission maxima.

Due to the high polarity of ethanol, it is expected that emission will be from the solvent stabilised ^1L_a state, consistent with the observation of a much larger Stokes shift than seen in isopentane. Notably, the Stokes shift for 5-methoxyindole is considerably lower than the other substituted indoles and is lower than that observed in isopentane. This is consistent with observations by Lami et al [15] who suggest that for 5-methoxyindole ^1L_a, ^1L_b level inversion does not occur in polar solvents. Thus for 5-methoxyindole in ethanol, the excitation maximum which corresponds to excitation of the ^1L_a state, is bathochromically shifted compared to that in isopentane, while the emission maximum (^1L_b state) is unaffected. This results in a smaller Stokes shift between excitation and emission maxima in

ethanol than in isopentane. Apart from the exceptional case of 5-methoxyindole, in polar solvents the emission properties of the 5-substituted indoles are dominated by the solvent effect, discussed below.

4.2.2 Solvent effects

The effects of solvent polarity on the emission properties of 5-cyanoindole and indole-5-carboxylic acid were studied. Indole-5-carboxylic acid exhibits more complex behaviour and will be discussed separately. 5-cyanoindole exhibits the solvent effects typical of an indole monomer. To quantify the variation in solvent properties the function *f(D,n)* was used:

$$f(D,n) = 2\left[\frac{D-1}{D-2} - \frac{n^2-1}{n^2+2}\right] \qquad \textbf{(4.3)}$$

where D represents the static dielectric constant of the solvent and n the solvent refractive index. The function $f(D,n)$ has been used in previous models [16] to test the hypothesis attributing the anomalous Stokes shift of indoles to solvent dipole relaxation following excitation. Since $f(D,n)$ depends strongly on the dielectric properties of the solvent, it is a useful parameter when investigating the effect of solvent on the energy of the excited states. The properties of the solvents used are shown in Table 4.4. The range of solvents was limited by the solubility of the monomers, which is very low in low polarity solvents.

Solvent	Dielectric constant, D	refractive index, n	$f(D,n)$
isopentane	1.843	1.356	0.003
DMSO	4.7	1.477	0.539
ether	4.33	1.352	0.619
THF	7.6	1.405	0.885
DMF	36.7	1.431	1.328
EtOH	24.3	1.361	1.329
MeOH	31.2	1.329	1.412
MeCN	38.8	1.344	1.429
H_2O	81	1.333	1.516

Table 4.4 Solvent properties

4.2.2.1 Effect of solvent on the emission properties of 5-cyanoindole

5-cyanoindole exhibits considerable bathochromic shifts in emission wavelength as the polarity of the solvent is increased, as illustrated in Figure 4.4. The wavenumbers of the excitation and emission maxima, along with the Stokes shift are presented in Table 4.5. The Stokes shift was calculated as the difference in wavenumber between the excitation peak and emission peak. The shortest emission wavelength and narrowest emission spectrum is observed in isopentane. This is consistent with the emission in this non-polar solvent originating from the ^1L_b state. There is a bathochromic shift of the emission and an increase in the Stokes shift as the value of $f(D,n)$ increases due to a stabilisation of the excited state by solvent–solute relaxation. The position of the excitation peak is less affected by solvent polarity, since solvent relaxation occurs after excitation.

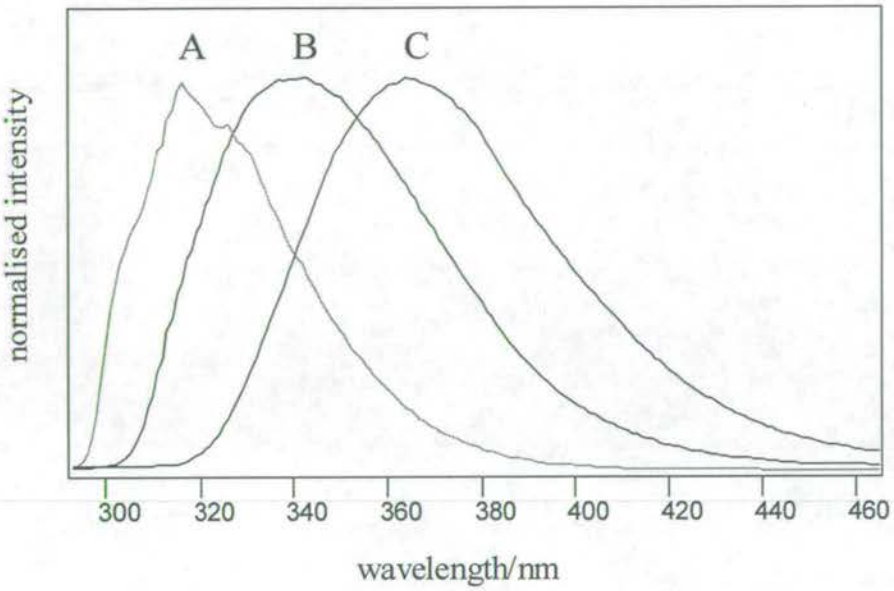

Figure 4.4 Effect of solvents on the emission spectra at room temperature of 5-cyanoindole. Emission spectra of 5-cyanoindole in isopentane (A), ether (B), and DMF (C).

In similar work, the Stokes-shifted emission has been attributed to both exciplex formation[16, 17] and inversion of the two low lying excited states ^1L_a and ^1L_b[18]. In non-polar media, emission occurs from the ^1L_b state, which has been shown to have a lower dipole moment than the ^1L_a state [19, 20], and therefore is less affected by the presence of a polar solvent. Due to the near degeneracy of these two states, the presence of a polar solvent can lower the energy of the ^1L_a state below that of the ^1L_b state and the ^1L_a becomes the emitting state, resulting in the observed broadening and bathocromic shift of the emission spectrum. There is a particularly large Stokes shift observed in EtOH, MeOH and H_2O and this is likely to be associated with the strong hydrogen bonding ability of these solvents. This effect is much greater for indole-5-carboxylic acid, as discussed below.

Solvent	f(D,n)	Excitation Maximum/cm^{-1}	Emission Maximum/cm^{-1}	$\Delta\bar{\nu}/cm^{-1}$
isopentane	0.003	35700	31500	4200
DMSO	0.539	31200	27000	4200
ether	0.619	34400	29300	5100
THF	0.885	34000	28600	5400
DMF	1.328	33300	27400	5900
EtOH	1.329	35300	27500	7800
MeOH	1.412	36600	27200	9400
MeCN	1.429	32600	27700	4900
H_2O	1.516	33000	25600	7400

Table 4.5 Excitation and emission data for 5-cyanoindole in a variety of solvents

4.2.2.2 Effect of solvent on the emission properties of Indole-5-carboxylic acid

The excitation, emission and Stokes shift values for indole-5-carboxylic acid are shown in Table 4.6. The emission properties of indole-5-carboxylic acid are more complex than those of 5-cyanoindole, as the carboxy functional group is subject to specific effects. Indole-5-carboxylic acid interacts strongly with protic solvents due hydrogen bonding, causing a further lowering in energy of the excited state and a greater shift of the emission to longer wavelength. It is also likely that indole-5-carboxylic acid will dimerise due to hydrogen bonding interactions between carboxylic acid groups, causing a broadening and bathochromic shift of the emission.

Solvent	f(D,n)	Excitation Maximum/cm^{-1}	Emission Maximum/cm^{-1}	$\Delta\bar{\nu}/cm^{-1}$
isopentane	0.003	36000	29800	6200
DMSO	0.539	34700	26300	8400
ether	0.619	36400	28600	7800
THF	0.885	36000	28000	7900
DMF	1.328	35500	27300	8100
EtOH	1.329	35700	26600	10500
MeOH	1.412	35200	24400	10800
MeCN	1.429	36900	26500	10400
H_2O	1.516	35700	25900	9800

Table 4.6 Excitation and emission data for indole-5-carboxylic acid in a variety of solvents

4.3 Electrochemical preparation and characterisation of polymers

All of the indoles examined above have been studied electrochemically[1-11] and all can form an electroactive film, except 5-aminoindole and 5-hydroxyindole which have soluble electropolymerisation products; these will be dealt with separately, as will indole which has different fluorescence properties.

Electropolymerisation of the monomer is carried out at its peak oxidation potential, determined using linear sweep voltammetry techniques, Table 4.7 shows the peak oxidation potential for the monomers studied. The electronic nature of the substituent in the 5-position has an effect on the peak oxidation potential, as the electron withdrawing nature of the substituent increases, oxidation becomes more difficult and a greater potential is required.

The Hammett substituent σ^+ is used to quantify the relative electron donating (or withdrawing) power of the functional group, the greater its value the greater the electron withdrawing power of the group. Figure 4.5 shows a plot of the peak oxidation potential versus the Hammett constant. The linear nature of the plot suggests that steric effects are not important in the initial formation of the radical cation. The monomers shown within the box all form electroactive films

MONOMER	POLYMERISATION POTENTIAL E_{pa}/V
Indole	+ 1.1
Indole-5-carboxylic acid	+ 1.46
5-cyanoindole	+ 1.64
5-bromoindole	+ 1.1
5-chloroindole	+ 1.3
5-methoxyindole	+ 0.83
5-nitroindole	+ 1.70
5-hydroxyindole	+ 0.93
5-aminoindole	+ 0.93

Table 4.7 Peak oxidation potentials for the indole monomers.

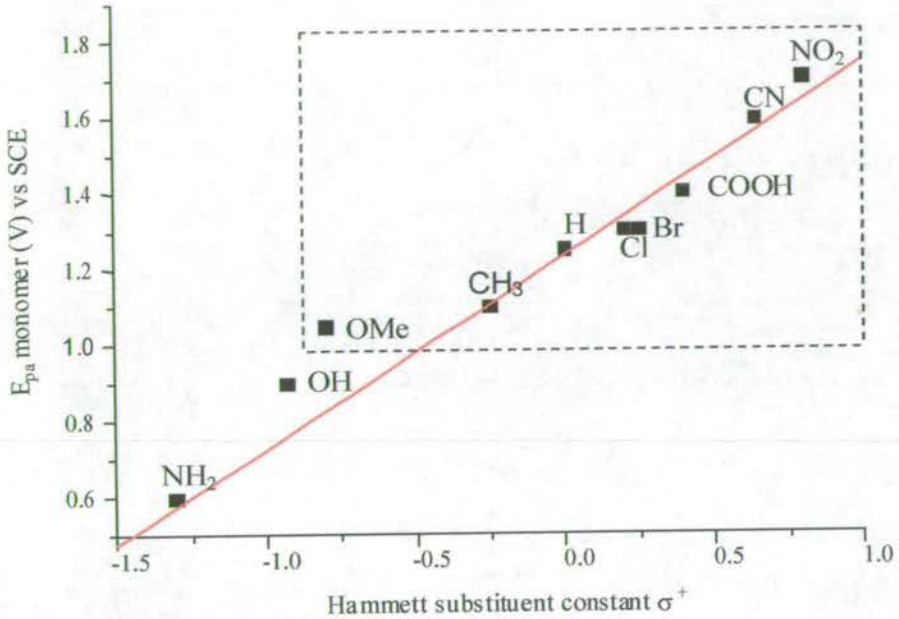

Figure 4.5 Plot of peak oxidation potential of a series of 5-substituted indoles versus their respective Hammett constant.

4.3.1 Polymerisation conditions

The composition and properties of the film can be altered by controlling the rotation speed of the electrode, duration of polymerisation and concentration of monomer solution. Previous chronamperometric studies at a rotating disc electrode [5, 6] for indole-5-carboxylic acid and 5-cyanoindole showed that initial formation of an asymmetric trimer (equation (4.1)) in the diffusion layer is followed by deposition of a monolayer onto the electrode surface. This layer acts as a site for further electrooxidation and adsorption of the monomer radical cation, which gives further cyclic trimer formation on the electrode surface. During the initial surface layer growth phase, the current changes with time. Once the layer is formed a steady

state current is observed, with the kinetics of deposition being first order in monomer, since oxidation and adsorption of monomer controls the linking process. The deposited cyclic trimer can act as a site for further trimerisation, or the trimers can link to form polymers of linked trimers according to equation (4.2).

Polymerisation (equations (4.1) and (4.2) combined) will dominate when the concentration of monomer at the surface falls, whereas trimerisation (equation (4.1) dominates when there is efficient supply of monomer to the surface for trimer formation. It has been found[1,3] that the former occurs when the bulk concentration of monomer is low (< 20mmol) and/or the rotation speed is slow (0-2 Hz), whereas the latter occurs at high concentrations (>50mmol) and high rotation speeds (> 5Hz). Therefore, at high rotation speed and high monomer concentration a film rich in trimer species is formed. At low monomer concentration and slow rotation speeds a film rich in polymer is formed. The polymerisation of each film is characterised by a current/time transient which allows the nature of the film to be assessed and the reproducibility of film production to be checked.

A typical current/time transient for the polymerisation of a 5-cyanoindole film is shown in Figure 4.6, where polymerisation takes place at a rotating electrode. The initial spike is the formation of the initial surface layer, after which the current approaches a steady state value, where the film surface is acting as a template for further film growth. When the electrode is held stationary, the steady state current is not achieved and the current steadily drops as the supply of monomer at the surface of the electrode is used up, as illustrated in Figure 4.7.

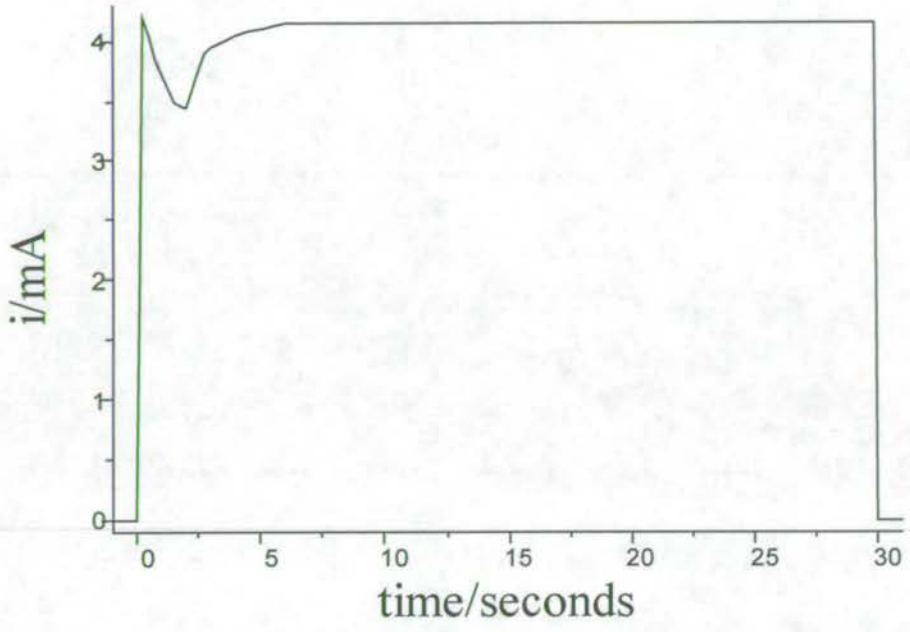

Figure 4.6 Typical current/time transient for the oxidation of 50mmol 5-cyanoindole at 1 Hz for 30 seconds with a disc potential of 1.64V.

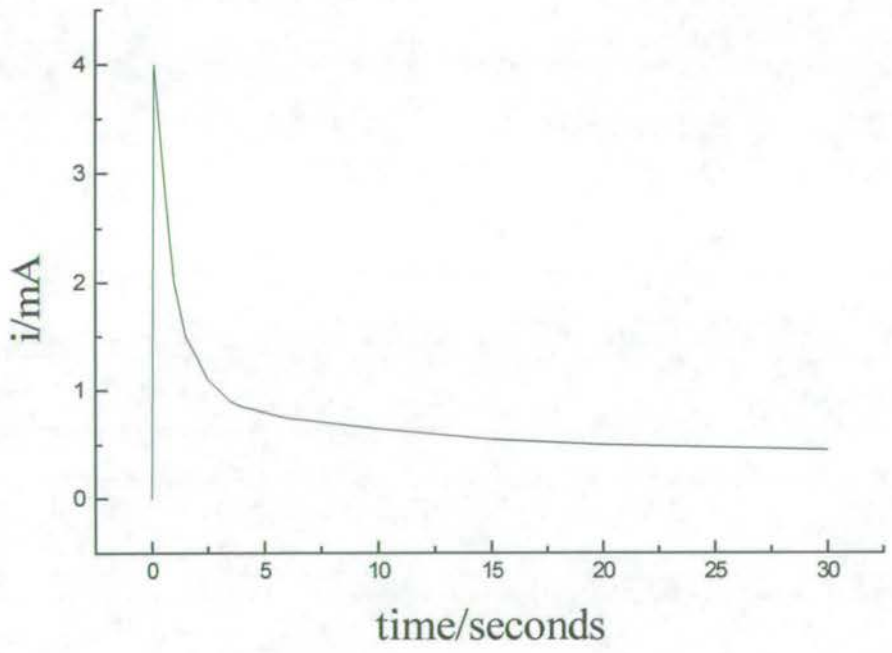

Figure 4.7 Typical current/time transient for the oxidation of 10 mmol indole-5-carboxylic acid at a stationary electrode with a disc potential of 1.46V.

When studying the unlinked trimer chromophore, typical film preparation conditions involved monomer concentrations higher than 50 millimolar, rotation speeds faster than 5 Hz and polymerisation times shorter than 10 seconds. In order to study the emission properties of the polymer species, electrochemical conditions were chosen to produce polymer-rich films. Typical conditions involved monomer solutions of 20 millimolar and less, a stationary working electrode and polymerisation times between one and five minutes.

4.3.2 Cyclic voltammetry

Cyclic voltammetry was used to verify that the electropolymerised films were consistent with previous work and also to further polymerise films which had been formed rich in trimer. Although all but two of the indoles studied formed electroactive films, the quality of these films varied greatly, along with the quality of electrochemical data obtained. 5-cyanoindole and indole-5-carboxylic acid produced the highest quality films and therefore have had the most extensive characterisation. Although similar in character, they posses distinct electrochemical differences. 5-cyanoindole is more difficult to oxidise than indole-5-carboxylic acid because electrochemical oxidation results in the production of an oxidised trimer species and the more electron withdrawing cyano group destabilises it, making the oxidation reaction energetically less favourable.

Let us first consider 5-cyanoindole. If a film is formed to favour trimer (in this case a 20 mmol solution, polymerised at 1.64V, with a rotation speed of 15 Hz for 20 seconds) then two different cyclic voltammetry experiments can be carried out. The film can be cycled from –100mv to +800mv and a reversible oxidation/reduction system is observed that can be

cycled many times with little change in the peak positions and heights as shown in the cyclic voltammogram (CV) in Figure 4.8.

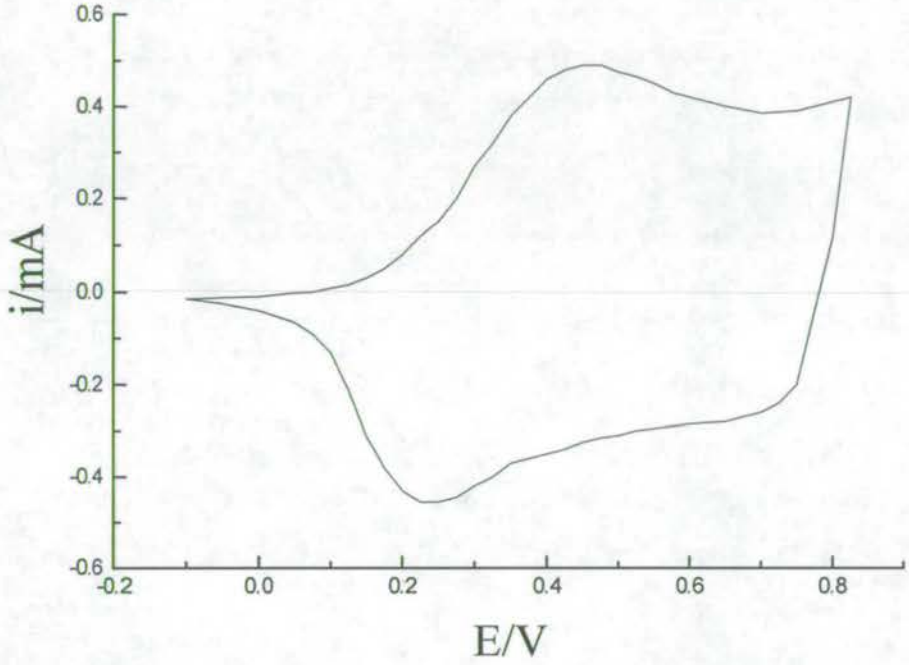

Figure 4.8 Typical CV for a film of 5-cyanoindole in background electrolyte, at a sweep rate of 20mV/s and sweeping from –0.1V to 0.8V (film polymerised from a 20mmol monomer solution at 15 Hz and an electrode potential of 1.64V).

If, however, the film is cycled up to 1200mV, then a second set of peaks appears, which drop significantly upon further cycles as shown in Figure 4.9 This is due to oxidative linking of trimer units in the film, to form polymer.

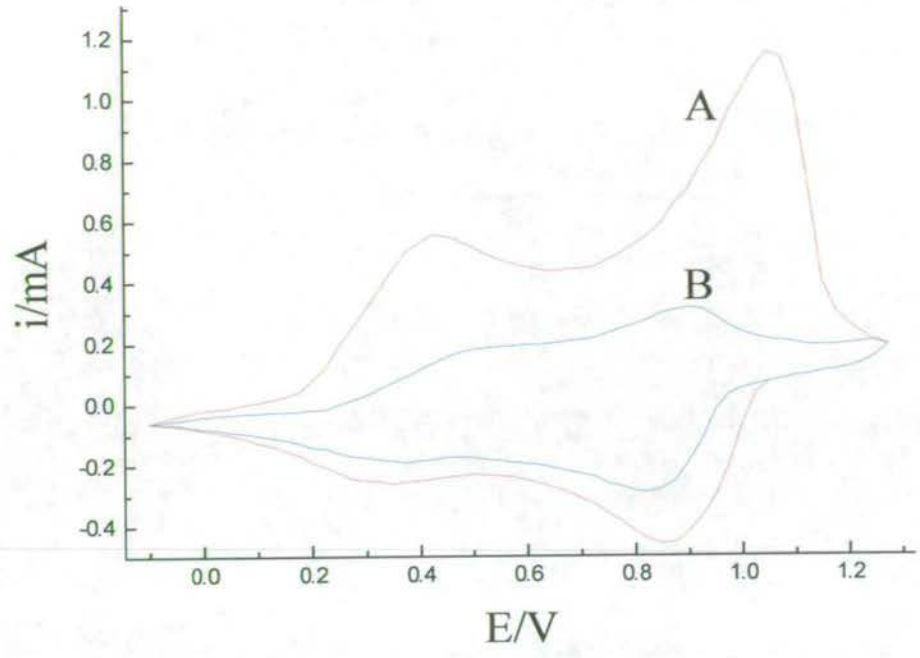

Figure 4.9 Typical CV for film of 5-cyanoindole in background electrolyte at a sweep rate of 20 mV/s, sweeping from –0.1V to +1.3V. A = first sweep, B = second sweep. (film polymerised from a 20mmol monomer solution at 15Hz and an electrode potential of 1.64V.)

Indole-5-carboxylic acid has similar redox behaviour, with a reversible oxidation-reduction CV being observed, but centred around 100mV rather than the 400mV observed for 5-cyanoindole. There is also an irreversible chemical change when the film is cycled up to 1V, with trimer units in the film linking to form polymer. However, the indole-5-carboxylic acid film displays a change in behaviour over time. If the film is cycled slowly around the oxidation/reduction cycle for an extended period, then the oxidation/reduction peaks are seen to increase in size and "grow in". This has been linked to the rearrangement of the trimer units in the film, with pores in the film opening up to allow the passage of counterions in and out of the film. This behaviour has been studied in detail using A.C. impedance techniques

and is reported elsewhere [3]. Chapter Seven of this thesis goes into greater depth concerning the electrochemical properties of the films and their relationship to emission properties.

4.4 Fluorescence properties of the trimer chromophore in solution

In this section, the fluorescence properties of the trimeric species of 5-cyanoindole, Indole-5-carboxylic acid, 5-bromoindole, 5-chloroindole and 5-methoxyindole in solution are considered. The trimers samples were produced by electrooxidation of monomer under conditions that were adjusted to favour trimer formation and minimise production of polymer. The fluorescence properties of the trimers are all very similar, but show a marked difference from the monomer species. A considerable bathochromic shift is seen between the spectra of the monomer and trimer species, accompanied by an increase in vibronic structure and a reduction in the Stokes shift. For example, the 0-0 transition in the excitation spectrum of 5-cyanoindole trimer in ethanol is shifted to lower energy by 10400cm^{-1} with respect to the monomer.

Figure 4.10 shows the excitation spectra (at an emission wavelength of 450nm) and emission spectra (at an excitation wavelength of 320nm) for trimers of indole-5-carboxylic acid, 5-bromoindole and 5-methoxyindole dissolved in ethanol. The wavelengths of peaks in the excitation and emission spectra for all the trimers are listed in Table 4.8. The value of the Stokes shift $\Delta\ \bar{\nu}$ is calculated as the wavenumber difference between the S_1 origin bands in the excitation and emission spectra. The Stokes shift is significantly lower for the trimer species than the corresponding monomer, as illustrated in Table 4.9.

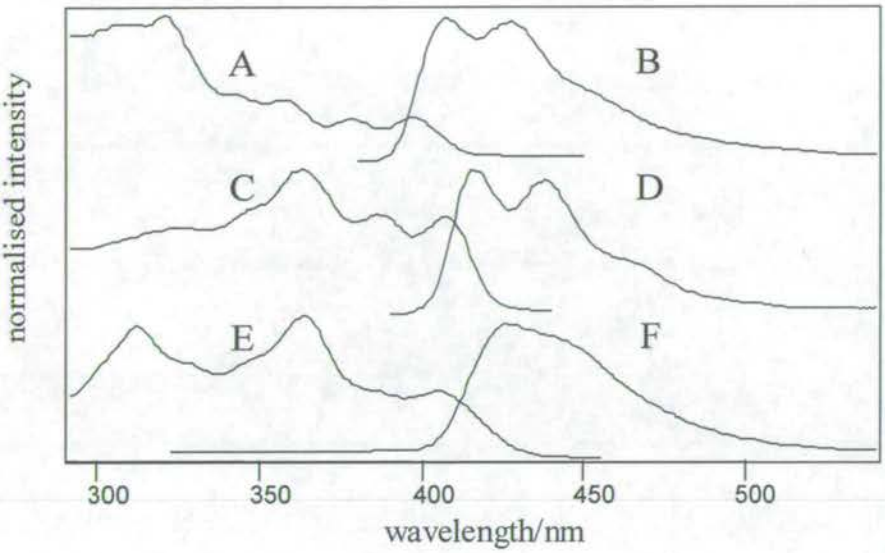

Figure 4.10 Excitation and emission spectra of: indole-5-carboxylic acid, excitation spectrum (A), emission spectrum (B); 5-bromoindole excitation spectrum(C), emission spectrum (D); 5-methoxyindole, excitation spectrum (E), emission spectrum (F), in ethanol.

Trimer	Excitation maxima /nm	Emission maxima /nm	Stokes shift $\Delta\bar{\nu}cm^{-1}$
Indole-5-carboxylic acid	397/378/357/343/320	408/428	700
5-cyanoindole	402/381/359/344/318	416/437	800
5-chloroindole	402/381/360/344/311	420/439	1200
5-methoxyindole	406/384/363/348/312	427/440	1200
5-bromoindole	400/380/356/340/310	417/438	1000

Table 4.8 Excitation and emission data for 5-substituted indole trimers in ethanol. The origin bands of the S_1, S_2 and S_3 states in the excitation spectra are underlined.

	Monomer Stokes Shift $\Delta\nu/cm^{-1}$	Trimer Stokes Shift $\Delta\bar{\nu}/cm^{-1}$
Indole-5-carboxylic acid	10500	700
5-cyanoindole	7800	800
5-bromoindole	6800	1000
5-chloroindole	5900	1200
5-methoxyindole	2900	1200

Table 4.9 A comparison of the Stokes shift, $\Delta\bar{\nu}$, of the monomer and trimer species in ethanol solution.

The reduction in excitation energy compared to the monomer is consistent with an increase in the delocalisation of the π-molecular orbitals around the trimer unit. The S_1 excitation spectra of the trimers show vibronic structure that mirrors that of the emission spectra. Transitions to higher excited singlet states, S_2 and S_3, are also apparent, as indicated in Table 4.8. The reduced Stokes shift of the emission and the enhanced vibronic structure both imply that there is a weaker interaction with the solvent and suggest a relatively non-polar excited state, more similar to the ^1L_b state of the monomer than the ^1L_a state. The small Stokes shift implies that there is little change in polarity between the ground and excited states. Unlike the monomers, the Stokes shift of the trimers is essentially independent of the substituent, suggesting that the nature of the substituent has little effect on solvent relaxation.

4.4.1 Substituent effect

5-bromoindole trimer has a greatly reduced quantum yield compared to the other trimer species. This reduction in quantum yield in 5-bromoindole trimer is attributed to the internal

heavy atom effect. The presence of the heavy bromine atom enhances spin-orbit coupling and increases the rate of intersystem crossing to the triplet manifold. This provides an efficient non-radiative pathway for decay of the excited singlet state and accounts for the reduced fluorescence quantum yield.

4.4.2 Effect of solvent on the trimer fluorescence

As for the monomers, the effect of solvent on the emission properties of indole-5-carboxylic acid and 5-cyanoindole was examined. It was found that the effect of increasing solvent polarity was much smaller than was seen for the monomers. The solubility of the trimers is much more limited than the monomers and the most non-polar solvents in which they dissolve are DMSO and ether. Figure 4.11 shows the emission spectra of 5-cyanoindole and indole-5-carboxylic acid in ether and DMF, it can be clearly seen that there is only a small bathocromic shift in the more polar solvent.

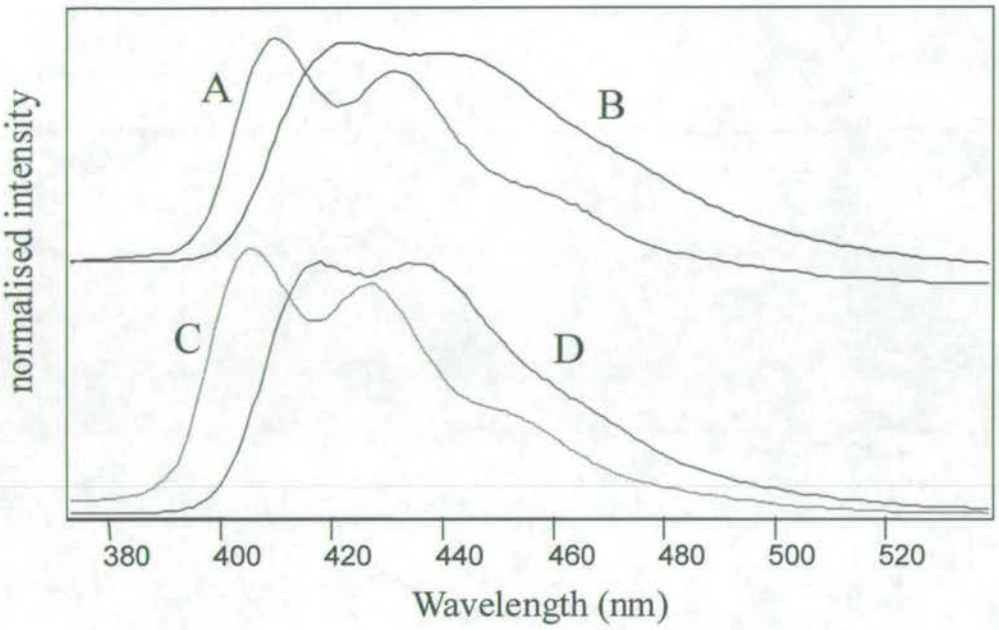

Figure 4.11 Effect of solvent on the emission spectra of: 5-cyanoindole in ether (A) and DMF (B) and Indole-5-carboxylic acid in ether (C) and DMF (D).

The results of a systematic study of the solvent effect on the emission of 5-cyanoindole and indole-5-carboxylic acid are summarised in Table 4.10, and Table 4.11, respectively. The excitation wavenumbers are essentially independent of solvent polarity and there is a much smaller Stokes shift than was observed for the monomer. The contrast in the response of monomer and trimer species to solvent polarity indicates that the first excited singlet state of the trimer has a smaller dipole moment than the monomer, hence it is less sensitive to solvent environment and experiences a reduced degree of solvent-solute relaxation in highly polar and protic solvents.

Solvents	Excitation maxima/cm^{-1}	Emission maxima/cm^{-1}	Stokes shift $\Delta\bar{\nu}/cm^{-1}$
DMSO	24800/26000/27600/28800/31000	23500/22700	1300
ether	25000/26400/28100/31800	24400/23200	600
DMF	24800/26100/27800/31500	23600/22600	1200
EtOH	24900/26200/27900/29100/31400	24000/22900	900
MeOH	25000/26300/27800/31800	24000/22900	1000
MeCN	25100/26500/28000/31700	24000/23100	1100

Table 4.10 Excitation and emission data for 5-cyanoindole trimer in a variety of solvents. The origin bands of the S_1, S_2 and S_3 states in the excitation spectra are underlined.

Solvents	Excitation maxima/cm^{-1}	Emission maxima/cm^{-1}	Stokes shift $\Delta\bar{\nu}/cm^{-1}$
DMSO	24900/ 26300/31200/35800	23900/22900	1100
ether	25300/26600/31500/ 36600	24600/23400	700
THF	24700/344500	24500/23300	200
DMF	25400/26700/31800/36200	24600/23400	800
EtOH	25500/26500/31700/35600	24500/23400	1000
MeOH	25500/26800/31600/36600	24300/23400	1200
MeCN	25500/26500/31700/35600	24100/23400	1400
H_2O	25600/26700/31600/36800	23300	2300

Table 4.11 Excitation and emission data for Indole-5-carboxylic acid trimer in a variety of solvents. Origin bands of the S_1, S_2 and S_3 states in the excitation spectra are underlined.

Indole-5-carboxylic acid trimer does not appear to be affected by aggregation in the same way as its monomer; however, the concentrations used for these measurements were very low, below $1x10^{-6}$ molar and therefore aggregation may not be apparent. This will be addressed further in chapter 6 where the fluorescence lifetimes are a much more sensitive probe of the molecular properties.

4.5 Fluorescence properties of the polymer chromophore.

In order to study the emission properties of the polymer species, electrochemical conditions were chosen to produce polymer-rich films. Typical conditions involved monomer solutions of 20 millimolar and less, a stationary working electrode and polymerisation times between one and five minutes. The more extensively polymerised films are less soluble than those rich in trimer (probably due to the presence of long chains of linked trimer units) and are less amenable to study in the solution phase. Because of this low solubility, it had originally been thought that the polymer emission was the same as that of the trimer, with the trimer being the fluorescing unit of the polymer chain. However, a red shift in the emission spectrum was noted in a low temperature sample as the excitation wavelength was increased to longer wavelengths, beyond the red edge of the absorption band for the trimer, as illustrated by Figure 4.12. The sample was excited from 400nm to 420nm at 5nm intervals and it was found that beyond 400nm, the emission spectrum began to shift to longer wavelength. It was thought that this shift in the emission wavelength could be due to excitation of species possessing a greater degree of electron delocalisation than the trimer, giving rise to emission at longer wavelengths than the trimer.

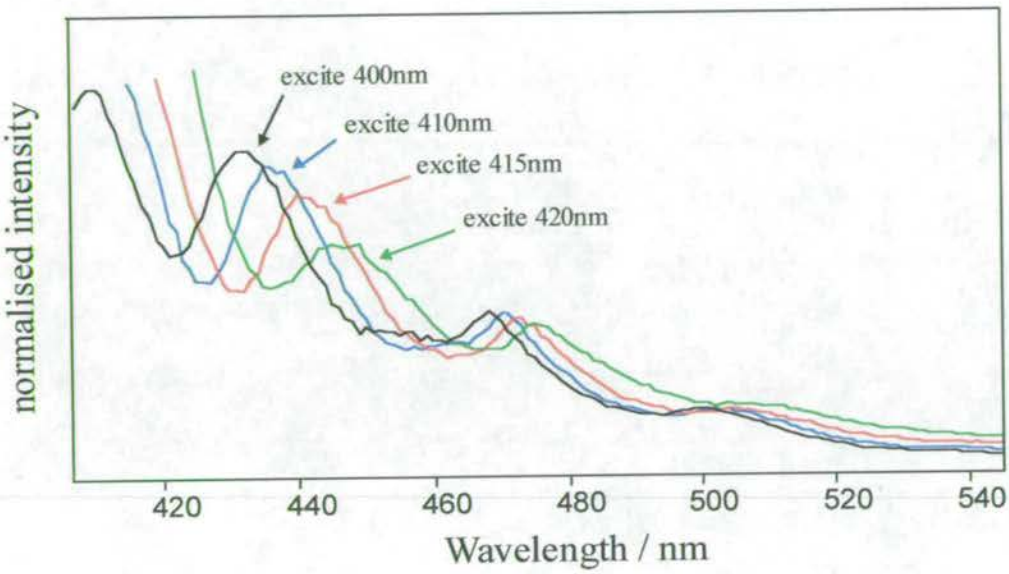

Figure 4.12 The shift to longer wavelength of the emission spectrum of electrooxidised 5-cyanoindole, dissolved in ethanol at 77K, with excitation at wavelengths on the red edge of the excitation spectrum.

It was not until 5-bromoindole was studied in detail that the existence of polymer fluorescence was confirmed. When electrooxidised, 5-bromoindole forms only a very thin film that is far more soluble than any of the other indole films. This meant that there was no doubt that all species produced during oxidation were dissolved in the solution, including any polymer. It was found that under conditions favouring polymer formation a peak was seen in the emission spectrum at longer wavelength than that attributed to the trimer. This is illustrated in Figure 4.13.

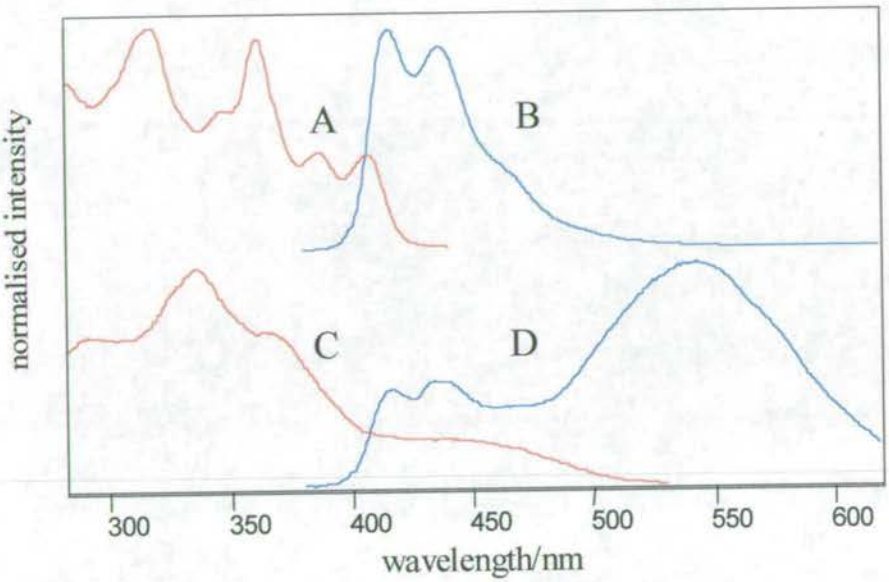

Figure 4.13 Excitation spectrum (A) for 5-bromoindole trimer at an emission wavelength of 450nm and emission spectrum (B) for 5-bromoindole trimer at an excitation wavelength of 335nm. Excitation spectrum (C) for 5-bromoindole polymer at an emission wavelength of 550nm and emission spectrum (D) for 5-bromoindole polymer and trimer at an excitation wavelength of 335nm, dissolved in ethanol.

For samples produced at high rotation speeds and high monomer solution concentrations, an emission spectrum characteristic of the trimer chromophore is seen. This is illustrated in Figure 4.13B, for the case of a film grown from a 150 millimolar monomer solution at a rotation speed of 10 Hz. However, for samples produced at low rotation speeds and low monomer concentration, the spectrum is dominated by a broad, longer wavelength emission band. This is exemplified in Figure 4.13D which shows the emission spectrum of a sample grown from a 10 millimolar monomer solution and with a stationary working electrode. The latter electrochemical conditions favour the formation of a film rich in polymer species. The

polymer emission has a characteristic, broad excitation spectrum that extends to lower excitation energies than the trimer spectrum, as shown in Figure 4.13C. This confirms that the broad red-shifted emission is due to excitation of ground state polymer species and is not excimer emission from the trimer species. If the sample is excited at longer wavelengths, in the tail of the polymer excitation spectrum, and beyond the absorption band of the trimer species, then the polymer can be excited exclusively as shown in Figure 4.14.

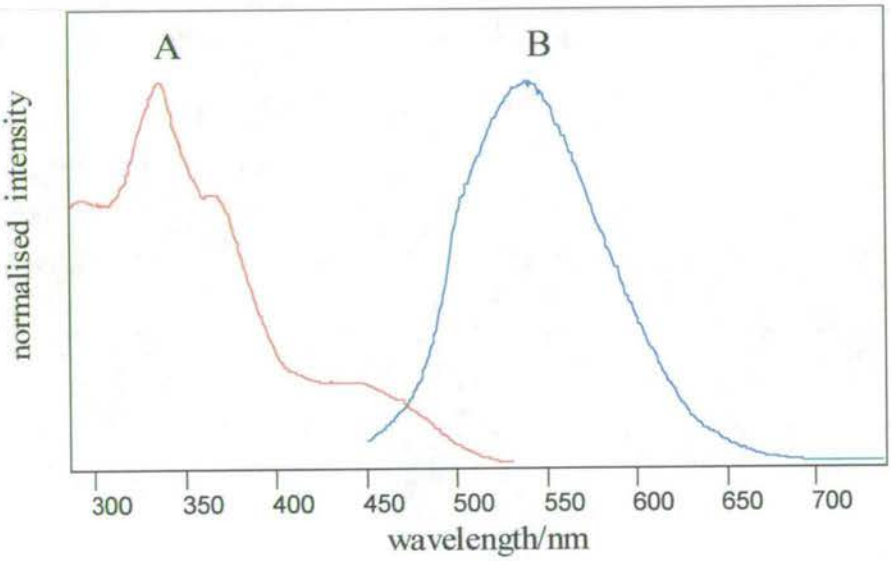

Figure 4.14 Excitation (A) and emission (B) spectra for 5-bromoindole polymer in ethanol. Excitation spectrum obtained using an emission wavelength of 550nm, emission spectrum obtained using an excitation wavelength of 440nm.

The fact that the polymer emission can be isolated from that of the trimer clearly shows that the trimer and polymer are distinct species that have their own characteristic absorption and emission spectra. The presence of emission with a bathochromic shift relative to the trimer

species is consistent with delocalisation of the excitation energy over several trimer units. The extent of this delocalisation, termed the conjugation length, rather than the overall length of the polymer chains will determine the optical properties of the sample. The broadness of the emission suggests a distribution of conjugation lengths and it is thought that each polymer chain will consist of conjugated segments of various lengths (extending over different numbers of trimer units). Thus, there exists a multiplicity of emitting species, a phenomenon that has been studied in detail for other conjugated polymer systems such as poly(phenylene-vinylene)[21] discussed in Chapter One section 1.4.

After confirming the presence of a polymer emission for 5-bromoindole, the other indoles were looked at more closely. A study of 5-cyanoindole and indole-5-carboxylic acid samples produced with electrochemical conditions tuned for high polymer yield has revealed similar emission properties as those seen for 5-bromoindole. However, the relative intensity of polymer to trimer emission is much lower than for 5-bromoindole. Since the peak of the polymer emission is in the same region as the tail of the trimer emission, it is hidden at all but the longest excitation wavelengths. The polymer emission can be revealed by exciting on the long wavelength edge of the excitation spectrum, as shown in Figure 4.15 for indole-5-carboxylic acid. The polymer appears to have a lower fluorescence quantum yield than the trimer, which is consistent with the polymer possessing a greater number of non-radiative pathways for excited state decay.

5-bromoindole polymer has a higher emission intensity relative to the trimer than the other 5-substituted indoles. As discussed in section 4.4.1 the fluorescence quantum yield of 5-bromoindole trimer is reduced by the internal heavy atom effect. The high intensity of the 5-bromoindole polymer emission, relative to the trimer, implies that intersystem crossing is

less favourable in the polymer species than in the trimer. This suggests that there is a closer coincidence of singlet and triplet states in the trimer than the polymer, allowing more efficient intersystem crossing in the trimer species.

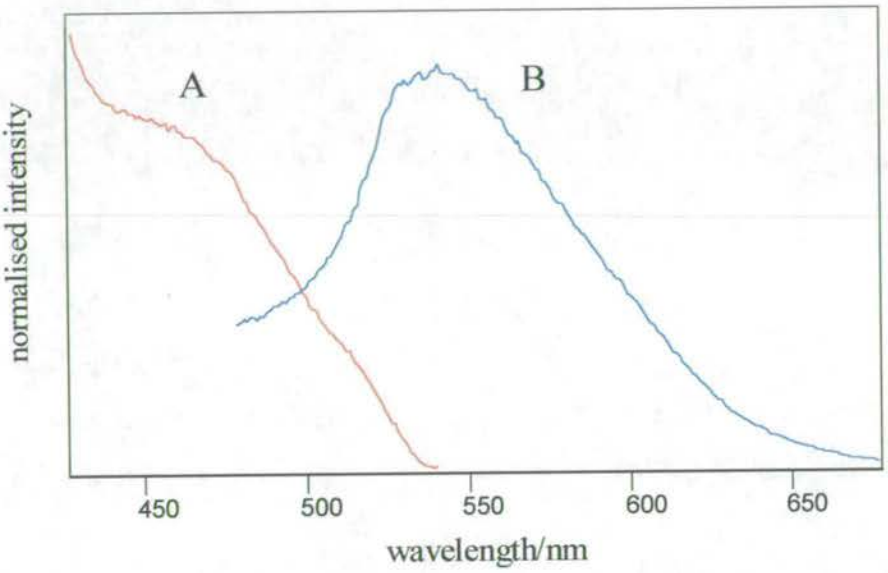

Figure 4.15 Excitation (A) and emission (B) spectra for indole-5-carboxylic acid polymer in ethanol; emission wavelength 550nm and excitation wavelength 440nm, respectively.

4.6 5-nitro indole trimer and polymer: a useful low intensity emission.

As was observed for 5-nitroindole monomer, the films produced electrochemically possessed very low intensity emission in solution. A weak emission band was seen at around 420nm, however, it was of a similar intensity to impurities found in the solvents and not reproducible, with no vibrational structure. This lack of fluorescence can be attributed, as for

the monomer, to the presence of an n-π^* state and consequent efficient intersystem crossing, which effectively quenches any fluorescence emission.

This lack of fluorescence proved to be very useful in the development of a novel electropolymerisation technique. Work was being carried out in an attempt to form polymer films from indole monomers that contain electron-donating substituents, such as 5-aminoindole and 5-hydroxyindole, as they would be very useful for the creation of a range of sensor devices. However, previous attempts at this had failed since the electrooxidation products were soluble and did not form an electroactive film. This problem was solved by carrying out the polymerisation on a pre-formed film of another indole.

The soluble trimers have a greater affinity for formation and linking on top of a pre-formed polymer layer than they do on a bare platinum electrode. Initially this was carried out using a thin layer of 5-cyanoindole as the template. As the oxidation proceeds, the film is seen to thicken and darken. Electrochemical analysis was consistent with the formation of a film, on top of the template, of further trimer units and polymer of linked trimer, from the desired monomer. However, since 5-cyanoindole trimer is so highly fluorescent, it was impossible to analyse the new films using fluorescence techniques. This is where 5-nitroindole proved to be very useful, as it forms a suitable template layer yet has only very weak fluorescence properties, allowing the fluorescence of the new polymer films to be studied. 5-nitroindole behaves in a similar fashion electrochemically to 5-cyanoindole and has the useful attribute that its oxidation potential is much higher than those of 5-aminoindole and 5-hydroxyindole, and therefore is not affected by their oxidation.

4.7 Fluorescence properties of soluble trimers.

To study 5-hydroxyindole and 5-aminoindole, the technique discussed above, using a pre-formed polymer layer, was used. However, it was noted that upon polymerisation there was a darkening of the monomer solution, indicating that there was still a considerable portion of the products remaining soluble. Therefore, both the films and the resulting solutions were examined.

4.7.1 Fluorescence of 5-hydroxyindole trimer

The results obtained for 5-hydroxyindole were much more straightforward than for 5-aminoindole. The film formed on a 5-nitroindole layer was dissolved off the electrode using DMSO to ensure complete dissolution. The fluorescence spectrum of the resulting solution was very similar to those previously observed for the other indole trimers. An excitation spectrum (measured at an emission wavelength of 460nm) and an emission spectrum (using an excitation wavelength of 320nm) is shown in Figure 4.16. These results support those from electrochemical analysis, that using a template film to produce a polymer film from an indole with an electron donating group results in the formation of the trimer species.

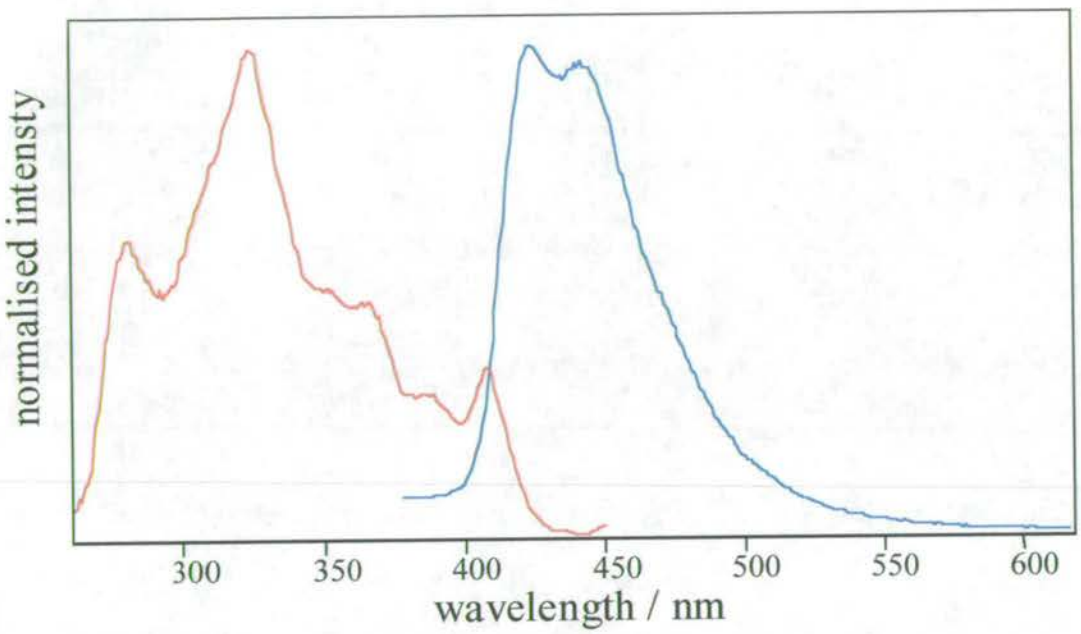

Figure 4.16 Excitation and emission spectra for a sample of 5-hydroxyindole trimer produced on a pre-formed film of 5-nitroindole and dissolved in DMSO.

When the background solution from polymerisation was examined it revealed the presence of a third species as well as the expected monomer and trimer. Each species can be seen individually by exciting at different wavelengths. The emission spectrum of the new species lies between the monomer and trimer emission and has a distinct excitation spectrum. The most likely explanation of the third species is that a dimer forms as a precursor of the trimer, but is completely soluble and, therefore, is not seen in the film. Figure 4.17 shows the excitation and emission spectra for each of the three species in the solution. The top spectrum is that of the monomer, the middle spectrum shows the postulated dimer and the bottom spectrum the trimer, each has a characteristic excitation spectrum.

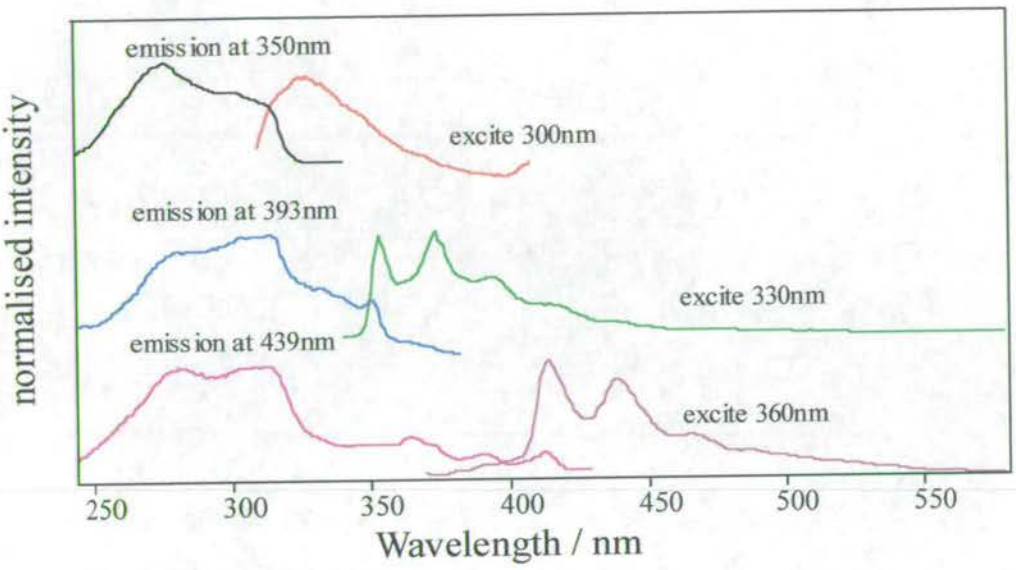

Figure 4.17 Excitation and emission spectra for the background solution from polymerisation of 5-hydroxyindole showing monomer, dimer and trimer species.

4.7.2 Fluorescence of 5-aminoindole trimer.

The electropolymerisation of 5-aminoindole on a pre-formed 5-nitroindole layer was similar to that of 5-hydroxyindole and suggested that again a trimer species was being formed. However, the results of fluorescence analysis were less conclusive due to poor film formation. During polymerisation the background solution became coloured deeply red due to the presence of soluble products. Analysis showed the presence of similar species to the 5-hydroxyindole background solution (Figure 4.18), with what appears to be a dimer species (C and D), large amounts of monomer (A and B), as expected, and an emission at longer wavelength, centred around 450nm (E and F). The latter emission is at longer wavelength than expected for a trimer species; this can be accounted for if aggregation of the trimer

molecules has occurred. The presence of a soluble trimer species is consistent with rotating ring disc studies carried out by other workers [2].

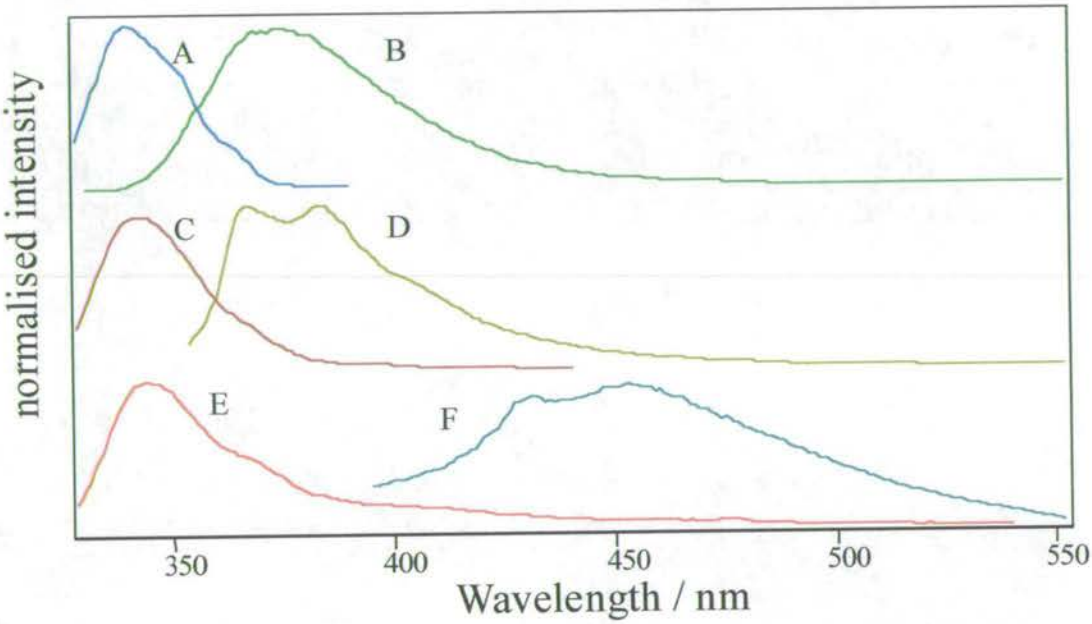

Figure 4.18 Excitation and emission spectra for the solution products of electropolymerisation of 5-aminoindole on top of a 5-nitro indole layer. With emission wavelengths of: A 380nm; C 420nm; E 500nm and excitation wavelengths of: B 300nm; D 340nm and F 380nm.

A similar result is seen for the film dissolved off the electrode. Figure 4.19 shows the emission and excitation spectra for a 5-aminoindole film formed on a template layer of 5-nitroindole polymer. Unlike the 5-hydroxyindole film, there appears to be a dimer species present on the film, which is seen when exciting at 340nm. As in the background solution, there is a long wavelength emission that is likely to be the trimer species, but shifted to

longer wavelengths due to the formation of an aggregate. Although not as conclusive as the results for the other trimer species, the fluorescence spectra along with the electrochemical results, prove good evidence for the formation of a layer of 5-aminoindole trimer and/or polymer on top of the 5-nitroindole polymer template layer.

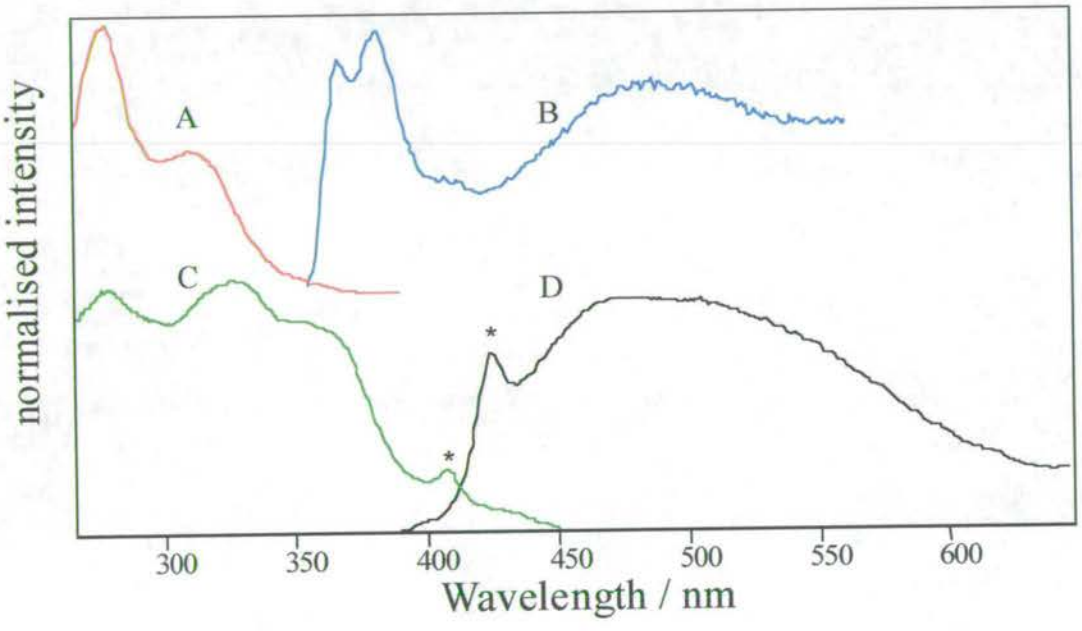

Figure 4.19 Excitation and emission spectra for a film of 5-aminoindole polymerised on top of a 5-nitroindole layer and dissolved in ethanol. With emission wavelengths: A 400nm; C 500nm and excitation wavelengths: B 340nm; D 380nm. Peaks marked * are due to Raman scattering by the solvent.

4.8 Fluorescence properties of unsubstituted indole trimer

Unsubstituted indole polymerises at a platinum electrode to form a film in the same way as the 5-substituted indoles. Its electrochemical properties are similar and laser desorption mass spectrometry showed the predominant species present to have a m/z of 345, corresponding to that of a cyclic trimer. However, there was another peak in the mass spectrum at a m/z of 573, which was thought to be a pentameric species. The origin of this pentamer has been the subject of considerable debate. The results of fluorescence studies were initially inconclusive, but also suggested the presence of a species other than the trimer species. Figure 4.20 shows the excitation and emission spectra for two samples of an electropolymerised indole film dissolved in ethanol.

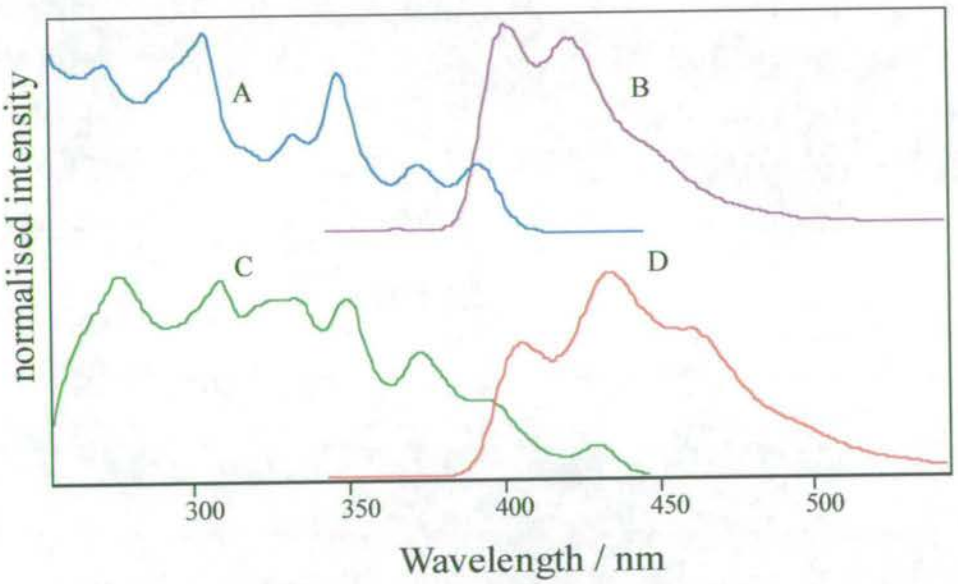

Figure 4.20 Excitation and emission spectra for films of electropolymerised unsubstituted indole in ethanol, with emission wavelengths: A 450nm; C 480nm and excitation wavelengths: B 320nm; D 320nm.

Excitation and emission spectra A and B are for a freshly prepared indole film dissolved in ethanol, displaying the characteristic features of a trimer species. However, some samples had different emission spectra and slightly altered excitation spectra (as shown in C and D), especially those that had been left in solution for extended periods. The origin of this new emission is uncertain, but there are several possible explanations. Initially, this emission was attributed to the pentamer species observed in the mass spectrum, although it is not known how this species would be generated. It was then found that adding a reducing or oxidising agent to the sample affected the emission characteristics. If the sample were oxidised, then only the characteristic trimer emission was seen. If a reducing agent was then added to the sample, the emission shifted to that seen in Figure 4.20D, with subsequent addition of an oxidant returning the emission to its previous state as illustrated in Figure 4.2. This behaviour can be explained in terms of aggregation of the trimer units in solution, leading to the formation of a π-complex of two trimer units, that has its own characteristic excitation and emission spectrum. No complexation is seen between oxidised (cationic) trimers since there is considerable charge repulsion between molecules, but in the reduced (neutral) state this repulsion no longer exists and the molecules can interact.

Returning to the mass spectrometry result, it is most likely that the pentamer peak is due to fragmentation of the aggregated trimer species in the desorption or ionisation process and is not a product of electropolymerisation, as had been originally thought. Work is presently underway to produce pure indole trimer via chemical methods with the hope of unambiguously determining its emission properties.

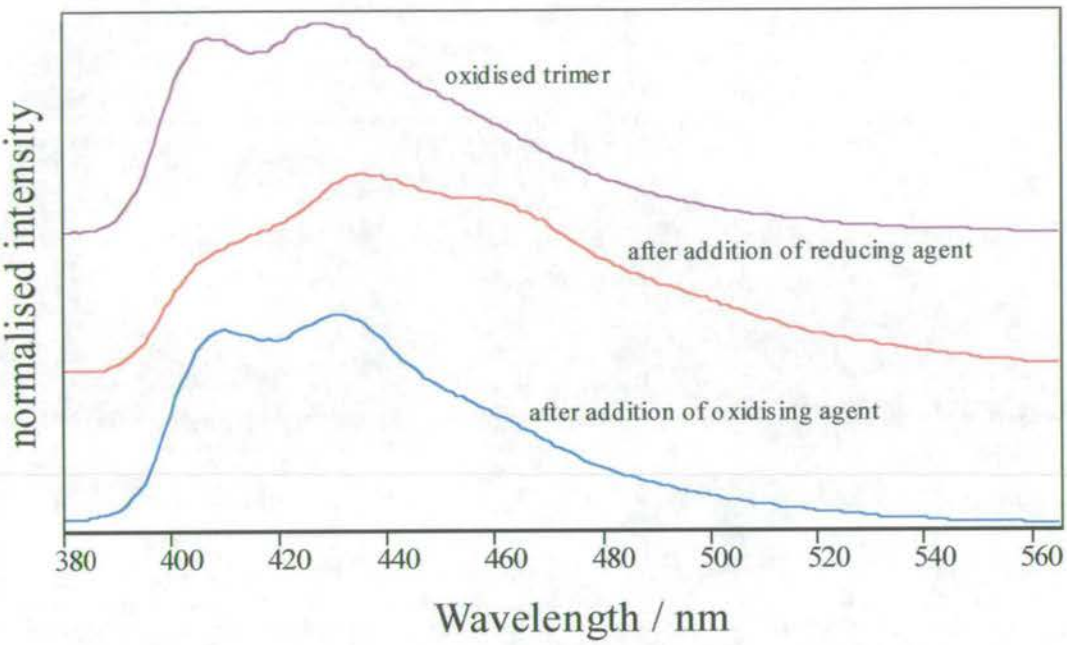

Figure 4.21 Emission spectra for a dissolved film of unsubstituted indole showing the effect of adding reducing and oxidising agents. Excitation wavelength for all spectra is 320nm.

4.9 Fluorescence properties of N-methylindole

From studies using infra-red spectroscopy [5] there is evidence that linking of 5-substituted indole trimers to form polymers occurs at the ring nitrogen. If this is so, N-methylation will prevent this and is expected to inhibit polymerisation of trimers. Therefore, the electrooxidation of N-methylindole was studied.

The electrochemical study gave evidence that a cyclic trimer species was being formed in the same fashion as for the other indoles, but the product was soluble, as for 5-aminoindole and

5-hydroxyindole. The presence of trimer was backed up by mass spectrometry (using the technique of matrix-assisted laser desorption ionisation mass spectroscopy, MALDI MS), with a dominant peak at 388 corresponding to the trimer unit. This is illustrated in Figure 4.22 [8] where it is also possible to see a series of other peaks that correspond to linear polymers of 2, 4, 5, 6 and 7 monomer units in length. Of particular note is the lack of any peaks due to linking of the trimer units, supporting the hypothesis that linking occurs at the nitrogen in the cyclic trimers.

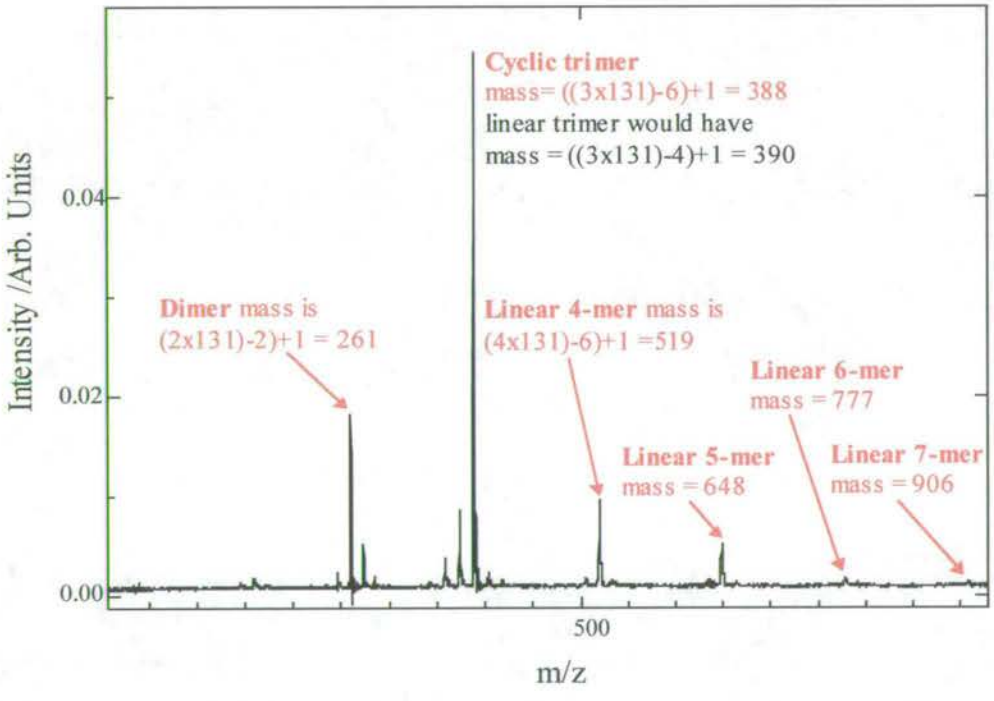

Figure 4.22 MALDI spectrum of electrooxidised N-methylindole solution products, taken from reference 8.

In order to examine the fluorescence of the polymerisation products of N-methylindole, a 50 mmol monomer solution was left polymerising at a platinum gauze for two hours. The initial

monomer solution is light yellow in colour; after polymerisation it is very dark brown, with a residue deposited on the platinum gauze. This residue was dissolved in ethanol and the fluorescence examined. The results are shown in Figure 4.23.

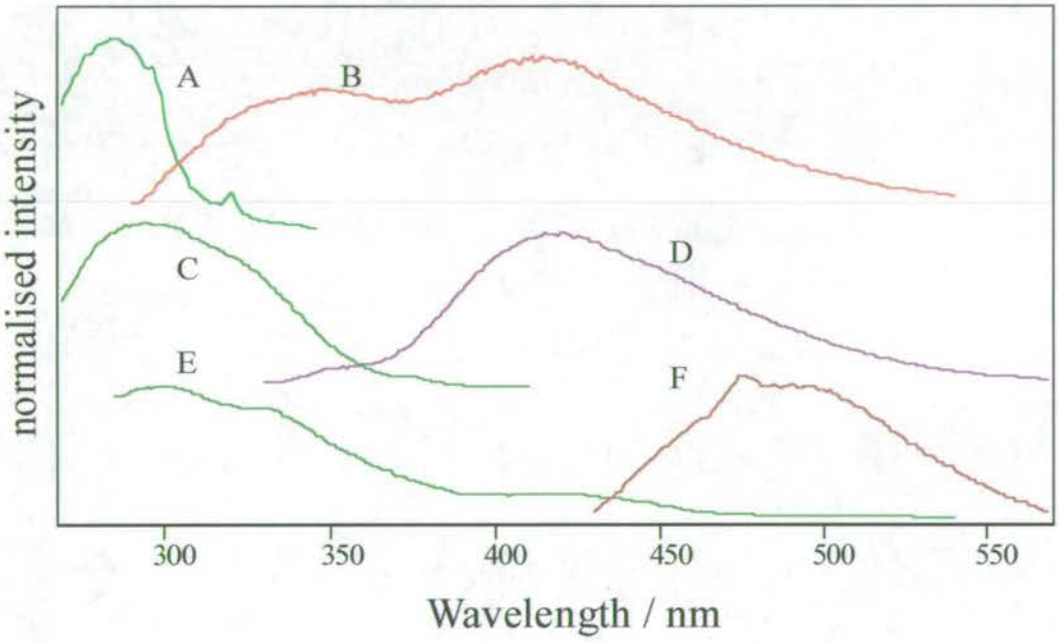

Figure 4.23 Excitation and emission spectra from the electrooxidised N-methylindole solution products. With emission wavelengths: A 360nm; C 450nm, E 550nm and excitation wavelengths: B 280nm; D 320nm; F 420nm.

There are three species present with different excitation and emission spectra. A small amount of residual monomer emission (B) is seen when exciting at shorter wavelengths (A), along with a longer wavelength broader emission. This broad emission peak is seen at 420nm (D) when exciting between 300 and 380nm; it has a broader excitation spectrum (C) than the monomer (A) and is in the correct region to be trimer, although it does not possess

any typical vibronic structure. When exciting at longer wavelengths (beyond 380nm) an emission is seen at even longer wavelength (F) with a corresponding extended excitation spectrum (E). This emission is at longer wavelength than the trimer species, but at shorter wavelength than the polymer species observed for the 5-substituted indoles, and is most likely to be from the linear polymers. The broad structureless nature of the trimer spectrum may be caused by underlying emission from the linear polymer species. The presence of a linear polymer, not observed for the 5-substituted indoles, can be attributed to the steric bulk of the N-methyl groups that hinder trimer formation, allowing linear polymerisation to compete.

Because of the soluble nature of the electropolymerisation products, the technique of using a thin layer of 5-nitroindole as a template on a rotating disc electrode was tried. Both the resulting solution and the dissolved film were analysed. The spectra of the background solution looked almost identical to the above (where a platinum gauze was used), with emission from the monomer, a broad trimer peak and a further peak due to the linear polymer. The emission of the dissolved film was somewhat different and is shown in Figure 4.24.

Exciting at 280nm produces the expected monomer emission peak (B), but when the sample is excited between 300 and 380nm a less broad emission (D) is seen, that much more closely resembles the trimer peaks of the 5-substituted indoles. Exciting at longer wavelengths reveals no further emission, indicating that no polymer is present in the film. The lack of any polymer emission accounts for the narrower emission band of the trimer species and suggests that the template forces trimer formation on the electrode, which cannot link due to the N-methyl groups. This is also in agreement with the mass spectrometric results that imply the

absence of polymer consisting of linked cyclic trimers. These results support the hypothesis that 5-substituted indole cyclic trimers link via the ring nitrogen positions.

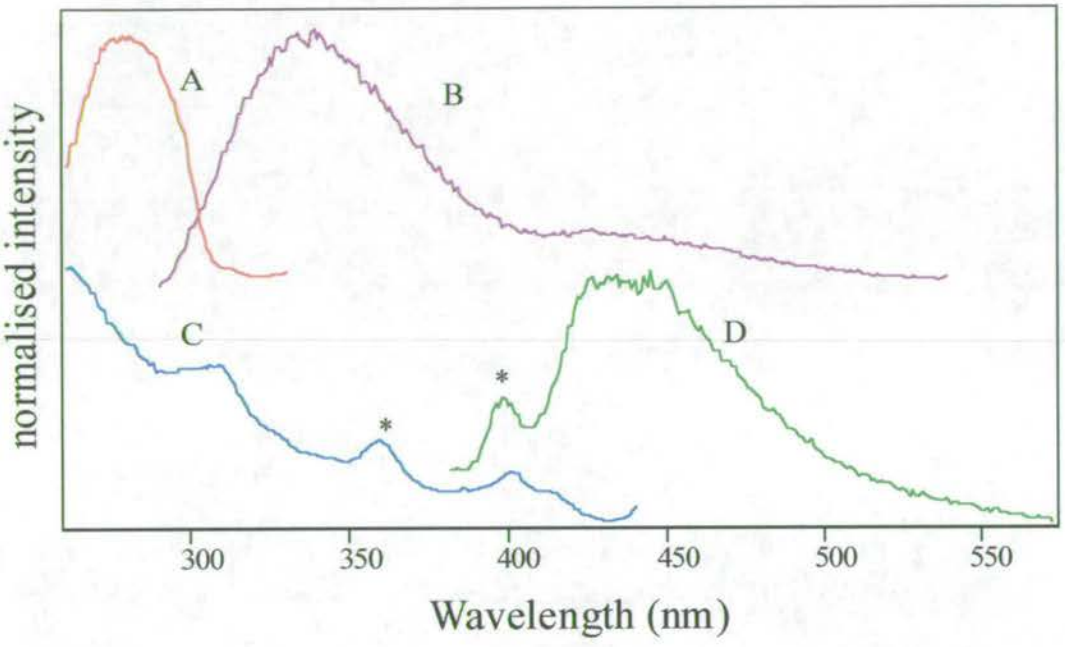

Figure 4.24 Excitation and emission spectra for a dissolved film of N-methylindole electropolymerised on top of a thin film of 5-nitroindole. With emission wavelengths: A 340nm; C 450nm and excitation wavelengths: B 280nm; D 360nm. Peaks marked * are due to Raman scattering by the solvent.

4.10 Chemically polymerised 5-substituted indoles.

It was of considerable interest to see if the species formed by electrochemical oxidation methods were the same as those produced using chemical oxidation. If this were the case, then it would be much easier to produce polymeric indoles on a bulk scale for any potential applications. The work detailed here is from initial studies concerning 5-cyanoindole, 5-

bromoindole, indole-5-carboxylic acid, 5-aminoindole and indole. There is ongoing work aimed at producing a pure trimer sample and controlling the proportion of trimer to polymer, as well as growing a suitable crystal for X-ray diffraction analysis to obtain a crystal structure of the trimer species. For all the polymerisation studies, iron(III) chloride was used as the oxidising agent. Theoretically, to produce a trimer without further polymerisation, the molar ratio of iron chloride to indole monomer should be 7:3. For all the results given here, iron(III) chloride and monomer solutions, both with concentrations of about 50 mmol, were rapidly mixed in various ratios; there is obviously considerable scope for fine-tuning the reaction procedure.

4.10.1 Chemically polymerised 5-cyanoindole.

The chemical polymerisation of 5-cyanoindole was carried out at different ratios of monomer to oxidant to see whether this affected the resulting products. Using a ratio of 7 parts iron(III) chloride to 3 parts monomer the resulting product appeared to be almost identical to the electropolymerised 5-cyanoindole. Upon addition of the oxidant a precipitate was formed which increased upon addition of water. The precipitate was filtered, washed with water then dissolved in ethanol. The emission was dominated by trimer (Figure 4.25 A and B) with a small amount of polymer being observed when the sample was excited beyond 400nm.

When a ratio of 4:1 iron(III) chloride to monomer was used, the emission was dominated by a broad polymer emission as shown in Figure 4.25 C and D. Such an intense polymer emission was never observed for the *electropolymerised* 5-cyanoindole, even when conditions were set to favour polymer production. This may be due to a number of effects.

The chemical polymerisation may be more efficient than electrochemical polymerisation, giving a higher yield of polymer and therefore an increase in the polymer emission. The product from chemical polymerisation was more soluble than the electrochemical product, possibly due to less cross-linking between polymer chains, therefore a greater proportion of the polymer will be present in the solution of the chemically produced sample. From the emission of the polymer, it is not possible to say conclusively how it is formed and it is possible that chemical polymerisation produces linear polymerisation products. However, the presence of a trimer emission implies that the polymer is composed of linked trimer units.

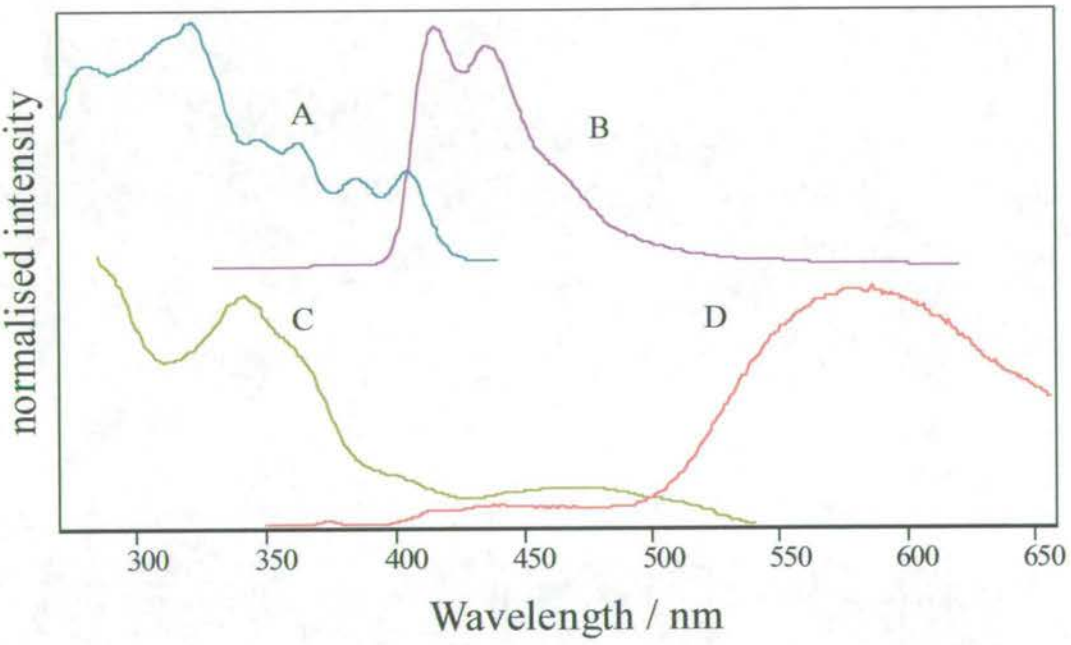

Figure 4.25 excitation and emission spectra of chemically polymerised 5-cyanoindole with oxidant to monomer ratios of: 2.3:1 (A, B) and 4:1 (C, D). Emission wavelengths of: A 450nm; C 550nm and excitation wavelengths of B 300nm and D 340nm.

4.10.2 Chemically polymerised 5-bromoindole.

A sample of 5-bromoindole was produced using an oxidant to monomer ratio of 7:3. The fluorescence of the resulting products was very similar to that of the electropolymerisation products under conditions set to favour the polymer. A trimer emission was seen, with peaks at 423nm and 440nm, and a longer wavelength polymer emission was also present with an emission maximum at 570nm, similar to the polymer emission observed for 5-cyanoindole. As for the electrochemical product, the trimer and polymer had individual excitation spectra and the polymer emission could be isolated by exciting at greater than 400nm.

4.10.3 Chemically polymerised 5-aminoindole.

The chemical polymerisation products of 5-aminoindole were all soluble, thus the fluorescence of the product solution was somewhat complex. Three definite species could be determined which correspond with those seen for the electrochemical oxidation. These are illustrated in Figure 4.26. When exciting at 280nm, the dominant emission is from the monomer, exciting at 355nm selects for what is most likely a trimer species and exciting at 440nm gives a typical polymer emission.

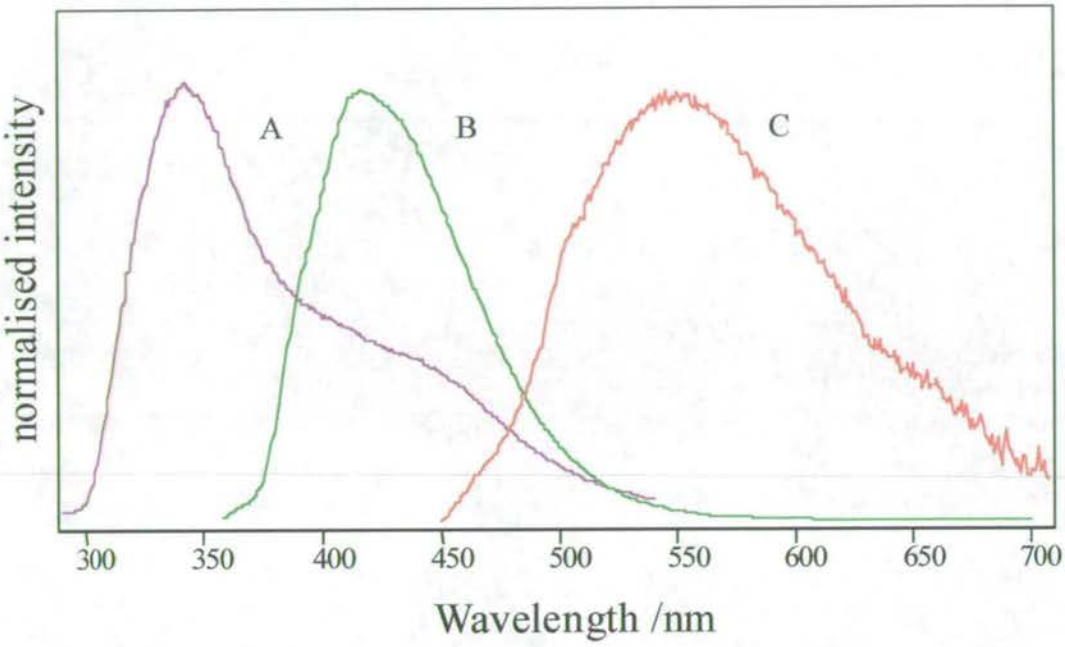

Figure 4.26 emission spectra for the chemical polymerisation products of 5-aminoindole with excitation wavelengths of A 280nm; B 355nm and C 440nm.

4.10.4 Chemically polymerised unsubstituted indole.

The chemically polymerised indole appeared to have identical properties to the electrochemical species. The oxidised species, displayed a typical trimer emission with peaks at 401nm and 422nm. Addition of a reducing agent caused aggregation and an emission shift with peaks at 405nm, 434nm and 460nm.

4.11 Quantum yield measurements for indole-5-carboxylic acid

Although the electropolymerised indoles in solution are visibly "highly fluorescent" it is important to try and quantify this statement. Measurements of absolute fluorescence quantum yields are not straightforward and beyond the experimental techniques available for this work. However, it is possible to make a comparative measurement using a known quantum yield of a similar molecule. The main difficulty is that to date a completely pure sample of the trimer has not been confirmed, since there is always the possibility of contamination with monomer or polymer species. This is not a problem for fluorescence spectroscopy work, since each species can be excited individually, however, it is difficult to give an accurate measure of the concentration of the sample. In order to obtain a comparative measure of the quantum yield, indole monomer was used as the standard; indole has a quantum yield of 0.4 in ethanol solution [21]. A chemically polymerised trimer of indole-5-carboxylic acid was used with an estimated 80% trimer proportion, the impurities being monomer and polymer (estimated from NMR analysis). Both the impurities can be excluded from the fluorescence emission by judicious selection of the excitation wavelength.

The emission spectra were measured with the concentration of indole monomer at $1x10^{-5}$ molar and trimer approximately $1x10^{-6}$ molar. At these concentrations any inner filter or self-absorbance effects are negligible. To correct for the difference in concentration, the absorption was measured for each sample. Emission spectra were collected using the same excitation wavelength of 280nm for both trimer and monomer. The results are as follows.

Indole monomer: Absorbance of $1x10^{-5}$ molar solution at 280nm = 0.049

Area under emission spectrum = $8.4719x10^{7}$ cps

Integrated emission intensity divided by absorbance = $\underline{1.729x10^{9}}$

Trimer: Absorbance of $\approx 1x10^{-6}$ molar solution at 280nm = 0.072.

Area under emission spectrum = $1.6867x10^{8}$ cps

Integrated emission intensity divided by absorbance = $\underline{2.346x10^{9}}$

$$\frac{\Phi_f \textbf{trimer}}{\Phi_f \textbf{indole}} = \frac{\textbf{2.346x10}^{9}}{\textbf{1.729x10}^{9}} = \textbf{1.35}$$ Hence the quantum yield of the trimer was estimated to be:

$\underline{0.54}$

4.12 Fluorescence emission from solid state indole films

To assess the viability of indole polymer films for applications involving fluorescence emission, the first step was to ascertain whether fluorescence was observable from a film. Detecting fluorescence from a solid sample is not as straight forward as for solution phase samples. The emission has to be detected from the front face of the sample and this introduces problems from scattered light. Initially no conclusive results were obtained using a fluorescence spectrometer and it was uncertain whether any of the polymer films did fluoresce. Preliminary results on the fluorescence of indole polymer films was obtained using a Nd:YAG laser excitation source as described in the following sections.

4.12.1 Laser induced fluorescence of a 5-cyanoindole film

A laser excitation source has the advantage of being much more intense and collimated than the xenon lamp source in the spectrometer and of being monochromatic. This means that scattered light could easily be discriminated from the emission. The output of the Nd-Yag laser was frequency tripled to give an excitation wavelength of 355nm which was known to be within the absorption band of the solution phase trimer and polymer species. The emission was collected through a long pass filter and a monochromator and detected by a photomultiplier tube. The films were examined in two forms, intact on the electrode and as a film drop-coated onto a glass slide from a DMF slurry. By using the disc electrode, films could be examined in their reduced and oxidised states. The results of this experiment were of particular importance as the basis for further studies, as discussed below. Emission could be clearly seen by the naked eye from the drop-coated film and the reduced film on the electrode.

The most intense emission was seen for the drop-coated film and by scanning the monochromator an emission spectrum was obtained as illustrated in Figure 4.27. Emission from the film was seen as a broad peak centred around 477nm. The peaks at 355nm and 532nm are due to the third and second harmonics from the laser respectively, and since they are sharp peaks, it can be inferred that scattered light is not contaminating the rest of the spectrum. Emission from the reduced film on the electrode was less intense than for the drop-coated film, but with the same emission maximum. Interestingly, no emission was detected from a film in the oxidised state.

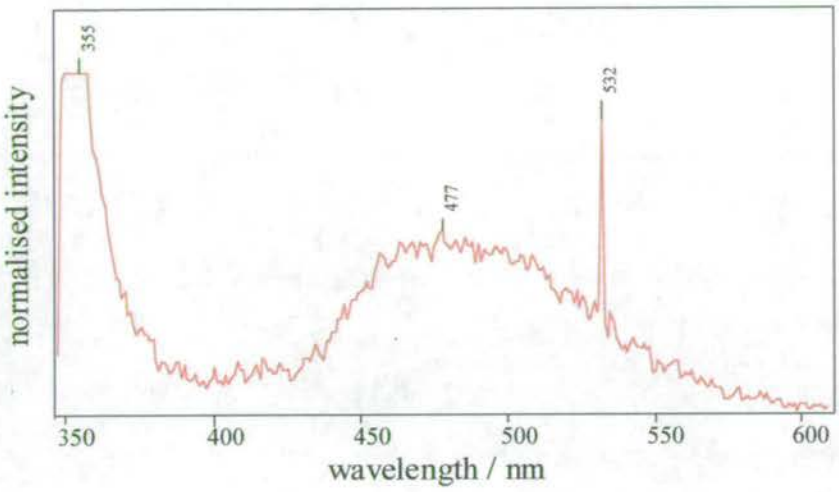

Figure 4.27 emission spectrum for a drop coated film of 5-cyanoindole. Peaks at 355nm and 532nm are due to scattered light from the laser.

4.12.2 Emission from a 5-cyanoindole film on a removable electrode.

Once it had been confirmed that emission was observable from a film of 5-cyanoindole, further investigations were made to obtain better results. An electrode with a removable tip was designed (as described in section 3.4.5) and this allowed much easier alignment within the sample chamber of the fluorescence spectrometer. This enabled spectra with much better resolution to be obtained. It was found that emission was only detectable from a reduced film and not from an oxidised film. Also, films produced at high rotation speeds and high monomer concentrations (conditions that favour trimer formation) were seen to have the most intense emission. An example of a 5-cyanoindole film produced from a 100mmol monomer solution at 10 Hz and then reduced in background electrolyte is shown in Figure 4.28.

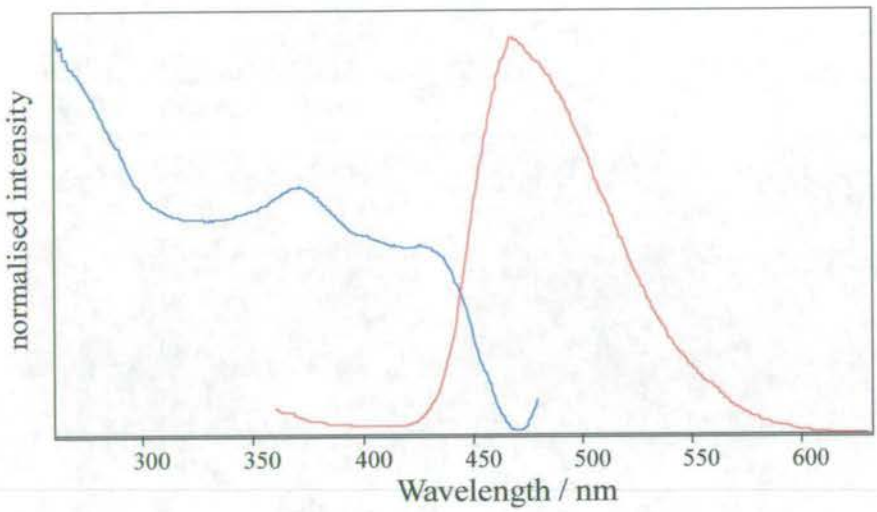

Figure 4.28 Excitation and emission spectra for a reduced film of 5-cyanoindole. With an emission wavelength of 500nm and excitation wavelength of 340nm.

The excitation and emission spectra of the reduced film are broader and shifted to longer wavelengths than those of the trimer in solution, having excitation peaks at 370nm and 440nm and the emission peak at 480nm. However, the emission is at shorter wavelength and less broad than the polymer emission in solution. The nature of the emitting species in the film is explored in much greater detail in Chapter Six, where lifetime measurements are used to probe the fluorescence properties.

The emission properties of the trimer and polymer species in solution are independent of redox state, unlike the emission from the films. The non-observance of any fluorescence emission from the oxidised state of the film implies that there is a structural difference between the reduced and oxidised forms of the films. The oxidised film must posses a very efficient quenching mechanism that is not present in the reduced film. The nature of this

quenching mechanism and the effect of structure on the properties of the solid films are discussed in Chapter Seven.

No fluorescence emission was observed for any of the other 5-substituted electropolymerised films, except for the reduced state of an indole-5-carboxylic acid film. This emission was just visible by the naked eye but it was too weak to be resolved from background noise and scattered light.

4.13 Conclusions

There is a considerable difference between the fluorescence properties of 5-substituted indole monomers and those of their electrochemically and chemically formed trimer and polymer species. The fluorescence properties of 5-substituted indole monomers are dependent upon the nature of the 5-substituent and the polarity of the solvating medium. In polar solvents there is a large Stokes shift (due to a considerable bathochromic shift in emission wavelength) which is attributed to the presence of a low-lying excited state that possesses a large dipole moment. The excitation and emission spectra of the trimer chromophore occur at longer wavelengths than those of the monomer, consistent with an increase in the delocalisation of the π-molecular orbitals around the trimer unit. The emission spectra of the trimers show little dependence on the polarity of the solvent or the nature of the 5-substituent. There is a much smaller Stokes shift and the spectra have resolvable vibronic structure. This indicates that there is less interaction of the excited state with the solvent, implying a lower excited state dipole moment than in the monomer and little change in polarity upon excitation. It is also apparent that the 5-substituent has little effect on solvent relaxation, indicating that the nature of the substituent has less effect on the

polarity of the excited state, relative to the ground state, than for the monomer. With the exception of 5-bromoindole, the 5-substituted trimers show intense fluorescence in solution. The quantum yield of indole-5-carboxylic acid in ethanol was estimated to be 0.54.

It was found that the 5-bromoindole trimer species has a much lower fluorescence quantum yield than the other 5-substituted trimer species. This is due to the presence of the heavy bromine atom which enhances spin-orbit coupling and leads to an increase in the efficiency of intersystem crossing to the triplet manifold. However, the fluorescence of the 5-bromoindole polymer species did not appear to be strongly quenched, implying that intersystem crossing is less favourable in the polymer species than in the trimer.

Control of the electrochemical conditions allows films rich in polymer species to be grown. The polymer fluorescence is observed in solution as a broad emission band at longer wavelength than the trimer spectrum, with a corresponding bathocromically shifted excitation spectrum. This confirms the presence of extended chains of linked trimer units with energy delocalised along the polymer chain. The broadness of the polymer emission suggests the presence of a broad distribution of local conformations, each with its own set of electronic states. The polymer appears to have a lower fluorescence quantum yield than the trimer species. This is attributed to an increase in the number of available non-radiative decay pathways for the electronic excitation in the polymer system.

The absence of fluorescence emission from electropolymerised 5-nitroindole proved to be useful in the study of the soluble trimers 5-aminoindole and 5-hydroxyindole. 5-nitroindole was used as a template for electropolymerisation. This assisted in confirming the trimer structure of 5-aminoindole and 5-hydroxyindole.

Electropolymerised N-methylindole has an emission similar to the other trimer species, but also shows a longer wavelength emission that corresponds to the presence of a linear polymer. Electropolymerised unsubstituted indole has similar fluorescence properties to the 5-substituted indoles, except that a π-complexed aggregate was formed by the reduced form of the trimer in solution, complicating the emission properties.

Chemically polymerising the 5-substituted indoles produced species which exhibited the same fluorescence spectra as the products of electropolymerisation. The products of electropolymerisation can therefore be assumed to be trimer and polymer species essentially identical to those formed electrochemically. The relative yield of trimer and polymer could be varied by altering the oxidant to monomer ratio and with variation of the reaction conditions. This gives a potential method for bulk production of the indole trimer and polymer chromophores.

Of particular importance for further studies was the observation of fluorescence emission from solid polymer films. Measurable emission was recorded from 5-cyanoindole films in the reduced state. Trimer rich films exhibited the most intense emission. There was no observable emission from oxidised films.

References

1. J.G. Mackintosh, *PhD Thesis*, The University of Edinburgh 1996.
2. A. D. Thomson, *PhD Thesis*, The University of Edinburgh 1996.
3. M. Robertson, *PhD Thesis*, The University of Edinburgh 1996.
4. J. G. Mackintosh, A.R. Mount, *J. Chem. Soc., Faraday Trans.*, 1994, **90**, 1121.
5. J. G. Mackintosh, C. R. Redpath, A C. Jones, P. R .R. Langridge-Smith, D. R. Reed, A.R. Mount, *J. Electroanal. Chem.*, 1994, **375**, 163.
6. J. G. Mackintosh, A.R. Mount, D. Reed, *Magn. Reson. Chem.*, 1994, **32**, 559.
7. A. R. Mount, A. D. Thomson, *J. Chem. Soc., Faraday Trans.*, 1998, **94(4)**, 553..
8. P. Jennings, A. C. Jones, A. R. Mount, A. D. Thomson, *J. Chem. Soc., Faraday Trans.*, 1997, **93**, 3791.
9. J. G. Mackintosh, C. R. Redapth, A. C. Jones, P. R. R. Langridge-Smith, A. R. Mount, *J. Electroanal. Chem.*, 1995, **388**, 179.
10. J. G. Mackintosh, S. J. Wright, P. R .R. Langridge-Smith, A.R. Mount, *J. Chem. Soc., Faraday Trans.*, 1996, **92(20)**, 4109.
11. C. A. Parker in, *Photoluminescence of solutions, Elsevier*, 1968.
12. J. N. Murrel in, *The theory of the electronic structure of organic molecules, J. Whiley & sons Inc. New York*, 1963.
13. J. J. Aaron, A. Tine, C. Villiers, C. Parkanyi, D. Bouin, *Croatica. Chemica. Acta.*, 1983 **56(2)**, 157.
14. J. Shorter in, *Correlation analysis in organic chemistry, Oxford Chem. Series*, 1973.
15. H. L. Lami and N. Glasser, *J. Chem. Phys.*, 1986, **84**, 597.
16. M. S. Walker, T. W. Bednar, R. L. Lumry, *J. Chem. Phys.*, 1966, **45**, 3455.
17. M. S. Walker, T. W. Bednar, R. L. Lumry, *J. Chem. Phys.*, 1967, **47**, 1020.

18. P. R. Callis, *J. Chem. Phys*., 1991, **95**, 4230.

19. D. K. Hahn, P. R. Callis, *J. Phys. Chem A.*, 1997, **101**, 2686.

20. Berlmann *Handbook of fluorescence spectra of aromatic molecules, 2nd ed. Academic Press, London*, 1971.

21. E. P. Kirby, R. F. Steiner, *J. Phys. Chem,* 1970, **74 (6)**, 4480.

Chapter Five – Steady-state, low temperature fluorescence and phosphorescence measurements

5.1 Introduction

The luminescence properties of the 5-substituted indole monomers are highly sensitive to the solvating environment, as has been illustrated in the previous chapter. The result of this sensitivity is a broadening of the spectra, with little vibrational structure apparent. In an attempt to obtain results with enhanced resolution, to enable the 0-0 transitions to be identified, the samples were cooled to 77K using liquid nitrogen. At this temperature the solvent freezes into a rigid glass and the emission properties of the solute molecules are modified. Diffusion of oxygen in a rigid glass is much slower than in a liquid, therefore the effect of oxygen quenching is greatly reduced. This gives a more intense fluorescence emission and allows phosphorescence, radiative emission from the longer-lived triplet state to be observed. The effect of solvent relaxation is also greatly reduced, since reorganisation of the solvent cage is inhibited in the solid matrix, this results in the fluorescence emission being at shorter wavelength with greater vibrational structure.

Initially the low temperature experiments were intended to provide more detail of the fluorescence properties; however, for both the monomer and trimer species a longer wavelength emission was observed that had a lifetime long enough to be discernible to the naked eye. This emission was without doubt due to decay of the triplet state, and investigations were extended to

include this phosphorescence emission. At the very end of the experimental period, a shutter system was installed in the fluorescence spectrometer that allowed the fluorescence emission to be gated out and the phosphorescence emission to be collected exclusively. The monomers and some of the trimer species were re-examined using the shutter system, allowing the triplet states to be characterised in greater detail, and the phosphorescence lifetime to be estimated.

5.2 Indole monomers

5.2.1 Fluorescence

All the 5-substituted indole monomers examined in chapter 4 were studied at low temperature, with a considerable effect being observed on the emission properties. These results were obtained using ethanol as a solvent, since it was the only solvent in which the monomers dissolve that forms a clear glass without cracking. As soon as the solvent glass cracks, there is a sharp increase in the level of scattered light, giving poor results.

At low temperature, vibronic structure is evident in both the excitation and emission spectra, this is most clearly observed for 5-methoxyindole, as shown in Figure 5.1. Considering first the excitation spectrum, the 0-0 transition of the ^1L_b state and associated vibronic structure can be clearly identified. At higher energy (shorter wavelength) the onset of transitions to the ^1L_a state can be observed. Considering next the emission spectrum, there is a clear 0-0 transition and resolved vibronic structure, which has a mirror image relationship to the excitation spectrum and

a small Stokes shift ($\Delta \bar{\nu}_{0\text{-}0}$, the difference between 0-0 transitions in the excitation and emission spectrum), characteristic of emission from the ^1L_b state.

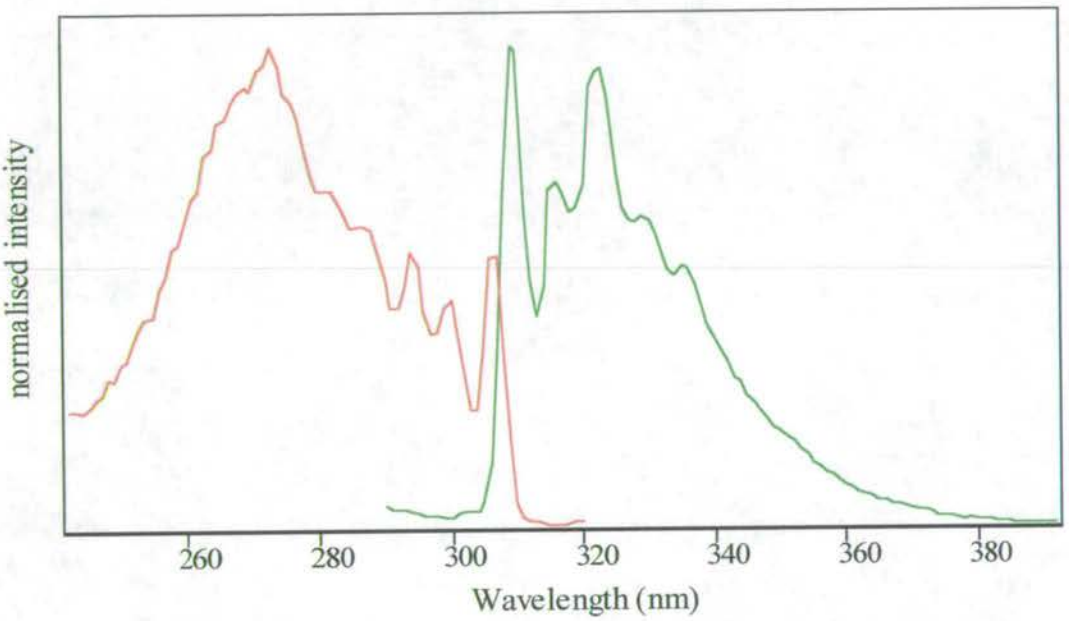

Figure 5.1 Excitation and emission spectra for 5-methoxyindole monomer in ethanol at 77K with an emission wavelength of 330nm and excitation wavelength of 280nm.

Fluorescence data for all the monomers at low temperature in ethanol is given in Table 5.1. In all cases emission is expected to be from the ^1L_b state, even though the solvent is highly polar. At room temperature, in the polar solvent ethanol, it is thought that emission occurs from the ^1L_a state (see discussion in section 4.2.2), due to solvent stabilisation of the ^1L_a state lowering it below the energy of the ^1L_b state. This accounts for the large Stokes shift and broad structureless emission spectrum observed in polar solvents. At low temperature the solvent is frozen into a rigid glass, therefore inhibiting the movement of solvent molecules and minimising the effect of

solvent-solute relaxation. Therefore, at low temperature the ^1L_a state will no longer be stabilised by the polar solvent, and emission is most likely to occur from the ^1L_b state.

monomer	Excitation maxima/nm	Fluorescence maxima/nm	Stokes shift $\Delta \bar{\nu}_{0\text{-}0}$ / cm^{-1}	Stokes shift $\Delta \bar{\nu}_{max}$ /cm^{-1}
5-cyanoindole	276, 282, 292, 300, <u>312</u>	<u>321</u>, 336, 351	900	5100
Indole-5-carboxylic acid	275, 283, 289, 306, <u>312</u>	<u>321</u>, 336, 344	900	5200
5-bromoindole	272, 277, 280, 286, <u>299</u>	<u>307</u>, 320, 326, 335, 340	900	3700
5-chloroindole	274, 280, 286, <u>296</u>	<u>301</u>, 306, 315, 327	600	3300
5-methoxyindole	273, 282, 287, 294, 300, <u>307</u>	<u>309</u>, 316, 323, 329, 335	200	4300
5-aminoindole	277, <u>308</u>	<u>321</u>, 327, 337, 353	1300	4900
5-nitroindole	272, 281, 288, 298, <u>308</u>	<u>314</u>, 320, 326, 335, 340	600	4900
Indole	272, 279, <u>288</u>	<u>295</u>, 307, 320, 326, 334	800	2900
5-hydroxyindole	275, 289, 300, <u>310</u>	<u>314</u>, 318, 328, 334	400	4500

Table 5.1 Fluorescence excitation and emission data for indole and some 5-substituted derivatives in ethanol at 77K. The origin bands of the S_1 state in the excitation and emission spectra are underlined. $\Delta \bar{\nu}_{0\text{-}0}$ is the difference between the excitation and emission 0-0 transitions. $\Delta \bar{\nu}_{max}$ is the difference between the excitation maximum and emission 0-0 transition.

The results in Table 5.1 indicate that for all the monomers emission is from the ^1L_b state, characterised by a small Stokes shift between the excitation and emission 0-0 transitions. This is markedly different from the behaviour at room temperature. For example the Stokes shift for 5-cyanoindole in ethanol at room temperature is 7800 cm^{-1} (due to excitation to the ^1L_a state and emission from the relaxed ^1L_a state) whereas at 77K it is 900 cm^{-1} (due to $^1L_{b\ 0\text{-}0}$ excitation and $^1L_{b\ 0\text{-}0}$ emission). Results from low temperature analysis of indole, Indole-5-carboxylic acid and 5-methoxyindole have been reported elsewhere [1, 2, 3], with the most notable observations being from Lami et al. They measured the Stokes shift as a function of temperature in glycerol, finding that below –50°C there was very little change in the Stokes shift, indicating the absence of any solvent relaxation during the excited state lifetime. Thus it was inferred that emission at low temperatures is from the ^1L_b state. In Table 5.1 values are given both for the Stokes shift between the 0-0 bands and for separation between the excitation maximum (onset of the ^1L_a state) and the 0-0 emission transition. The latter gives an indication of the ^1L_a-^1L_b separation. The values of both of these parameters are similar to those observed in isopentane at room temperature, confirming that in ethanol at 77K, emission is from the ^1L_b state.

The vibrational progression in the emission spectrum is a mirror image of the excitation spectrum, with a separation between each peak in the progression of approximately 700cm^{-1}. Each peak in the excitation and emission progression is likely to be the superposition of a number of vibronic transitions, but the 700 cm^{-1} interval is dominant. A fundamental mode of approximately 700 cm^{-1} has been observed [4, 5] as the predominant vibronic transition in the supersonic jet spectrum of the ^1L_b state of indole. This mode probably corresponds to a symmetric ring breathing vibration.

5.2.1.1 Substituent effects

In section 4.2.1 there is a discussion concerning the effect of substituent upon the emission properties in the low polarity solvent isopentane. At low temperature in ethanol there is a similar solvent environment, with emission being observed from the ^1L_b state, allowing a comparison with the room temperature isopentane measurements. A plot of the Hammett constant versus emission wavenumber for the monomers in ethanol at low temperature is shown in Figure 5.2. A very similar trend is observed compared to the room temperature results. As the Hammett constant increases to both positive and negative values, the position of the 0-0 emission transition moves to longer wavelength (lower energy). The anomalous value for indole-5-carboxylic acid may be due to a specific ground state hydrogen-bonding interaction with ethanol.

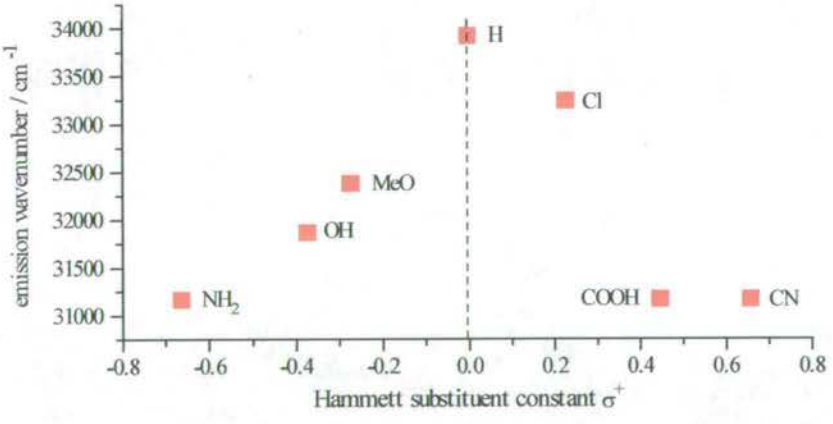

Figure 5.2 Plot of emission wavenumber (for the 0-0 transition) against the Hammett Substituent constant for indole and a selection of 5-substituted derivatives in ethanol at 77K.

Another interesting observation at low temperature is the emission spectrum for 5-nitroindole. At room temperature there is only a very weak emission, which is difficult to resolve. However, at low temperature the fluorescence emission is observable and has a very similar vibrational structure to the other indole monomers. This similarity implies that the first singlet excited state (S_1) of 5-nitroindole is of a similar nature to the other indoles resulting from a π-π^* transition. This suggests that the n-π^* state invoked to explain the low quantum yield of this molecule is a triplet state; this is discussed further in section 5.2.2.

5.2.2 Phosphorescence

All of the monomers examined have further emission peaks at longer wavelengths due to phosphorescence emission, as illustrated for 5-cyanoindole in Figure 5.3. For all the monomers except 5-nitroindole, there is considerable vibronic structure in the phosphorescence emission with spacing of approximately 450cm^{-1}. Excitation spectra were collected using emission wavelengths in the fluorescence and phosphorescence regions. These were found to be identical, which confirmed that the emission was in fact phosphorescence and arose from the triplet state of the same species as the fluorescence.

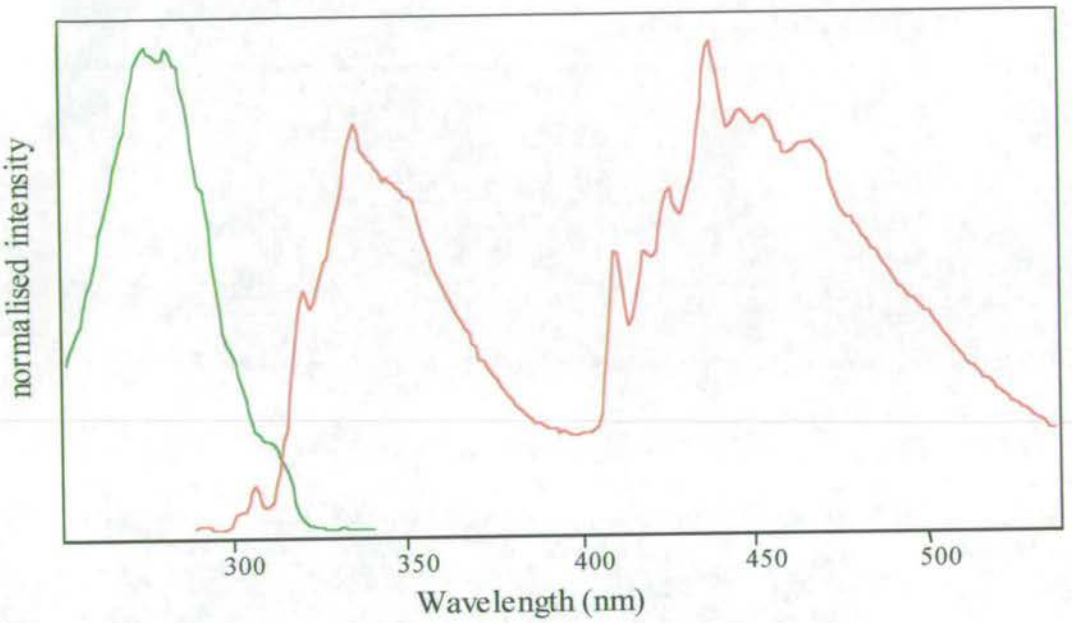

Figure 5.3 Excitation and emission spectra for 5-cyanoindole monomer in ethanol at 77K, with an emission wavelength of 350nm and excitation wavelength of 280nm.

The phosphorescence properties of the various monomers are summarised in Table 5.2. The relative intensity of the fluorescence to phosphorescence emission is calculated as the ratio of the integrated area under the fluorescence emission spectrum (corrected for photomultiplier response) to the area under the phosphorescence spectrum.

monomer	Phosphorescence maxima/nm	$S_1 - T_1$ separation / cm^{-1}	Relative intensity fluorescence/phosphorescence
5-cyanoindole	<u>411</u>, 418, 426, 438, 447,453, 467	6822	0.582
Indole-5-carboxylic acid	<u>409</u>, 415, 424, 435, 451, 464	6703	0.204
5-bromoindole	<u>408</u>, 413, 423, 436, 450, 464	8663	0.029
5-chloroindole	<u>409</u>, 414, 422, 436, 442, 446, 451, 466	8773	0.314
5-methoxy indole	<u>401</u>, 417, 435, 432, 439, 447, 454, 464	7425	5.895
5-aminoindole	<u>416</u>, 431, 446, 462, 469, 474	7114	4.400
5-nitroindole	470	Not applicable	0.110
indole	<u>405</u>, 417, 432, 446, 458	9207	2.943
5-hydroxy indole	<u>410</u>, 417, 425, 432, 439, 447, 454, 464	7457	3.421

Table 5.2 Phosphorescence emission values, relative intensity of fluorescence to phosphorescence and separation between the 0-0 transitions of the singlet and triplet states. The origin bands of the T_1 state are underlined.

All of the monomers have similar structure in their phosphorescence emission spectra except for 5-nitroindole, which has a very broad, featureless spectrum as shown in Figure 5.4. At room temperature there is very little fluorescence emission from 5-nitroindole implying efficient intersystem crossing because of a low lying n-π^* state. This could be the triplet state, singlet state or both. At room temperature, intersystem crossing acts as a non-radiative pathway, since emission from the triplet state is quenched; however, at low temperature this results in a very intense phosphorescence emission. The very different appearance of the phosphorescence emission of 5-nitroindole compared to the other indole monomers can be attributed to the T_1 state being an n-π^* state rather than a π-π^* state, as in the other indoles. As previously mentioned, the fluorescence emission of 5-nitroindole at low temperature is very similar to the other indoles, therefore the S_1 state is likely to be a π-π^* state.

The intensity of the phosphorescence emission is highly dependent upon the functional group, as can be seen from the values of relative intensities of fluorescence to phosphorescence in Table 5.2. This effect is most noticeable for 5-bromoindole where the intensity of phosphorescence emission is far greater than the intensity of fluorescence emission. The excitation, fluorescence and phosphorescence spectra for 5-bromoindole are shown in Figure 5.5. The presence of the heavy atom, bromine, greatly enhances spin-orbit coupling, and increases the rate of intersystem crossing from the singlet to the triplet manifold as discussed in Chapter Two. The intensity of phosphorescence depends upon both the efficiency of (S_1-T_1) intersystem crossing and on the quantum yield of the radiative phosphorescence transition, from the T_1 state to the S_0 ground state. There is an interesting comparison between 5-nitroindole and 5-bromoindole. At room temperature 5-bromoindole has a more intense fluorescence emission than 5-nitroindole,

implying that (S_1-T_1) intersystem crossing is more efficient for 5-nitroindole. However, at low temperature there is a greater relative intensity of 5-bromoindole phosphorescence, implying that there is a higher quantum yield of emission from the T_1 state of 5-bromoindole than 5-nitroindole.

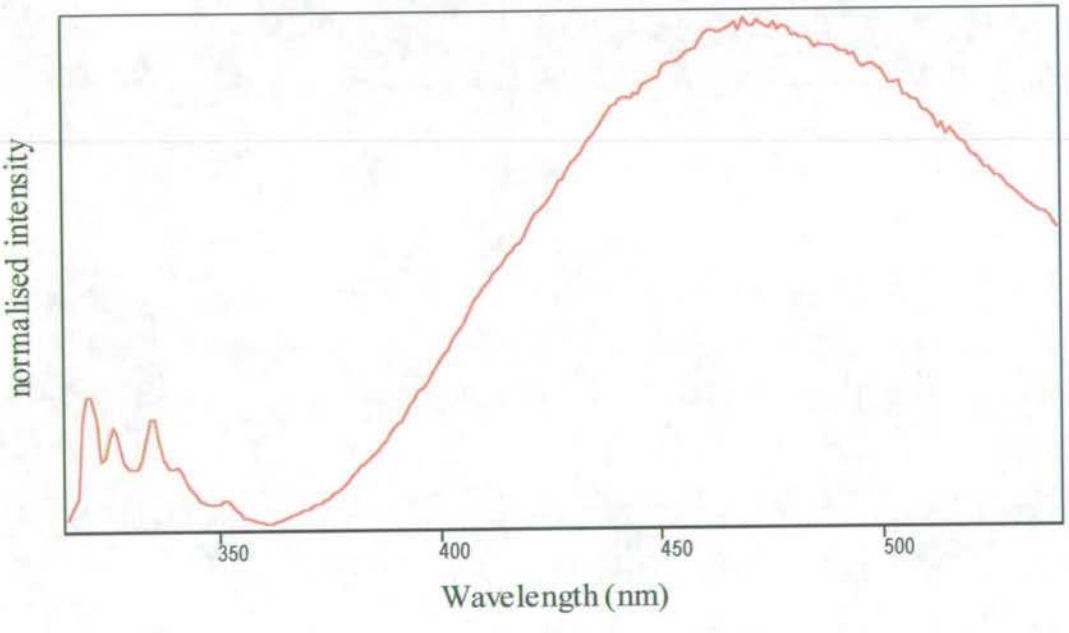

Figure 5.4 Emission spectrum for 5-nitroindole in ethanol at 77K using an excitation wavelength of 280nm.

Both 5-cyanoindole and indole-5-carboxylic acid have a relatively intense phosphorescence emission, although they have no heavy atom effect or n-π^* state to explain this. These monomers also have an intense fluorescence emission, implying that the rate of intersystem crossing (k_{isc}) is not very great. Therefore, they must have a phosphorescence quantum yield (ϕ_p) close to unity.

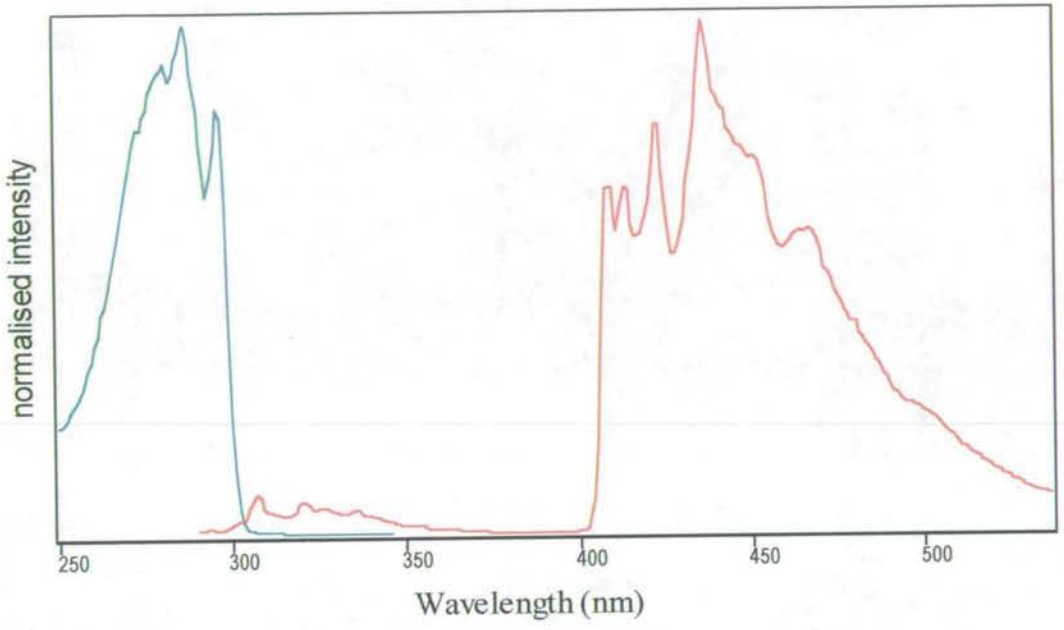

Figure 5.5 Excitation and emission spectra for 5-bromoindole monomer in ethanol at 77K with an emission wavelength of 450nm and excitation wavelength of 280nm.

There is little variation in the wavelength of phosphorescence for the different monomers. The value of the singlet triplet separation (given in Table 5.2) varies due to the variation in the wavelength of the fluorescence emission. This shows that although the energy of the emitting singlet excited state (shown to be the ^1L_b state at 77K) is greatly affected by the functional group, there is little effect on the energy of the triplet state. Since at this temperature there is no environmental effect (such as solvent relaxation) this observation implies that the energy of the T_1 state is insensitive to the nature of the substituent. The nature of the triplet state in indoles has been studied theoretically by Callis et al [7] who find that the triplet ^3L_a state has a much smaller permanent dipole moment than the singlet ^1L_a state.

5.3 Electrooxidised indole trimers

All the electrooxidised indoles examined in Chapter Three were studied at low temperature, with the aim of obtaining better resolution in the fluorescence excitation and emission spectra and ascertaining the presence and nature of any phosphorescence emission.

5.3.1 Fluorescence of the trimer species

Initially, samples for study were produced with a high trimer content, so that the emission spectra would be less complicated. Cooling the trimer samples down to 77K had the expected effect of shifting the emission to slightly shorter wavelengths, reducing the Stokes shift and providing far better vibronic resolution. The fluorescence data are presented in Table 5.1 along with a calculation of the Stokes shift. Figure 5.6 shows the excitation and emission spectra at 77K for 5-cyanoindole trimer, illustrating the increased resolution of excitation and emission peaks. The shift to shorter wavelengths of the emission spectrum is much smaller for the trimer species than was seen for the monomer, with emission peaks moving by only a couple of nanometers. This is consistent with the much smaller solvent effect observed for the trimer species as illustrated in Chapter 4. The resolution of peaks in the emission spectrum is far greater at 77K and a vibronic progression is seen with a spacing of 1300 cm^{-1}. As in the monomer, this may be due to a symmetric ring breathing mode.

Trimer	Excitation maxima/nm	Fluorescence maxima/nm	Stokes shift $\Delta \bar{\nu}$ /cm^{-1}
5-cyanoindole	408, 386, 360, 346, 319, 275.	416, 440, 468.	471.
Indole-5-carboxylic acid	404, 384, 360, 348, 323, 273.	408, 431, 455.	243.
5-bromoindole	405, 384, 359, 343, 314, 267.	412, 432.	419.
5-chloroindole	405, 383, 364, 314, 279.	412, 435, 461.	420.
5-methoxyindole	406, 384, 368, 314, 277.	412, 434, 460.	359.
5-nitroindole	372, 330.	N/A	N/A
5-hydroxyindole dimer	350, 333, 324, 293, 260	354, 374, 396, 415	323
5-hydroxyindole trimer	412, 391, 366, 350, 314, 282	414, 439, 465	117
Indole trimer	397, 377, 350, 335, 305, 275	399, 422, 447	126
Aggregated indole trimer	434, 374, 349, 332, 310, 275	403, 425, 433, 460	

Table 5.3 Fluorescence excitation and emission data for the electrooxidised indoles. The origin bands of the S_1, S_2 and S_3 states in the excitation spectra are underlined. The Stokes shift is calculated as the difference between excitation and emission 0-0 transitions.

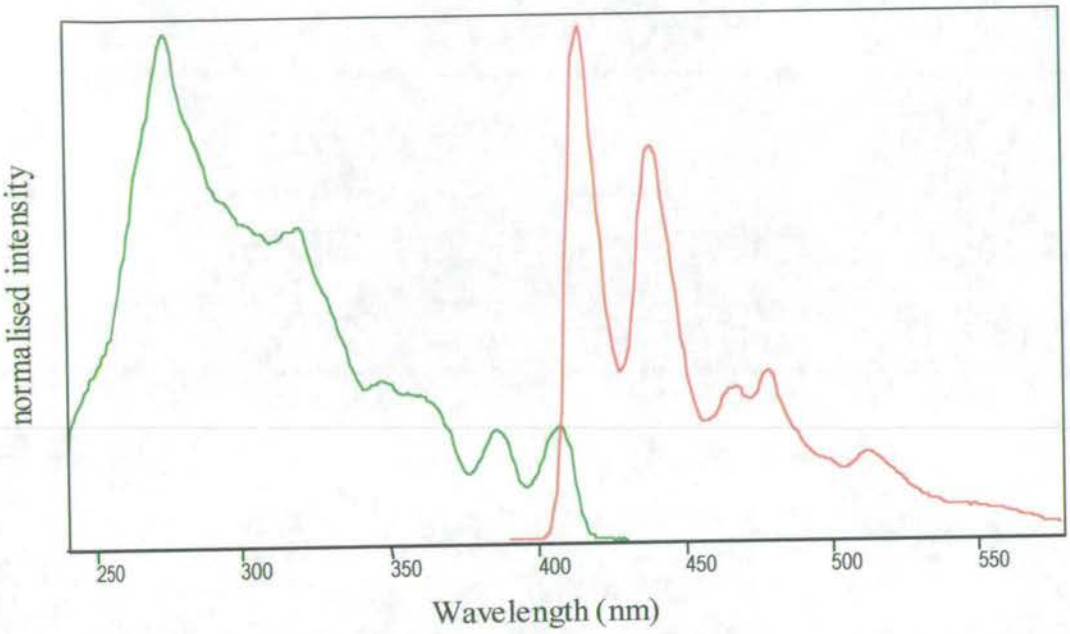

Figure 5.6 Excitation and emission spectra for 5-cyanoindole trimer in ethanol at 77K, using an emission wavelength of 450nm and an excitation wavelength of 320nm respectively.

5.3.2 Phosphorescence of the trimer species

The trimers were observed visually to have a phosphorescence emission, but it appeared to underlie the fluorescence emission and was therefore difficult to quantify. As can be seen in Figure 5.6 there are further peaks in the emission spectrum that do not fit into the vibronic progression and may be due to phosphorescence. The 5-bromoindole trimer was the exception in that it displayed a very intense phosphorescence emission, far greater than the fluorescence emission. This is shown in Figure 5.7, for a sample of 5-bromoindole electropolymerised to

favour the trimer species. As explained for the monomer, the intense phosphorescence is due to the presence of a heavy atom. This very intense phosphorescence confirms that there is efficient intersystem crossing from the singlet excited state, giving a much lower fluorescence quantum yield than for the other electrooxidised indoles.

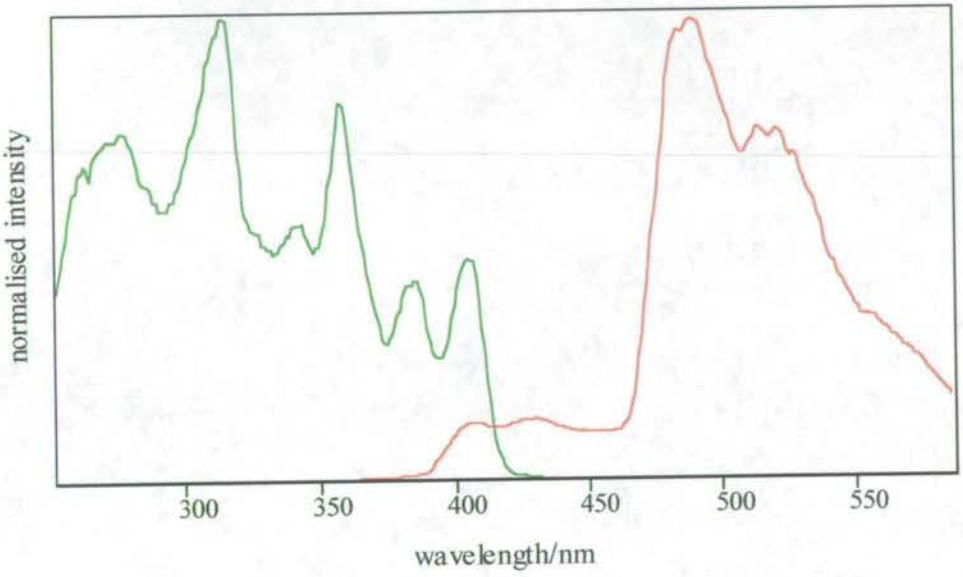

Figure 5.7 Excitation and emission spectra for 5-bromoindole trimer in ethanol at 77K, with an emission wavelength of 500nm and an excitation wavelength of 320nm.

In order to observe the phosphorescence spectra of the other indole trimers, a shutter system was used allowing fluorescence emission to be eliminated and only the phosphorescence emission to be collected (refer to section 3.4.4 for details). This was very effective in providing well resolved phosphorescence spectra. Figure 5.8 shows the emission spectra of indole-5-carboxylic acid in ethanol at 77K. Spectrum A is the combination of fluorescence and phosphorescence emission

observed without using the shutters. The phosphorescence emission can be seen in the long wavelength tail of the fluorescence spectrum. Spectrum B was collected using a 10ms delay between the excitation and emission shutters, allowing any fluorescence emission to decay before the emission shutter opens. The result is a phosphorescence spectrum with no contaminating fluorescence, with well-resolved peaks showing a vibronic progression of $1300cm^{-1}$ as seen for the fluorescence.

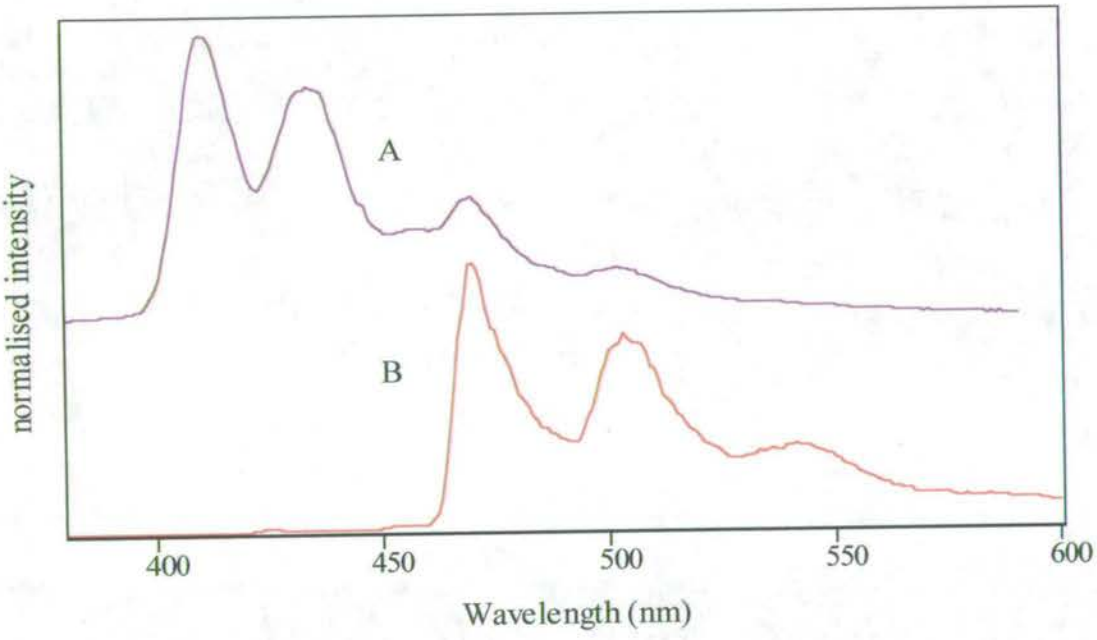

Figure 5.8 Fluorescence (A) and phosphorescence (B) emission spectra for indole-5-carboxylic acid in ethanol at 77K. For both spectra an excitation wavelength of 320nm was used. A was collected without the use of the shutter system. B was collected with a 10ms delay between excitation and emission shutters.

The data for phosphorescence emission from the series of indole trimer species is shown in Table 5.4, along with the separation between the 0-0 transitions of the S_1 and T_1 states. The increased resolution gained by using the shutter system allows an energy level diagram to be constructed for the singlet and triplet states, as shown for 5-cyanoindole trimer in Figure 5.9.

Trimer	Phosphorescence maxima/nm	S_1 - T_1 separation/cm^{-1}
5-cyanoindole	480, 514, 551	3205
Indole-5-carboxylic acid	469, 503, 536	3188
5-bromoindole	490, 519	3864
5-chloroindole	481, 500	3482
5-methoxyindole	480, 514	3439
5-nitroindole	539	N/A
5-hydroxyindole Trimer	487, 522	3621
Indole trimer	466, 499	3603

Table 5.4 Phosphorescence emission values and separation between the 0-0 transitions of the S_1 and T_1 states for the electrooxidised indoles. The origin bands of the T_1 state are underlined.

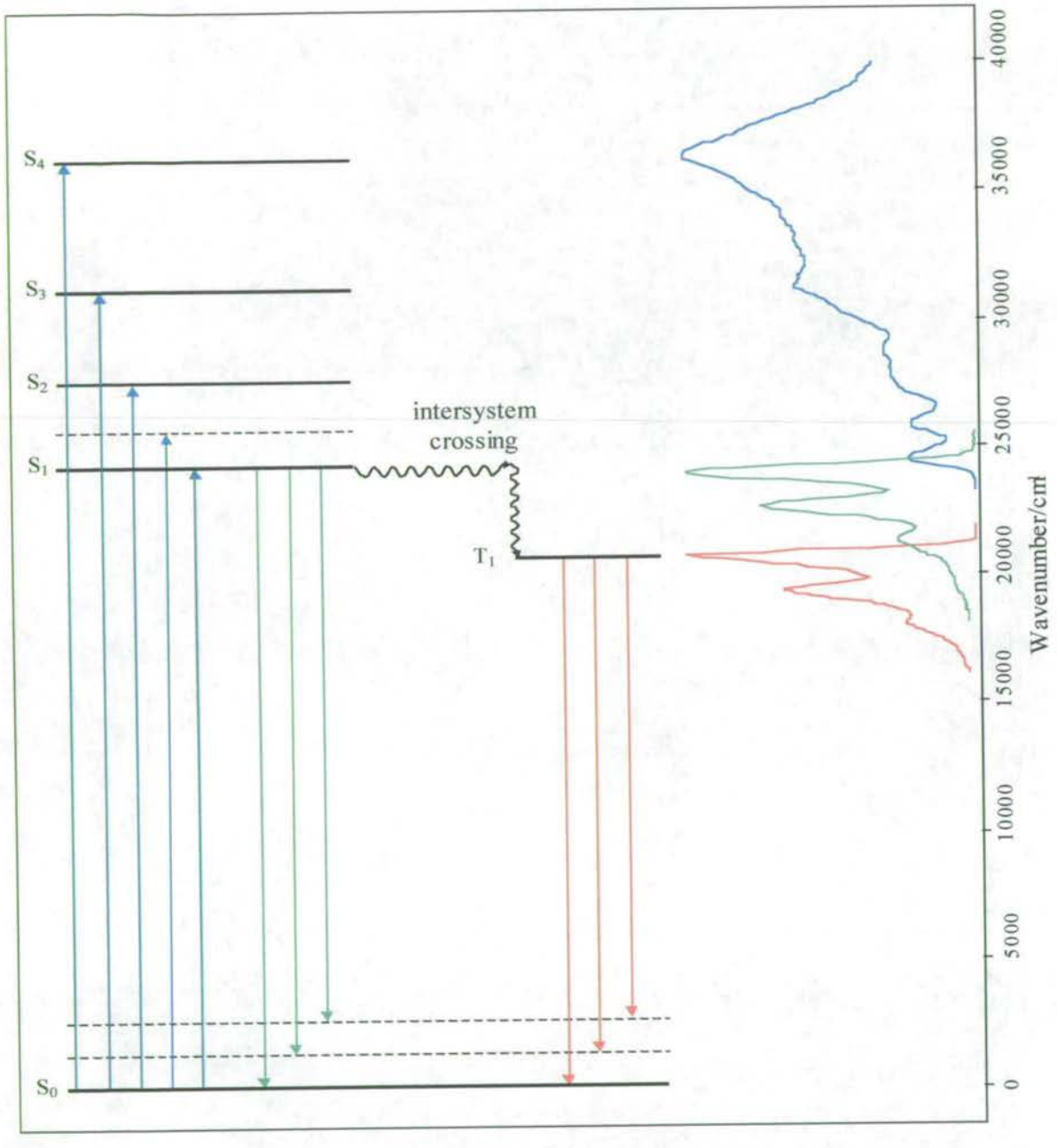

Figure 5.9 Energy level diagram for 5-cyanoindole showing singlet and triplet states.

The T_1 state of the trimer species is at lower energy than the T_1 state of the monomers species. This is consistent with the energy difference between the S_1 states of the monomer and trimer. The difference in S_1 energies between the trimer and monomer varies between 7000 cm^{-1} and 9000 cm^{-1} whilst the difference in T_1 energies vary between 3000 cm^{-1} and 4000 cm^{-1}, as summarised in Table 5.5. This lowering in energy can be explained by a greater delocalisation of the π-electrons in the trimer species. The S_1-T_1 separation is considerably smaller for the trimer species than is observed for the monomer; the S_1 and T_1 states of the trimer are very close in energy with a separation of only 3000 cm^{-1}.

	$S_{1\ 0\text{-}0}$ trimer – S_1 (^1L_b)$_{0\text{-}0}$ monomer $\Delta\bar{\nu}$ /cm^{-1}	T_1 (trimer) – T_1(monomer) $\Delta\bar{\nu}$ /cm^{-1}
5-cyanoindole	7110	3500
Indole-5-carboxylic acid	6640	3130
5-bromoindole	8300	4102
5-chloroindole	8950	3660
5-methoxyindole	8090	4100
5-nitroindole	N/A	(2720)
Indole	8830	2930

Table 5.5 Separation in energy between the S_1 and T_1 0-0 transitions of the monomer and trimer.

5.3.3 Electrooxidised indoles with unusual behaviour

Studies at room temperature showed that not all the 5-substituted indoles possessed identical fluorescence properties, with 5-aminoindole and 5-hydroxyindole giving soluble electropolymerisation products, 5-nitroindole being non-fluorescent and unsubstituted indole subject to aggregation effects. The use of low temperature analysis has allowed further insight into some of these differences.

5.3.3.1 5-nitroindole trimer

At room temperature no fluorescence emission was observed for the electrooxidised 5-nitroindole species. This proved to be very useful for studying films of the insoluble trimers grown on a 5-nitroindole template. The absence of fluorescence, as for the monomer species, was attributed to an n-π^* state associated with the nitro group, enhancing intersystem crossing. Analysis at low temperature gave the expected result of a large, broad, phosphorescence emission centred at 539nm, with very little, if any, fluorescence being observed. The presence of a broad phosphorescence emission meant that films of the insoluble trimers grown on 5-nitroindole could not be studied easily at low temperature, since any emission would be confused with that of the 5-nitroindole phosphorescence. The nature of the phosphorescence of the trimer species is very similar to that of the monomer species, with little or no fluorescence emission at room temperature and a broad phosphorescence emission at low temperature. The phosphorescence emission of the 5-nitroindole trimer is very different to that of the other trimer species, implying a difference in the nature of the T_1 state. In light of the monomer results, it is likely that phosphorescence from the trimer originates from an n-π^* T_1 state.

5.3.3.2 Indole trimer

Room temperature analysis of electropolymerisation products of unsubstituted indole showed that under certain conditions a further species was present as well as the expected trimer. It appeared that this species could be a π-complex formed between trimer species in the reduced state manifested by additional emission peaks at longer wavelength, whereas in the oxidised state only trimer emission was observed. By cooling the samples down to 77K the differences in the emission of these two species were much better resolved. This can be seen in Figure 5.10. The uncomplexed trimer species exhibits the expected excitation and emission spectra as illustrated by A and B, with the longer wavelength emission peaks being due to phosphorescence. When a reducing agent is added additional peaks are observed as seen in C and D, these peaks are better resolved in the low temperature spectrum than at room temperature (see figure 4.19). This better resolution clearly shows the presence of two distinct species, although it does not help in determining exactly what the second species is.

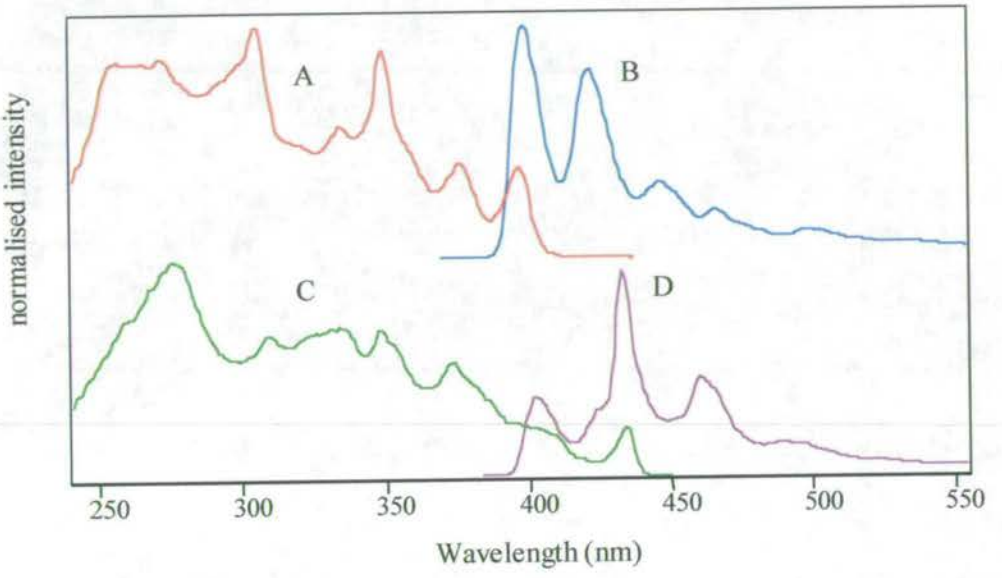

Figure 5.10 Excitation and emission spectra for unsubstituted indole trimer in its oxidised state (A and B) and reduced state (C and D). A and C were collected with an emission wavelength of 460nm. B and D were collected with an excitation wavelength of 320nm.

5.4 Indole polymers

After the trimer species had been characterised at low temperature, samples were produced with conditions favouring linking to form the polymer. Chemically polymerised samples, that had been synthesised using an excess of oxidant to encourage polymer formation, were also examined. In all these cases no phosphorescence emission was observed from the polymer and the polymer fluorescence emission was hidden under phosphorescence from any remaining trimer. A wide range of samples was examined with a systematic variation of excitation and emission wavelengths, with the same negative result. There are a two predominant factors

affecting the phosphorescence intensity, one is the efficiency of $S_1 - T_1$ intersystem crossing, the other is the radiative efficiency, or quantum yield, of phosphorescence. From fluorescence lifetime measurements (presented in Chapter Six) we know that there are more non-radiative decay channels in the polymer, therefore there are more non-radiative pathways to compete with S_1-T_1 intersystem crossing. These non-radiative channels which quench the fluorescence emission are likely to have a similar effect on the phosphorescence, therefore reducing the phosphorescence quantum yield. Therefore a combination of reduced intersystem crossing and increased phosphorescence quenching compared to the trimer species is likely to lead to the observed absence of phosphorescence in the polymer.

5.5 Phosphorescence lifetimes

Installation of the shutter system (described in section 3.4.4) not only allowed phosphorescence spectra to be collected, but also made the measurement of the relatively long phosphorescence lifetimes possible. The technique involved closing the excitation shutter, then opening the emission shutter after all fluorescence had decayed. The emission shutter was left open until the phosphorescence had decayed and the data was collected using a time base scan. Since the light source is not pulsed, the decay is only collected for the equivalent of one light pulse, therefore the results are not as reliable as the fluorescence lifetimes derived from single photon counting data presented later in this thesis. Nevertheless, a good estimate of the phosphorescence lifetime can be obtained. Phosphorescence lifetime data was collected for all the monomer species and a selection of the trimer species.

5.5.1 Phosphorescence lifetimes of the monomer species.

For all the monomers examined above, a measurement of the phosphorescence lifetime was made. Table 5.6 gives the phosphorescence lifetimes of the monomer species, measured in ethanol at 77K.

Monomer	Phosphorescence lifetime / seconds
5-cyanoindole	6.9
Indole-5-carboxylic acid	4.9
5-methoxyindole	3.9
Indole	3.2
5-hydroxyindole	3.1
5-aminoindole	2.5
5-chloroindole	1.1
5-nitroindole	0.72
5-bromoindole	0.05

Table 5.6 Phosphorescence lifetimes for indole and its 5-substituted derivatives. The samples were dissolved in ethanol and measurements taken at 77K with an excitation wavelength of 280nm and emission wavelength of 440nm.

Figure 5.11 shows the raw data obtained using the shutter system for a sample of 5-bromoindole monomer. An estimate of the phosphorescence lifetime is made and the emission shutter held

open until the phosphorescence has completely decayed. The data is collected on a time-base scan with more than one decay collected to ensure reproducibility. The decay portion of the data is then removed to a spreadsheet and fitted to a single exponential function as illustrated in Figure 5.12 for a sample of 5-chloroindole monomer.

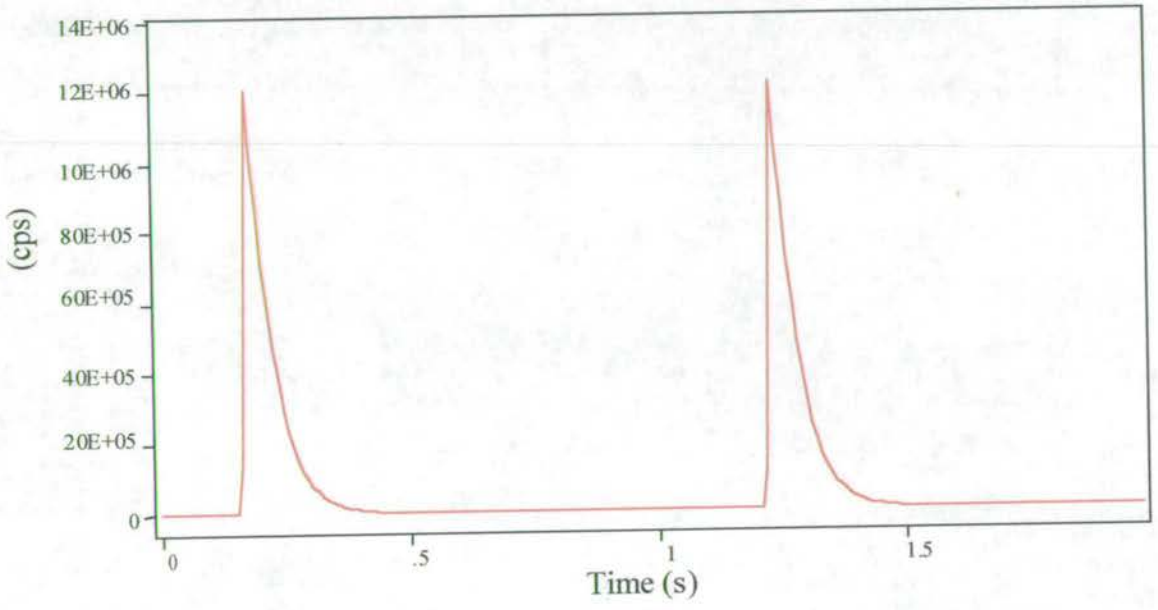

Figure 5.11 Raw data showing the phosphorescence decay of 5-bromoindole monomer in ethanol at 77K, with a delay of 10 milliseconds between the opening of the emission shutter and closing of the excitation shutter and with the emission shutter remaining open for 1 second. An excitation wavelength of 280nm and emission wavelength of 440nm was used.

Since the monomers are a single species and are at low temperature and low concentration, there should be very little solvent or self-absorption effect. Therefore the phosphorescence emission is

expected to follow single exponential decay kinetics; this has been assumed in obtaining the fitted lifetimes given in Table 5.6. However some of the fits were not very good and could have been better fitted by bi-exponential functions. This is most likely to be due to impurities in the samples and solvents. Also, because the low intensity and long lifetime of phosphorescence emission from some of the samples, the signal to noise ratio is rather low.

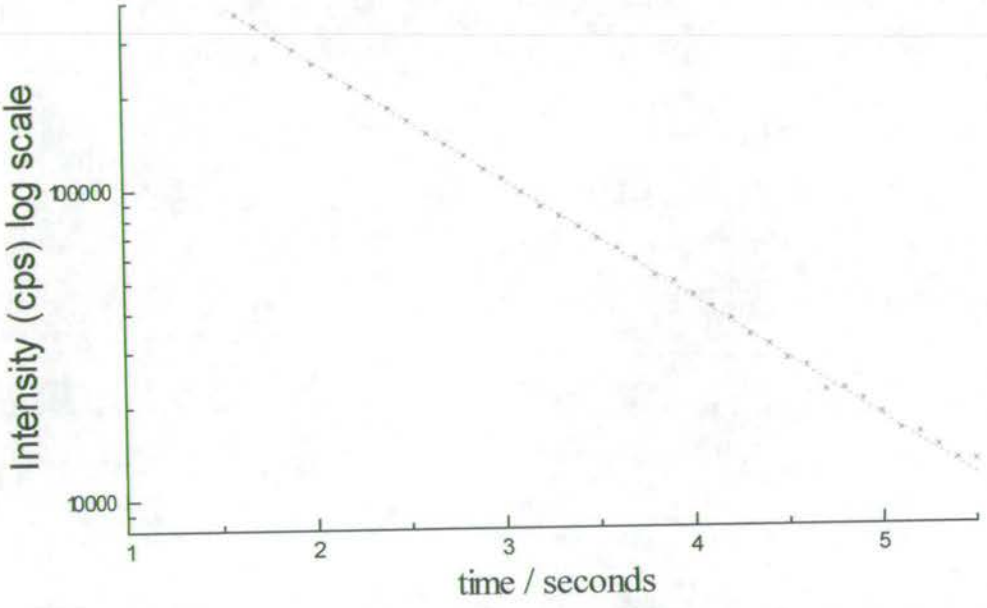

Figure 5.12 Processed data for the phosphorescence decay of 5-chloroindole monomer in ethanol at 77K using an excitation wavelength of 280nm and emission wavelength of 440nm. The data is shown as points (x) and a fitted single exponential decay is shown as a dashed red line.

The results for the monomers presented in Table 5.6 show several expected features. The shortest lifetime is that of 5-bromoindole with a value of only 50 milliseconds compared to almost 7 seconds for 5-cyanoindole. Once again this can be attributed to the presence of enhanced spin-orbit coupling generated by the heavy bromine atom. Due to this spin orbit coupling there is greater mixing of the singlet and triplet states allowing the spin forbidden transition between the T_1 and S_0 states to occur much more rapidly, therefore reducing the lifetime of the triplet state. The presence of the less heavy chlorine atom in 5-chloroindole can be seen to have some effect, with a lifetime of 1.1 seconds. The lifetime of 5-nitroindole is also much shorter than the other indoles with a value of 0.72 seconds. This is consistent with the suggestion that the triplet state has n-π^* character, therefore enhancing spin orbit coupling and allowing the spin forbidden transition between T_1 and S_0 to occur more rapidly. Of the species which do not have a heavy atom (or n-π^* state), it is notable that 5-cyanoindole and indole-5-carboxylic acid, which showed the greatest phosphorescence to fluorescence ratio, also have the longest phosphorescence lifetimes. This is consistent with these molecules having a high quantum yield of phosphorescence.

5.5.2 Phosphorescence lifetimes of the trimer species.

Phosphorescence lifetime measurements were made for the trimer species of 5-cyanoindole, indole-5-carboxylic acid and 5-bromoindole, since these were the only samples ready for study in the short period that the shutter system was available. These samples give a representative illustration of the extremes of the phosphorescence lifetimes expected. The results obtained from single exponential fits of the phosphorescence decay data are given in Table 5.7.

Trimer	Phosphorescence lifetime / seconds
5-cyanoindole	4.5
Indole-5-carboxylic acid	4.2
5-bromoindole	0.1

Table 5.7 Phosphorescence lifetimes for a selection of 5-substituted indole trimers. The samples were dissolved in ethanol and measurements taken at 77K with an excitation wavelength of 320nm and emission wavelength of 520nm.

It is highly possible that electrooxidation of the monomer does not produce solely individual trimer units, but trimers, dimers of trimers and oligomers of trimers (this will be explored in greater detail in Chapter 6). No phosphorescence emission has been observed from the long chain length polymer species, however, much shorter oligomers may well have a phosphorescence emission. This is not resolved in the steady state phosphorescence emission, but may have considerable effect on the decay behaviour. The quality of data from these phosphorescence measurements is not good enough to make quantitative multiexponential fits, therefore only single exponential estimates have been made. However, it is apparent that more than one species is contributing to the phosphorescence decay. This is illustrated in Figure 5.13 for a sample of 5-cyanoindole trimer in ethanol at 77K. The decay has been fitted to a bi-exponential function, giving lifetimes of 4.5 seconds (as obtained from a single exponential fit) and 0.2 seconds. The decay for indole-5-carboxylic acid can be fitted to lifetimes of 4.2 seconds and 0.45 seconds, with the decay for 5-bromoindole fitting to 0.13 seconds and 0.08 seconds. These lifetimes are only estimates but give an idea of the presence of other emitting species. The

time resolution of the shutter system is limited and decays of less than 10 ms, which may be present, will not be detected. The lifetimes of several seconds for electropolymerised 5-cyanoindole and indole-5-carboxylic acid are comparable to those observed for the monomer and are assumed to be due to trimer species. The much shorter decay component may be due to polymeric species with much enhanced rates of non-radiative decay of the T_1 state.

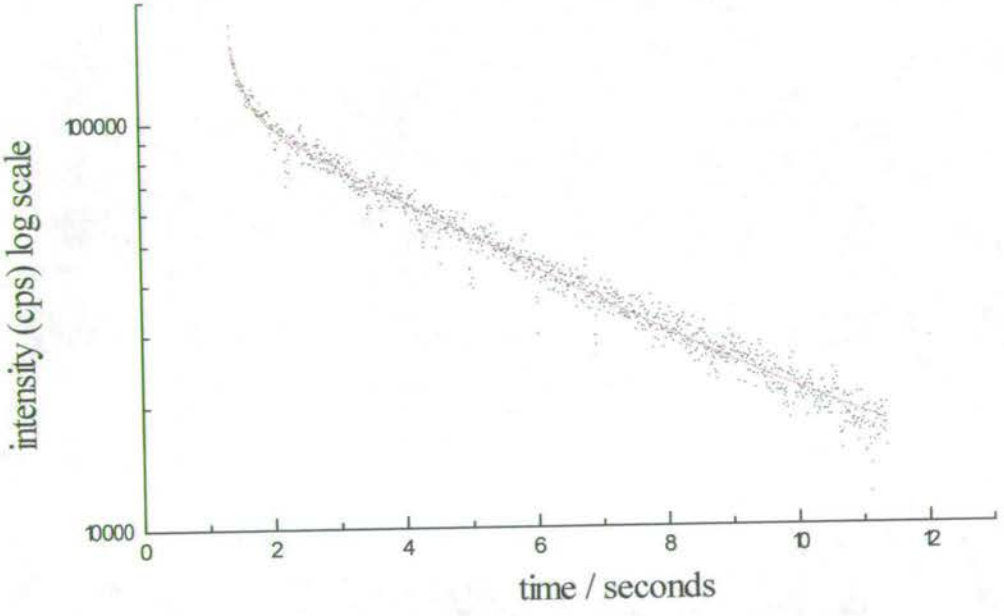

Figure 5.13 Processed data for the phosphorescence decay of Indole-5-carboxylic acid trimer in ethanol at 77K using an excitation wavelength of 320nm and emission wavelength of 520. The data is shown as points (x) and a fitted double exponential decay is shown as a solid red line.

The phosphorescence lifetimes for the trimer species are similar to those of the monomer, with a similar effect observed for both the presence of a heavy bromine atom and a nitro group. This similarity implies that the rates of radiative and non-radiative decay from the T_1 state are very similar for both monomer and trimer species.

5.6 The potential importance of the triplet state for electrogenerated chemiluminescence.

Polymerised 5-substituted indoles have been proposed as potential materials for electroluminescent devices and the mechanism of electrogenerated chemiluminescence (ECL) is presently being studied. ECL is the emission of light from intermediates produced during electrochemical reactions where the energy liberated is sufficient to generate an electronically excited species. For the propagation of an ECL reaction, radical ions are generated electrochemically, giving an electron acceptor $A^{\bullet+}$ and an electron donor $D^{\bullet-}$ which diffuse together forming an encounter complex. This complex may then dissociate via electron transfer to form either an emitting excited singlet state $^1A^*$ or a non-emitting excited triplet state $^3A^*$. This is illustrated by the following reaction scheme:

$$A - e^- \rightarrow A^{\bullet+} \qquad (5.1)$$

$$D + e^- \rightarrow D^{\bullet-} \qquad (5.2)$$

$$A^{\bullet+} + D^{\bullet-} \rightarrow {}^1A^* + D \qquad (5.3)$$

$$\rightarrow {}^3A^* + D$$

$$^1A^* \rightarrow A + h\upsilon \qquad (5.4)$$

There are two possible routes to the generation of $^1A^*$, by direct excitation, or via triplet-triplet annihilation. In systems where there is insufficient energy to directly produce the excited singlet state, it is possible for the singlet excited state to be produced via triplet-triplet annihilation where two excited triplet states diffuse together and transfer energy to form an excited singlet state and a ground state molecule:

$$^3A^* + {}^3A^* \rightarrow {}^1A^* + A \qquad (5.5)$$

$$^1A^* \rightarrow A + h\upsilon \qquad (5.6)$$

The mechanism of triplet-triplet annihilation allows ECL reactions to proceed where there is insufficient electrochemical energy to generate the excited singlet state directly. This mechanism is attractive for practical uses since it requires a lower redox potential to be applied to produce each triplet state than directly to produce the singlet state. Therefore the potential applied to generate luminescence, which if too high might damage the system, can be kept lower. In order to identify systems which can generate ECL by the triplet-triplet annihilation route, it is neccessary to know the energy of the triplet state relative to the ground and singlet states. This has been achieved using low temperature analysis to obtain phosphorescence emission spectra.

5.7 Conclusions

Cooling samples down to 77K using liquid nitrogen has been shown to be of considerable benefit for collecting a greater wealth of information about the luminescence properties of both the monomer and trimer species. The resolution of the fluorescence excitation and emission

spectra are greatly increased upon cooling giving data on the 0-0 transition and the vibronic progressions of the monomer and trimer species. Freezing the solvent into a solid matrix reduces any solvent relaxation effects giving more intense spectra with shorter wavelength emissions than at room temperature. Freezing the solvent also reduces oxygen quenching of the triplet state and phosphorescence emission has been observed for all the monomer and trimer species. This allows the energy of the triplet state to be measured relative to the ground and first singlet excited states with potential importance in the investigation of electrogenerated chemiluminescence. No phosphorescence emission was observed for the polymer species implying that non-radiative decay of the S_1 state competes with intersystem crossing and that the T_1 state is subject to similar non-radiative channels.

The use of a shutter system to gate out the fluorescence emission allowed phosphorescence spectra to be recorded and phosphorescence lifetimes to be estimated. Similar effects of the bromo and nitro substituents on the phosphorescence emission were seen for both the monomer and trimer species. The presence of the heavy bromine atom greatly increased the intensity of phosphorescence and shortened the phosphorescence lifetime due to enhanced spin orbit coupling. In 5-nitroindole an n-π^* transition also enhances intersystem crossing and an intense phosphorescence emission with a short lifetime is observed. For both the 5-nitroindole monomer and trimer species, the triplet T_1 state has been identified as an n-π^* state and the singlet S_1 state as a π-π^* state.

References

1. P. S. Song, W. E. Kurtin, *J. Am. Chem. Soc.*, 1969, 4892.
2. J. J. Aaron, A. Tine, C. Villiers, C. Parkanyi, D. Bouin, *Croatica Chem. Acta.*, 1983, **56(2)**, 157.
3. H. Lami, N. Glasser, *J. Chem. Phys.*, 1986, **84(3)**, 597.
4. M. J. Tubergen, D. H. Levy, *J. Phys. Chem.*, 1991, **95**, 2175.
5. R. Bersohn, U. Even, J. Jortner, *J. Chem. Phys.*, 1984, **80(3)**, 1050.
6. J. N. Murrel in: *The Theory of The Electronic Spectra of Organic Molecules, J. Wiley and Sons, New York*, 1963.
7. D. K. Hahn, P. R. Callis, *J. Phys. Chem.*, 1997, **101**, 2686.

Chapter Six – Time-resolved fluorescence studies

6.1 Introduction

The steady state luminescence measurements presented in the preceding chapters provide considerable insight into the properties of the indole polymer systems. However, due to the complex, multicomponent nature of such systems, the scope of steady state studies is limited. Therefore, the time-resolved technique of time-correlated single photon counting was used to measure fluorescence lifetimes and time-resolved emission spectra (TRES). This method is a very powerful tool for gaining a greater depth of understanding of the photophysical properties of complex systems.

All time-resolved fluorescence measurements were made at the Lasers for Science Facility of the Rutherford Appleton Laboratories, using a picosecond laser system, as outlined in Chapter Three section 3.5. This chapter presents analysis of the lifetime measurements for the solution phase monomer, trimer and polymer systems of 5-cyanoindole, indole-5-carboxylic acid and 5-bromoindole, as well as a preliminary examination of solid state 5-cyanoindole films. Time-resolved emission spectroscopy was used to assist the interpretation of the fluorescence lifetime data and to provide a more immediate, pictorial representation of the species present. The aims of this work were to characterise the species present in the electropolymerised indoles and their relationships to each other and to gain an insight into the excitonic processes occurring in these systems. Samples were produced using differing electrochemical conditions to vary the proportions of trimer and polymer. The lifetimes of the monomers were measured for

comparison. The analysis of 5-cyanoindole films is limited here to presenting a discussion of the species present, a more detailed analysis of the influence of various factors on the luminescence properties of films can be found in Chapter Seven.

A significant limitation of the experimental technique employed for measuring time-resolved properties was the wavelength of excitation. The excitation source was a frequency-doubled, Nd:YAG-pumped dye laser, with Rhodamine 6G being used as the dye. The frequency-doubled output could be tuned from 290nm to 315nm, offering only a very narrow range of excitation wavelengths. From steady state data it is known that the different components in the trimer/ polymer system can be excited selectively using judicious selection of excitation wavelength, a technique that has been utilised by other workers [1] to simplify the data from a multicomponent system. Exciting between 290nm and 315nm is known to excite all the components in the system, resulting in more complex data. To obtain as full a picture as possible, lifetimes were measured as a function of emission wavelength, across the entire emission spectrum.

When a multiexponential fit is made to the lifetime data, the lifetimes are presented along with a value of the A factor and the %-contribution, which quantify the contribution of each lifetime to the total decay. For multiexponential fits, the total fluorescence response function is given by:

$$\mathbf{I_{(t)} = A_1 \exp(-t/\tau_1) + A_2(-t/\tau_2) + \cdots\cdots} \qquad \textbf{(6.1)}$$

where A_1, A_2 are the pre-exponential A factors for each lifetime. The %-contribution is the % of total steady state fluorescence intensity at that emission wavelength for the given lifetime component.

6.2 Checking experimental reliability.

In order to be certain that the lifetimes presented here are accurate, standard samples of known lifetime were initially run and the experiment optimised until a range of lifetimes could be accurately and consistently measured. These standards were repeated regularly to ensure consistency of results. 2,5-diphenyloxazole (PPO) and 1-cyanonaphthalene were used as standards. These were found to give results consistent with those given in the literature [2], with the experimental fluorescence response function being well fitted by a mono-exponential decay function. The experimental decay data and fitted function for PPO dissolved in cyclohexane are shown in Figure 6.1 together with a plot of the residuals. A very good single exponential fit is achieved; giving a chi squared value of 1.07 and Durbin Watson value of 1.84, along with residual and autocorrelation functions that have a low amplitude and are spread evenly and randomly about the zero point. The lifetime of 1.28 ns is identical to that given in reference 2. Consistent results were also found for 1-cyanonapthalene in both hexane and cyclohexane. In cyclohexane a lifetime of 10.15ns was found. In order to check that multicomponent systems with different lifetimes could be accurately measured a mixture of PPO and 1-cyanonapthalene in cyclohexane was prepared. The fluorescence response function, instrument response function and fitted functions are illustrated in Figure 6.2. An excellent bi-exponential fit was obtained, giving lifetimes of 1.26ns and 9.7ns, very close to the individual component lifetimes. The small, secondary pulse marked in Figure 6.2 arises from the cavity dumper, where a low intensity pulse is emitted exactly 12.156ns after the primary pulse. This initially posed a problem in measuring lifetimes that had to be fitted beyond this pulse. However, after careful adjustment this effect was reduced to a negligible level.

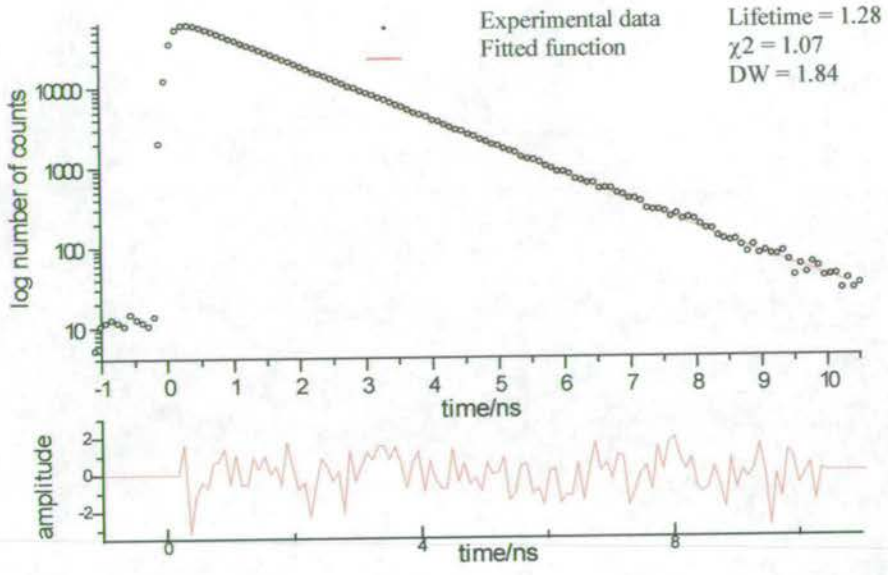

Figure 6.1 Experimental decay data, fitted single exponential function and residuals for PPO in cyclohexane.

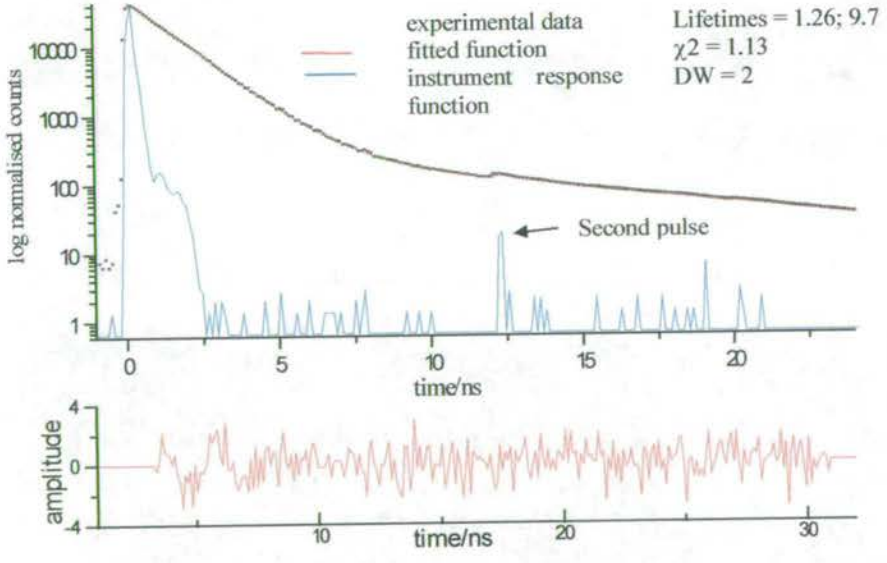

Figure 6.2 Experimental decay data, instrument response function, fitted bi-exponential function and residuals for a mixture of PPO and 1-cyanonaphthalene in cyclohexane.

6.3 Monomer lifetimes

The indole monomers, 5-cyanoindole, 5-bromoindole and indole-5-carboxylic acid, were all examined in ethanol as this was the main solvent used for the trimer and polymer species. Lifetimes were measured for solutions with and without degassing to monitor the effect of oxygen quenching, and also at a variety of solution concentrations. The results for 5-cyanoindole and 5-bromoindole were simple, giving mono-exponential decays, whereas those for indole-5-carboxylic acid were somewhat more complicated and are dealt with separately.

6.3.1 5-cyanoindole and 5-bromoindole monomer.

The lifetime data for 5-cyanoindole and 5-bromoindole is shown in Table 6.1 and the experimental data and fitted function for 5-cyanoindole is shown in Figure 6.3. The fluorescence decays of 5-cyanoindole and 5-bromoindole could both be satisfactorily fitted to single exponential functions, but the quality of the fits obtained were not as high as expected for a single component system, where the value of χ^2 should be well below 1.5 and DW above 1.8. Since the experimental set-up had been rigorously validated, the reason for this is most likely to be the quality of the sample. In both cases there was some difficulty in recrystallisation, as the melting point of each monomer is well below the boiling point of the solvent used, leading to possible impurities in the products. The lifetimes for these monomers are very similar: 4.32 ns for 5-cyanoindole and 4.5 ns for 5-bromoindole. When degassed there is a small increase in the value of the lifetime, indicating that there is a degree of oxygen quenching of the fluorescence in the aerated sample. The lifetimes were independent of concentration over the range $1x10^{-4}$ molar

to $1x10^{-6}$ molar, indicating that there is no complexation or aggregation effect at higher concentrations.

monomer	Not degassed			Degassed		
	Lifetime/ns	χ^2	DW	Lifetime/ns	χ^2	DW
5-cyanoindole	4.32	1.79	1.5	5.23	1.4	1.3
5-bromoindole	4.5	1.3	1.8	6.55	1.4	1.6

Table 6.1 Fitted lifetimes for 5-cyanoindole and 5-bromoindole in Ethanol.

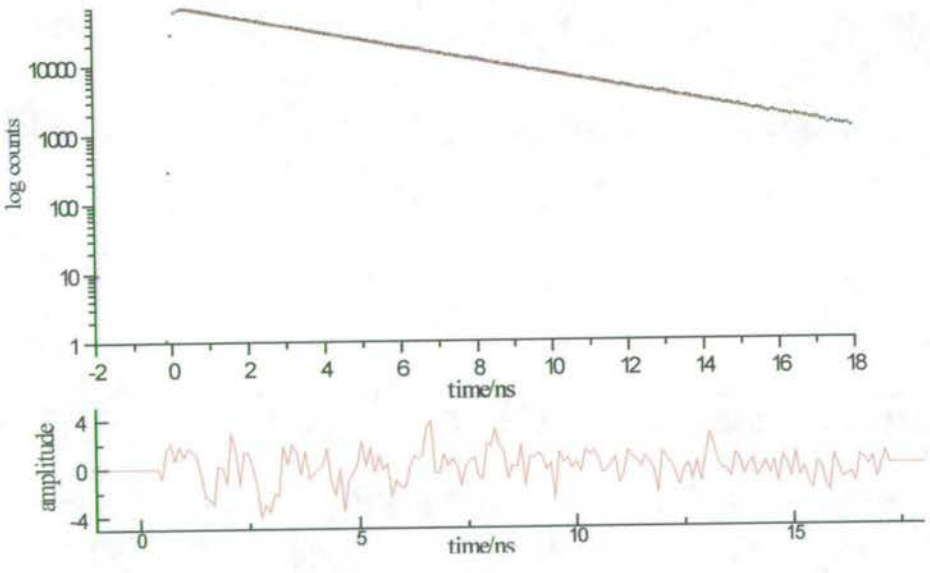

Figure 6.3 Experimental decay data, fitted single exponential function and residuals for a non de-gassed sample of 5-cyanoindole monomer in Ethanol.

6.3.2 Indole-5-carboxylic acid monomer.

In contrast to 5-cyanoindole and 5-bromoindole, the fluorescence decay of indole-5-carboxylic acid monomer is greatly affected by solution concentration. At concentrations below $1x10^{-6}$ molar a single exponential decay is observed, with a lifetime of 1.19ns. This is considerably lower than the other two monomers, implying a lower quantum yield. At higher concentrations, the decay becomes bi-exponential with a longer lifetime component appearing, whose contribution increases with concentration. This can be clearly seen in the values presented in Table 6.2 for a range of solution concentrations, and in the decay function shown in Figure 6.4. When the solution is degassed, there is very little change to the shorter wavelength component, which is unaffected by oxygen quenching, whereas the longer lifetime component is increased. The lifetime of a 3×10^{-6} molar degassed solution is 1.2ns, a degassed 1×10^{-4} molar solution has lifetimes of 12ns and 1.3ns.

	Concentration / mol dm^{-3}		
	1×10^{-4}	5×10^{-5}	1.55×10^{-6}
Lifetime / ns	1.18	1.20	1.19
A factor	86.9	90.2	
% contribution	48.4	57.6	
Lifetime / ns	8.37	8.13	
A factor	13.1	9.8	
% contribution	51.6	42.4	
χ^2	1.5	1.27	1.24
DW	1.44	1.85	1.5

Table 6.2 Fluorescence lifetimes of indole-5-carboxylic acid in ethanol at different concentrations.

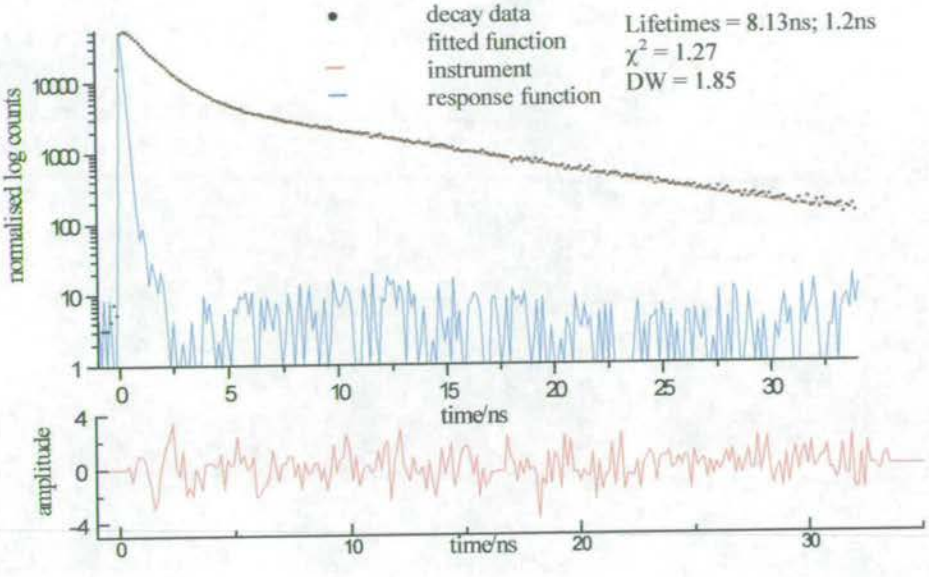

Figure 6.4 Experimental decay data, fitted bi-exponential function, instrument response function and residuals for a 5 x 10^{-5} molar solution of indole-5-carboxylic acid in ethanol.

The appearance of a longer lifetime component at higher concentrations can be attributed to an aggregation effect, with a ground state species being formed due to the hydrogen bonding capabilities of the carboxy group present on the monomer. No such effect is observed for the non-hydrogen bonding cyano and bromo substituents. Aggregation also accounts for the broadening of the emission spectrum at higher concentrations. The effect of the carboxy group on the sensitivity to solvent environment was also noted in Chapter 4

6.4 Lifetimes of the electropolymerised indoles

When measuring the lifetimes of the electropolymerised indoles, an important factor was the solubility of the product. 5-bromoindole was the most soluble, dissolving fully in ethanol, even when containing high quantities of polymer. This has been mentioned previously in Chapter 4 as it provides the best example of a mixed trimer and polymer system, where both components are easily distinguishable. It is the first of the indoles to be discussed in this section, since we can be certain that all species are present in the solution. Indole-5-carboxylic acid is only partially soluble in ethanol, but almost entirely soluble in DMF, except for samples with very high polymer content, and therefore gives comparable results to 5-bromoindole. The solubility of 5-cyanoindole is much lower, even in solvents such as DMF and DMSO; therefore it is difficult to predict the proportions of trimer and polymer present in solution. Throughout this discussion, the results of time-resolved emission spectroscopy will be presented alongside the lifetime data to provide a clearer picture of the fluorescence behaviour.

6.4.1 Electropolymerised 5-bromoindole

By altering the electrochemical conditions, it is possible to control the amount of trimer and polymer in the electropolymerised film. This has been discussed in Chapter 4, where it was shown that a high monomer concentration and high rotation speeds result in films that display predominantly trimer emission characteristics. When low concentration monomer solutions and low rotation speeds are used, then the films are rich in polymer species. These effects are illustrated in Figure 6.5. From the steady state results, it is clear that at least two emitting species are present, both of which are excited at 300nm. It is expected that the lifetime data will

correspond to the steady state observations, with the lifetimes measured at short wavelength being dominated by emission from a trimer species and at long wavelength by polymer species.

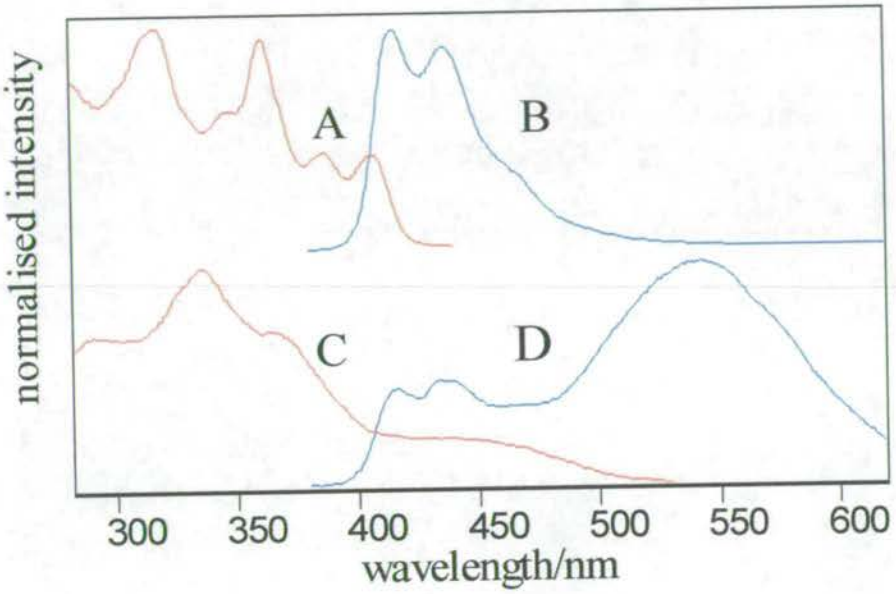

Figure 6.5 Excitation spectrum (A) for 5-bromoindole trimer at an emission wavelength of 450nm and emission spectrum (B) for 5-bromoindole trimer at an excitation wavelength of 335nm. Excitation spectrum (C) for 5-bromoindole polymer at an emission wavelength of 550nm and emission spectrum (D) for 5-bromoindole polymer and trimer at an excitation wavelength of 335nm, dissolved in ethanol.

Samples were prepared using a range of polymerisation conditions to give either a high trimer or high polymer content. Lifetime measurements were made on more than one set of samples produced using the same reaction conditions to check for consistency of results. As will become

apparent, differences between batches of samples are revealed. This is due to the difficulty in reproducing identical conditions, since factors such as the quality of monomer and electrode surface, which are hard to quantitatively control, will affect the sample. Because of this, direct comparisons are only made between samples produced from the same monomer solution and on the same day.

6.1.1.1 Lifetime data

The reaction conditions for the first set of samples examined are shown in Table 6.3. After polymerisation the films were dissolved off the electrode with ethanol. It is expected that the samples produced at a stationary electrode, 1a and 2a, will have a high polymer content, with the low concentration solution 1a having a greater proportion of polymer than 2a. The samples produced at high rotation speeds, 1b and 2b should be rich in trimer, with the high concentration monomer solution 2b giving a higher proportion of trimer than 1b. Lifetimes were measured at wavelengths across the trimer and polymer emission spectra at regular intervals from 420nm to 580nm.

Concentration of 5-bromoindole	Rotation speed and polymerisation time	
	0Hz 1 minute	15Hz 20 seconds
20 mmol	Sample 1a	Sample 1b
200mmol	Sample 2a	Sample 2b

Table 6.3 Polymerisation conditions for first batch of 5-bromoindole samples.

For all the samples and at nearly all emission wavelengths at which decays were measured, it was necessary to use a tri-exponential function to give an adequate fit to the decay data. The three lifetime components have values of approximately 5ns, 2ns and 0.3ns, which are essentially consistent across the different samples and are separate enough to imply they represent different emitting species. To simplify the analysis of data, the lifetime components have been labelled as τ_1, τ_2 and τ_3, corresponding to the approximate values of 5ns, 2ns and 0.3ns, respectively. Due to the complex, multicomponent nature of these systems, a fit of three lifetimes is not assumed to indicate the presence of only three individual species, but is assumed to be characteristic of a distribution of emitting species whose lifetimes are centred on those calculated.

The lifetime data for samples 1a and 1b are shown in Table 6.4, giving the lifetimes at wavelengths from 420nm to 580nm along with A factor, % contribution, χ^2 value and DW value. Most of the fits were acceptably good, with χ^2 values close to 1.5 and DW values close to 2. In some cases the fits were not as good, but these values are still included to provide a comparison between the different samples and different emission wavelengths. For some of the fits, the value of χ^2 is greater than 2 (indicating a poor fit), but the value of DW is close to 2 (indicating a good fit), implying that although the data varies considerably from the fitted function, this variation is random above and below that function. Figure 6.6 shows an example of the fluorescence decay and fitted functions for sample 1b at wavelengths corresponding to the peak of trimer emission at 420nm and polymer emission at 560nm, illustrating the variation in decay profile with wavelength and the obviously multi-exponential nature of the decay.

	20 mmol/ 0 Hz/ 1 minute sample 1a / very high polymer content				20 mmol/ 15 Hz/ 20 seconds sample 1b / high trimer content			
λ / nm	τ_1 / ns	τ_2 / ns	τ_3 / ns		τ_1 / ns	τ_2 / ns	τ_3 / ns	
420	5.46 0.2 5.9	0.63 1.8 5.4	0.19 98 88.7	1.5 2	4.77 2 32	0.55 5 10	0.18 93 58	1.1 1.9
440	4.30 0.2 4	0.57 1.7 5.2	0.18 98 91	1.2 2	4.70 1.3 24	0.50 5 10	0.18 94 66	1 2
460	3.94 0.3 6.8	0.55 3.2 8.8	0.18 97 84.4	1.4 1.9	4.63 1.3 23	0.52 6.4 13	0.18 92 64	1.3 1.9
480	4.25 0.4 8	1.00 1.5 6.3	0.21 98 85.7	2.6 1.9	4.39 1.1 18	0.59 5.9 14	0.18 93 67	1 1.9
500	4.80 1.2 18	1.40 4 17.5	0.20 95 64.5	1.5 1.95	4.39 1.5 22	1.04 4.9 17	0.20 94 61	1.2 1.6
520	5.09 1.7 21.6	1.70 5.3 22	0.24 93 56.3	2 1.6	4.76 4.1 38	1.42 9.6 26	0.22 86 36	1.5 1.8
540	5.13 3 27.6	1.83 8 27.9	0.28 88.6 44.6	1.57 1.65	4.75 7 44	1.55 12 26	0.26 81 30	1.45 1.6
560	5.13 4.1 30	1.93 11.5 32	0.31 85 38	2.6 1.5	4.92 9 45	1.78 18 32	0.30 74 23	1.2 1.8
580	5.17 4.6 30	2.00 13.5 34	0.34 82 36	1.9 1.7				

Table 6.4 Lifetime data for 5-bromoindole samples 1a and 1b, produced from a 20 mmol solution at 0 Hz for 1 minute and 15 Hz for 20 seconds.

Data consists of:

Lifetime A factor % contribution	χ^2 value DW value

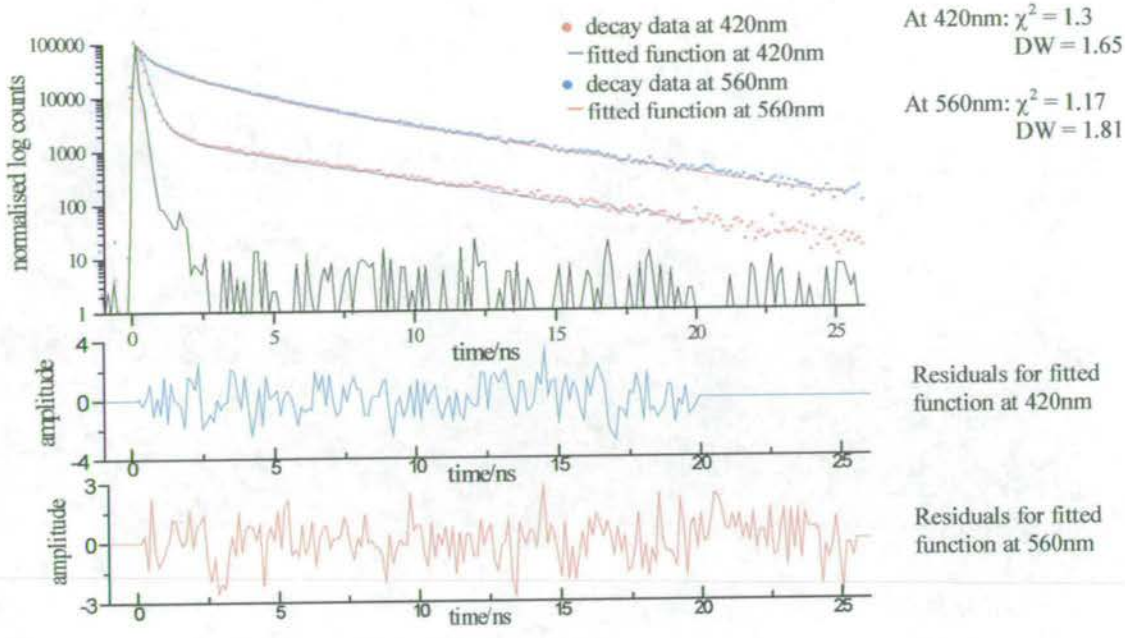

Figure 6.6 Log plot of experimental decay data, instrument response function, fitted tri-exponential functions and residual plots for sample 1b at 420nm and 560nm.

To compare between samples, graphs of A factor and % contribution vs. emission wavelength for τ_1, τ_2 and τ_3 have been plotted and are shown in Figures 6.7 and 6.8. From these plots, the contribution from each lifetime can be followed as the wavelength is increased and preparation conditions altered. For both samples, the short lifetime component, τ_3 has the greatest contribution at short wavelength, decreasing towards longer wavelength, but it has a considerably greater contribution in the high polymer sample. In both samples τ_2 steadily increases its contribution as the wavelength increase. The longest lifetime component, τ_1, has a considerably greater contribution in the higher trimer sample. Its contribution remains approximately constant in the short wavelength region up to 480nm and then increases with increasing wavelength.

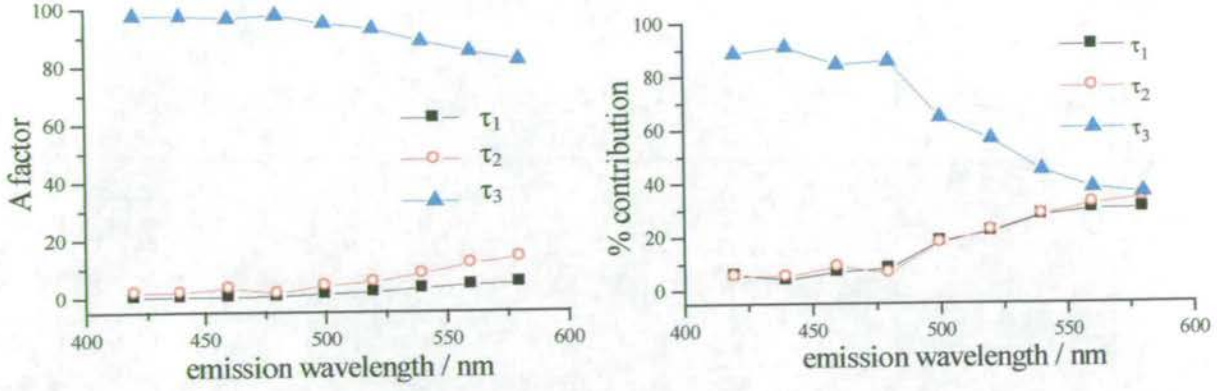

Figure 6.7 Plots of A factor and % contribution vs. wavelength for each of the three characteristic component lifetimes for sample 1a dissolved in ethanol, produced using a 20 mmol 5-bromoindole monomer solution and a rotation speed of 0 Hz for 1 minute to give a high polymer content.

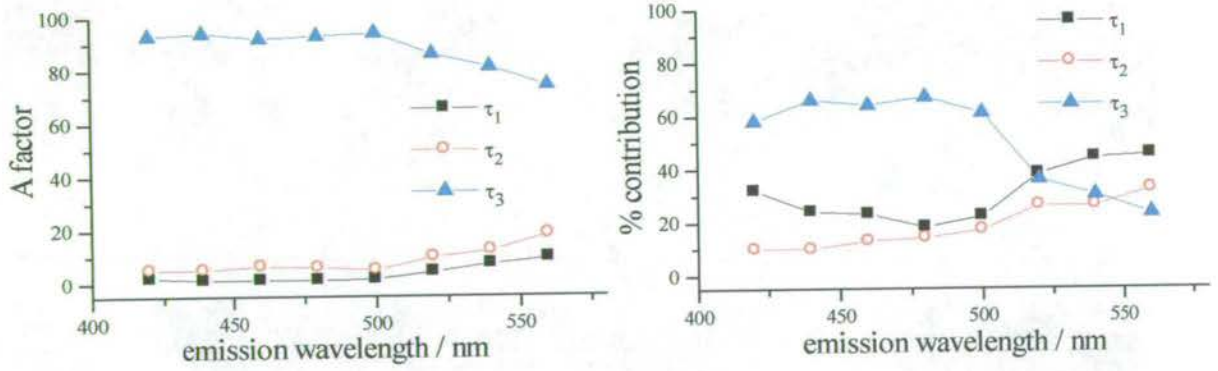

Figure 6.8 Plots of A factor and % contribution vs. wavelength for each of the three characteristic component lifetimes for sample 1b dissolved in ethanol, produced using a 20 mmol 5-bromoindole monomer solution and a rotation speed of 15 Hz for 20 seconds to give a high trimer content.

Samples 2a and 2b were prepared using the same rotation speeds and polymerisation times as samples 1a and 1b, but the monomer solution concentration was much higher, at 200 mmol. It is expected that the higher monomer concentration should give samples that have a higher proportion of trimer than samples 1a and 1b, prepared using a lower monomer concentration. As for samples 1a and 1b, it is expected that sample 2a polymerised at a stationary electrode will be richer polymer and sample 2b, polymerised at fast rotation speed will be trimer rich. The lifetime data for samples 2a and 2b is presented in Table 6.1 along with χ^2 and DW values. As with the previous 5-bromoindole samples, suitable fits cannot be achieved with fewer than three exponentials, giving similar lifetimes of approximately 5ns, 2 ns and 0.3ns. Plots of A factor and % contribution for each of these dominant lifetimes are shown in Figure 6.9 and Figure 6.10.

In the high polymer sample, 2a, the short lifetime component τ_3 is very dominant at short wavelength, its contribution dropping towards longer wavelengths. Due to the very high contribution of τ_3 at short wavelengths, the values of the other two components are likely to be unreliable. Both τ_1 and τ_2 grow in contribution at a similar rate as the wavelength increases.

For the very high trimer sample, 2b, this situation is reversed, with the long lifetime component τ_1 being dominant at short wavelength and dropping in contribution at longer wavelengths. As for all the samples, the intermediate lifetime τ_2 steadily grows in as the wavelength increases. The short lifetime component τ_3 shows a decrease in A factor and an increase in contribution from short to long wavelength.

	200 mmol/ 0 Hz/ 1 minute sample 2a / high polymer				200 mmol/ 15 Hz/ 20 seconds sample 2b / very high trimer			
λ / nm	τ_1 / ns	τ_2 / ns	τ_3 / ns		τ_1 / ns	τ_2 / ns	τ_3 / ns	
420	5.92 0.06 1.95	0.92 0.2 0.9	0.17 99.8 97.1	1.56 1.73	5.5 26 94	1.64 4 4	0.14 71 2	1.86 1.5
440	3.46 0.06 1.24	0.47 1.0 2.5	0.17 99 96.3	1.5 1.6	5.5 9.0 82	1.53 3.0 8	0.06 88 10	1.8 1.5
460	6.25 0.03 0.82	1.34 0.3 1.7	0.19 99.7 97.4	2.6 1.6	5.56 18 83	1.33 13 15	0.05 69 3.0	1.5 1.34
480	3.64 0.14 2.5	0.98 0.7 3.3	0.19 99 94	2.3 1.5	6.63 19 55	2.12 27 25	0.83 54 20	1.8 1.3
500	4.54 0.4 7.5	1.00 2.0 10	0.19 97 83	2.3 1.6	7.36 12 45	2.00 31 32	0.80 57 23	1.5 1.8
520	5 0.7 12	1.2 3.0 12	0.23 96 76	2.6 1.6	7.9 8 37	1.90 33 36	0.78 59 26	1.6 1.54
540	5.17 1.7 23.4	1.25 5.7 19	0.24 97 58	2 1.8	7.86 6.5 33	1.73 38 42	0.73 56 26	1.4 1.5
560	5.23 2.0 27	1.33 7.0 19	0.27 91 54	2.3 1.5	7.81 5 29	1.72 37 43	0.73 57 28	1.6 1.7
580					7.81 5 25	1.74 36 44	0.73 60 31	1.7 1.9

Table 6.5 Lifetime data for 5-bromoindole samples 2a and 2b dissolved in ethanol, produced from a 200 mmol 5-bromoindole monomer solution at 0 Hz, 1 minute and 15 Hz 20 seconds.

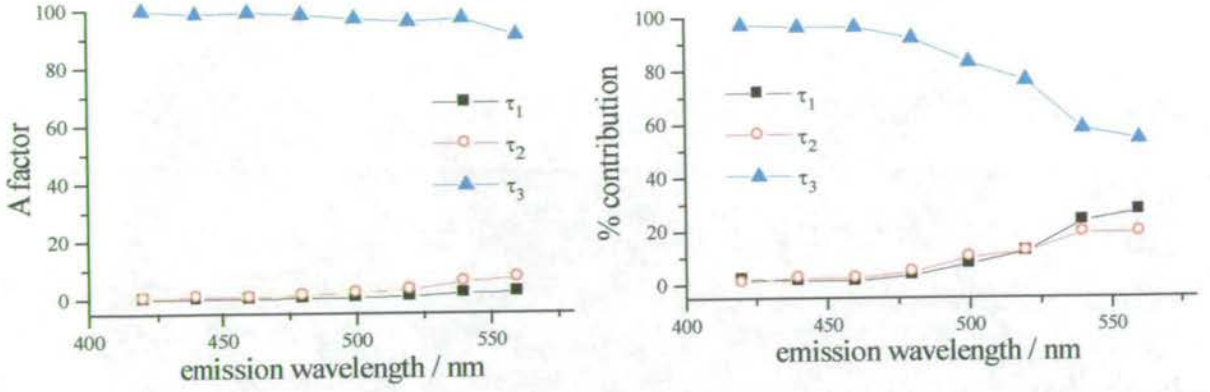

Figure 6.9 Plots of A factor and % contribution vs. wavelength for each of the three characteristic component lifetimes for sample 2a dissolved in ethanol, produced using a 200 mmol 5-bromoindole monomer solution and a rotation speed of 0 Hz for 1 minute to give a high polymer content.

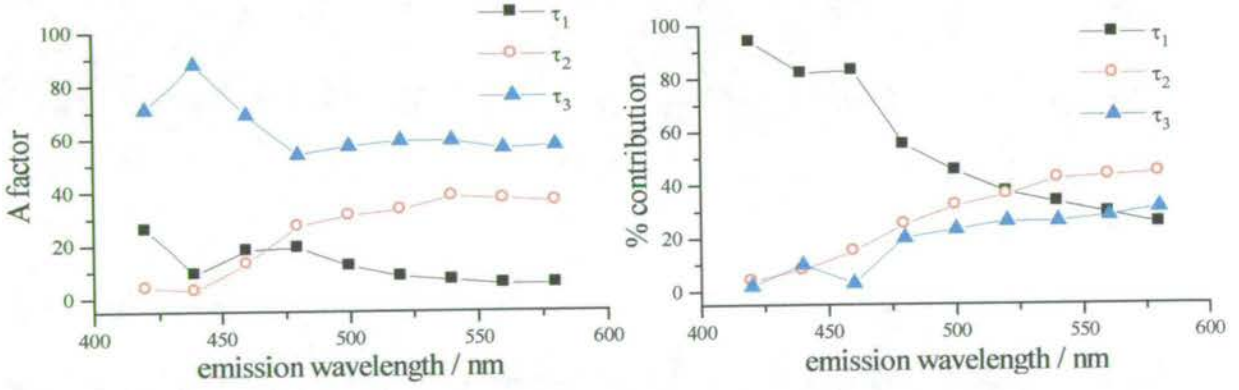

Figure 6.10 Plots of A factor and % contribution vs. wavelength for each of the three characteristic component lifetimes for sample 2b dissolved in ethanol, produced using a 200 mmol 5-bromoindole monomer solution and a rotation speed of 15 Hz for 20 seconds to give a high trimer content.

Although the lifetime data presented above has been separated into the three characteristic components τ_1, τ_2 and τ_3, the lifetimes of these components do change between short and long emission wavelengths and this change is consistent across the samples. The value of the long lifetime component τ_1 lies between 5 and 6 ns at short wavelength and shows little change as the wavelength increases, except in very the high trimer sample 2b, where it increases to 7.8ns at a wavelength of 500nm. The intermediate lifetime component τ_2 shows a significant increase as the wavelength gets longer, lying between 0.5 and 1 ns at short wavelength, increasing to around 2ns at long wavelength for most of the samples. The short lifetime species, τ_3 also shows an increase, with values between 0.06 and 0.2 ns at short wavelength and greater than 0.3ns at longer wavelength.

6.4.1.1 Time-resolved emission spectra of 5-bromoindole

Time-resolved emission spectroscopy presents essentially the same information as a series of lifetime measurements at successive emission wavelengths. However, it gives a much more concise picture of the components present and aids in interpretation of the lifetime data. Shown in Figure 6.11 are a selection of gated spectra measured for a sample of 5-bromoindole produced to give a high polymer content. The spectrum of the full decay, as expected, displays both trimer and polymer emission peaks. The polymer peak at 530nm is small compared to the trimer peaks at 416nm and 434nm because the excitation wavelength of 300nm is well below the 340nm excitation maximum of the polymer, but very close to one of the trimer excitation maxima as can be seen in Figure 6.5. Collecting only photons arriving in the first 500 picoseconds after excitation gives a spectrum which has predominantly trimer characteristics, losing the peak at

530nm due to the polymer. By gating out the first 500 picoseconds of the decay, the polymer emission reappears and is more intense with respect to the trimer emission.

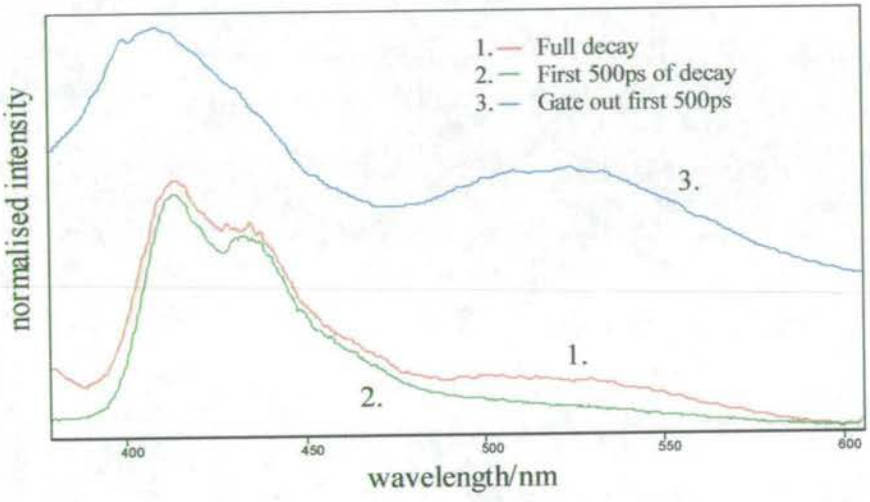

Figure 6.11 Time-resolved emission spectra for 5-bromoindole polymerised from a 10 mmol monomer solution at 0 Hz for 2 minutes, giving a high polymer content, dissolved in ethanol.

6.1.1.2 Discussion of time-resolved data and a proposed model.

Examining the results presented above, the most significant feature is the change in contribution of the component lifetimes between the different samples and at different wavelengths. The shortest lifetime species τ_3, which varies from 0.06ns to 0.78ns, consistently has the highest A factor, and in the high polymer samples 1a and 2a it has the greatest % contribution. The contribution from τ_3 steadily drops as the wavelength is increased, implying that it is associated

with a short wavelength emitting species. The longest living species τ_1, with a lifetime around 5ns shows a small increase in contribution as the wavelength increases; it has a markedly greater influence in the high trimer samples, 1b and 2b, than in the high polymer samples.

The most obvious difference between samples is seen in the % contribution plots of Figure 6.9 and Figure 6.10. For the high trimer sample 2b, τ_1 has the greatest contribution at short wavelengths, rapidly dropping off as the wavelength increases, whereas for the high polymer sample 2a, τ_3 has most influence at short wavelength, dropping off as the wavelength increases. This implies that τ_1 is associated with the trimer species and that τ_3 is associated with the polymer species; however, the short-lived species τ_3 has its greatest contribution at shorter wavelengths, where the trimer emits. This suggests that τ_3 is associated with a trimer-like chromophore within the polymer chain. In the high polymer sample the longest lived component, τ_1, shows little contribution at short wavelength and increasing contribution with increasing wavelength above 500nm; this is essentially the inverse of the trend observed for high trimer samples. This can be explained if τ_1 is associated with different emitting species in the short wavelength and long wavelength regions. The third lifetime, τ_2, of around 2 ns shows a very similar trend for all the samples, with a gradually increasing contribution as the wavelength increases, implying that it is associated with the polymer emission.

These observations are consistent with the time-resolved emission spectra. At short time intervals, the emission spectrum has a short wavelength, trimer-like character, with no emission at longer wavelength. This implies that the short-lived emission originates from a trimer-like

species; however, from the lifetime measurements, we know that this species is more prevalent in samples with a high polymer content. At longer time intervals, an emission at long wavelength is observed, consistent with a polymer species, but there is also emission at short wavelength characteristic of the trimer. This corresponds with the observation that in samples with a high trimer content, the longest lifetime species, τ_1, has a greater contribution at short wavelengths than in samples with a high polymer content.

From these observations, the following model is proposed, which will be developed further by examining 5-cyanoindole and indole-5-carboxylic acid time-resolved data.

- The short lifetime component τ_3 corresponds to a high excitation energy species from which there is efficient non-radiative decay, through energy-transfer, to lower excitation energy (greater conjugation length) segments. The trimer-like emission spectrum of this species, at short wavelengths (between 420nm and 500nm), but prevalence in high polymer samples, implies that it is due to excitation localised on an intra-chain trimer unit; i.e. an intra-chain trimer chromophore which is isolated from the conjugated system and constitutes the shortest possible conjugation length species. At wavelengths greater than 500nm the value of τ_3 increases, which can be attributed to contribution from short conjugation length oligomers, with a length greater than one trimer unit. As the wavelength increases the distribution of emitting species consists of longer conjugation lengths. The contribution of τ_3 decreases at longer emission wavelengths as the other lifetime components become more dominant.

- The intermediate lifetime component τ_2 originates from polymer segments of intermediate conjugation length and intermediate excitation energy. They are quenched by energy transfer to lower excitation energy species, but less so than the high excitation energy species τ_3. The contribution of τ_2 increases with increasing emission wavelength as does the value of τ_2. This is characteristic of the distribution of emitting species shifting to longer conjugation lengths.

- At short wavelengths, the longest lived component τ_1 corresponds to the free trimer species in solution, for which there is little contact with the polymer species, minimising non-radiative decay pathways via energy transfer. It is expected that the lifetime of the free trimer will be comparable in magnitude to the free monomer lifetime, as is observed. At longer emission wavelengths, τ_1 corresponds to the lowest excitation energy segments of the polymer chain (the deepest energy traps) which are least prone to non-radiative decay by energy transfer, therefore decaying with a long lifetime. At intermediate wavelengths the value of τ_1 will result from a mix of the free trimer species and the longer conjugation length species.

6.4.1.2 Reproducibility of results

These experiments were repeated at a later date using a fresh batch of 5-bromoindole and slightly different experimental conditions to check how consistent and reproducible the results are. The polymerisation conditions for samples 3a, 3b, 4a and 4b are shown in Table 6.6.

Concentration of 5-bromoindole	Rotation speed and polymerisation time	
	0Hz 1 minute	15Hz 1 minute
20 mmol	Sample 3a	Sample 3b
200mmol	Sample 4a	Sample 4b

Table 6.6 polymerisation conditions for second batch of 5-bromoindole samples.

Samples 3a and 4a should give a high polymer content, with 3a being the highest. Samples 3b and 4b should give a high trimer content, with 4b giving the highest. Due to the longer polymerisation time of samples 3b and 4b, compared to 1b and 2b, they are expected to contain a higher amount of polymer. Table 6.7 shows the lifetime data for samples 3a and 3b, and Table 6.8 shows the lifetime data for samples 4a and 4b. Most of the decays have been fitted to a tri-exponential function as for the previous samples, however some of the shorter wavelength decays will fit satisfactorily to a bi-exponential function, with the intermediate lifetime τ_2 not appearing until a wavelength of 500nm. Most of the fits were acceptably good with χ^2 values below 1.5 and DW values close to 2.

	20 mmol/ 0 Hz/ 1 minute sample 3a / high polymer				20 mmol/ 15 Hz/ 1 minute sample 3b / high trimer			
λ / nm	τ_1 / ns	τ_2 / ns	τ_3 / ns		τ_1 / ns	τ_2 / ns	τ_3 / ns	
420	5.10 22 84	0.60 4 2	0.28 74 15	1.4 1.7	5.10 33 89		0.30 67 11	1.4 1.5
460	5.08 13 73	0.51 7.9 4.4	0.26 79 22	1.5 1.7	5.10 21 82		0.30 80 18	1.6 1.3
500	5.12 7.3 52.1	1.51 7.6 15.9	0.27 85 32	1.2 1.9	5.00 6 51	1.10 5 9	0.30 90 40	1.6 1.9
540	4.90 10 55	1.50 11 20	0.30 79 25	1.4 1.8	5.10 10 58	1.55 10 18	0.30 80 25	1.4 1.5
580	4.90 17 59	1.90 18 23	0.40 66 18		5.00 17 63	1.7 17 21	0.30 66 16	1.4 1.5

Table 6.7 Lifetime data for 5-bromoindole samples 3a and 3b dissolved in ethanol, produced from a 20 mmol 5-bromoindole monomer solution at 0 Hz, 1 minute and 15 Hz 1 minute.

	200 mmol/ 0 Hz/ 1 minute sample 4a, high polymer				200 mmol/ 15 Hz/ 1 minute sample 4b, high trimer			
λ / nm	τ_1 / ns	τ_2 / ns	τ_3 / ns		τ_1 / ns	τ_2 / ns	τ_3 / ns	
420	5.00 1.6 29	0.50 5 8.5	0.20 93 63	1.6 1.8	5.00 17 78		0.30 83 22	1.3 1.4
460	4.80 1 23	0.50 4 8	0.20 95 69	1.5 1.8	5.00 13 73		0.30 87 27	1.4 1.6
500	4.40 2 28	0.80 7 18	0.20 91 54	1.7 2	5.10 9 62	1.10 3 5	0.30 88 33	1.4 2
540	5.00 10 55	1.50 12 20	0.30 79 25	1.5 1.7	5.50 17 70	2.00 7 10	0.30 76 20	1.3 1.5
580	5.10 20 64	1.90 20 23	0.40 60 13	1.4 1.8	5.50 50 85	2.30 14 10	0.50 36 6	1.4 1.6

Table 6.8 Lifetime data for 5-bromoindole samples 4a and 4b dissolved in ethanol, produced from a 200 mmol 5-bromoindole monomer solution at 0 Hz, 1 minute and 15 Hz 1 minute.

The results have again been grouped into the three dominant lifetimes of 5ns, 2 ns and 0.3ns, labelled τ_1, τ_2 and τ_3. The values of A factor and % contribution have been plotted against wavelength as illustrated in Figure 6.12, Figure 6.13, Figure 6.14 and Figure 6.15 for samples 3a, 3b, 4a, and 4b respectively.

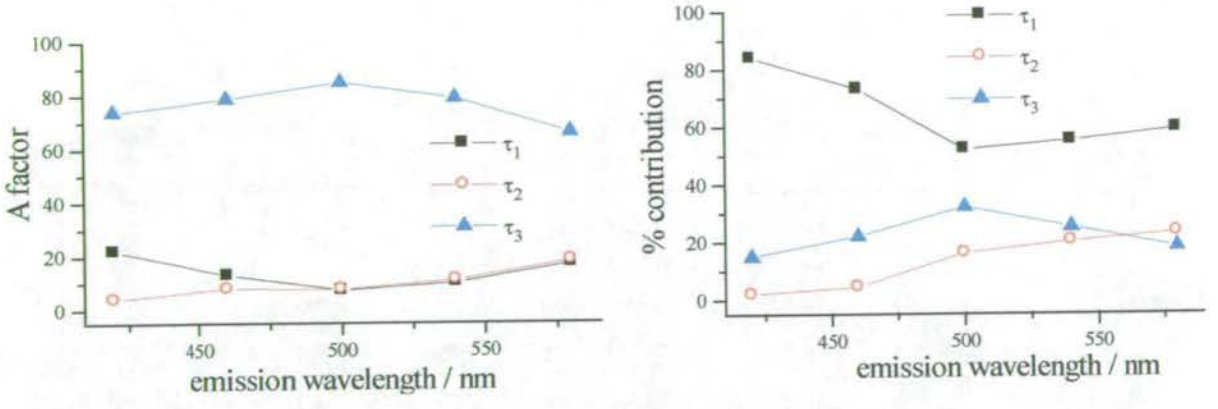

Figure 6.12 Plots of wavelength vs. A factor and % contribution for each of the three characteristic component lifetimes for sample 3a dissolved in ethanol, produced using a 20 mmol 5-bromoindole monomer solution and a rotation speed of 0 Hz for 1 minute to give a high polymer content.

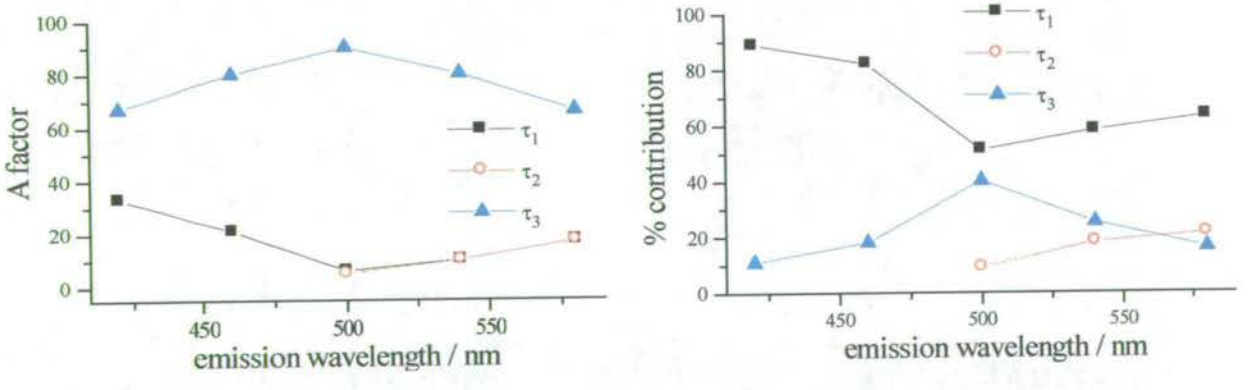

Figure 6.13 Plots of wavelength vs. A factor and % contribution for each of the three characteristic component lifetimes for sample 3b, produced using a 20 mmol 5-bromoindole solution and a rotation speed of 15 Hz for 1 minute to give a high trimer content.

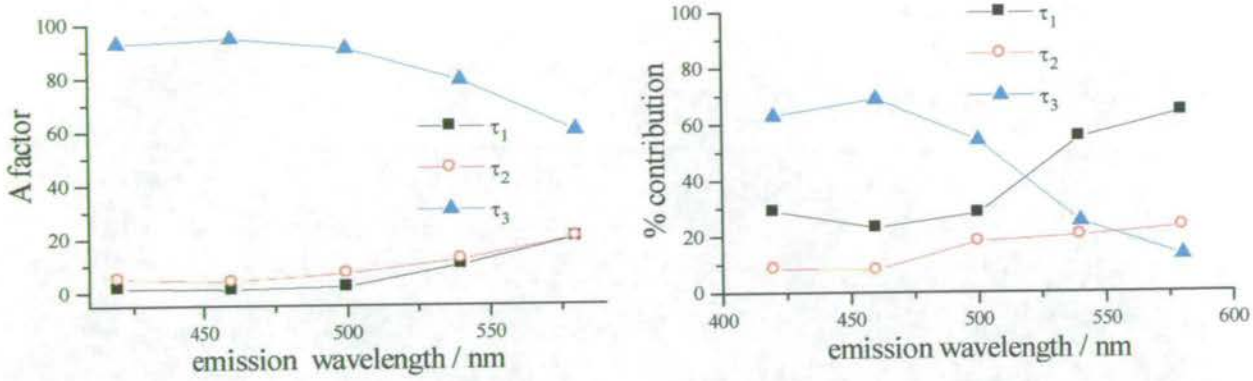

Figure 6.14 Plots of wavelength vs. A factor and % contribution for each of the three characteristic component lifetimes for sample 4a dissolved in ethanol, produced using a 200 mmol 5-bromoindole monomer solution and a rotation speed of 0 Hz for 1 minute to give a high polymer content.

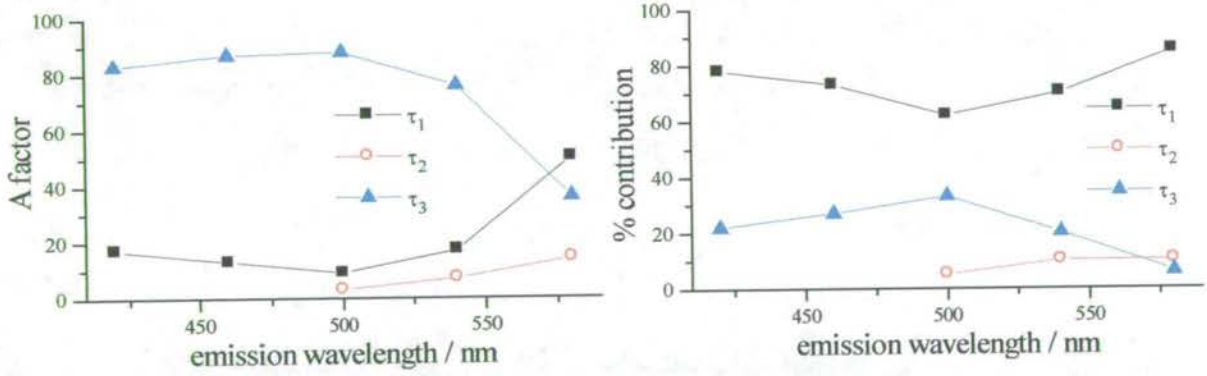

Figure 6.15 Plots of wavelength vs. A factor and % contribution for each of the three characteristic component lifetimes for sample 4b dissolved in ethanol, produced using a 200 mmol 5-bromoindole monomer solution and a rotation speed of 15 Hz for 1 minute to give a high trimer content.

Similar trends are observed to those of the first batch of samples, reinforcing the proposed model. The contribution of τ_1 at short wavelengths is higher in the trimer-rich samples than the polymer-rich samples and at long wavelengths it shows a considerable contribution in all samples. This is consistent with τ_1 originating at short wavelengths from a free trimer species, with a similar lifetime to the monomer. The presence of τ_1 at long wavelengths corresponds to the longest conjugation segments, with lowest excitation energy, acting as energy wells, from which no further energy transfer can occur.

The contribution of τ_3 at short wavelengths is greatest in the high polymer samples, reducing at longer wavelengths in all the samples. This is consistent with τ_3 being the lifetime of a high energy, trimer- like species, located on the polymer chain, from which non-radiative decay by energy transfer is rapid. The effect of preparation conditions on the contributions of τ_1 and τ_3 is seen clearly in Figure 6.14 and Figure 6.15 for samples 4a and 4b. In the polymer-rich sample 4a, the contribution of τ_3 is much higher than for τ_1 at short wavelengths. This is in contrast to the trimer-rich sample 4b for which the contribution of τ_1 is much greater than τ_3 at short wavelengths. For all samples the contribution of τ_2 increases with increasing wavelength and is consistent with emission from polymer segments of intermediate conjugation length. The lifetimes for samples 3a and 3b show similar trends, although the differences are not as great between samples.

The results for the second batch of samples, although showing the same trends in their lifetimes, do show some differences to the first batch of samples. There is considerably more free trimer,

characterised by the lifetime τ_1, in sample 3a than was observed in 1a, even though identical preparation conditions were used. This highlights the difficulty in reproducing an identical sample, when using different batches of monomer and not having a quantitative method for polishing the electrode. Due to the sensitivity of electropolymerisation to other species in solution, there will be a perturbation of the polymerisation conditions after a monomer solution has been used to generate a single polymer film. Ideally a fresh monomer solution would be prepared for each new film, however, this was neither practical in terms of cost nor time.

6.4.2 Electropolymerised indole-5-carboxylic acid

As has previously been noted, the solubility of indole-5-carboxylic acid is lower than that of 5-bromoindole in ethanol, nevertheless most of the sample can be dissolved using a sonic bath and it is expected that only the longer chain polymers remain insoluble. It is notable that the solubility of the high polymer samples is lower than high trimer samples, this implies that for all the samples, there will be a larger proportion of free trimer due to its preferential solubility. Samples were produced using the preparation conditions shown in Table 6.9 to give trimer-rich and polymer-rich samples. Lifetimes were measured at a range of wavelengths and the results presented below exhibit the same trends as were seen for 5-bromoindole. A similar pattern to the 5-bromoindole samples was observed where the fluorescence decays would fit to no fewer than three exponentials, giving well-spaced lifetimes that can be grouped into three categories; 5ns, 1ns and 0.5 ns, labelled τ_1, τ_2, and τ_3 respectively.

Concentration of indole-5-carboxylic acid monomer	Rotation speed and polymerisation time	
	5 Hz 30 seconds	15Hz 10 seconds
100 mmol	Sample 5a	Sample 5b

Table 6.9 Polymerisation conditions for indole-5-carboxylic acid samples.

The results given in Table 6.10 show the lifetime data for samples 5a and 5b, where 5a will be polymer-rich and 5b trimer-rich.

	100 mmol/ 5 Hz/ 30 seconds sample 5a/ higher polymer content				100 mmol/ 15 Hz/ 10 seconds sample 5b/ higher trimer content			
λ / nm	τ_1 / ns	τ_2 / ns	τ_3 / ns		τ_1 / ns	τ_2 / ns	τ_3 / ns	
420	5.00 13 90	1.21 3 5	0.05 84 5	1.16 2	5.07 23 96	1.13 2 2	0.04 75 2	1.59 1.4
460	4.88 13 69	1.18 19 24	0.10 68 8	1.37 1.7	5.00 17 82.5	1.08 13 13.7	0.056 70 3.8	1.3 1.6
500	4.58 7 26	1.34 60 62	0.50 33 13	1.2 1.8	4.87 10 34	1.34 54 51	0.57 36 15	1.3 1.9
540	4.2 3.5 13	1.37 58 69	0.56 38 19	1.1 1.8	4.14 4.4 16	1.29 59 67	0.54 36.6 17	1.1 1.44
580	4.32 3 12	1.42 53 64	0.62 44 24	1.4 1.7	3.96 4 14	1.27 60 70	0.47 36 16	1.38 1.6

Table 6.10 Lifetime data for indole-5-carboxylic acid samples 5a and 5b produced from a 100 mmol sample at 5 Hz, 30 seconds and 15 Hz 10 seconds.

Figure 6.16 shows the experimental decay data and fitted tri-exponential functions for sample 5a at wavelengths of 420nm and 540nm, illustrating the change in decay profile from the trimer emission region to the polymer emission region. In both cases the tri-exponential function fits very well with χ^2 values close to one, DW values close to 2 and residuals plots with low amplitude and a random distribution of points.

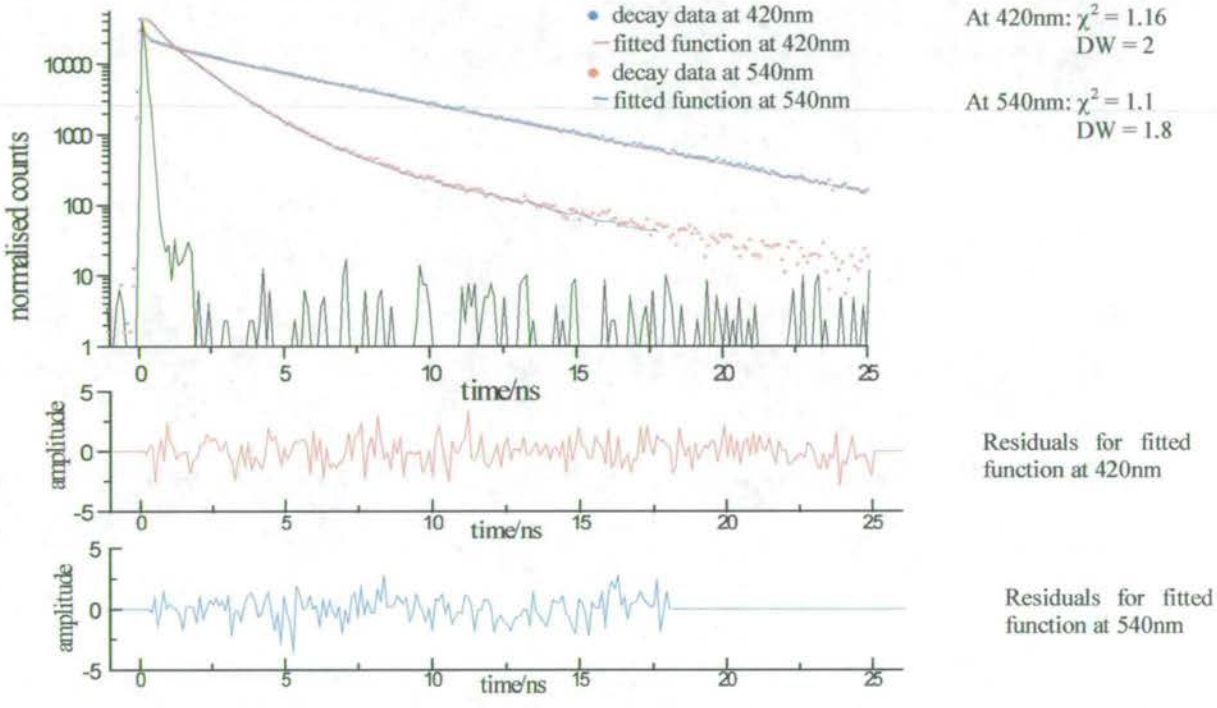

Figure 6.16 Log plot of experimental decay data, instrument response function, fitted tri-exponential functions and residual plots for sample 5a dissolved in ethanol at 420nm and 540nm, made from a 100mmol Indole-5-carboxylic acid monomer solution at 5 Hz for 30 seconds to give a sample with a higher polymer content.

As for 5-bromoindole the results have been presented as plots of A factor and % contribution versus wavelength for each of the three lifetimes τ_1, τ_2 and τ_3, shown in Figure 6.17 and Figure 6.18 for samples 5a and 5b respectively.

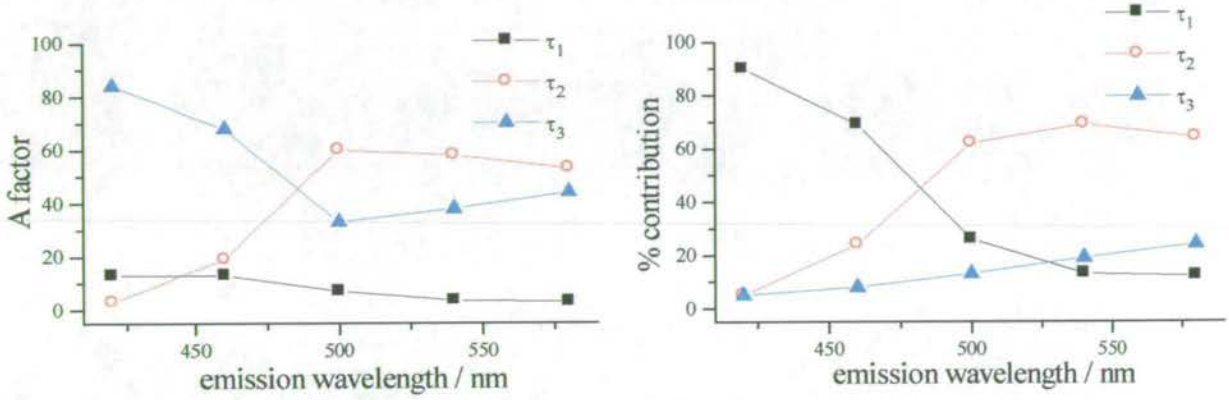

Figure 6.17 Plots of A factor and % contribution versus wavelength for each of the three characteristic component lifetimes for sample 5a dissolved in ethanol, produced using a 100 mmol indole-5-carboxylic acid monomer solution using a rotation speed of 5 Hz for 30 seconds to give a higher polymer content.

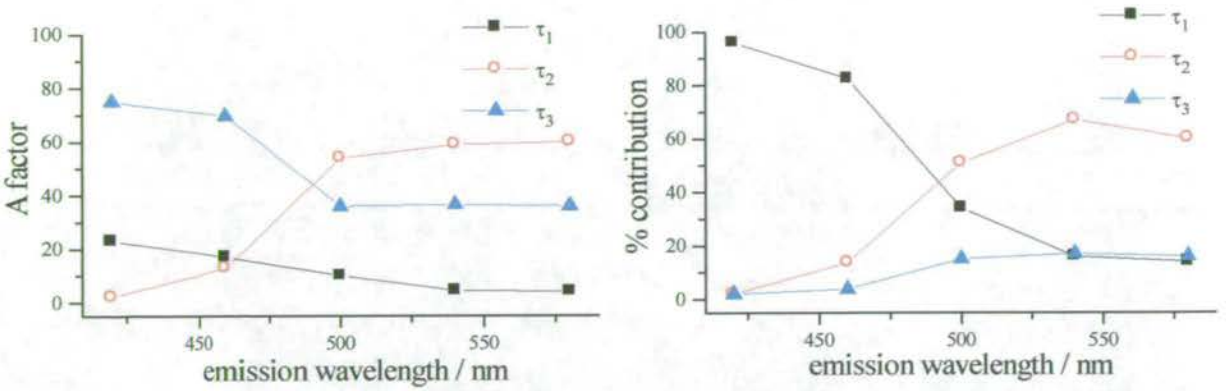

Figure 6.18 Plots of A factor and % contribution versus wavelengthfor each of the three characteristic component lifetimes for sample 5b dissolved in ethanol, produced using a 100 mmol indole-5-carboxylic acid monomer solution using a rotation speed of 15 Hz for 10 seconds to give a higher trimer content.

As expected from the preferential solubility of the trimer in ethanol, at short wavelengths, τ_1, the longest lived component, is dominant for both samples. In the polymer-rich sample 5a, the A factor and % contribution of τ_1 is lower and of τ_3 higher at short wavelengths than in the trimer-rich sample 5b. This is consistent with the proposal that τ_1 is due to a free trimer species and τ_3 to an intra-chain trimer chromophore from which energy transfer is very efficient. In both samples, as the wavelength increases, there is an increasing influence from τ_2. In the polymer emission region, above 500nm this component becomes dominant, with τ_1 still present, but with a much smaller contribution. This again corresponds with the previous conclusions, that τ_2 results from a distribution of intermediate conjugation length polymer segments, of increasing length as the wavelength increases. This is also supported by the observation that the value of τ_2 increases with increasing wavelength. The remaining presence of the longest component, τ_1, at

longer wavelength implies that it now corresponds to the longest conjugation lengths segments of the polymer. The contribution of the longest component, τ_1 in the polymer emission region (from 500 to 580nm) is a lot smaller than was seen for 5-bromoindole. This is consistent with the reduced solubility of the polymer sample compared to 5-bromoindole, hence a lower proportion of longer chain length polymers contributing to the emission.

6.4.2.1 Repeating indole-5-carboxylic acid experiments

A number of further indole-5-carboxylic acid samples were produced using higher and lower monomer concentrations and a range of rotation speeds and polymerisation times. The analysis of the experimental data for these samples produced very similar results to those presented above. Since the results are very similar, they have been placed in Appendix I along with plots of A factor and % contribution against wavelength. All of the samples examined so far have shown the same trends with regards to wavelength dependence and preparation conditions.

6.4.2.2 Time-resolved emission spectroscopy on indole-5-carboxylic acid

As for 5-bromoindole, time-resolved emission spectra were measured for some of the indole-5-carboxylic acid samples. Due to the reduced solubility of the indole-5-carboxylic acid polymer, the steady-state emission results discussed in Chapter Four only ever showed low intensity emission in the longer wavelength polymer emission region. This is also noted in the time-resolved emission spectra, where the longer wavelength emission was of low intensity. However the results are similar to those of 5-bromoindole and examples of short lifetime and long lifetime spectra are shown in Figure 6.19.

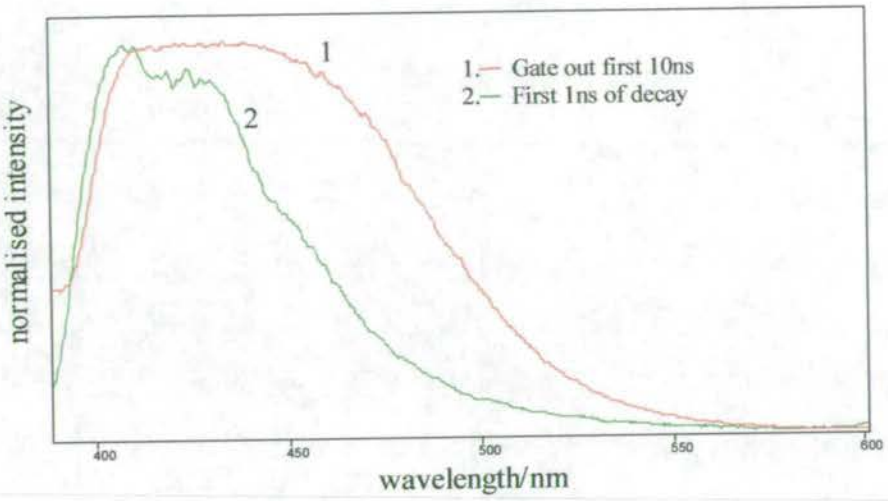

Figure 6.19 Time-resolved emission spectra for indole-5-carboxylic acid polymerised from a 100 mmol monomer solution at 5 Hz for 30 seconds and dissolved in ethanol.

The emission from the short lifetime species is seen to be of a trimeric nature, confirming that it is due to excitation localised on an intra-chain trimer chromophore within the polymer. At longer lifetimes, the emission shifts to longer wavelength, corresponding to the presence of emission from longer conjugation length polymer species. The trimer like emission that is still present at longer lifetime confirms the assumption that the 5 ns lifetime corresponds to the free trimer species, which has little contact with the polymer species.

6.4.3 Electropolymerised 5-cyanoindole

5-cyanoindole is much less soluble than both 5-bromoindole and indole-5-carboxylic acid. It is only slightly soluble in ethanol, more soluble in DMF and almost fully soluble in DMSO except when the polymer content is very high. Therefore the results obtained are slightly different from those already presented, with solutions likely to contain high amounts of free trimer regardless of the polymerisation conditions. Samples were prepared using a variety of polymerisation conditions and lifetimes were measured for solutions of 5-cyanoindole in ethanol, DMF and DMSO, however the fits obtained for all these solutions were not as good as those previously measured. The best fits were achieved for samples dissolved in DMF whose preparation conditions are shown in Table 6.11. Figure 6.20 is an example of the experimental results and fitted functions for sample 6a of 5-cyanoindole polymerised from a 50 mmol monomer solution at 1 Hz for 30 seconds to give a high polymer content, with decays measured at 420nm and 580nm. The difference between the decay of emission from the trimer region and the polymer region can be clearly seen. The complete set of data is shown in Table 6.12.

Concentration of 5-cyanoindole monomer	Rotation speed and polymerisation time	
	1 Hz 30 seconds	15Hz 5 seconds
50 mmol	Sample 6a	Sample 6b

Table 6.11 Polymerisation conditions for 5-cyanoindole samples.

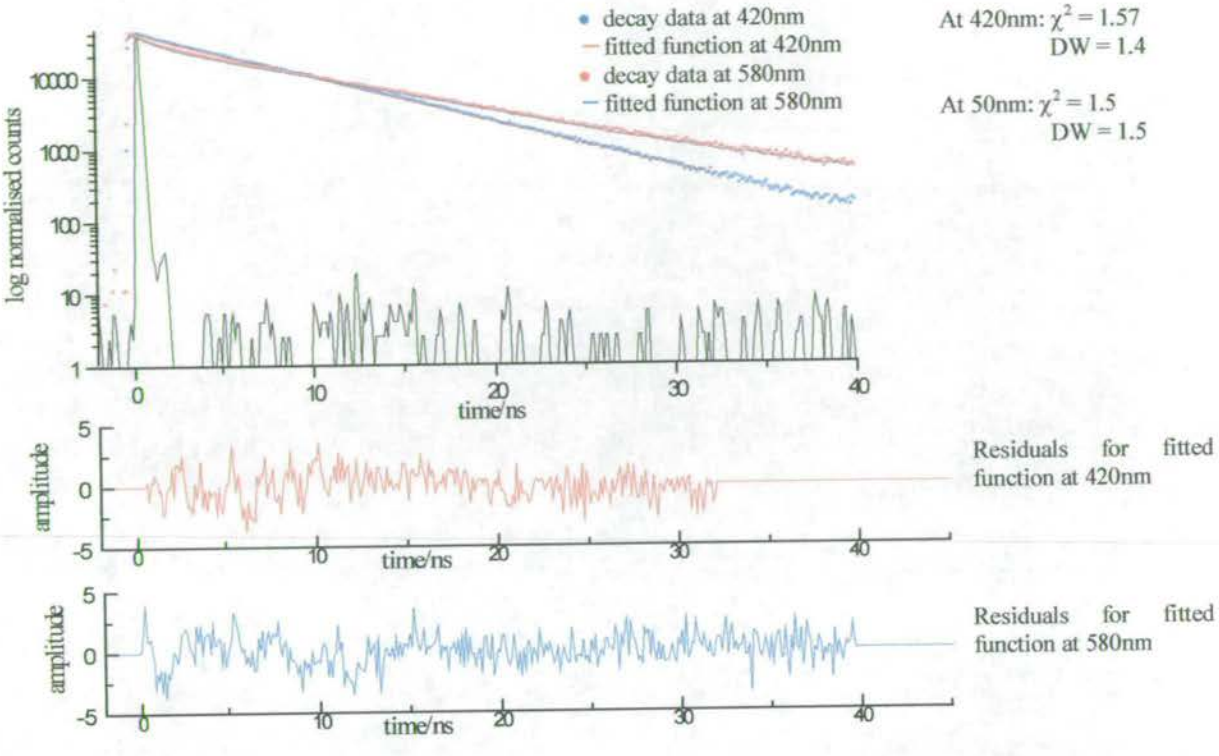

Figure 6.20 Log plot of experimental decay data, instrument response function, fitted bi-exponential functions and residual plots for sample 6a at 420nm and 580nm, made from a 50mmol 5-cyanoindole monomer solution at 1 Hz for 30 seconds to give a high polymer content, then dissolved in DMF.

Unlike the 5-bromoindole and indole-5-carboxylic acid, the fitted functions were not all tri-exponential. At short wavelength, bi-exponential fits were possible, with only some of the long wavelength decays needing a tri-exponential function to give a satisfactory fit. This complies with the lower solubility of electropolymerised 5-cyanoindole, where fewer polymer species will be dissolved, therefore there will be a smaller proportion of the intra-chain trimer species to

contribute to the short wavelength emission. The longest lifetime is also slightly longer than for the other indoles, with values of almost 9ns, however this would appear to be a solvent effect as the decay times measured in ethanol solution (a full set of results can be found in appendix II) are shorter. The lifetimes can be split into a short and long-lived species, with an even shorter-lived species present in one of the samples at long wavelength. As previously, the characteristic component lifetimes are labelled τ_1, τ_2, and τ_3. The contribution of the species with respect to wavelength is presented in Figure 6.21 and Figure 6.22.

	50 mmol/ 15 Hz/ 5 seconds sample 6b, high trimer				100 mmol/ 1 Hz/ 30 seconds sample 6a, high polymer		
λ / nm	τ_1 / ns	τ_2 / ns	τ_3 / ns		τ_1 / ns	τ_2 / ns	
420	6.91 90 99	0.59 10 1.0		1.78 1.4	6.81 85 99	0.24 15 1	1.57 1.4
460	7.22 92 99	0.53 8 1.0		1.9 1.12	7.14 91 99.5	0.34 9 0.5	1.9 1.3
500	7.86 44 83	1.29 56 17		1.4 1.34	7.81 93 99	1.13 7 1.0	1.6 1.5
540	8.91 9.0 51	3.82 5.0 13	0.69 86 36	1.5 1.4	8.56 74 92	2.20 27 8.0	1.4 1.3
580	8.74 4.1 47.1	2.09 2.5 6.7	0.38 93.4 46.2	1.9 2	8.84 27 69	1.45 74 31	1.5 1.5

Table 6.12 Lifetime data for 5-cyanoindole samples 6a and 6b produced from a 50 mmol sample at 15 Hz, 5 seconds and 1 Hz 30 seconds, then dissolved in DMF.

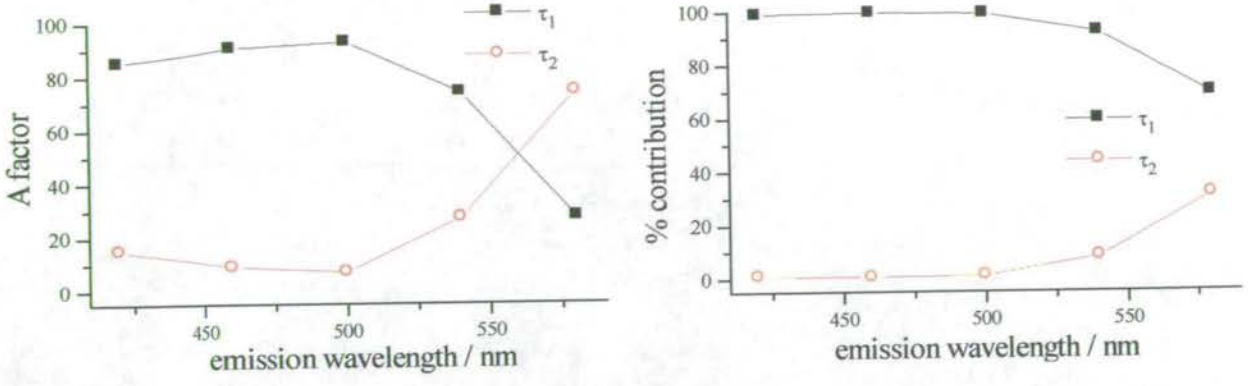

Figure 6.21 Plots of wavelength vs. A factor and % contribution for each of the two characteristic component lifetimes for sample 6a produced using a 50 mmol Indole-5-carboxylic acid solution and a rotation speed of 1 Hz for 30 seconds, to give a high polymer content.

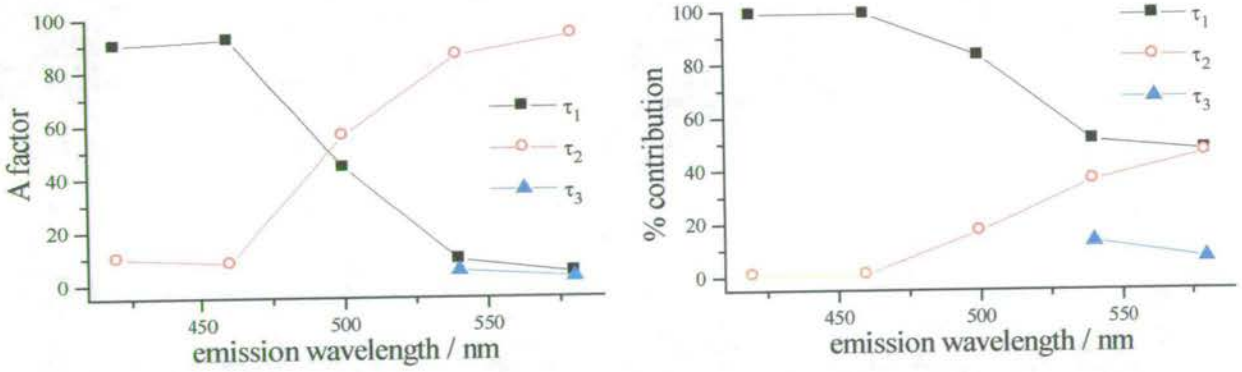

Figure 6.22 Plots of wavelength vs. A factor and % contribution for each of the three characteristic component lifetimes for sample 6b produced using a 50 mmol Indole-5-carboxylic acid solution and a rotation speed of 15 Hz for 30 seconds to give a high trimer content.

Although the results differ from the other indoles, similar patterns are observed. The lower solubility results in a more dominant long lifetime emission, τ_1, at short wavelength that corresponds to a high proportion of the free trimer species. As the wavelength increases, this lifetime increases in value and shows a significant reduction in contribution, consistent with there being a contribution from a longer conjugation length polymer species.

The reduced solubility of the longest polymer chains reflects in a smaller difference between the higher polymer sample 6a and the higher trimer sample 6b. The presence of a short lifetime species, τ_3, at short wavelengths is consistent with an intra-chain trimer chromophore, however due to the lower solubility, it has a much smaller contribution. As was noted for the other indoles, there is an increasing contribution as the wavelength is increased from a species with an intermediate lifetime, τ_2, that corresponds to a distribution of intermediate conjugation length polymer segments.

6.4.3.1 Time-resolved emission spectroscopy on 5-cyanoindole.

The time-resolved emission spectra presented in Figure 6.23 are from a sample of 5-cyanoindole polymerised from a 50 mmol monomer solution at 1 Hz for 30 seconds to give a polymer-rich sample, dissolved in ethanol.

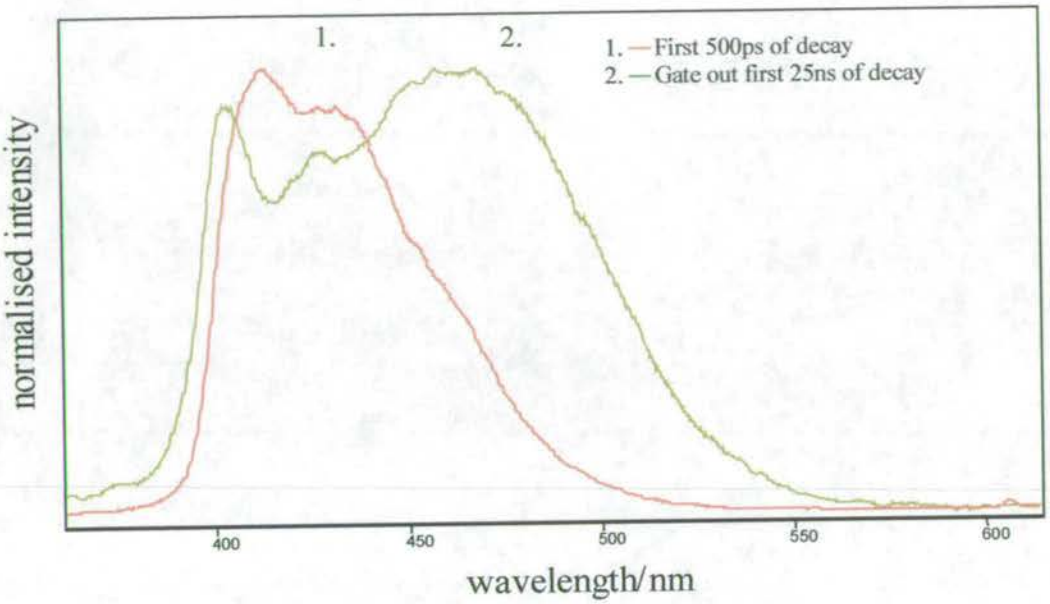

Figure 6.23 Time-resolved emission spectra for 5-cyanoindole polymerised from a 50 mmol monomer solution at 1 Hz for 30 seconds, to give a high polymer content and dissolved in ethanol.

Although the lifetime data from ethanol solutions did not give very good fits, the time-resolved emission spectra give the clearest view of the different components, although it is noted that only the trimer and shorter polymer chain lengths will be observed due to the lower solubility. The time resolved spectra confirm the conclusions drawn from the lifetime data. The very short lifetime species is seen to have a trimer like emission profile, which is consistent with it being the result of excitation of an intra-chain trimer. If only the emission from the very tail of the decay is collected then an obvious polymer emission is observed at longer wavelength. This is consistent with the model that the longest conjugation length polymer segments act as energy

traps into which the mobile excitation energy is transferred to before returning to the ground state. Also present in the spectrum corresponding to the tail of the decay are peaks that correspond to a trimer species. This confirms that the free trimer species is responsible for the longest lived decay at short wavelengths.

6.5 Lifetime measurements on intact electropolymerised films

In chapter four the steady state emission of electropolymerised indole films was discussed with only the reduced form of 5-cyanoindole being found to be fluorescent. Because of this, lifetime measurements were only made on such films. Films were produced using a wide range of solution concentrations, rotation speeds and polymerisation times to investigate their influence on properties. Experiments were also carried out where the film was electrochemically cycled between the reduced and oxidised states to see the long-term effect on emission as well as to higher potentials to see the effect of further linking of the film. This section will examine the overall trends observed for the films, the number of lifetimes that fit to the decays and the effects of polymerisation conditions and wavelength of emission. The next chapter will deal in greater detail with the effects of film structure on the emission, how cycling to higher potential effects the film and how the emission changes when the film is cycled between redox states.

6.5.1 Effect of wavelength on lifetimes

Emission is seen only from the reduced form of the films. Additionally, there is a significant effect of the polymerisation conditions on the intensity of emission and hence the lifetime. This is dealt with in the next section, however, it should be noted that the most intense emission is

seen from films that are made from high concentration monomer solutions and at fast rotation speeds. Therefore in this discussion concerning the effect of wavelength, an example will be used that was prepared using such conditions, from a 50 mmol monomer solution, at 2 Hz for 20 seconds. Shown in Figure 6.24 is an example of the decay data and fitted functions for the film at short and long wavelengths.

It is clear both that the decay is multiexponential and that there is a significant increase in the lifetimes as the wavelength is increased. The full set of data for this film is shown in Table 6.13. As can be seen from the fitted data, none of the decays will fit satisfactorily to less than four exponentials. It is accepted that fitting to such a number of exponentials can be misleading, however every film produced has a very similar multiexponential nature, with a similar distribution of lifetimes. In fitting the data in such a way, the resulting lifetimes are not being presented as a measurement of the exact lifetimes of the species present, but as a representation of the system, allowing comparisons between samples and general features to be observed. In fact, the very multiexponential nature of these decays indicates the complex nature of a system that possesses multiple emitting species. Although the decay of the films fluorescence is being quantified by four lifetimes, it is expected that each of these lifetimes will represent a distribution of emitting species.

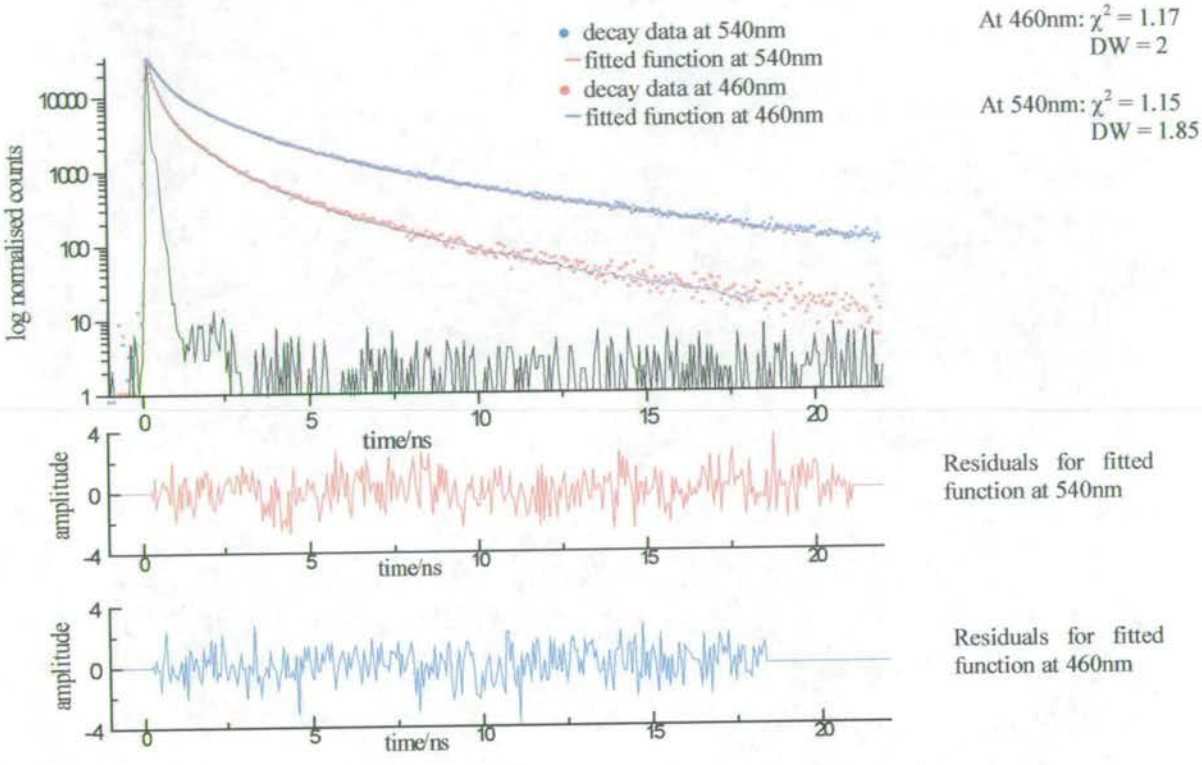

Figure 6.24 Log plot of experimental decay data, instrument response function, fitted four exponential functions and residual plots for a 5-cyanoindole electropolymerised film at 460nm and 540nm, made from a 50mmol 5-cyanoindole monomer solution at 2 Hz for 20 seconds.

λ / nm	50 mmol/ 20 seconds/ 2 Hz				
	τ_1 / ns	τ_2 / ns	τ_3 / ns	τ_4 / ns	
460	4.02 1 17	1.25 7 31	0.38 24 34	0.072 68 18	1.17 1.85
480	4.39 2 20	1.26 10 35	0.35 27 32	0.076 58 13	1.1 1.8
500	4.71 2 21	1.35 9 34	0.38 30 32	0.083 59 14	1.2 1.8
520	5.12 2 24	1.45 10 35	0.41 30 30	0.081 57 11	1.3 1.84
540	6.52 4 31	1.88 17 41	0.5 37 23	0.085 43 5	1.2 1.8

Table 6.13 Lifetime data for a 5-cyanoindole electropolymerised film produced from a 50 mmol 5-cyanoindole monomer solution at 2 Hz for 30 seconds.

From the results in Table 6.13 and the decays illustrated in Figure 6.24, it can be seen that all the lifetimes increase with increasing wavelength. This is a feature that is observed for all the films examined, regardless of polymerisation conditions. The plot in Figure 6.25 shows this increase in lifetime with wavelength. Unlike the solution phase lifetime measurements, there is no great change in the values of A factor and % contribution for each lifetime as the wavelength is increased. As for the solution phase results, the characteristic component lifetimes have been classified as τ_1, τ_2, τ_3 and τ_4, with graphs of A factor and % contribution vs. emission wavelength plotted and shown in Figure 6.26.

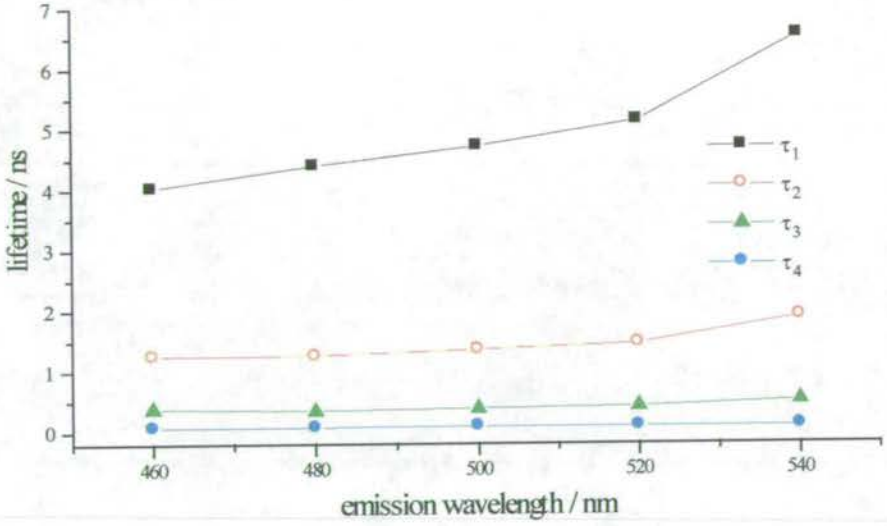

Figure 6.25 Plot of lifetime against wavelength for the four lifetimes fitted to the decay of a 5-cyanoindole film polymerised from a 50 mmol monomer solution at 2 Hz for 20 seconds.

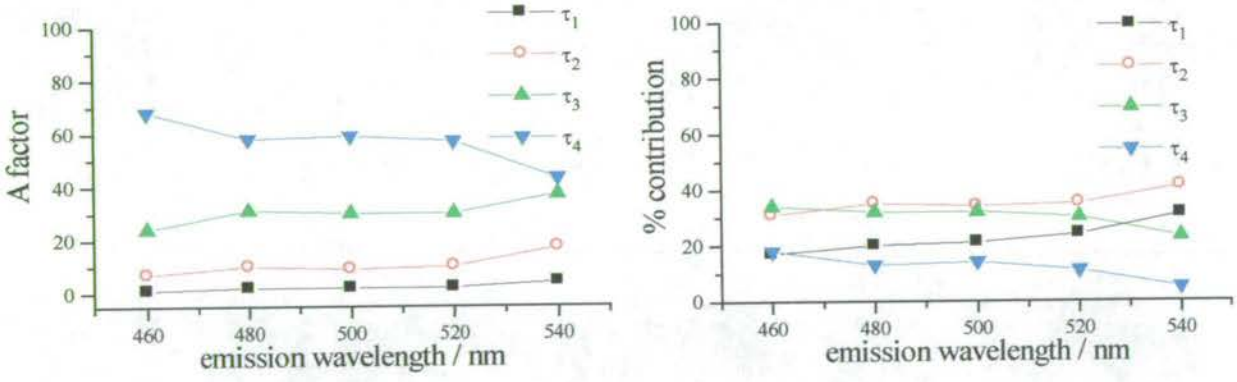

Figure 6.26 Plots of wavelength vs. A factor and % contribution for each of the four characteristic component lifetimes for a 5-cyanoindole film polymerised using a 50 mmol monomer solution and a rotation speed of 2 Hz for 20 seconds.

Although the variation in A factor and % contribution is small, there is a general trend, which is observed for all the films examined. As the wavelength increases, there is a greater contribution from the longer-lived species. This feature, along with the increase in the value of the lifetimes with wavelength, provides an indication of the emitting species present in the film. Unlike the solution phase samples, there will be no isolated free trimer species in the film, since even an isolated trimer unit will be in close contact to any polymer species. Due to the short wavelength of the excitation source, the higher energy trimer and short polymer units will be preferentially excited. Because of the close contact in the film it is expected that any isolated trimer units, or short conjugation length polymer segments will rapidly lose their excitation energy via energy transfer to longer conjugation length, lower energy polymer units. Therefore the short wavelength emission that originates from the higher energy species will have the shortest lifetime due to efficient energy transfer. This explains the general increase in lifetime at longer wavelengths and the decrease in contribution from the short-lived species at longer wavelengths.

In the intact films, there is no evidence of emission from an inter-chain excimer, although it is expected that there will be some energy transfer between chains due to their close proximity. These results are similar to experiments carried out on the conjugated polymer poly(p-phenylene vinylene) (PPV), which is discussed in Chapter One (section 1.4). Lifetime measurements on films of PPV were consistent with photo-excitation giving an intra-chain singlet exciton, whereas the derivative CN-PPV, showed evidence of energy migration to form an inter-chain excimer. It would appear that the fluorescence emission from 5-cyanoindole films is similar in nature to that from PPV films, even though they are quite different in terms of both chemical composition and synthesis.

6.5.1.1 Time-resolved emission spectroscopy on the 5-cyanoindole film

In order to confirm the findings concerning emission lifetime and wavelength, time-resolved emission spectra were collected. As has been previously mentioned, this allows a more graphic interpretation of the emitting species. A film was prepared from a 50 mmol monomer solution at 10 Hz to give a highly fluorescent film and the emission spectra were measured at different time gates. The time-resolved emission spectra for this film are shown in Figure 6.27 from which it can be seen that the short-lived species have a narrower emission at shorter wavelength than the long-lived species. This is consistent with the short wavelength emission being the result of trimer units or short conjugation length polymers, which have a short-lived emission due to efficient energy transfer to longer conjugation length polymer segments. The narrower emission is a reflection of a limited distribution of short conjugation lengths, whereas at longer wavelength there will be emission from a large distribution of longer conjugation lengths with longer lifetimes, resulting in the broader, longer wavelength emission from the long-lived species.

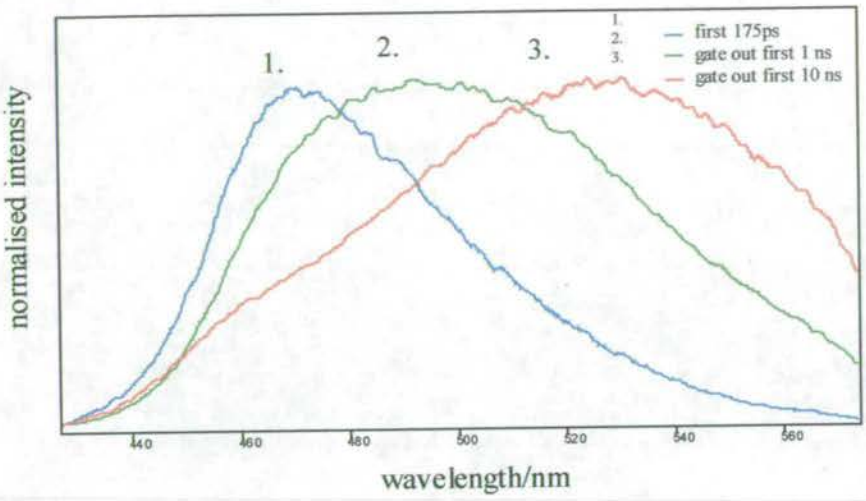

Figure 6.27 Time-resolved emission spectra for a 5-cyanoindole film polymerised from a 50 mmol monomer solution at 15 Hz for 30 seconds.

6.5.2 Effect of polymerisation conditions on lifetimes

The three main variables of the polymerisation conditions are monomer solution concentration, rotation speed and polymerisation time. These have been discussed previously with the view of controlling the trimer and polymer content of the films. These conditions have a significant effect on the emission properties of the films, which can vary from highly fluorescent with relatively long lifetimes to completely non-fluorescent. This variation in the emission properties will be related to the composition of the film and also its structure, which is discussed in more detail in the next chapter. The effect of changing each of these conditions will be presented, then the results will be discussed as a whole.

6.5.2.1 Variation of lifetime with rotation speed.

Regardless of the monomer solution concentration and polymerisation time, the rotation speed has a very large effect on the emission properties. This effect is greatest when the monomer solution concentration is low, which is consistent with electrochemical results. The example given below is for films electropolymerised from a 50 mmol monomer solution.

	λ = 460nm				λ = 540nm			
Rotation speed	τ_1 / ns	τ_2 / ns	τ_3 / ns	τ_4 / ns	τ_1 / ns	τ_2 / ns	τ_3 / ns	τ_4 / ns
0 Hz	1.11	0.48	0.16	0.036	1.46	0.53	0.18	0.047
1 Hz	3.05	0.85	0.24	0.047	4.55	1.21	0.32	0.074
2 Hz	4.02	1.25	0.38	0.072	6.52	1.88	0.5	0.085
3 Hz	4.39	1.23	0.34	0.063	6.44	1.74	0.45	0.097

Table 6.14 Data for the variation of lifetime with rotation speed for a 5-cyanoindole film polymerised from a 50 mmol monomer solution at the given rotation speeds for 20 seconds with lifetimes measured at a wavelength of 460nm and 54onm.

From the data shown in Table 6.1 it can be seen that small changes in the rotation speed have a considerable effect on the emission lifetimes. This can be seen more clearly in Figure 6.28 where the four fitted lifetimes are plotted against rotation speed. The response of lifetime to rotation

speed is shown at short and long emission wavelengths to illustrate that a similar effect is seen at all emission wavelengths.

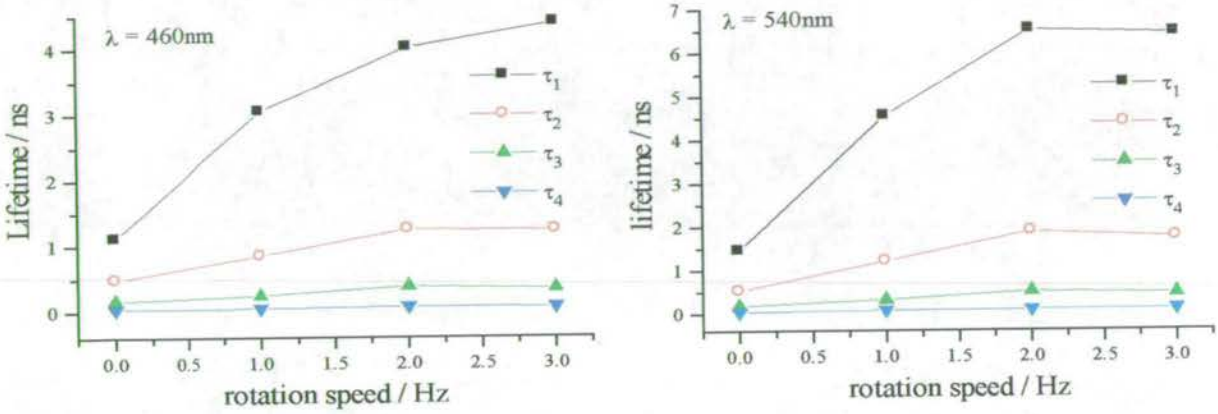

Figure 6.28 Plots of lifetime against rotation speed for 5-cyanoindole films polymerised for 20 seconds from a 50 mmol monomer solution at a wavelength of 460nm and 540nm.

6.5.2.2 Variation of lifetime with concentration

Rotation speed and monomer solution concentration are both used for controlling the trimer and polymer content of a film, therefore the effect of altering the concentration is expected to be similar to that of altering the rotation speed. This is seen to be the case, which is illustrated in the example shown below. The rotation speed and polymerisation time were kept constant at 5 Hz and 30 seconds, and the monomer solutions made up to 20 mmol, 50 mmol and 100 mmol. The results are shown in Table 6.1 and graphically in Figure 6.29.

concentration	τ_1 / ns	τ_2 / ns	τ_3 / ns	τ_4 / ns
20 mmol	1.13	0.37	0.132	0.039
50 mmol	4.09	1.14	0.3	0.06
100 mmol	6.26	1.77	0.44	0.076

Table 6.15 Data for the variation of lifetime in relation to monomer solution concentration for 5-cyanoindole film electropolymerised at 5 Hz for 30 seconds. Measured at a wavelength of 500nm.

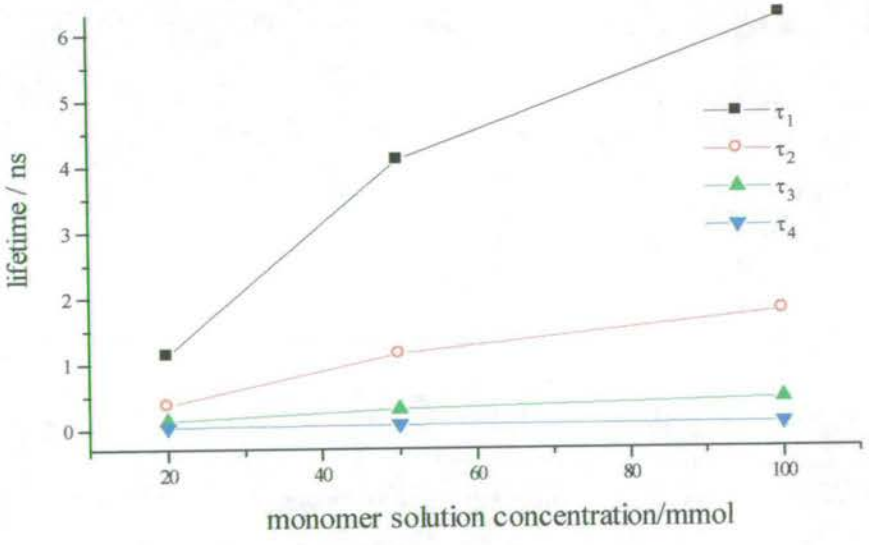

Figure 6.29 Plot of lifetime against monomer solution concentration for 5-cyanoindole film electropolymerised at 5 Hz for 30 seconds. Measured at a wavelength of 500nm.

The trend for changing the monomer solution concentration is very similar to that seen for rotation speed. As the concentration increases, so do the lifetime values. The emission wavelength at which the lifetimes were measured was 500nm, however the same effect is observed at all emission wavelengths, as was observed for the rotation speed.

6.5.2.3 Variation of lifetime with polymerisation time.

The effect of altering the polymerisation time was not as great as the solution concentration and rotation speed, however, there is a noticeable difference in the lifetimes. In order to see any changes, the solution concentration and rotation speed were kept constant at 100 mmol and 5 Hz and the polymerisation time set at 10 seconds, 30 seconds and 1 minute. This has a considerable effect on the physical appearance of the film, with it becoming thicker as the polymerisation time is increased. Table 6.16 and Figure 6.30 show the results of this experiment.

Polymerisation time	τ_1 / ns	τ_2 / ns	τ_3 / ns	τ_4 / ns
10 seconds	5.3	1.75	0.493	0.114
30 seconds	5.09	1.51	0.4	0.072
60 seconds	4.14	1.27	0.353	0.086

Table 6.16 Data for the variation of lifetime with polymerisation time for 5-cyanoindole films polymerised from a 100 mmol monomer solution at 5 Hz and measured at a wavelength of 460nm.

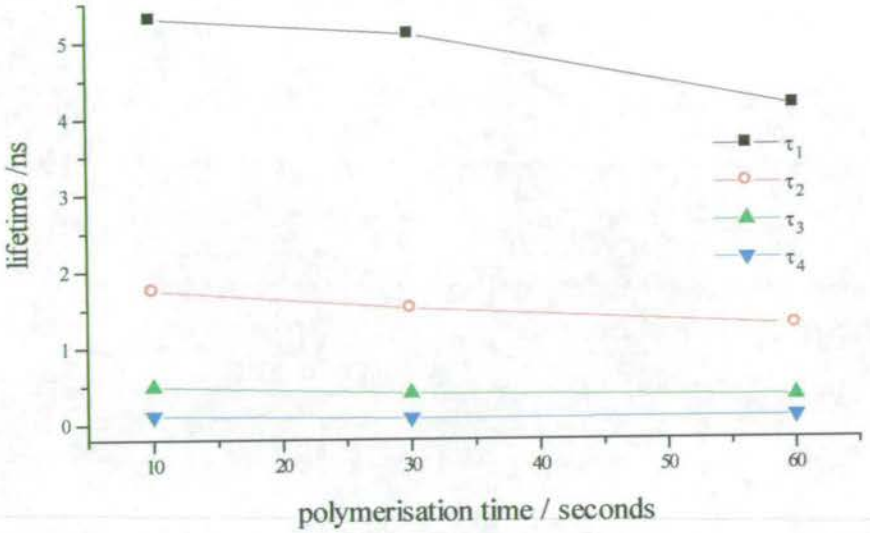

Figure 6.30 Plot of lifetime against polymerisation time for 5-cyanoindole films polymerised from a 100 mmol monomer solution at 5 Hz and measured at a wavelength of 460nm.

As the polymerisation time is increased there is a small decrease in each of the fitted lifetimes. The example above shows the lifetime data measured at 460nm; the same pattern is seen at all emission wavelengths.

6.5.2.4 Discussion of the effect of polymerisation conditions

Briefly recapping on the effect of polymerisation conditions on the composition of a film, high monomer concentrations and fast rotation speeds will result in a trimer-rich film whilst low concentrations and slow rotation speeds will give a polymer-rich film. Short polymerisation times will result in a thin film, which will have had less time to undergo further polymerisation,

whilst long polymerisation times will give a thicker film that is more likely to contain long chain polymer.

With these facts in mind, it would appear that the most highly fluorescent 5-cyanoindole films with the longest lifetimes are those that are rich in trimer. From the results presented above it can be seen that the most fluorescent film will be one that has been polymerised from a high concentration monomer solution at a fast rotation speed for a short time. It would require further work to establish the precise optimum conditions for a highly fluorescent film. From these results, it cannot be established whether the emission properties of a highly fluorescent film are the direct result of the presence of a high trimer concentration, or the influence of composition on the structure of the film. This is explained further in the next chapter.

6.6 Conclusions

Picosecond time-correlated single photon counting was used to measure the fluorescence lifetimes of electropolymerised 5-bromoindole, indole-5-carboxylic acid and 5-cyanoindole in solution and their associated monomers as well as intact films of 5-cyanoindole. The experiment was assessed for reliability and was found to give consistent, reproducible lifetimes using standard reference samples.

5-cyanoindole and 5-bromoindole monomers were found to have single exponential decays with lifetimes of 4.32 ns and 4.5 ns, respectively, when not degassed and 5.23 ns and 6.55 ns when degassed. The lifetime of indole-5-carboxylic acid monomer was found to be dependent upon

solution concentration. At concentrations below 1 x 10^{-6} molar, a single exponential function fits the decay data, with a lifetime of 1.2 ns. At higher concentrations, a lifetime of approximately 8 ns becomes dominant, thought to be the result of an aggregation effect due to the hydrogen-bonding ability of the carboxy group.

Solutions of electropolymerised 5-bromoindole were used to build a model of the fluorescence decay behaviour of the trimer and polymer species. Films of 5-bromoindole are fully soluble in ethanol, therefore all species produced during electropolymerisation are known to be present in solution. Samples were produced using a range of polymerisation conditions to give trimer-rich and polymer-rich solutions. It was found that the decay data would not fit satisfactorily to fewer than three exponentials, with the resulting lifetimes taken as being representative of a distribution of emitting species. Each of the three lifetimes consistently fell into a defined lifetime range, with a long-lived component of approximately 5 ns (τ_1), an intermediate length component of approximately 2 ns (τ_2) and a short-lived component of approximately 0.3 ns (τ_3). Lifetime measurements were made at a range of emission wavelengths to investigate the relationship between the lifetimes and the emitting trimer and polymer species.

A model has been proposed to account for the time-resolved fluorescence properties. The short lifetime component, τ_3, is attributed to a high excitation energy species, where the excitation is localised on an intra-chain trimer chromophore, isolated from the conjugated system. Very efficient non-radiative decay, through energy transfer will occur from this species, to lower energy, longer conjugation length segments, hence the very short lifetime. The intermediate lifetime component, τ_2, corresponds to intermediate conjugation length segments, which lose

their excitation energy by transfer to longer conjugation length segments, but less efficiently so than the high excitation energy species, hence the increased lifetime. The long lifetime component, τ_1, corresponds at short emission wavelengths (420 nm-480 nm) to the free trimer species in solution, which has little contact with the polymer and therefore is subject to minimal non-radiative decay via energy transfer. At longer emission wavelengths (above 500nm) τ_1 corresponds to the lowest excitation energy segments of the polymer with the longest conjugation lengths. Non-radiative decay via energy transfer to longer conjugation lengths no longer occurs, therefore the lifetime is much greater. This relates to solution phase time-resolved studies on the conjugated polymer PPV, where there is strong evidence for a distribution of conjugation lengths (see discussion in Chapter One section 1.4.3.1). Excitation at short wavelengths is thought to generate excitons on the shorter, higher energy segments, with this energy then migrating to longer, lower energy segments

The single photon counting experiment was set up to collect time-resolved emission spectra, a powerful method of visualising the variation in lifetime with emission wavelength. The TRES for 5-bromoindole supported the above model, showing a trimer like emission at very short lifetimes and at longer lifetimes both polymer and trimer emission.

Samples of electropolymerised 5-cyanoindole and indole-5-carboxylic acid were examined using the same systematic variation of preparation conditions as for 5-bromoindole. Due to the lower solubility of the samples, the lifetime data was not as good and was less representative of the system as a whole. However, the same trends were observed as for 5-bromoindole, both in the lifetime data and the time-resolved emission spectra, supporting the proposed model.

Fluorescence lifetimes were collected for intact films of 5-cyanoindole in the reduced state, with films produced using a wide range of preparation conditions. The emission from the intact film was found to be multiexponential, adequately fitting to no fewer than four exponentials, which varied from 40 ps to 6.5 ns. The lifetimes were found to increase at longer emission wavelengths, reflected in the appearance of the time-resolved emission spectra, which shift to longer wavelength and become broader at longer lifetimes. In the film, there is not the same distinction between trimer and polymer species as in solution, due to the close interaction of all species present. The increase in lifetimes at longer emission wavelengths is thought to correspond to a transfer of the excitation energy from high excitation energy, short conjugation length species, to lower energy, longer conjugation length segments, acting as energy traps. There is no evidence of photo-excitation generating an inter-chain excimer species, as has been reported for the conjugated polymer CN-PPV.

It was found that the polymerisation conditions had a considerable effect on the emission properties of the film, with a high trimer content giving the most fluorescent films with the longest lifetimes. Increasing the rotation speed, increasing the monomer solution concentration, and decreasing the polymerisation time, which are all associated with increasing the trimer content, all served to increase the lifetimes and hence the luminescence efficiency.

Chapter Seven – Effects of structure and redox state on the emission properties of electropolymerised 5-cyanoindole and Indole-5-carboxylic acid films

7.1 Introduction

The previous chapter discussed the fluorescence lifetimes of electropolymerised 5-bromoindole, indole-5-carboxylic acid and 5-cyanoindole in the solution phase and 5-cyanoindole as a solid film. The fluorescence lifetimes were used as an indication of photoluminescence efficiency, making the assumption that the natural radiative lifetime, k_r, is constant for all the emitting species, therefore changes in the fluorescence lifetime, τ_f, indicate changes in the rates of non-radiative decay, k_{nr}. This chapter takes the discussion of the emission properties of the 5-cyanoindole films further, examining the effect on decay times of electrochemically cycling the film and further polymerisation of the film by cycling to higher potentials. In order to do this a novel, in-situ fluorescence apparatus was developed and used, allowing emission intensities to be measured as the film was cycled between redox states.

7.2 Effect on the fluorescence lifetimes of electrochemically cycling a 5-cyanoindole film.

Electrochemical experiments have shown [1] that a 5-cyanoindole film can be repeatedly cycled between its reduced and oxidised states with very little change in the electrochemical

properties of the film. This is illustrated by the CV in Figure 4.5 (Chapter 4). However, if the film is taken to potentials higher than the oxidation peak, an irreversible peak is seen due to the linking of residual trimer units in the film to form a more extensive polymer system (Figure 4.6). Since a potential use of the polymerised indoles is as an electroluminescent material, it is important to gain an understanding of the relationship between electrochemical and photophysical behaviour of trimer and polymer species, in their oxidised and reduced forms, in a film.

7.2.1 Cycling between the redox peaks.

The first experiment was to find out if the reversible cycling of a film had a significant effect on its emission properties. A high trimer content film was made to give an intense fluorescence emission, according to the conditions discussed in chapter 6, using a 100 mmol monomer solution with a rotation speed of 10 Hz for 20 seconds. Since only the reduced form of the film is fluorescent, all measurements given here are for reduced films i.e. after cycling the current is switched off at the negative end of the sweep. To examine the films, the electrode is removed from the solution and the electrode tip dismounted (as described in Chapter 3 section 3.4.5), allowing lifetimes for an intact film, as formed on the electrode, to be measured. The first film was removed without any cycling and its fluorescence decay measured. Further films were prepared using the same conditions but were cycled either once, twice or twenty times between –0.1V and 0.8V before having their decays measured. The cyclic voltammogram in Figure 7.1 shows the first three cycles, illustrating the reversible nature of the redox behaviour. After an initial small drop in the current, the CV settles into a reversible cycle.

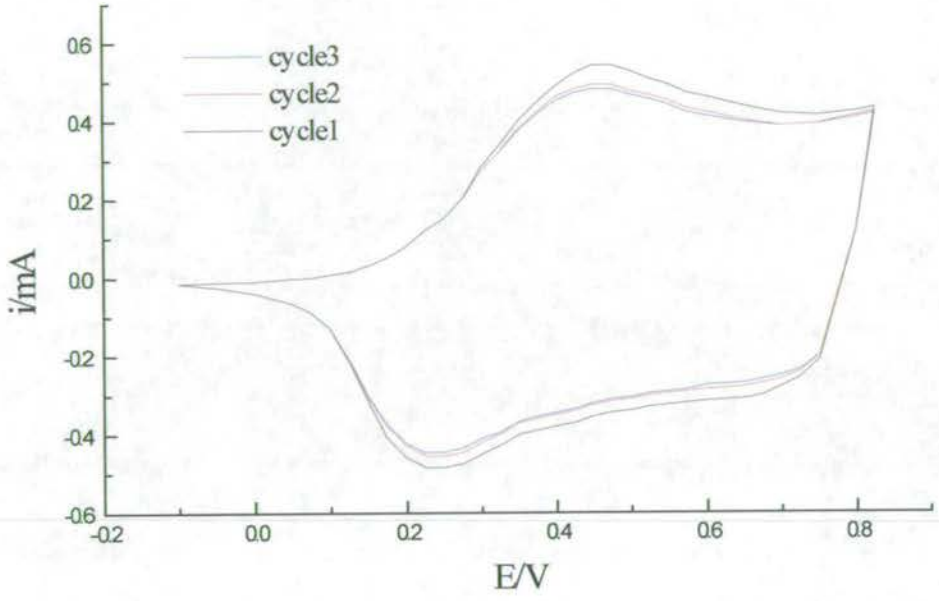

Figure 7.1 Cyclic voltammogram at 20mv/s for the first three cycles of a 5-cyanoindole film polymerised from a 100 mmol monomer solution at 10 Hz for 20 seconds.

The lifetimes for each of the films prepared are shown in Table 7.1, having been measured at emission wavelengths of 460nm, 500nm and 540nm. The small variation in lifetimes that is observed over a small number of cycles is probably due to the difficulty in exactly reproducing the experimental conditions for each film, as was discussed in section 6.4.1, with the reversible cycling between oxidation states having little effect. After 20 cycles there is a slight decrease in the lifetimes. This can be attributed to a small amount of polymerisation occurring at the higher potential, where it can be seen on the CV that the current begins to increase. This process of polymerisation is discussed in the next section.

		τ_1 / ns	τ_2 / ns	τ_3 / ns	τ_4 / ns
λ = 460nm	Uncycled	3.7	1.1	0.3	0.03
	CV x 1	4.2	1.1	0.3	0.06
	CV x 2	4.2	1.2	0.3	0.05
	CV x 20	3.1	0.93	0.26	0.034
λ = 500nm	uncycled	4.4	1.2	0.33	0.062
	CV x 1	5.54	1.3	0.3	0.01
	CV x 2	5.53	1.42	0.38	0.096
	CV x 20	3.4	1.02	0.31	0.064
λ = 540nm	uncycled	5.32	1.53	0.415	0.157
	CV x 1	7.14	2	0.55	0.015
	CV x 2	5.91	1.34	031	0.04
	CV x 20	4.34	1.24	0.35	0.085

Table 7.1 Lifetimes for a series of 5-cyanoindole films polymerised from a 100 mmol monomer solution at 10 Hz for 20 seconds and cycled between –0.1V and 0.8 V for the given number of cycles. Lifetimes were measured at emission wavelengths of 460nm, 500nm and 540nm.

To confirm that cycling of the film was not having a significant effect on the emission properties, the above experiment was repeated, but the film was only cycled between –0.1V and +0.5V to ensure no polymerisation of the film can occur. The fluorescence lifetimes from an uncycled film and a film cycled 20 times are shown in Table 7.2. The differences between the lifetimes for the uncycled and cycled films were very small, confirming that the reversible electrochemical redox process has little or no effect on the emission properties of the film.

		τ_1 / ns	τ_2 / ns	τ_3 / ns	τ_4 / ns
λ = 460nm	Uncycled	4.38	1.26	0.33	0.06
	CV x 20	4.6	1.23	0.33	0.084
λ = 500nm	uncycled	5.34	1.5	0.37	0.035
	CV x 20	6.64	1.87	0.51	0.13
λ = 540nm	uncycled	7.23	2.65	1.1	0.35
	CV x 20	7.0	1.75	0.46	0.12

Table 7.2 Lifetimes for a series of 5-cyanoindole films polymerised from a 100 mmol monomer solution at 10 Hz for 20 seconds and cycled between –0.1V and 0.5 V for the given number of cycles. Lifetimes were measured at wavelengths of 460nm, 500nm and 540nm.

7.2.2 Cycling beyond the redox peaks

Subjecting a fluorescent 5-cyanoindole film to potentials higher than 0.8V has a considerable effect on the emission properties. The voltage to which the film is cycled and the sweep rate at which it is cycled determine the magnitude of this effect. The electrochemical response of a 5-cyanoindole film that is cycled to higher potentials is exemplified by the CVs shown in Figure 7.2. An oxidation peak at 1.06V is seen that becomes much smaller on each subsequent cycle. This peak is attributed to the linking of residual free trimer units in the film to form extended polymer chains [2]. The example in Figure 7.2 shows a film that is taken well beyond the potential at which polymerisation occurs. A considerable difference is seen between each subsequent cycle.

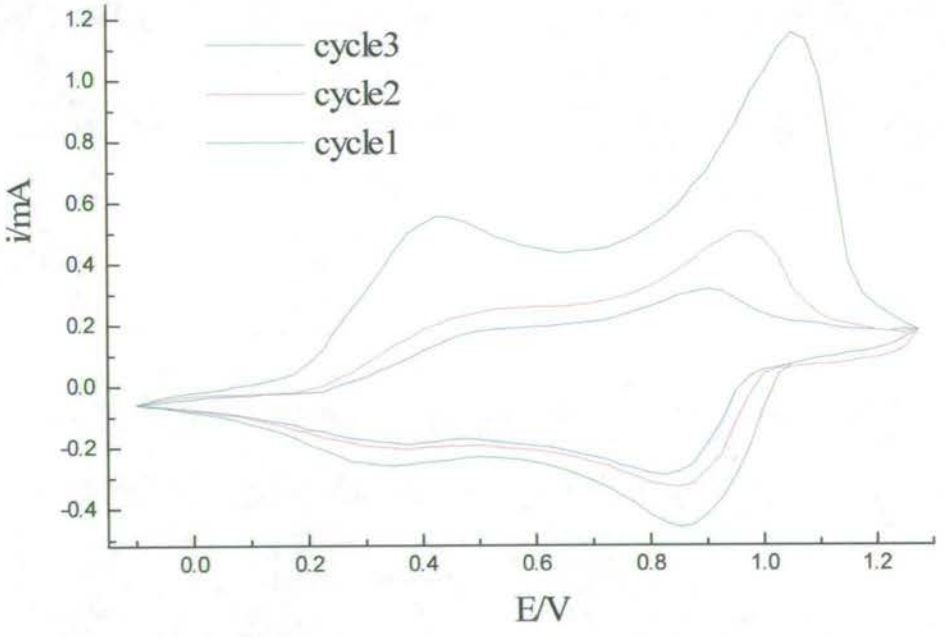

Figure 7.2 Cyclic voltammogram at 20mv/s for the first three cycles of a 5-cyanoindole film from –0.1V to +1.3V, polymerised from a 100 mmol monomer solution at 10 Hz for 20 seconds.

Without exception, cycling the film to potentials greater than 0.8V causes a drop in the emission intensity and a reduction in the fluorescence lifetimes. To follow this loss of emission a series of films were made using identical polymerisation conditions and then subjected to a number of cycles between –0.1V and +1V at 20 mV/second. The fluorescence decay of each film was then measured at emission wavelengths of 460nm, 500nm and 540nm. The lifetime data obtained are shown in Table 7.3 and a selection of the decays are shown in Figure 7.3

	Number of cycles	τ_1 / ns	τ_2 / ns	τ_3 / ns	τ_4 / ns
λ = 460nm	0	5.09	1.51	0.4	0.072
	2	2.44	0.8	0.27	0.061
	4	1.7	0.62	0.24	0.06
	6	0.42	0.135	0.034	--
λ = 500nm	0	6.26	1.77	0.44	0.076
	2	3.5	1.1	0.34	0.076
	4	2.75	0.88	0.3	0.08
	6	0.61	0.2	0.065	0.023
λ = 540nm	0	8.47	2.17	1.23	0.4
	2	3.9	1.13	0.36	0.08
	4	3.45	1.12	0.36	0.091
	5	2.43	0.84	0.29	0.08

Table 7.3 Lifetimes for a series of 5-cyanoindole films polymerised from a 100 mmol monomer solution at 5 Hz for 30 seconds and cycled between –0.1V and +1 V for the given number of cycles. Lifetimes were measured at emission wavelengths of 460nm, 500nm and 540nm

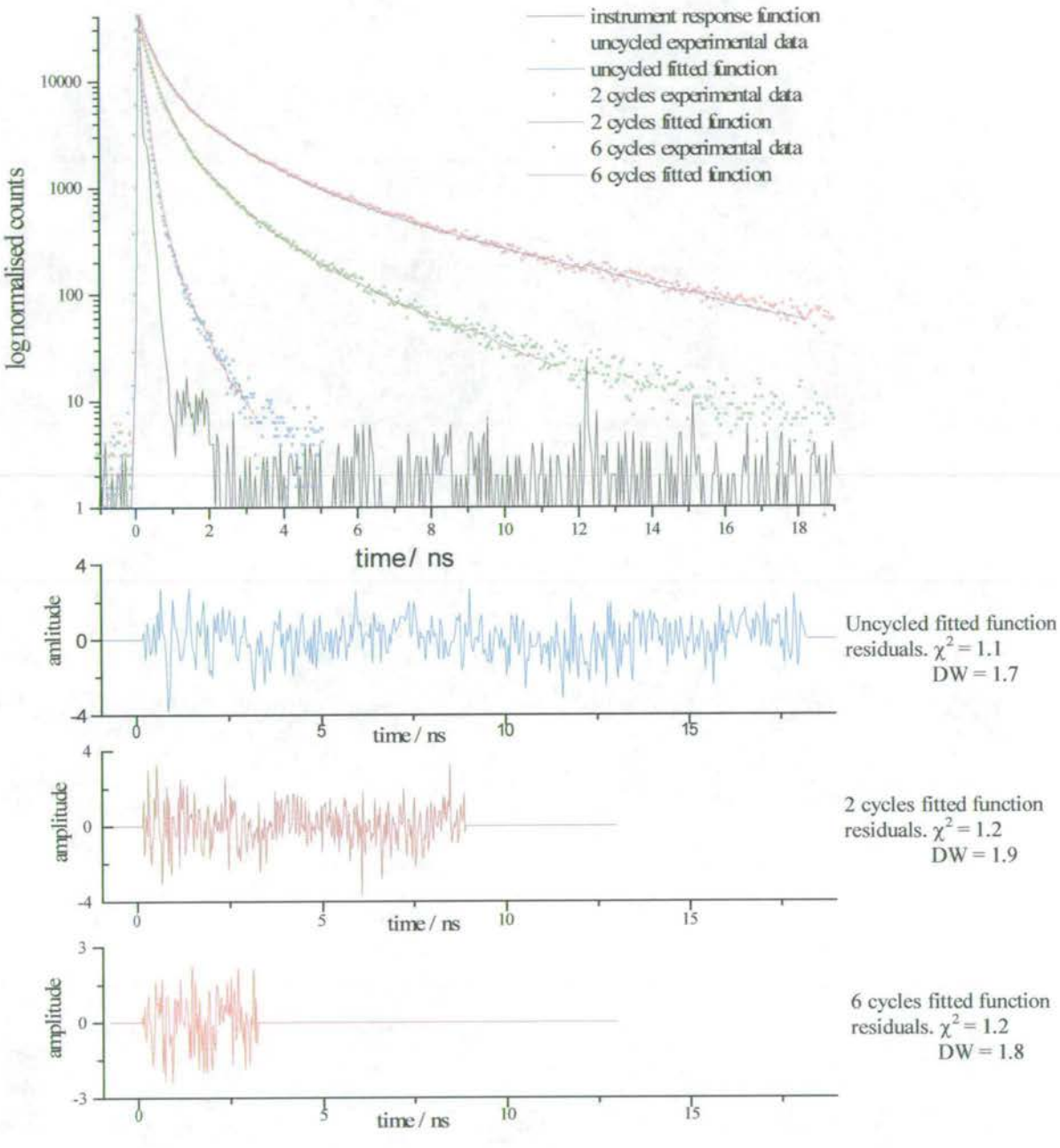

Figure 7.3 Experimental data, instrument response function, fitted four-exponential functions and residual plots for the fluorescence decay of 5-cyanoindole films polymerised from a 100 mmol monomer solution at 5 Hz for 30 seconds. The films were cycled for the number of times given, between –0.1V and + 1V, at a sweep rate of 20 mv/second. The decays were measured at an emission wavelength of 480nm.

The decrease in the lifetimes of the films with increasing number of cycles can be seen quite clearly, with the lifetimes becoming appreciably much shorter after 6 cycles. When a film was cycled more than six times, the emission intensity dropped too low to be experimentally measurable. The data in Table 7.3 are represented by plots of lifetime against the number of cycles in Figure 7.4. The decrease in the lifetimes occurs regardless of the emission wavelength at which the decay is collected.

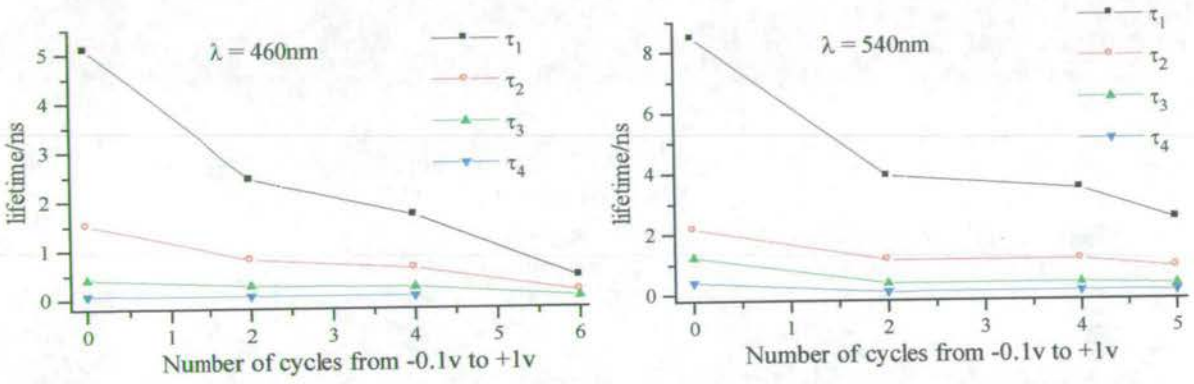

Figure 7.4 Plots of lifetime against number of cycles for 5-cyanoindole films polymerised from a 100 mmol monomer solution at 5 Hz for 30 seconds. The films were cycled at 20 mv/second between –0.1V and 1 V and the lifetimes measured at 460nm and 540nm.

Altering the cycling voltage

If the film is cycled to a voltage higher than 1V as for the example Figure 7.2, then there is a much greater drop in the emission intensity and lifetimes after the first cycle. To try and find the point at which the greatest change occurred, several films were made and cycled once up to different voltages. The lifetimes were then measured at a range of wavelengths, a selection of which are shown in Table 7.4. The same trend is seen at all emission

wavelengths. The greatest drop in lifetime occurs when the film is cycled above +1.1V, which corresponds, to the potential of the "linking" peak shown in Figure 7.2.

	τ_1 / ns	τ_2 / ns	τ_3 / ns	τ_4 / ns
uncycled	3.49	0.914	0.255	0.051
-0.1V to 1 V	2.93	0.866	0.267	0.056
-0.1V to 1.1V	2.21	0.683	0.202	0.04
-0.1V to 1.2V	0.83	0.21	0.042	

Table 7.4 Lifetimes for 5-cyanoindole films polymerised from a 100 mmol monomer solution at 10 Hz for 20 seconds then cycled once to the voltages shown at 20 mv/s. The lifetimes were measured at an emission wavelength of 460nm.

7.2.2.2 Altering the sweep rate

The sweep rate has a considerable effect on electrochemical studies as it controls the rate at which further polymerisation of the film occurs. To investigate the effect of sweep rate on the emission properties, several films were made then cycled once between –0.1V and 1.1V using sweep rates from 5 mV/s to 100 mV/s. The lifetimes were measured at a range of emission wavelengths, a selection of which are given in Table 7.5.

		τ_1 / ns	τ_2 / ns	τ_3 / ns	τ_4 / ns
λ = 480nm	no cycles	3.3	0.9	0.25	0.048
	100 mv/s	3.27	0.96	0.29	0.06
	50 mv/s	2.36	0.73	0.22	0.05
	20 mv/s	1.45	0.4	0.16	0.04
	10 mv/s	0.62	0.21	0.08	0.025
	5 mv/s	0.32	0.1	0.023	N/A
λ = 520nm	no cycles	4.09	1.14	0.3	0.06
	100 mv/s	4	1.1	0.3	0.065
	50 mv/s	3.2	0.9	0.26	0.058
	20 mv/s	1.9	0.6	0.17	0.045
	10 mv/s	0.9	0.3	0.11	0.031
	5 mv/s	0.5	0.16	0.05	0.01

Table 7.5 Lifetimes for 5-cyanoindole films polymerised from a 50 mmol monomer solution at 5 Hz for 30 seconds then cycled once from –0.1V to 1.1V at the sweep rates given. The lifetimes were measured at emission wavelengths of 480nm and 520nm.

It was found that the sweep rate has a significant effect on the emission properties. At very fast sweep rates, there is very little difference between the cycled and uncycled film. As the sweep rate slows down, so the effect on the film increases, with the lifetimes decreasing. At 5 mV/s there is a large reduction in the lifetimes and the intensity of emission is only just

detectable. Although only the lifetimes measured at two wavelengths are shown above, the effect is the same at all wavelengths.

The results presented above show how the emission characteristics of a 5-cyanoindole film are affected by electrochemically altering the composition of that film. The trends observed are consistent with the conclusions drawn in chapter 6 concerning the polymerisation conditions for the films. The experiments presented in that chapter showed that films produced under conditions favouring a high trimer content had a greater fluorescence yield and longer lifetimes than those produced to favour a high polymer content. The results from the experiments described here show how the emission intensity and lifetime decrease as the film is further polymerised by cycling it beyond its redox potentials. The reason why more extensive polymerisation leads to a reduced quantum yield is discussed further in section 7.3.1. The effect is greatest when the voltage to which the film is subjected is greater than the linking potential and when the sweep rate is slowest. The effect of sweep rate is a kinetic one, with a greater degree of linking occurring when the sweep rate is slow than when it is fast. An important observation to note from the above results is the minimal effect on the emission properties of cycling the film between redox states and returning to the reduced state. This suggests that 5-cyanoindole films are stable within set electrochemical conditions even when cycled for an extended period of time. This point will be discussed in more detail later in the chapter.

7.3 Direct comparison of solid state and solution phase electropolymerised 5-cyanoindole.

The fluorescence emission from an electropolymerised 5-cyanoindole film has been shown to be very sensitive to polymerisation conditions and further electrochemical processes. For example, a film made to favour a high trimer content is very fluorescent, whereas a film with a high polymer content has little or no fluorescence emission. If a film rich in trimer is cycled once beyond the redox region then the fluorescence intensity drops considerably. The composition of the film is obviously affecting its emission properties, however, whether this is due to the species present, the structure of the film, or a combination of both, is difficult to say. The drop in emission intensity between films rich in trimer and polymer implies that in the polymer-rich film there are efficient quenching pathways for the excitation energy. To see whether this quenching was a result of the presence of polymer or its morphology in the film, films were prepared with varying composition and some were cycled. A direct comparison between the fluorescence properties of the solid and solution was made by measuring the fluorescence decays for the films before they were dissolved off the electrode, then examining them in solution. To examine the effect of film structure on fluorescence properties a comparison was made between electropolymerised films and films drop coated onto a quartz slide. This was carried out for films that were in both the reduced and oxidised states.

7.3.1 Effect of polymer content on film and solution emission.

The lifetime data presented in Table 7.6 are for an uncycled and a cycled intact film and solutions of those respective films in ethanol. The film was cycled to a point where the emission intensity was reduced but still detectable. The decrease in the lifetimes of the cycled film can clearly be seen.

Wavelength / nm		No cycles					3 cycles				
		τ_1	τ_2	τ_3	τ_4		τ_1	τ_2	τ_3	τ_4	
Intact film	460	3.23 1 14	1 7 31	0.3 25 34	0.07 68 20	1.5 1.9	1.09 0.2 5	0.37 3 16	0.13 15 36	0.03 82 43	1 2
	500	3.94 1.6 22	1.12 10 38	0.3 28 30	0.05 61 10	1.3 1.7	1.57 0.5 8	0.49 4 23	0.16 21 38	0.04 74 32	1.4 1.9
	540	4.57 2.5 24	1.3 14 38	0.38 34 27	0.1 50 11	1.5 1.6	1.98 0.6 9	0.64 5 26	0.19 25 39	0.05 69 39	1.3 2
Solution	420	5.76				1.5 1.4	5.8 94 98.6	1.36 6 1.4			1.5 1.4
	500	5.8 97 99	1.52 3 1			1.7 1.3	5.79 82 94	1.8 18 7			1.5 1.7
	580	5.78 85 95	1.7 15 5			1.6 1.5	5.8 93 98	1.6 7 2			1.6 1.5

Table 7.6 Lifetime data for a film and the film dissolved in ethanol, polymerised from a 20 mmol monomer solution at 10 Hz for 1 minute. The cycled film was cycled three times from –0.1V to +1V then held at –0.1V to give a reduced film.

Data consists of:

Lifetime A factor % contribution	χ^2 value DW value

The considerable difference seen in the emission properties of the cycled and uncycled films is not mirrored by the emission properties of the respective solutions. The intensity of the emission from the solutions of cycled and uncycled films is comparable and the lifetimes are very similar. The only notable difference is the presence of a small contribution at 420nm

from a short-lived lifetime in the solution of the cycled film. These are very similar to results presented in chapter six, where a solution sample of 5-cyanoindole, with a high polymer content, has an additional short lived decay at short wavelengths due to excitation localised on an intra-chain trimer chromophore. There is a possibility that due to the lower solubility of polymerised 5-cyanoindole in ethanol, only the free trimer and short chain polymer species are present in the solutions examined above i.e. the composition of the solution and film are different. Therefore some experiments were carried out using DMF as the solvent, to insure complete dissolution of the polymer film. A 5-cyanoindole film was produced that had been cycled six times from –0.1V to 1.25V to ensure it had been fully linked. The resulting film was dark black in colour even in the reduced state compared to the light green of a fluorescent film. This film was then dissolved in DMF and the emission examined. The fitted lifetime data is shown in Table 7.7.

Wavelength / nm	uncycled				6 cycles			
	τ_1	τ_2	τ_3		τ_1	τ_2	τ_3	
420 nm	6.91 90 99	0.59 10 1		1.78 1.4	8.13			1.4 1.6
500 nm	7.86 44 83	1.29 56 17		1.9 1.12	9.56 87 93	4.682 14 7		1.3 1.7
580 nm	8.74 4.1 47.1	2.09 2.5 6.7	0.378 93.4 46.2	1.9 2	11.93 28 72	4.67 22 22	0.49 51 5	1.2 1.8

Table 7.7 Lifetime data for two films dissolved in DMF. The films were polymerised from a 50 mmol monomer solution at 10 Hz for 30 seconds. The cycled film was cycled six times from –0.1V to +1.25V.

Although the quality of fit for the lifetimes presented in Table 7.7 were not good, the trend is clear. There is no decrease in lifetime (reduction in luminescence efficiency) for the cycled sample compared to the uncycled sample, in fact the lifetimes for the cycled sample are slightly longer. The above experiments, where films were cycled then dissolved off the electrode, were repeated a number of times using different initial polymerisation conditions, the results are shown in Appendix III. In all cases, the same trend was observed, with the film emission being very sensitive to polymerisation conditions and cycling whereas the solution phase emission showed only small changes, with no detectable drop in the emission intensity.

These results suggest that the significant change in the emission properties of 5-cyanoindole films with respect to polymerisation conditions and cycling are due a structural effect associated with the presence of extended polymer chains. When there is a high proportion of polymer present there appears to be a very efficient quenching mechanism, removing the excitation energy via a non-radiative pathway. This structural effect is lost when the film is dissolved and the emission intensity is similar to that of a high trimer sample. This implies that in the intact electropolymerised film there are inter- as well as intra-chain processes influencing its emission properties. Due to the close contact of polymer chains in the film, the excitation energy is easily transferred between chains and can decay via efficient non-radiative mechanisms. In solution these non-radiative mechanisms are lost, implying that only intra-chain processes are involved in the decay of the excited state. Upon dissolution, the close contact between polymer chains is lost and inter-chain interaction can no longer occur.

7.3.2 Emission characteristics of drop coated films.

It has been shown that the fluorescence emission of an intact film is far more sensitive to variations in preparation conditions and subsequent cycling than that of a dissolved film and that it appears to be the structure of the film that influences the emission characteristics. To determine whether this influence is due to the specific structure of the film as laid down during electropolymerisation, or simply the fact that it is in the solid phase, an experiment was carried out where a non-fluorescent, cycled film was dissolved off the electrode then drop coated onto a quartz slide. This was also carried out for an oxidised film, which has no fluorescence emission on the electrode and for an indole-5-carboxylic acid film which showed no fluorescence emission. The difficulty in carrying out this experiment was in producing a drop-coated film of sufficient quality. This was never fully achieved, with films being of uneven thickness and subsequent lifetime measurements being dependent upon the spatial location of the excitation beam. Therefore, the lifetimes presented here are not very reproducible, but are useful for comparison with the intact electropolymerised films and for picking out trends in the lifetimes.

7.3.2.1 Cycled and uncycled 5-cyanoindole films

The decay data and fitted function shown in Figure 7.5 is for a film as prepared on the electrode. This film was then dissolved off using DMF then drop coated onto a quartz slide, the decay data and fitted function for the drop coated film are shown in Figure 7.6. The decay shown in Figure 7.7 is for a drop coated film that was prepared using the same conditions as the previous two films, but was then cycled repeatedly between –0.1V and +1.25V to link the film. The fitted lifetime data for all these films at 460nm and 500nm is presented in Table 7.8.

The most notable result is that the drop-coated film that was prepared from a cycled, non-fluorescent film shows an intense fluorescence emission. This implies that the lack of fluorescence in the film on the electrode is due to a quenching mechanism that occurs as a result of the films structure, not its composition, since a film of the same composition is fluorescent after being dissolved off the electrode then drop coated. Both the solution of the dissolved film and its drop-coated film are fluorescent whereas the intact film on the electrode is not.

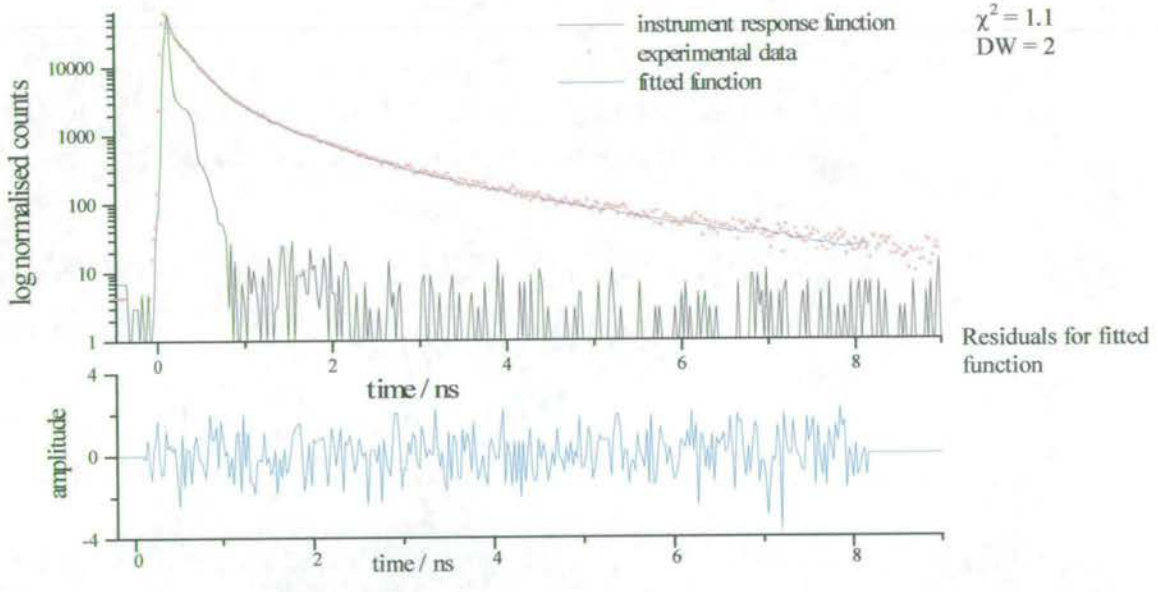

Figure 7.5 Experimental data, fitted function and residual plot for a 5-cyanoindole electropolymerised onto a Pt electrode from a 50 mmol monomer solution at 10 Hz for 30 seconds.

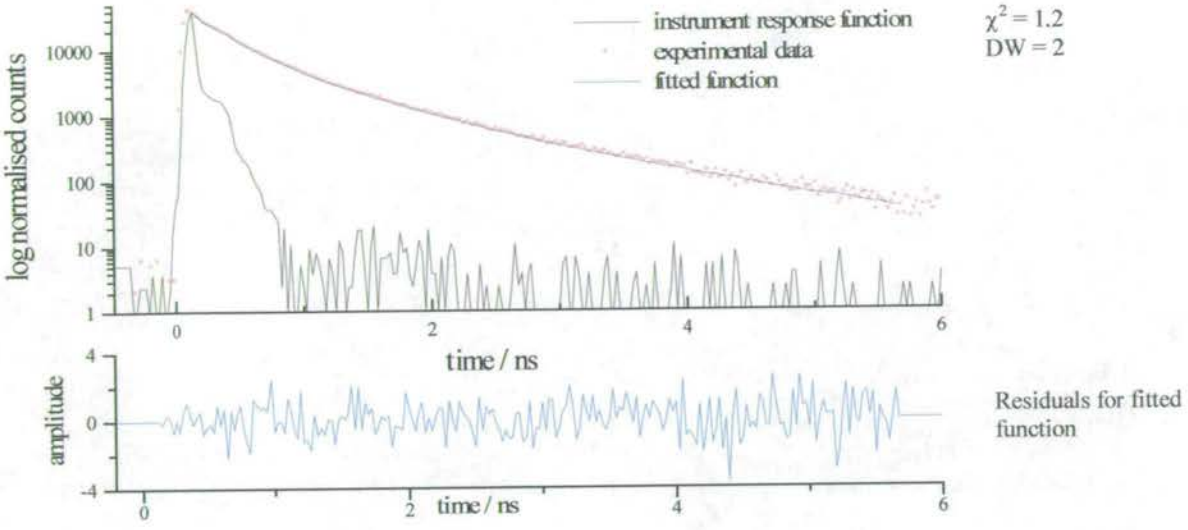

Figure 7.6 Experimental data, fitted function and residuals plot of 5-cyanoindole film drop coated from a DMF solution of the film shown in Figure 7.5 (from a 50 mmol monomer solution at 10 Hz for 30 seconds) onto a quartz slide.

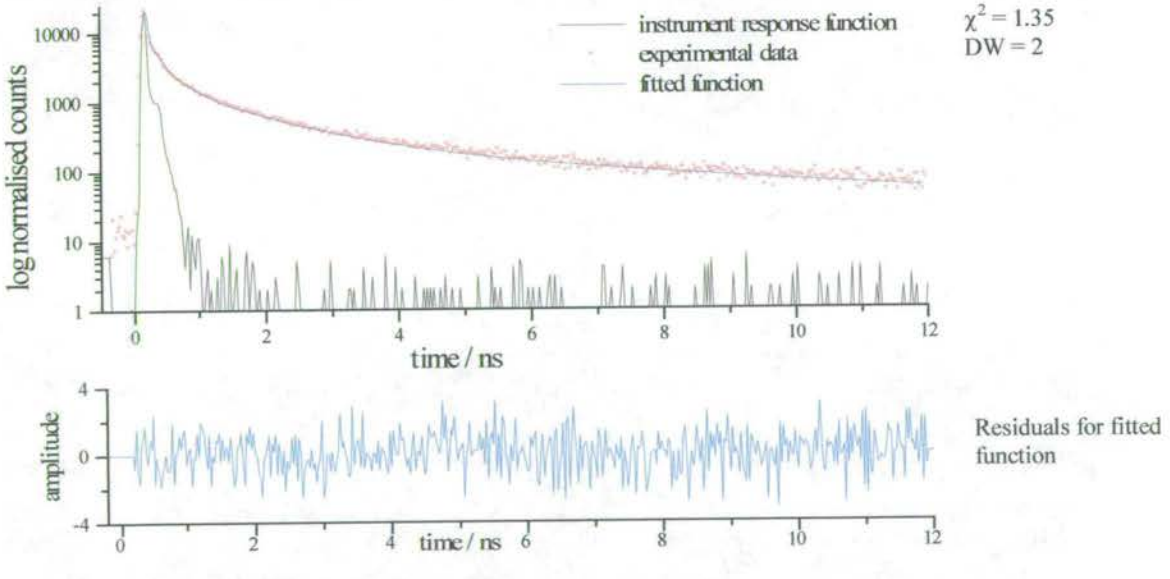

Figure 7.7 Experimental data, fitted function and residuals plot for a 5-cyanoindole drop coated film. The original film was polymerised from a 50 mmol monomer solution at 10 Hz for 30 seconds then cycled from 0.1V to 1.25V six times before dissolving in DMF.

	Wavelength / nm	Fitted lifetimes / ns				
		τ_1	τ_2	τ_3	τ_4	
Uncycled film on electrode	460	2.05 0.6 10	0.63 5 26	0.19 23 38	0.04 72 26	1.1 2
	500	2.53 0.9 15	0.72 6 30	0.21 26 35	0.05 67 20	1.2 1.9
Uncycled drop coated film	460	6.71 0.4 21	1.45 3 36	0.34 6 16	0.03 91 26	1.4 2
	500	6.3 0.6 30	1.42 3 30	0.3 6 13	0.04 91 26	1.5 1.75
Cycled drop coated film	460	7.75 0.4 25	1.26 2.5 29	0.275 7.4 19	0.03 90 27	1.35 2
	500	8.13 0.5 33	1.27 3 29	0.26 8 16	0.04 88 23	1.3 2

Table 7.8 Lifetime data for films of 5-cyanoindole on the electrode and drop coated from a DMF solution. Films were polymerised from a 50 mmol monomer solution at 10 Hz for 30 seconds. The cycled film was cycled from –0.1V to 1.25V six times.

From the data in Table 7.8 it can be seen that there is some variation in lifetime between the intact films on the electrode and the drop coated films. The lifetimes of the drop-coated films are considerably longer than the intact film, although there are still four components with comparable contributions to those in the intact film. The longer lifetimes implies that there is less efficient non-radiative decay in the drop-coated film. The cycled and uncycled drop-coated films have very similar lifetimes, which implies that there is a similar distribution of emitting species and similar fluorescence efficiencies for both films. These observations are consistent with structural effects influencing the emission properties of the intact film.

7.3.2.2 Reduced and oxidised films

So far all the results presented have been for 5-cyanoindole films in their reduced state since no emission is seen from films in the oxidised state. This may be due to structural differences between the reduced and oxidised states with an efficient quenching mechanism being present in the oxidised film. To investigate this, an oxidised film was prepared then dissolved off the electrode and drop coated onto a quartz slide, then examined to see if it was fluorescent. As for the cycled film, the drop-coated oxidised film was highly fluorescent, compared with no fluorescence from the intact film on the electrode. The lifetimes for the oxidised drop-coated film are shown in Table 7.9. The distribution of lifetimes and their respective contributions are very similar to the reduced films examined in the previous section (Table 7.8). There is no effect of redox state on the emission properties of the drop coated film, compared to the considerable effect on intact films. This is consistent with oxidation of an intact film causing a structural change that opens up efficient non-radiative pathways. These pathways are lost upon dissolution and redeposition of the film. The nature of the redox behaviour and its influence on emission is discussed further in section 7.4.

Wavelength / nm	Fitted lifetimes / ns				
	τ_1	τ_2	τ_3	τ_4	
460	6.71 0.4 21	1.45 3 36	0.34 6 16	0.03 91 26	1.4 2
500	6.29 0.6 30	1.42 3 30	0.3 6 13	0.04 91 26	1.5 1.75

Table 7.9 Lifetime data for an oxidised 5-cyanoindole film drop-coated from a DMF solution. Polymerised from a 50 mmol monomer solution at 10 Hz for 30 seconds.

7.3.2.3 Drop coated films of Indole-5-carboxylic acid

So far fluorescence data for only 5-cyanoindole films has been presented, since no detectable emission was measured from any of the other indole films. Indole-5-carboxylic acid did appear to have a very weak emission, but the lifetime was too short to be detected. The lack of emission may be due to the fact that polymerised indole-5-carboxylic acid in the solid state is inherently non-fluorescent, or may be a structural effect resulting from electropolymerisation. Once again, this was addressed by dissolving a non-fluorescent film off the electrode then drop coating it onto a quartz slide. The result was a fluorescent drop-coated film in both the oxidised and reduced states.

The lifetime data for the oxidised and reduced films are presented in Table 7.10 and the experimental data and fitted functions for the oxidised film at 460nm and 540nm are shown in Figure 7.8. The lifetime data for indole-5-carboxylic acid drop-coated films is very similar to that for 5-cyanoindole drop–coated films (Table 7.8 and Table 7.9). They both have a similar multi-exponential decay character, with 4 components of similar magnitudes. The shorter lifetimes observed for the oxidised indole-5-carboxylic acid film is probably due to the poor quality of the drop-coated film and not an effect of oxidation. The absence of fluorescence emission from indole-5-carboxylic acid films intact on the electrode must be due to the structure of the electropolymerised film, with a more efficient non-radiative decay than an equivalent 5-cyanoindole film, and not because the solid state indole-5-carboxylic acid polymer is non-fluorescent.

Both 5-cyanoindole and indole-5-carboxylic acid show little difference in the emission properties of drop-coated reduced and oxidised films, in contrast to the intact films on the electrode. This suggests that there is a change in the structure of the film as it is oxidised and

reduced, altering the non-radiative decay pathways available for the excitation energy. This is explored in greater detail in the next section.

To investigate whether the absence of fluorescence from an intact electropolymerised indole-5-carboxylic acid film was due to the presence of the electrode, a layer of film was peeled off the electrode and placed in the excitation beam. As for the film on the electrode, no fluorescence emission was detectable, implying that quenching of the fluorescence was occurring via an internal mechanism, and did not rely upon contact with the electrode surface.

Wavelength / nm	Lifetimes for a reduced, drop coated film					Lifetimes for an, oxidised drop coated film				
	τ_1	τ_2	τ_3	τ_4		τ_1	τ_2	τ_3	τ_4	
460	3.66 0.3 13	0.7 2.5 21	0.19 13 31	0.03 84 34	1.5 2	1.11 0.4 5.4	0.37 6 29	0.13 23 38	0.032 71 29	1.2 2
500	4.55 0.2 11	0.76 2.4 19	0.22 16 38	0.04 81 32	1.4 2	2.53 0.2 5.4	0.54 6.4 32	0.17 26 41	0.04 67 22	1.6 2
540	7.5 0.2 15.6	0.67 3 18	0.21 19 39	0.03 78 27	1.3 2	2.22 0.5 8	0.52 10 36	0.18 30 38	0.04 60 19	1.5 1.7

Table 7.10 Lifetime data for a film of indole-5-carboxylic acid drop coated from a DMF solution. The original film was polymerised from a 50 mmol monomer solution at 10 Hz for 20 seconds and either left in the oxidised state or held at reducing potential.

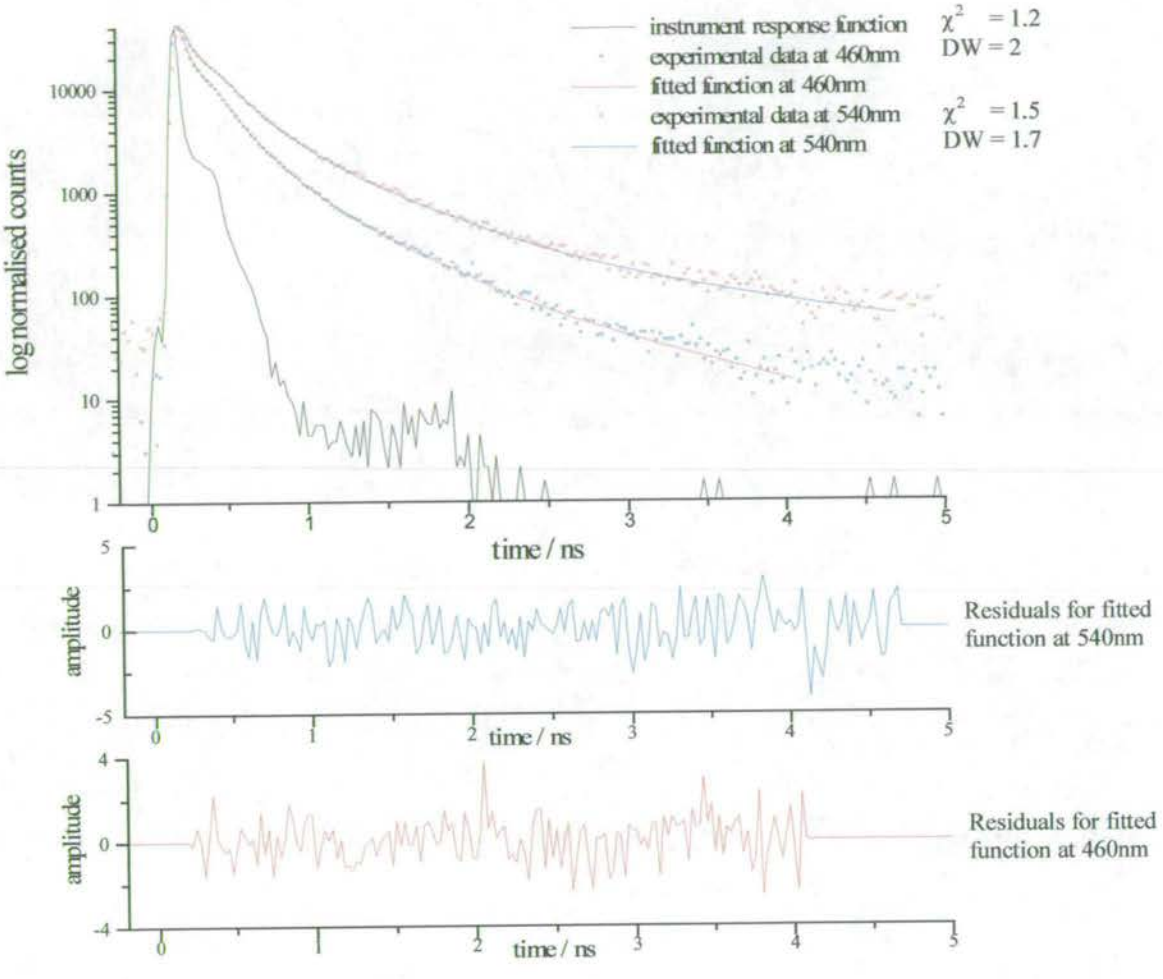

Figure 7.8 Decay data and fitted functions for films of oxidised indole-5-carboxylic acid drop-coated from a DMF solution. Decays were measured at 460nm and 540nm. The original film was polymerised from a 50 mmol monomer solution at 10 Hz for 20 seconds.

7.4 In-situ cyclic voltammetry (CV)/emission experiments

To gain a better understanding of the processes occurring when a film is cycled between a fluorescent reduced state and a non-fluorescent oxidised state, the experiment described in section 3.7 was set up. This allowed in-situ measurement of the emission intensity as the film was cycled within the redox region and then to higher linking potentials. Initially it was attempted to measure fluorescence lifetimes of the films in-situ in background electrolyte, to see if there was a difference between the solvated and non-solvated films. However, due to the slight solubility of the films in the electrolyte and the highly fluorescent nature of the dissolved films, there was always a background emission present making lifetime measurements unfeasible. This background emission was not a problem when measuring changes in the emission intensity of the film, as it is constant. Films of both 5-cyanoindole and indole-5-carboxylic acid were examined and were polymerised using a range of conditions, to determine whether the proportion of trimer and polymer had any effect. The variation in emission intensity was measured as a function of the changing voltage at sweep rates from 2 mv/s to 200 mv/s and at wavelengths ranging from 420nm to 540nm.

7.4.1 Effect of sweep rate on the CV/emission response of 5-cyanoindole films

A series of films were studied, with polymerisation conditions varied according to the details given in Table 7.1. They are designated films 1-5 in this work. The intensity of emission from the film was then measured as it was cycled at a range of sweep rates between the reduced and oxidised states, with electrochemical and emission data collected synchronously. Looking first at the results for film 1, plots of current against voltage (a CV) and emission intensity against voltage (which shall henceforth be referred to as a fluorescogram) for two cycles at a sweep rate of 20 mV/s are shown in Figure 7.9

	50 mmol	100 mmol
5 Hz 10 seconds	film 1	
1 Hz 10 seconds	film 2	
10 Hz 30 seconds		film 3
1 Hz 30 seconds		film 4
0 Hz 15 seconds		film 5

Table 7.11 Polymerisation conditions for the CV/emission experiments on 5-cyanoindole films.

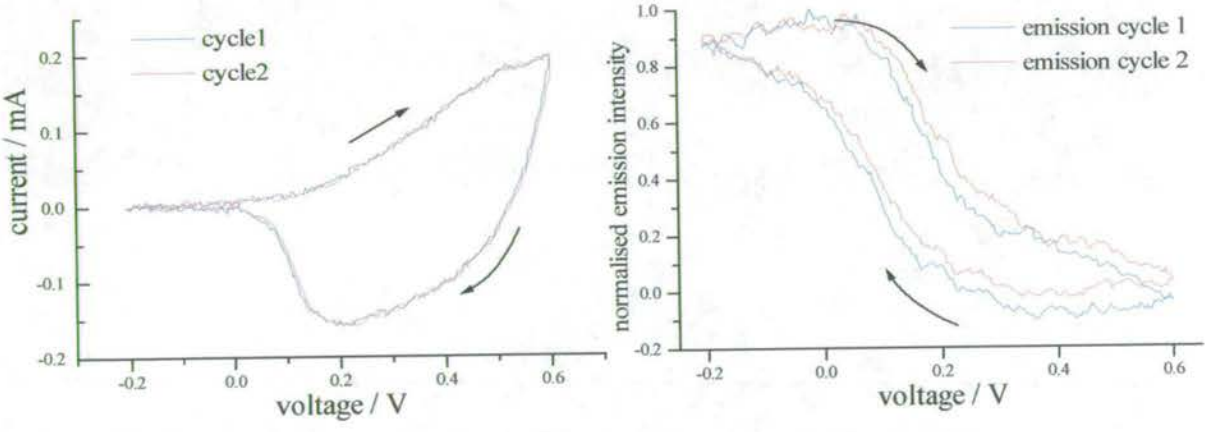

Figure 7.9 A cyclic voltammogram and fluorescogram (collected at an emission wavelength of 460nm) at a sweep rate of 20 mV/s for 5-cyanoindole film 1 (polymerised from a 50 mmol monomer solution at 5 Hz for 10 seconds). The arrows indicate the direction of the cycle.

The plots shown in Figure 7.10 illustrate both the electrochemical reversibility of the redox cycle and the equivalent reversible change in fluorescence intensity. Apart from a very small difference in the emission intensity for each cycle, they are almost identical. This is still the case even after multiple cycles. The longest period for which a film was examined was 5 hours of repeated cycling, over which time there was no apparent drop in the emission intensity. The decrease in emission intensity as the film is oxidised and the subsequent increase as it is reduced can be clearly seen. In order to relate the emission intensity to the extent of oxidation of the film, the charge passed was calculated. In Figure 7.10 plots of charge against voltage and emission intensity against charge are shown for the first cycle.

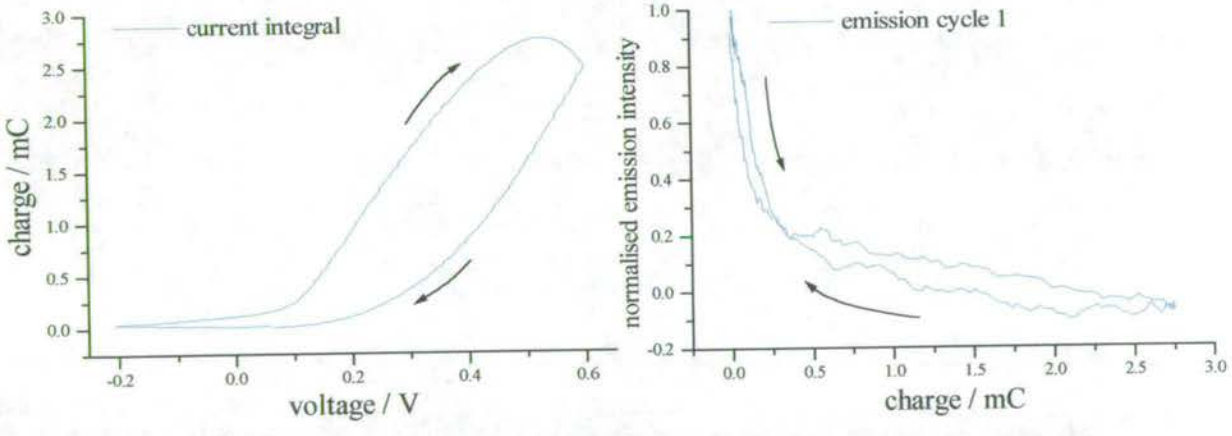

Figure 7.10 Plots of charge against voltage and emission intensity against charge for film 1 with a sweep rate of 20 mV/s, polymerised from a 50 mmol monomer solution at 5 Hz for 10 seconds.

From the plot of emission against charge, it can be seen that the maximum emission intensity is shown by the film in its fully reduced state. As the film is oxidised the emission intensity decreases, falling to zero in the fully oxidised state. The majority loss of fluorescence intensity occurs after only approximately 10 % of the film has been oxidised, suggesting that oxidation of only a small fraction of the film opens an efficient non-radiative channel. When the sweep is reversed and the film reduced, the fluorescence intensity is restored, with a steep increase in intensity once approximately 90% of the film has been re-reduced, closing the efficient non-radiative channel. The emission intensity shows a reversible dependence on the oxidation state of the film and, at this sweep rate, the relationship between emission intensity and charge is very similar for the forward (oxidation) and reverse (reduction) sweeps. Upon oxidation, anions move into the film to balance the charge (hence doping the film) and upon reduction these anions are expelled to give an undoped film. It has been reported [3] that in the oxidised (doped) state, the films are more conducting than the reduced (undoped) state. It is possible that the efficient non-radiative mechanism, present in the oxidised films, is associated with the increased conductivity, providing an efficient channel for electron transfer. It is also a possibility that the anions present in the oxidised film are responsible for quenching the fluorescence.

An interesting effect on the fluorescence response is observed as the sweep rate is increased. The plots in Figure 7.11, Figure 7.12 and Figure 7.13 are all for film 1, but with increasing sweep rates.

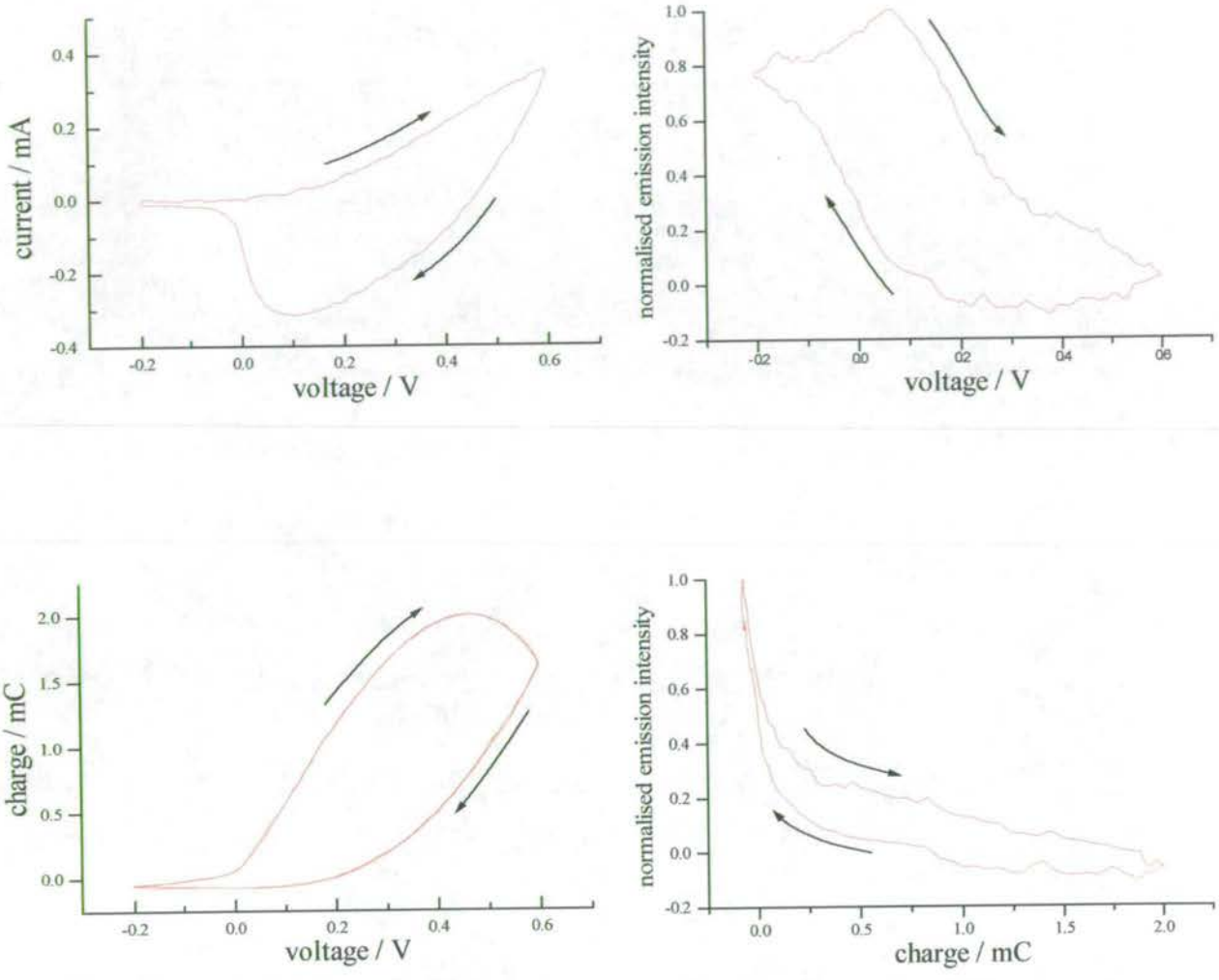

Figure 7.11 Plots of current, charge and emission intensity against voltage and emission intensity against charge for film 1, with a sweep rate of 50 mV/s, collected at an emission wavelength of 460nm.

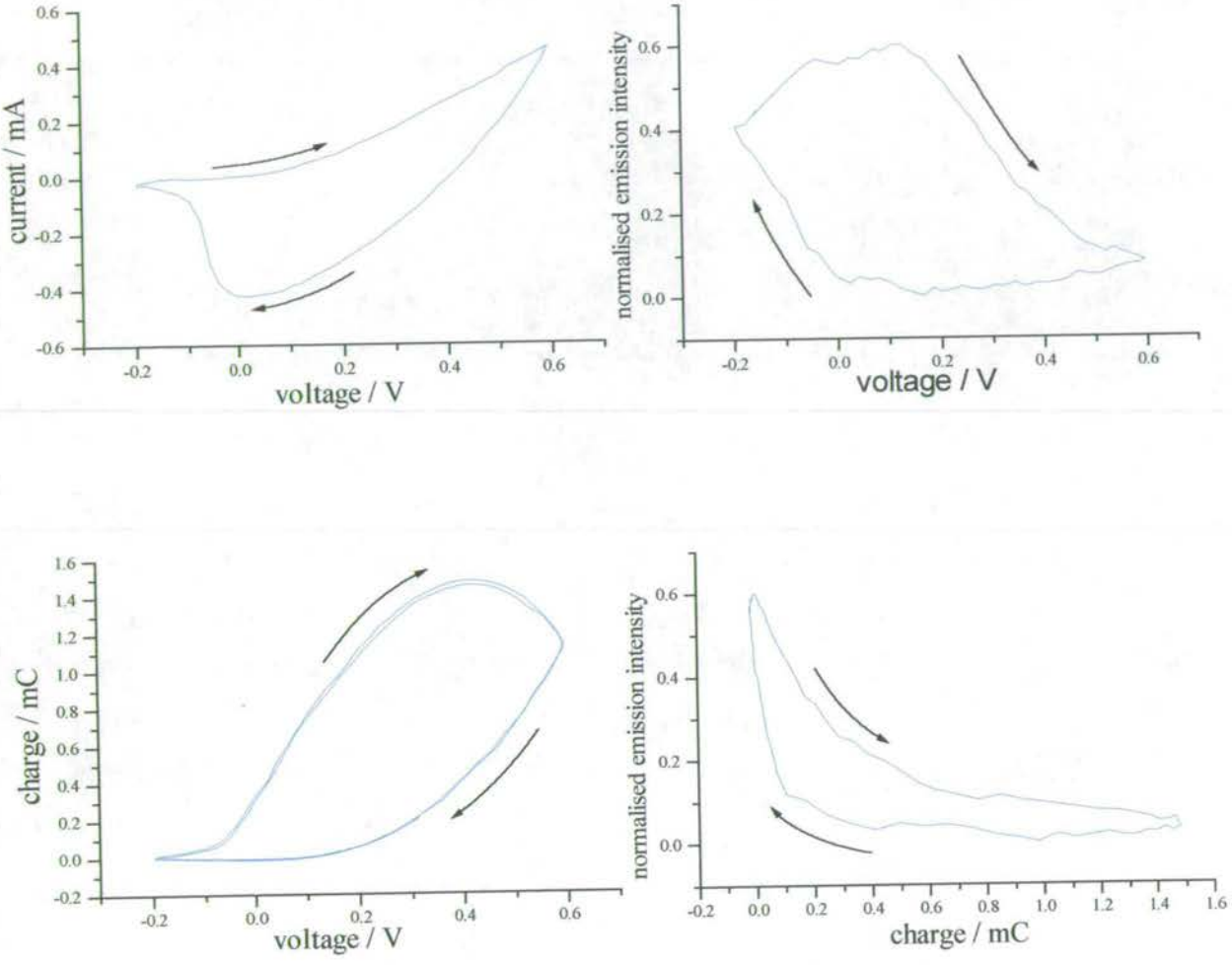

Figure 7.12 Plots of current, charge and emission intensity against voltage and emission intensity against charge for film 1, with a sweep rate of 100 mV/s, collected at an emission wavelength of 460nm

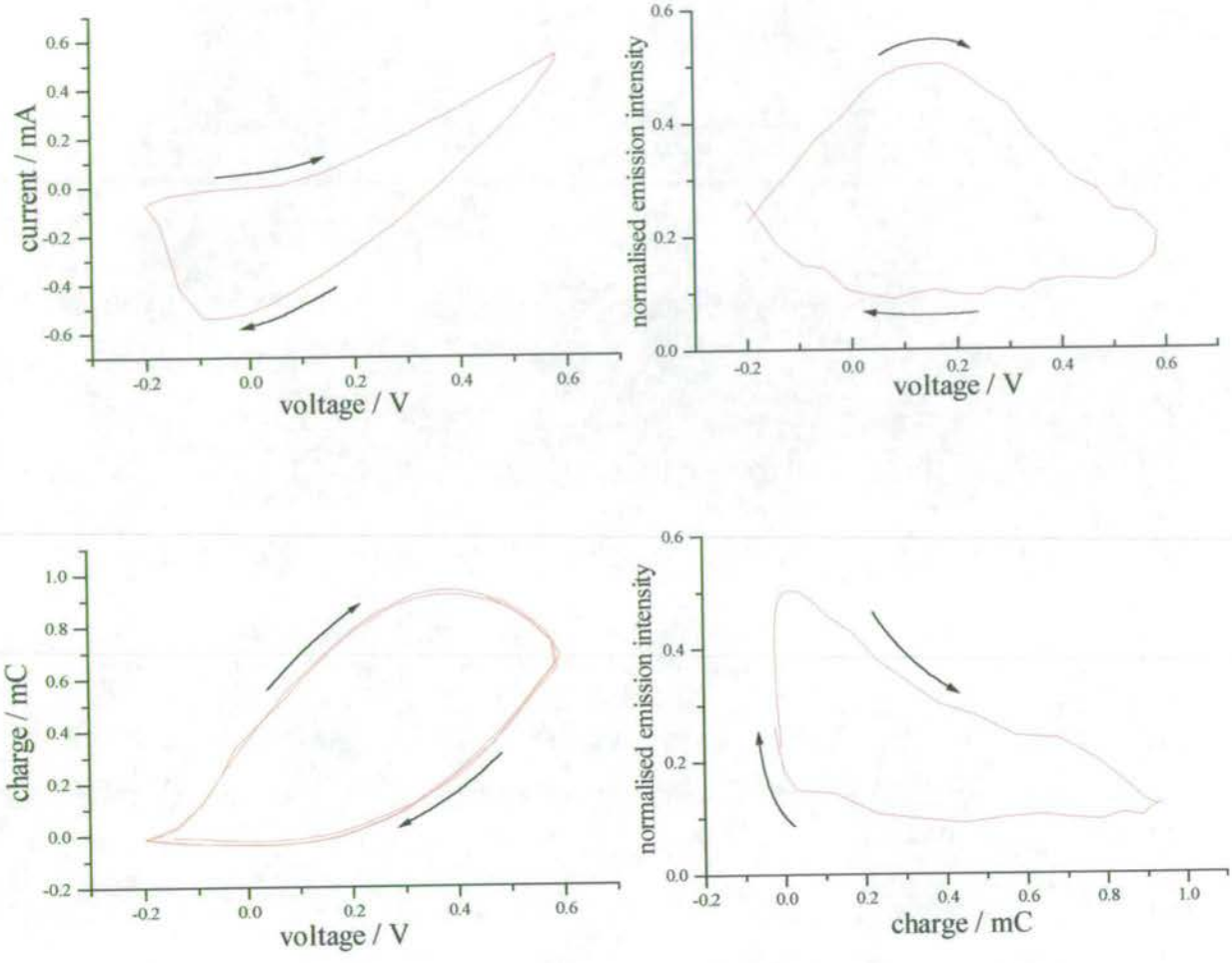

Figure 7.13 Plots of current, current integral and emission intensity against voltage and emission intensity against current integral for film 1, with a sweep rate of 200 mV/s, collected at an emission wavelength of 460nm.

As the sweep rate increases, the response of the emission changes significantly. At slow sweep rates, the change in emission intensity is very similar on forward and reverse sweeps, however as the sweep rate increases, a significant difference develops. This is seen most clearly on the plots of emission intensity against charge. As the sweep rate increases, the initial steep drop in intensity, as the fully reduced film is oxidised, becomes less evident; at

the highest sweep rate of 200mV/s (Figure 7.13) a gradual decline in intensity is seen as the oxidation proceeds. On reversal of the sweep, the intensity continues to decrease initially and does not start to increase until later in the reduction sweep. The intensity recovers at the greatest rate at the very end of the reduction sweep and as the sweep is reversed. This recovery of intensity occurs over part of the CV where very little charge is passed and is seen on the plot of intensity against charge as a very sharp rise. Thus, there is a time-lag in the response of the emission to the change in redox state of the film. This hysteresis results in a separation (along the intensity axis) of the fluorescence-charge response curves for the forward and reverse sweeps; the greater the hysteresis the greater the separation. It can be seen in Figures 7.10 to 7.13 that the hysteresis increases as the sweep rate increases.

The observation of hysteresis implies that the dependence of fluorescence intensity on the redox state of the film is not simply a function of the redox charge, but is due to a change in the structure of the film, associated with the change in redox state. At high sweep rates, the rate of structural rearrangement is slower than the rate of oxidation (or reduction) of the film leading to the hysteresis in fluorescence response. It is apparent from figures 7.10 to 7.13 that as the sweep rate increases the charge passed decreases and the oxidation is incomplete. Consequently, as the sweep rate increases, the difference in emission intensity between the reduced and oxidised states decreases.

The movement of anions in and out of the film upon oxidation and reduction has a considerable effect on the structure of the film. It is thought [3] that in the fully reduced (undoped) form, the film has a compact, insulating structure. In the fully oxidised (doped) form it is though to have a more open, conducting structure. When sweeping from the fully oxidised state to the reduced state, anions are expelled from the film, which should occur

easily due to the open structure of the film, therefore the structural rearrangement can happen at the same rate as the redox change. However, when sweeping from the fully reduced state to the oxidised state, the film is initially more compact and there is a barrier to the insertion of anions. Therefore the structural rearrangement of the film is though to be delayed relative to the redox change. This may explain why a greater degree of hysteresis is observed on the forward oxidation sweep than the reverse reduction sweep.

The next set of results is for film 2, which was polymerised from the same 50 mmol monomer solution as film 1, but at 1 Hz rather than 5 Hz. This should result in a film with a higher polymer content. There appears to be a significant effect on the emission response of the film due to the increased polymer content. The plots shown in Figure 7.14 are the cyclic voltammogram and emission intensity against charge at a sweep rate of 20 mV/s; this data should be compared with the plots in Figure 7.10. Whereas there was no hysteresis apparent in film 1 at 20 mV/s, there is a considerable degree present in film 2 at this sweep rate. As for film 1, the degree of hysteresis increases with sweep rate, but only becomes insignificant when the sweep rate drops to 5 mV/s and below. These results imply that the film with a higher polymer content has a greater barrier to structural reorganisation, and hence change in emission intensity, than the film with a high trimer content. This is an intuitive result, since the polymer will have a much less flexible structure and would be expected to be more resistant to reorganisation.

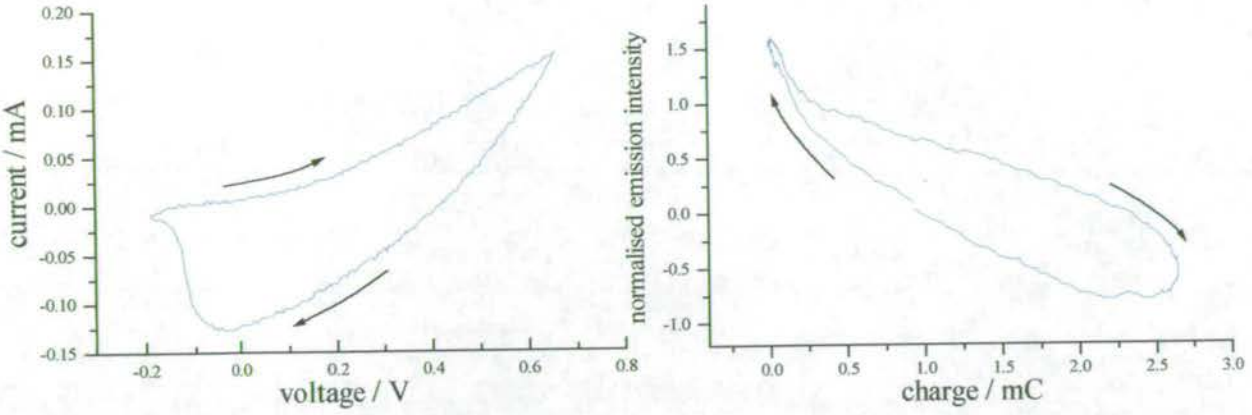

Figure 7.14 Plots of current against voltage and emission intensity against charge for film 2, with a sweep rate of 20 mV/s, collected at an emission wavelength of 460nm. Polymerised from a 50 mmol monomer solution at 1 Hz for 10 seconds.

To confirm the relationship between rate of fluorescence and polymer content, the experiments were repeated using films 3, 4 and 5, polymerised using a different concentration of monomer solution at 100 mmol. The plots shown in Figure 7.15 are for film 3, which should contain a higher level of trimer than films 1 and 2 (due to the fast rotation speed and high concentration of monomer solution). At a sweep rate of 10 mV/s, the emission against charge plot shows no hysteresis. As for the samples produced from the 50 mmol monomer solution, as the sweep rate is increased, the degree of hysteresis increases, with the greatest change in emission intensity occurring at negative potentials. Film 5 was polymerised from the same solution, but with a stationary electrode and is therefore expected to contain a higher proportion of polymer. The plots shown in Figure 7.16 are consistent with a higher polymer level, as there is a considerably greater degree of hysteresis in the response of the emission with respect to the charge. This is consistent with the conclusion that it is more difficult to rearrange the structure of a film with a higher polymer content.

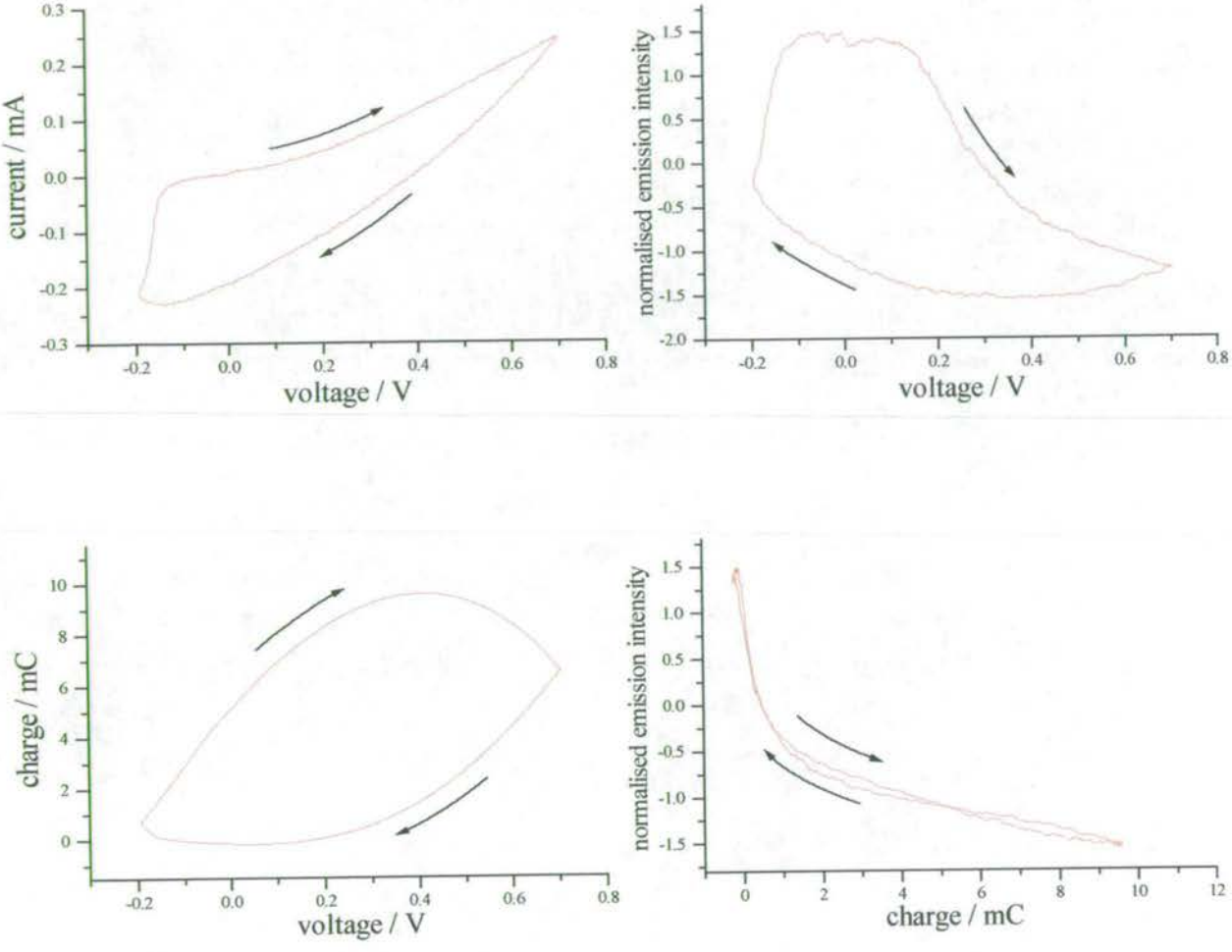

Figure 7.15 Plots of current, charge and emission intensity against voltage and emission intensity against charge for film 3, with a sweep rate of 10 mV/s, collected at an emission wavelength of 460nm. Polymerised from a 100 mmol monomer solution at 10 Hz for 30 seconds.

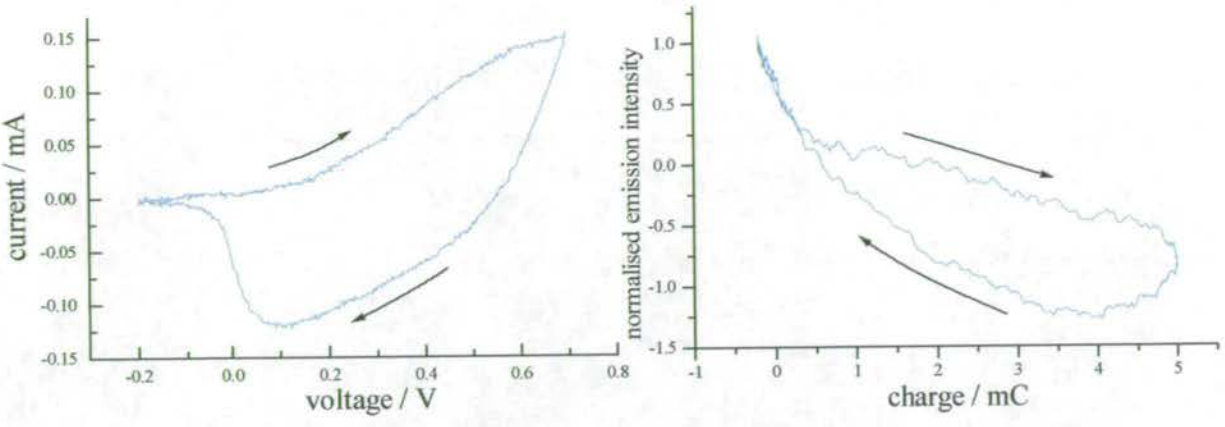

Figure 7.16 Plots of current against voltage and emission intensity against charge for film 5, with a sweep rate of 10 mV/s, collected at an emission wavelength of 460nm. Polymerised form a 100 mmol monomer solution at 0 Hz for 15 seconds.

7.4.2 Effect of sweep rate on the CV/emission response of indole-5-carboxylic acid films.

Although no usable lifetime data was obtained for the indole-5-carboxylic acid films, there was sufficient emission intensity from films with a high trimer content to carry out CV/emission experiments. The example presented here was polymerised from a 70 mmol monomer solution at 10 Hz for 10 seconds. This can be compared to film 3 for 5-cyanoindole, produced using similar conditions and shown in Figure 7.15. The plots shown in Figure 7.17 for indole-5-carboxylic acid are similar to those in Figure 7.15, with minimal hysteresis in the fluorescence-charge response curves. However, the plots in Figure 7.17 were collected using a sweep rate of 2mV/s, five times slower than the 10 mV/s sweep rate for the 5-cyanoindole film in Figure 7.15.

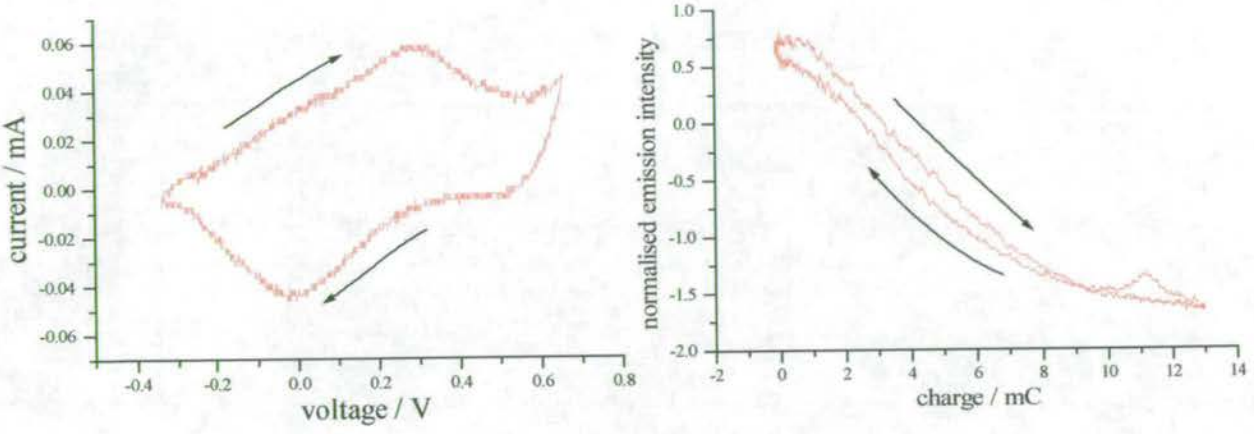

Figure 7.17 Plots of current against voltage and emission intensity against charge for an indole-5-carboxylic acid film, at a sweep rate of 2 mV/s, collected at an emission wavelength of 460nm. Polymerised from a 70 mmol monomer solution at 10 Hz for 10 seconds.

When the sweep rate is increased to 20 mV/s as shown in Figure 7.18, the degree of hysteresis in the fluorescence-charge response curve is very large. Even 5-cyanoindole films with a high polymer content, when cycled at 20 mV/s (Figure 7.14) have much less hysteresis. The plots shown in Figure 7.19 are for a sweep rate of 50 mV/s. There is a very small change in fluorescence intensity, with the sweep rate being too fast for any change in morphology.

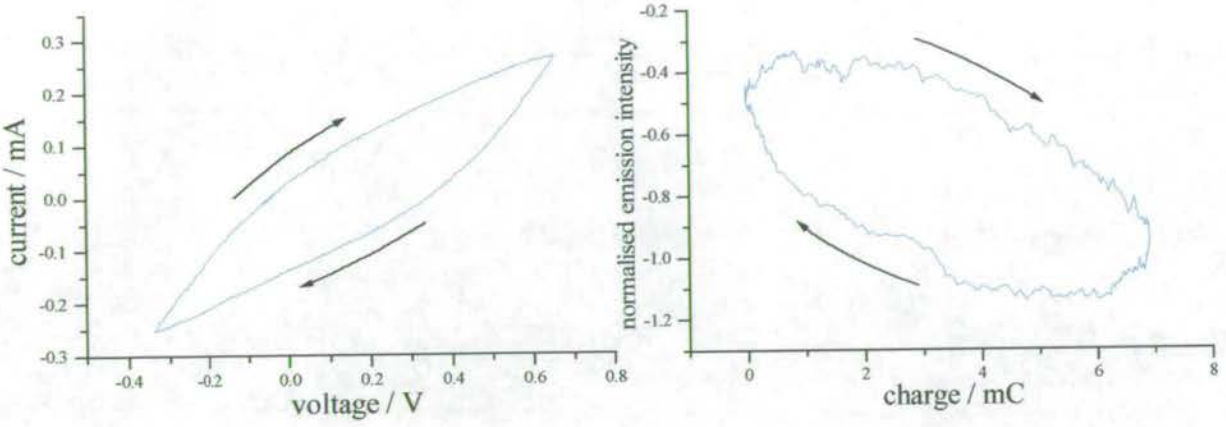

Figure 7.18 Plots of current against voltage and emission intensity against charge for an indole-5-carboxylic acid film, at a sweep rate of 20 mV/s, collected using an emission wavelength of 460nm. Polymerised from a 70 mmol monomer solution at 10 Hz for 10 seconds.

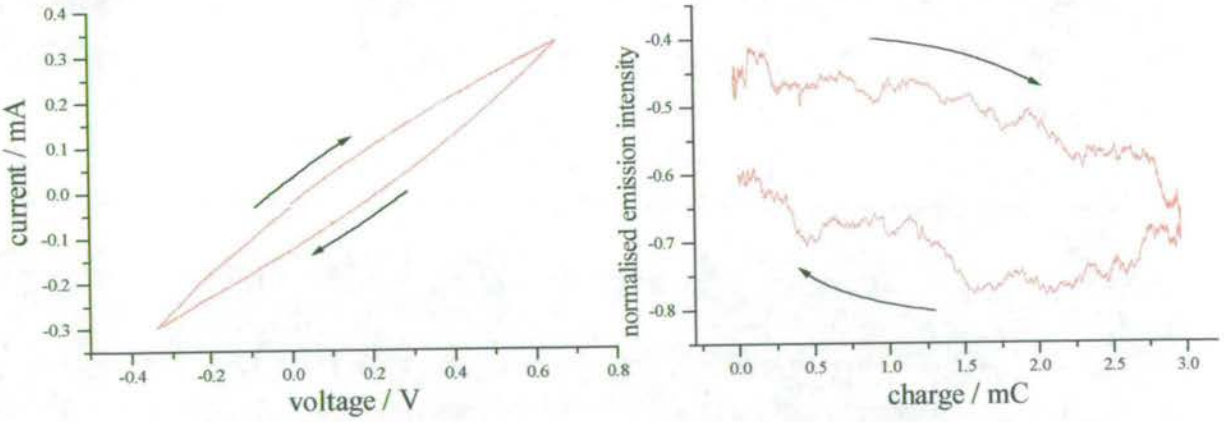

Figure 7.19 Plots of current against voltage and emission intensity against charge for an indole-5-carboxylic acid film, at a sweep rate of 50 mV/s, collected at an emission wavelength of 460nm. Polymerised from a 70 mmol monomer solution at 10 Hz for 10 seconds.

The emission response of the indole-5-carboxylic acid film is different to that of the 5-cyanoindole film, with hysteresis being observed at slower sweep rates than for 5-cyanoindole films. The increased hysteresis implies that there is a larger barrier for the structural rearrangement of indole-5-carboxylic films when they are oxidised and reduced, compared to equivalent 5-cyanoindole films. Due to the presence of the carboxy group, intermolecular hydrogen bonding interactions are likely. These intermolecular interactions will be a barrier to the morphological rearrangement of the film as it is oxidised and reduced, therefore creating a time-lag in the response of the emission from the film to the redox change.

7.4.3 Dependence of CV/emission response on emission wavelength

To see if the emission response was wavelength dependent, the sweep rate was fixed at 20 mV/s and the change in emission intensity recorded at emission wavelengths between 420nm and 540nm. This was carried out for several of the 5-cyanoindole films and for the indole-5-carboxylic acid film. Figures 7.20 to 7.23 show results for 5-cyanoindole film 1. In Figure 7.20 all four plots of current, emission and current integral against voltage and emission against current integral are shown. All subsequent diagrams only show the emission vs. voltage and current integral since the other two plots are invariant throughout.

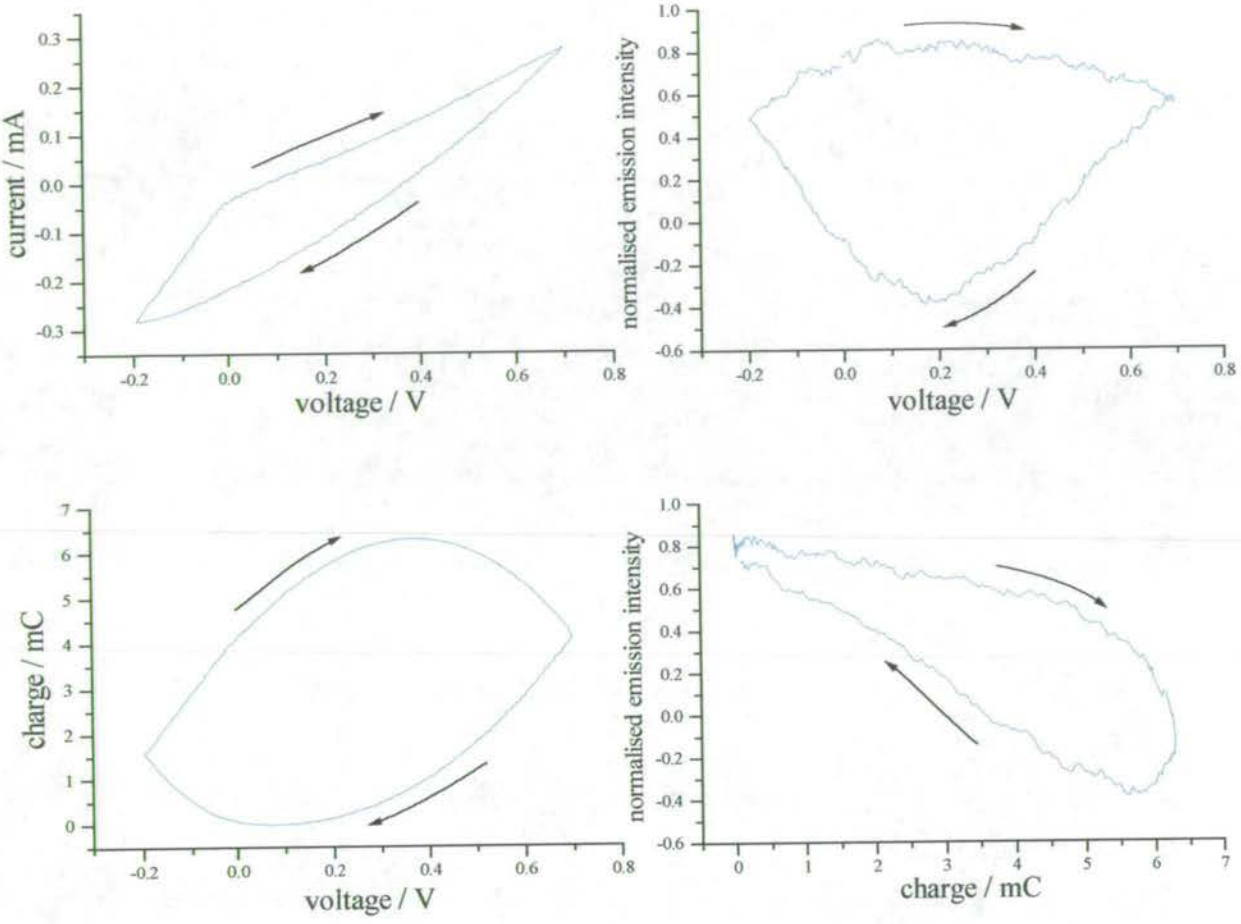

Figure 7.20 Plots of current, charge and emission intensity against voltage and emission intensity against charge for film 3, with a sweep rate of 20 mV/s measured at a wavelength of 420 nm.

The emission intensity response at 420nm, as shown in Figure 7.20 shows a considerable degree of hysteresis. As the wavelength increases to 460nm, Figure 7.21, there is a decrease in hysteresis. The hysteresis is further decreased for emission at 500nm, Figure 7.22, and almost completely absent at 540nm, Figure 7.23.

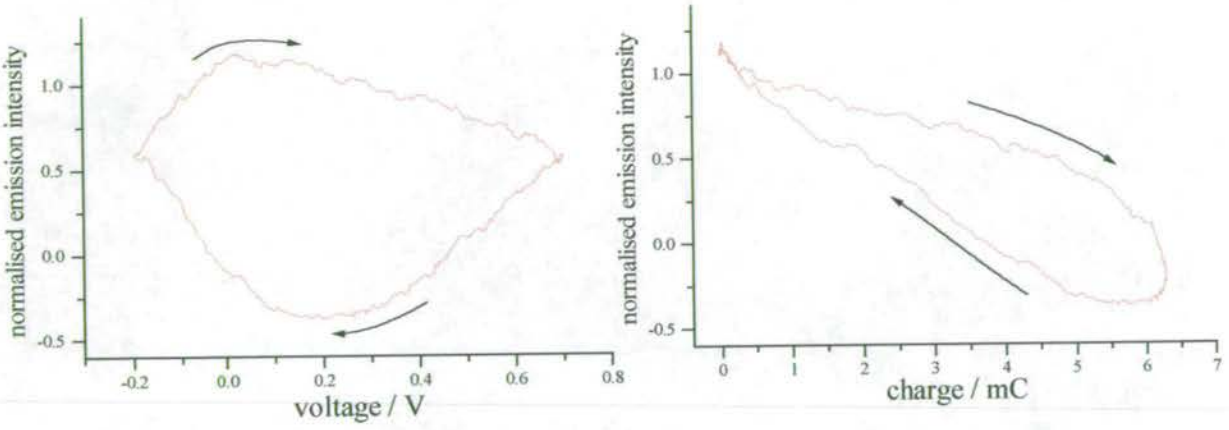

Figure 7.21 Plots of emission intensity against voltage and emission intensity against charge for film 3, with a sweep rate of 20 mV/s measured at a wavelength of 460 nm

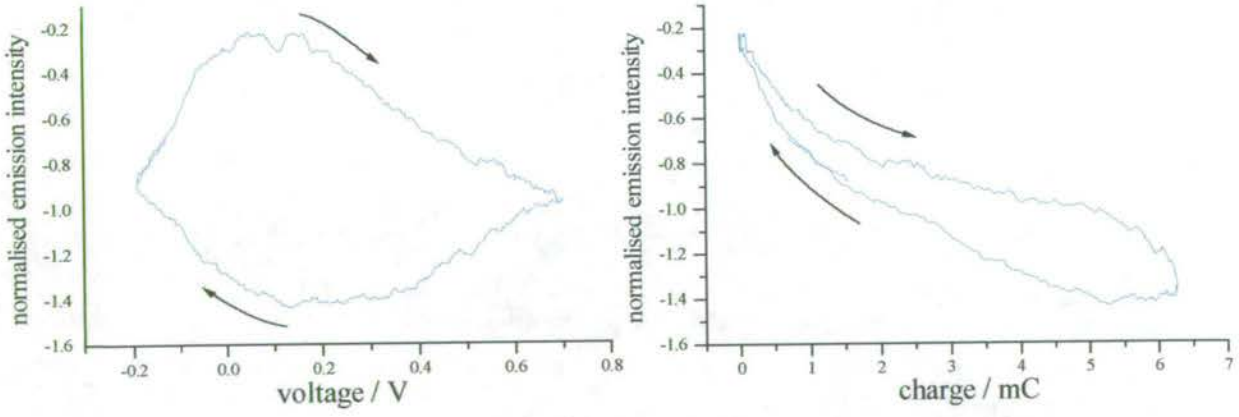

Figure 7.22 Plots of emission intensity against voltage and emission intensity against charge for film 3, with a sweep rate of 20 mV/s, measured at a wavelength of 500 nm.

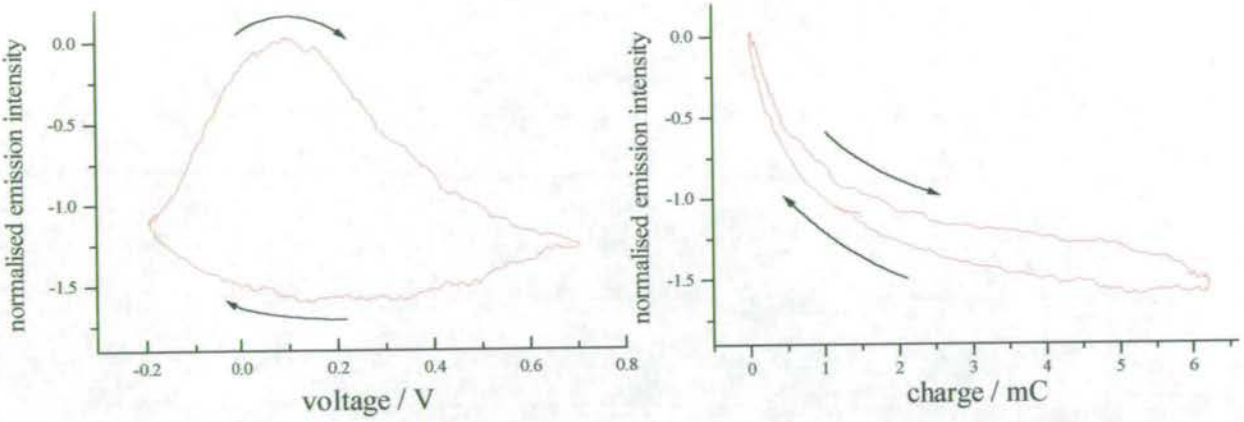

Figure 7.23 Plots of emission intensity against voltage and emission intensity against charge for film 3, with a sweep rate of 20 mV/s, measured at a wavelength of 540 nm.

At short wavelength, the emission will be from free trimer and polymer segments of short conjugation length. As the wavelength increases, the emission will be from polymer segments of longer conjugation length, as has been discussed in chapter six. Thus longer chain emitting species appear to experience less hysteresis than short chain species. This suggests that the structure of the film is anisotropic. It is possible to explain these observations if the mechanism of polymerisation is considered. When a film is formed, the layer closest to the electrode is laid down first, with further layers being deposited on top. The outside layer will be the last to be deposited and is likely to be rich in trimer, since it has had no chance to undergo further oxidation. The inside layer however is more likely to have undergone further oxidation to form polymer. When the film is cycled from the reduced to the oxidised state the film undergoes a structural change, which is reflected in the emission intensity. The reduction reaction involves the expulsion of counter-anions at the film/electrolyte interface, but the outside of the film will remain rich in anion until all the trimer centres have been reduced. This occurs because there is a kinetic barrier to anion

transfer to the solution at the film surface [3]. Therefore the inner layers of the film will be the first to change structurally, which will be reflected in the emission properties. At short wavelength, only the short chain polymer and trimer species are emitting; since these will lie on the outer layer of the film, they will be the last to be affected by the change in oxidation state and will therefore display a degree of hysteresis. At long wavelength the longer chain polymer species are emitting; these will be the first to change, as they are closest to the electrode. This will result in the observed reduction in hysteresis.

At a sweep rate of 20 mV/s ,no large differences were observed at different wavelengths for indole-5-carboxylic acid. This is because at this sweep rate there is such a large degree of hysteresis due to the effect of the carboxy group that wavelength-dependence is not apparent. These differences would be expected to be observable at or below 5 mV/s, where hysteresis is starting to occur.

7.4.4 The effect on the emission response of sweeping the film to linking potentials

Earlier in this chapter, results from lifetime measurements were presented for films that had been cycled to potentials beyond the redox region, causing further polymerisation of trimer units. It was found that as further polymerisation occurred, the emission intensity irreversibly dropped and the lifetimes became shorter. This process was followed in situ using the cv/emission set-up. A similar effect was seen for both 5-cyanoindole and indole-5-carboxylic acid films. The example given below is for the 5-cyanoindole film 5. In Figure 7.24 there is a CV and fluorescogram for all the cycles of the film. The first cycle is in the reversible redox region, with subsequent cycles illustrating the irreversible polymerisation of the film. After

each sweep to higher potential the fluorescence intensity is seen to drop and the next sweep results in a less fluorescent film.

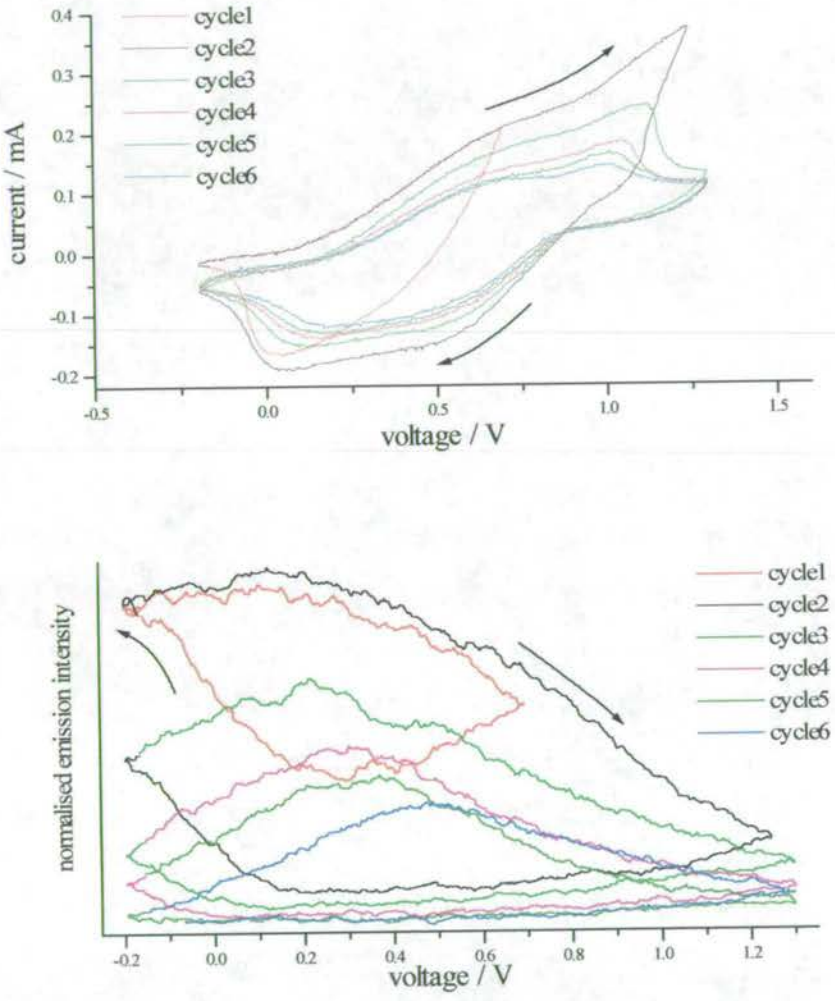

Figure 7.24 Cyclic voltammogram and fluorescogram for a 5-cyanoindole film at a sweep rate of 20 mV/s, collected at an emission wavelength of 460nm. Polymerised from a 100 mmol monomer solution at 0 Hz for 15 seconds. The first cycle shows the redox region, subsequent cycles link the film.

It is hard to pick out the individual cycles in Figure 7.24, therefore plots of the fluorescogram and emission intensity against charge for the first and final cycles have been given in Figure 7.25. It can be seen that not only has the emission intensity dropped with increasing polymerisation, but the emission response has changed, with emission intensity against charge plot for the highly polymerised film showing increased hysteresis. This is consistent with the previous observation that a film with a high polymer content shows a greater degree of hysteresis in the emission response with respect to the redox change, due to the greater difficulty in reorganising the structure of longer chain polymers.

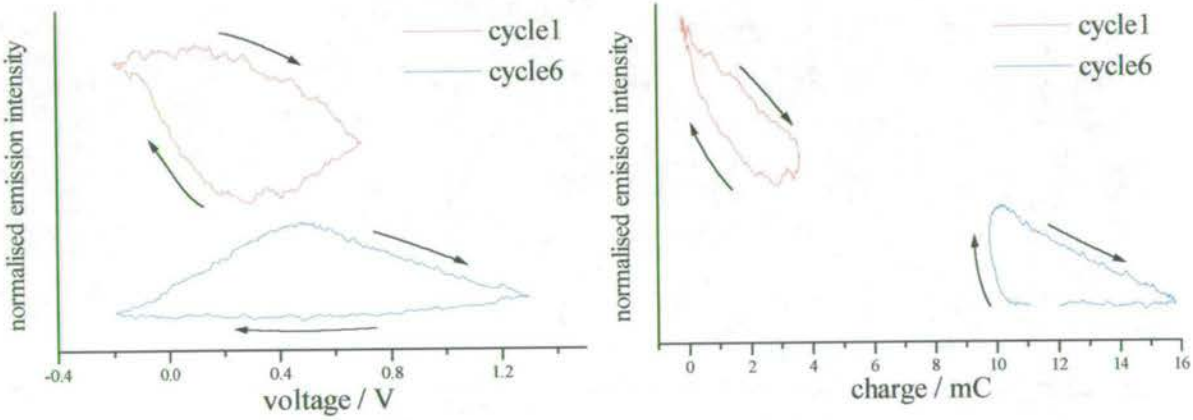

Figure 7.25 Fluorescogram and plot of emission intensity against charge for the first and final cycles of film 5 at a sweep rate of 20 mV/s, collected at an emission wavelength of 460nm.

7.5 Conclusions.

Fluorescence lifetime data and a novel, in-situ experimental technique have been used to probe the structural properties of 5-cyanoindole and indole-5-carboxylic acid electropolymerised films in greater detail.

From the lifetime measurements, it was found that fluorescent 5-cyanoindole films could be repeatedly cycled within the redox region, with little effect on the intensity of emission or value of the lifetimes. This was in contrast to cycling a film beyond the redox region, where polymerisation of residual trimer occurs to form a more extensive polymer system, and the magnitude of the fluorescence lifetimes drop significantly. The faster the sweep rate and the higher the potential to which the film is cycled, the greater the drop in lifetime. An equivalent effect is not observed when the films are dissolved and examined in solution. It is suggested that the presence of a high proportion of polymer in the intact film opens up efficient non-radiative pathways with inter- as well as intra-chain mechanisms influencing the emission properties.

Films of 5-cyanoindole drop coated from solution were found to be fluorescent, regardless of oxidation state or polymer content. This implies that the efficient non-radiative channels present in the intact, electropolymerised films are a feature of the films structure and are lost when the film is dissolved and drop coated. It was also found that drop coated films of indole-5-carboxylic acid were fluorescent, implying that the non-observance of emission from such a film as formed on the electrode is again due to a structural effect.

The development of a new, in-situ technique, allowed the fluorescence response of an intact film in an electrochemical cell to be examined, relating the emission properties to

electrochemical observations. This provides a useful technique for assessing the potential of a material for electroluminescent applications. There also exists the possibility of examining emission changes as a function of spatial location and quenching of emission as a function of conductivity within the film.

This technique was used to examine the appearance and disappearance of fluorescence emission as films of 5-cyanoindole and indole-5-carboxylic acid were cycled between the reduced and oxidised states. It was found that at faster sweep rates, there is a time-lag in the response of the emission to the change of redox state of the film, observed as hysteresis in the fluorescence-charge response curves. This hysteresis implies that the variation in emission with redox state is not just a function of the redox charge, but is associated with a change in the structure of the film. Films with a higher polymer content were found to display a greater hysteresis, implying that the presence of extended polymer chains are a barrier to structural reorganisation of the film. A film of indole-5-carboxylic acid was found to have a greater degree of hysteresis than a comparable 5-cyanoindole film. This has been related to the presence of the carboxy group, which may form inter-molecular hydrogen bonds and reduce the mobility of the polymer chain.

It was found that the degree of hysteresis in a 5-cyanoindole film was a function of the emission wavelength, with less hysteresis observed at longer wavelengths. A possible explanation is that reorganisation of the film as it is oxidised and reduced occurs initially adjacent to the electrode, where there is known to be a greater concentration of polymer species than at the film/electrolyte interface, where there will be more trimer.

7.6 References

1. J. G. Mackintosh, A.R. Mount, *J. Chem. Soc., Faraday Trans.*, 1994, **90**, 1121.
2. J.G. Mackintosh, *PhD Thesis*, The University of Edinburgh 1996.
3. M. Robertson, *PhD Thesis*, The University of Edinburgh 1996.

Chapter Eight - Conclusions

A comprehensive photophysical characterisation of electropolymerised indole and its 5-substituted derivatives has been carried out using the techniques of steady state and time-resolved fluorescence spectroscopy. Steady state techniques were used to characterise the fluorescence properties of the monomer, trimer and polymer species in solution at room and low temperature and to investigate the emission from intact films. This gave a background for measuring the fluorescence lifetimes and time-resolved emission spectra of the solutions and films to gain a greater understanding of the excitonic properties of the electropolymerised indoles.

A considerable difference was observed between the steady state emission properties of the monomer, trimer and polymer species in solution. The emission of the monomers was highly dependent upon the solvent polarity with 5-cyanoindole and indole-5-carboxylic acid monomers being examined in a variety of solvents. A considerable bathochromic shift and an increase in the Stokes shift was observed as the solvent polarity was increased, due to the solvent-stabilisation of the ^1L_a state. It was found that the nature of the 5-substituent strongly affects the emission properties, with a bathochromic shift being observed as the electron withdrawing or donating power of the 5-substituent is increased.

Emission from the trimer chromophore was found to be at longer wavelength with greater vibrational structure than the monomer, attributed to an increase in delocalisation of the π-

molecular orbitals. The trimer emission showed little dependence upon solvent polarity or the nature of the 5-substituent; suggesting that the first singlet excited state of the trimer has a smaller dipole moment than the monomer. The quantum yield of indole-5-carboxylic acid trimer was estimated to be 0.54, illustrating the highly fluorescent nature of the indole trimer.

5-bromoindole trimer was found to have a much lower fluorescence quantum yield than the other trimers, attributed to the presence of the heavy atom bromine, increasing the rate of quenching via intersystem crossing. This quenching was not found to affect the polymer species, allowing the fluorescence emission from the polymer to be isolated. It was found to be much broader and at longer wavelength than the trimer emission, due to increased delocalisation of the π-molecular orbitals along the polymer chain. The very broad nature of the polymer emission was thought to be the result of a wide distribution of different polymer conjugation lengths. Apart from 5-bromoindole, the polymer had a much lower quantum yield than the trimer species, attributed to an increase in the number of available non-radiative pathways.

Both 5-nitroindole monomer and trimer were found to be non-fluorescent at room temperature, attributed to the presence of an n-π^* transition due to the nitro group. This made 5-nitroindole films very useful as a template onto which films of 5-hydroxyindole and 5-aminoindole, both soluble when polymerised on a platinum electrode, could be grown. In this way the emission properties of 5-hydroxyindole and 5-aminoindole trimers were found to be very similar to the previously studied trimer species. N-methylindole was found to have a trimer-like emission as well as a longer wavelength emission corresponding to a linear polymer. The emission properties of unsubstituted indole were complicated by the presence of an additional peak, in the emission

spectrum, at slightly longer wavelength than the trimer emission. It is though that this is due to the presence of a π-complexed aggregate, formed by the reduced form of the trimer.

Chemically polymerised 5-substituted indoles were prepared for comparison with the electropolymerised samples. Very similar emission properties were observed, with characteristic emission from the trimer and polymer species. It was found that controlling the reaction conditions could vary the relative proportions of trimer and polymer.

By freezing the solvent to a rigid glass at 77K, fluorescence spectra were collected with an increased resolution of the vibronic structure, allowing the location of the excitation and emission 0-0 transitions, and identification of vibronic progressions of the monomer and trimer species. At 77K, phosphorescence emission was observed for all the monomer and trimer species, but not for the polymer, attributed to efficient non-radiative decay from the S_1 state competing with intersystem crossing and similar non-radiative decay from the T_1 state. The energy of the triplet state for the trimer species was measured relative to the ground and first singlet excited states, being of potential importance for electrogenerated chemiluminescence studies.

A shutter system was used to collect phosphorescence spectra, separated from the fluorescence emission, and to measure phosphorescence lifetimes. The presence of the heavy atom Bromine had a considerable effect on the phosphorescence emission due to an enhancement of spin-orbit coupling, giving a much greater phosphorescence quantum yield and a reduced phosphorescence lifetime. The n-π^* transition present in 5-nitroindole monomer and trimer species was also found

to give an increased intensity of phosphorescence emission and a reduced lifetime. The triplet T_1 state was identified as the n-π^* state for both the monomer and trimer, with the singlet S_1 state having π-π^* character.

The use of picosecond time-resolved fluorescence measurements in conjunction with electrochemical control of the polymerisation conditions gave a very useful insight into the factors influencing the luminescence efficiency of these systems. The monomers of 5-cyanoindole, 5-bromoindole and indole-5-carboxylic acid were found to have mono-exponential decays with lifetimes of 4.5 ns, 4.32 ns and 1.2 ns respectively. The fluorescence decays of the trimer and polymer species were characteristically multiexponential, typically fitting to a tri-exponential function. By measuring the lifetimes of samples with high trimer and high polymer contents, a general model of the emission properties has been proposed. The tri-exponential fit gives three lifetimes, each in a well-defined lifetime range. The longest lived component, of approximate 5ns, is attributed at short emission wavelengths to the free trimer species in solution, and at long emission wavelengths to the longest conjugation length, lowest energy segments of the polymer. The shortest lived component of approximately 0.3ns, is attributed to a high excitation energy species, with the excitation localised on an intra-chain trimer chromophore, from which very efficient energy transfer will occur to longer conjugation length, lower energy segments. The intermediate lifetime component, of approximately 2ns, is attributed to the presence of intermediate conjugation length segments, from which energy transfer will occur to longer conjugation length, lower energy segments.

Investigations of the intact electropolymerised films found that only films of 5-cyanoindole in the reduced state were fluorescent, with a broad emission spectrum at longer wavelength than the solution phase trimer emission, but shorter wavelength than the polymer emission. The broad featureless emission is consistent with a distribution of emitting species. A systematic variation of the polymerisation conditions found that the most intense emission was observed from films with a very high trimer content. Lifetime measurements were made on the films, finding the emission to be highly multiexponential, fitting to no fewer than four exponentials, with lifetimes varying from 40 ps to 6.5 ns. The lifetimes increased with increasing emission wavelength, consistent with the transfer of excitation energy from short conjugation length, high excitation energy species, to longer conjugation length, lower energy species.

A novel in-situ technique allowed measurements of the fluorescence emission from a film on the working electrode surface in an electrochemical cell, thereby relating the fluorescence and electrochemical properties of the film. There is a dramatic dependence of the fluorescence efficiency on oxidation state, which can be related to the morphology and conductivity of the film. In the reduced state the film is highly fluorescent, whereas in the oxidised state it is completely non-fluorescent. The fluorescence of non-emitting oxidised films is restored when the films are dissolved, indicating that it is the morphology of the film, not its composition that is responsible for the quenching of the fluorescence. The film can be cycled repeatedly, within the redox region, with no noticeable drop in the emission intensity when returned to the reduced form. This process was followed and it was found that at faster sweep rates there is a time-lag in the response of the emission to the change of redox state of the film, observed as hysteresis in the fluorescence-charge response curves. A high polymer content was found to increase this

hysteresis, thought to be due to the presence of extended polymer chains being a barrier to the structural reorganisation of the film. When a film was cycled beyond the redox region, polymerisation of residual trimer occurs, accompanied by a rapid drop in the fluorescence intensity, thought to be due to the presence of a greater number of non-radiative pathways. When dissolved off the electrode, fluorescence is restored, implying that the non-radiative channels present in the film due to the extended polymer chains are lost in solution.

There is an interesting parallel with the work presented here and the studies on the conjugated polymer PPV. In the solution phase, the steady state and time-resolved data for the electropolymerised indoles give evidence for photo-excitation generating an intra-chain exciton, localised on the free trimer species (from which no energy transfer occurs), or short conjugation length segments of the polymer (from which intra-chain energy transfer then occurs to longer conjugation length segments). This is similar to PPV, which is thought to only form an intra-chain exciton, with energy transfer from short to long conjugation length segments. With 5-cyanoindole as an intact film, there is no evidence of emission from an inter-chain excimer species, although it is expected that due to the close contact environment of the film, there will be some energy transfer between polymer chains. Again this is similar to work presented on PPV, but different to the derivative CN-PPV, for which there is strong evidence of emission from an inter-chain excimer in both the solution and solid phase.

These similarities are particularly interesting, considering the very different chemical nature of PPV and indole and the difference in the methods of synthesis. These similarities are also interesting when considering the potential applications of such polymer systems in the

fabrication of light emitting devices. PPV and its derivatives have been the subject of very intensive research and are presently close to a commercial use. Very little work has been carried out on the polyindoles and from this study, they have shown a very real potential for further development.

Appendix I

Supplementary lifetime data for electropolymerised indole-5-carboxylic acid in ethanol solution.

	20 mmol/ 0 Hz/ 1 minute high polymer				200 mmol/ 15 Hz/ 20 seconds High trimer			
λ	τ_1	τ_2	τ_3		τ_1	τ_2	τ_3	
420	5.24 7.5 78	1.50 5 15	0.04 87.5 7.1	1.79 1.45	5.34 12.5 91	1.75 2.4 6	0.03 85 3.2	1.7 1.4
460	5.13 7.5 54	1.38 20 39	0.07 73 7	2.00 1.40	5.24 8 79	1.25 8 18	0.02 84 3.4	1.8 1.24
500	5.15 5 17	1.55 759 67	0.61 36 16	1.50 1.80	5.22 10 34	1.45 53 52	0.56 38 14	1.5 1.7
540	5.29 2.6 11	1.55 57 69	0.64 41 21	1.50 2.00	4.81 4 15	1.41 54 65	0.57 42 20	1.3 1.7
580	5.45 3 13	1.57 52 63	0.7 45 24	1.25 1.83	4.70 3 11	1.45 50 64	0.61 43 26	1.65 1.4

Table 1: Lifetime data for indole-5-carboxylic acid samples polymerised from 20 mmol monomer solution at 0 Hz for 1 minute and 200 mmol monomer solution at 15 Hz for 20 seconds to give a high polymer and high trimer content respectively. Dissolved in ethanol.

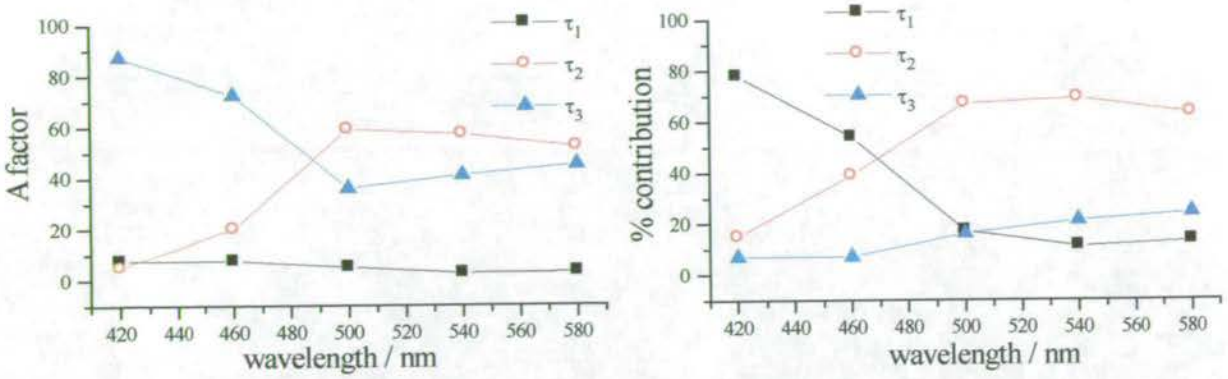

Figure 1 A factor and % contribution versus wavelength for an indole-5-carboxylic acid sample polymerised from a 20 mmol monomer solution at 0 Hz for 1 minute, to give a high polymer content.

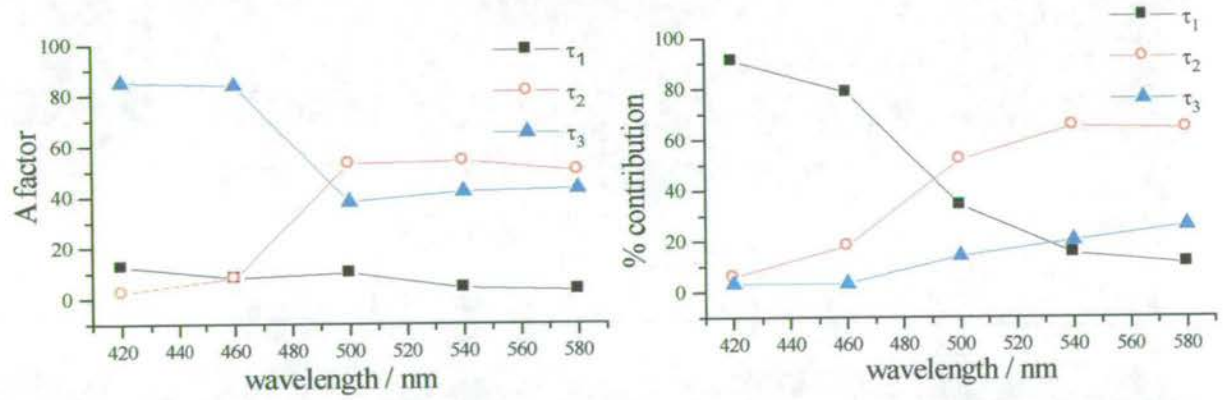

Figure 2 A factor and % contribution versus wavelength for an indole-5-carboxylic acid sample polymerised from a 200 mmol monomer solution at 15 Hz for 20 seconds, to give a high trimer content.

	200 mmol/ 0 Hz/ 1 minute high polymer				200 mmol/ 15 Hz/ 10 seconds High trimer			
λ	τ_1	τ_2	τ_3		τ_1	τ_2	τ_3	
420	4.77 12 72	1.52 13 24	0.4 75 4	1.8 1.5	5.5 26 94	1.64 4 4	0.04 71 2	1.86 1.5
460	5.07 7.4 42	1.58 24 42	0.21 69 16	2 1.5	5.56 18 83	1.33 13 15	0.05 69 3	1.8 1.3
500	8.2 9.5 39	1.96 47 45	0.75 44 16	1.5 1.6	7.4 12 45	2 31 32	0.81 57 23	1.6 1.5
540	8.25 7.5 34	1.82 48 49	0.7 44 17	1.7 1.7	7.86 7 33	1.73 38 42	0.73 56 25	1.4 1.5
580	7.5 6.4 29	0.7 43 18	1.71 51 53	1.3 1.9	7.81 5 25	1.74 36 44	0.73 60 31	1.7 1.9

Table 2 Lifetime data for indole-5-carboxylic acid samples polymerised from 200 mmol monomer solution at 0 Hz for 1 minute 15 Hz for 10 seconds to give a high polymer and high trimer content respectively. Dissolved in ethanol.

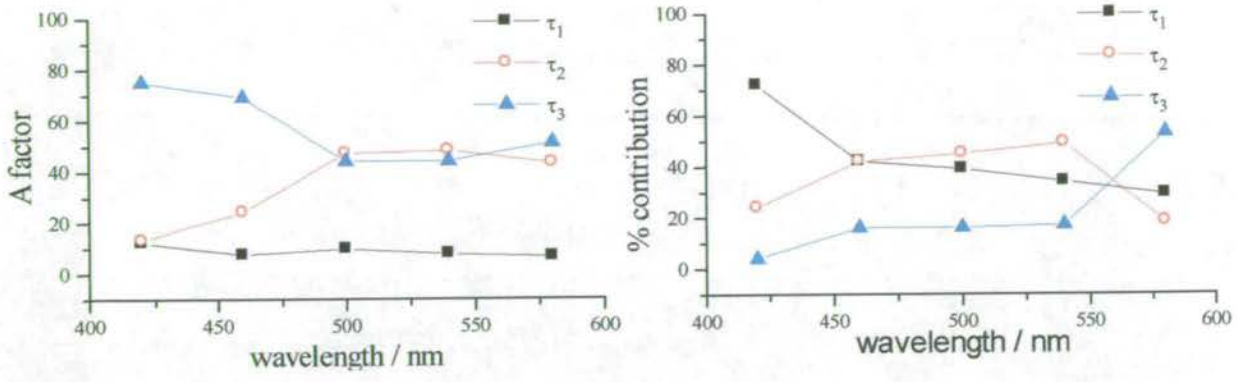

Figure 3 A factor and % contribution versus wavelength for an indole-5-carboxylic acid sample polymerised from a 200 mmol monomer solution at 0 Hz for 1 minute, to give a high polymer content.

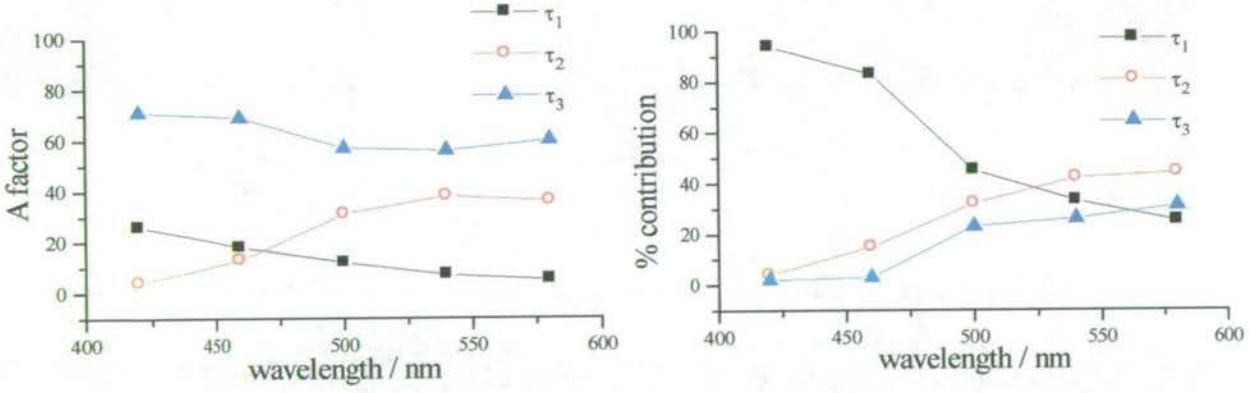

Figure 3 A factor and % contribution versus wavelength for an indole-5-carboxylic acid sample polymerised from a 200 mmol monomer solution at 15 Hz for 10 seconds, to give a high trimer content.

Appendix II

Supplementary lifetime data for electropolymerised 5-cyanoindole in ethanol solution

	10 mmol/ 0 Hz/ 10 seconds not degassed				10 mmol/ 0 Hz/ 10 seconds degassed			
λ / nm	τ_1 / ns	τ_2 / ns	τ_3 / ns		τ_1 / ns	τ_2 / ns	τ_3 / ns	
420	5.75			2.5 1.2	7.97			2.2 0.93
460	5.78			1.8 1.2	7.96			2.4 0.8
500	5.75			2.1 1.1	797 97.8 99.4	2.35 2.2 0.6		2 1.2
540	5.80 61 94	1.94 9 5	0.21 30 2	1.75 1.5	8.14 67 93.5	2.73 12 5.7	0.24 21 0.8	7.76 1.9
580	5.71 16.5 62	2.37 12.5 20	0.38 71 18	1.45 1.72	8.23 33.5 74	2.86 30 23	0.36 37 4	1.46 1.6

Table 1 Lifetime data for a degassed and non-degassed sample of indole-5-carboxylic acid in ethanol, polymerised from a 10 mmol monomer solution at 0 Hz for 10 seconds, to give a high polymer content.

	20 mmol/ 15 Hz/ 20 seconds high trimer			200 mmol/ 0 Hz/ 1 minute seconds increased polymer		
λ / nm	τ_1 / ns	τ_2 / ns		τ_1 / ns	τ_2 / ns	
420	5.85 98 99	2.15 2 1	2.1 1.2	5.75 97 98.4	2.8 3.3 1.6	4 0.5
460	5.84 99.3 99.7	2.25 0.7 0.3	2.9 0.8	5.71 98 99	2.84 2 1	3.7 0.7
500	5.87 98.8 99.5	2.42 1.2 0.5	2.8 0.9	5.74 94 98	2 6 2	2.7 0.9
540	5.94 93.6 97.3	2.43 6.4 2.7	1.8 1.3	5.74 77.6 93.4	1.4 22.4 6.6	3.8 0.7
580	5.79 32 82	0.6 68 18	1.6 1.2	5.6 30 68	1.11 70 32	3.3 0.7

Table 2 Lifetime data for a sample of indole-5-carboxylic acid in ethanol, polymerised from a 200 mmol monomer solution at 15 Hz for 20 seconds, to give a high trimer content and 0 Hz for 1 minute to give an increased polymer content.

Appendix III

Supplementary lifetime data for electropolymerised 5-cyanoindole films and the films dissolved in ethanol.

Wavelength / nm		No cycles					2 cycles				
		τ_1 / ns	τ_2 / ns	τ_3 / ns	τ_4 / ns		τ_1 /ns	τ_2 / ns	τ_3 / ns	τ_4 / ns	
Intact film	460	2.15 0.6 9	0.68 5 28	0.21 26 28	0.05 68 24	1.3 2	0.7 1 10	0.2 14 37	0.045 86 54		1.4 1.9
	500	3.06 2 18	0.94 10 34	0.3 32 33	0.07 56 14	1.3 2	1.19 0.8 9	0.37 7 27	0.13 26 37	0.04 63 27	1.3 2
	540	2.24 4 26	0.7 16 35	0.3 25 20	0.11 55 19	1.4 2	1.23 1.5 13	0.43 9 26	0.18 24 29	0.07 66 32	1.2 2
Ethanol solution	420	5.73				1.8 1.2	5.8 98 99.5	1.42 2 0.5			1.5 1.6
	500	5.73				2 1.2	5.78 98 99.75	0.7 2 0.25			1.5 1.3
	580	5.52 87 96	1.41 13 4			1.7 1.8	5.75 94 98.8	1.1 6 1.2			1.5 1.6

Table 1: Lifetime data for an uncycled and a cycled 5-cyanoindole film and the film dissolved in ethanol, polymerised from a 50 mmol monomer solution at 0 Hz for 10 seconds

Wavelength / nm		No cycles					1 cycle				
		τ_1 / ns	τ_2 / ns	τ_3 / ns	τ_4 / ns		τ_1 /ns	τ_2 / ns	τ_3 / ns	τ_4 / ns	
Intact film	460	4.07 1.4 20	1.20 8 31	0.35 26 32	0.08 65 17	1.4 1.9	1.38 0.4 7	0.46 4 24	0.16 17 37	0.03 78 32	1.2 1.9
	500	4.88 2.4 27	1.30 12 34	0.38 31 27	0.10 56 12	1.4 1.8	1.57 1 14	0.47 8 34	0.15 23 33	0.03 69 19	1.3 1.9
	540	5.38 2.6 29	1.41 12 36	0.38 33 26	0.09 52 9	1.3 1.9	2.06 1 13	0.63 7 33	0.19 25 36	0.04 67 18	1.2 1.6
Solution	420	5.80				1.6 1.2	5.71				1.5 1.4
	500	5.78				1.6 1.4	5.85 97 99.5	0.96 2.7 0.5			1.7 1.4
	580	5.83 97 99	1.38 3 1			1.3 1.9	5.85 94 99	0.9 6 1			1.4 1.7

Table 1: Lifetime data for an uncycled and a cycled 5-cyanoindole film and the film dissolved in ethanol, polymerised from a 50 mmol monomer solution at 10 Hz for 10 seconds

Appendix IV

Postgraduate courses and lectures

Intermediate Microsoft Word.

Advanced Microsoft Word.

Advanced Microsoft PowerPoint.

Basic HTML programming.

Electrochemistry.

Colloquia and physical section meetings.

EPSRC "Insight into management" course.

Transferable skills course.

Conferences and Meetings

Butler meeting, University of Edinburgh, 1996.

Electrochem '96, University of Bath, 1996.

Butler meeting, Glasgow Caledonian University, 1997.

The 193rd meeting of the Electrochemical Society, San Diego, California, 1998.

Central Laser Facility Users Meeting, Rutherford Appleton Laboratory, 1998.

Firbush Physical Section Meetings, 1995-1998.

Appendix V

Reprints of Publications

Electrooxidation of 5-substituted indoles

Peter Jennings, Anita C. Jones, Andrew R. Mount* and Alastair D. Thomson
University of Edinburgh, Department of Chemistry, The Joseph Black Building, West Mains Road, Edinburgh, UK EH9 3JJ

The electrochemical oxidation of a wide variety of 5-substituted indole monomers at a platinum electrode results in the formation of a redox active film. Electrochemical and spectroscopic evidence is consistent with the redox species in the film being a cyclic trimer. In contrast, the electropolymerisation of 5-aminoindole and 5-hydroxyindole on a platinum electrode does not result in redox active film formation. This is attributed to the adsorption of the monomer onto the metal electrode *via* the substituent, which inhibits this reaction. However, electropolymerisation of these monomers onto a predeposited film of 5-cyanoindole or 5-nitroindole results in the formation of the cyclic trimer. Electrochemical studies using a rotating-ring disc electrode (RRDE) have confirmed the stoichiometry of the trimerisation reaction and also that the redox active cyclic trimer species shows reversible one electron redox activity. The half-wave potential for the reduction of each of these trimers shows a linear dependence with the Hammett substituent constant, σ^+ or σ^-, as appropriate, determined for a *para*-substituted aromatic indicating that the 5-substituent is conjugated into the π-electron system of the trimer. This indicates that judicious choice of substituents allows control of the trimer redox potential.

Introduction

In our previous papers,[1,2] we showed that electropolymerisation of the 5-substituted indoles (**1**) indole-5-carboxylic acid (R = COOH) and 5-cyanoindole (R = CN) both involved the formation of a cyclic trimer, which was then deposited onto an electrode surface and linked to form a redox active polymer of linked trimers.

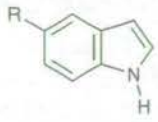

Formula 1

Our previous chronamperometric studies at a rotating disc electrode (RDE) for indole-5-carboxylic acid and 5-cyanoindole[1,2] showed that electrooxidation involved the initial formation of an asymmetric cyclic trimer (**2**) in the diffusion layer, which is then deposited onto the electrode surface.

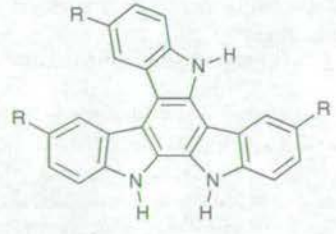

Formula 2

This deposited monolayer then acts as a site for electrooxidation and adsorption of the monomer radical cation, so that cyclic trimer is then formed by coupling on the electrode surface. In the initial growth phase, when the surface layer is being deposited, the current is observed to change with time, whereas once the film is formed, steady-state currents are observed and the kinetics of deposition become first order in monomer, as oxidation and adsorption of the monomer control the linking process. The reaction is, therefore, that given in eqn. (1):

$$3n\ \mathrm{In} \rightarrow n(\mathrm{In})_3{}^+(\mathrm{s}) + 7\mathrm{e}^- + 6\mathrm{H}^+ \quad (1)$$

with the cyclic trimer being deposited in its oxidised form onto the electrode surface. Once deposited, the trimer centre can act as a site for further trimerisation (the coat grows) and/or the trimers can link on the surface to form a polymer of linked trimers [eqn. (2)][1,2]

$$n(\mathrm{In})_3{}^+(\mathrm{s}) \rightarrow -[(\mathrm{In})_3{}^+]_n-(\mathrm{s}) + 2\mathrm{e}^- + 2\mathrm{H}^+ \quad (2)$$

Polyindoles have been proposed as potential candidates for fast response potentiometric sensors[3] and for the direct oxidation and reduction of biomolecules.[4] For many of these applications, it is desirable to produce electroactive indole layers with a wide variety of substituents. The most obvious method for achieving this would be the electrooxidation of a wide variety of 5-substituted indole monomers. These molecules have been the subject of a previous preliminary investigation by Waltman *et al.*,[5] who electropolymerised some commercially available 5-substituted indoles, including 5-cyanoindole and indole-5-carboxylic acid, and suggested that the polymerisation of the indoles occurred at the 1- and 3-positions, resulting in a linear polymer, and that electropolymerisation and film formation on the electrode could only be observed for those monomers which oxidised in a limited range of electrode potentials. In the light of our results for indole-5-carboxylic acid and 5-cyanoindole, which contradict some of these findings, we now present results for the electropolymerisation of other 5-substituted indoles.

Experimental

All chemicals used in these experiments were of AnalaR grade or equivalent and were used as received unless otherwise stated. Electrochemical control of the RRDE and RDE studies was by an Oxford Electrodes bipotentiostat, with the data being collected on a *x*–*y*–*t* chart recorder (Bryans Instruments). An Oxford Electrodes motor controller was used to rotate the electrode. A 2 cm^2 platinum gauze was used as the counter-electrode, whilst the working electrode was a Pt–Pt RRDE (Oxford Electrodes, disc area 0.387 cm^2, measured collection efficiency, $N_0 = 0.21$, as measured by the ferrocene/ferrocinium couple). The reference electrode was

made in house and consisted of a silver wire dipping into a solution of silver perchlorate (0.01 mol dm^{-3}) in background electrolyte solution. All potentials are reported with respect to this electrode, which has a potential of +0.437 V *vs.* SCE. The background electrolyte solution consisted of 0.1 mol dm^{-3} anhydrous lithium perchlorate (Aldrich) in acetonitrile (Fisons, dried distilled). Indole-5-carboxylic acid was recrystallised twice in an oven and dried at 130 °C for several days prior to use. Fluorescence measurements were performed on a Spex Fluoromax spectrophotometer.

Results and Discussion

Electropolymerisation of indoles at the RDE

Initially electropolymerisation studies were performed at our platinum RDE. Table 1 presents the peak oxidation potentials (the potential at which the peak in oxidation current is observed) measured for each indole by linear sweep voltammetry (LSV), and the oxidation potential chosen for the chronoamperometric polymerisation studies. As with most polymers formed by electrooxidation, it is not easy to measure the true oxidation potential of the monomer, as coupling of the radical cations complicates the reaction and there is a change in the nature of the electrode surface as reaction proceeds owing to deposition of oligomeric product. However, under the same conditions, the variation in the peak oxidation potential as the monomer is changed should mirror changes in the oxidation potential. As with our previous studies, we have ensured that this electrode potential is equal to or more positive than the oxidation potential of the monomer[5] in order to ensure that the electrode kinetics of monomer oxidation are not rate limiting. To confirm this, under these conditions we observe little variation in the oxidation current with potential.

In contrast to some of the results obtained by Waltman *et al.*,[5] electrooxidation of 0.1 mmol dm^{-3} 5-nitroindole produced similar chronoamperometric transients compared with indole-5-carboxylic acid and 5-cyanoindole[1,2] [Fig. 1(a)], and resulted in film formation. This may be because we have chosen to perform our electropolymerisation experiments at high monomer concentrations and higher oxidation currents. This will lead to higher concentrations of monomer radical cations near the electrode surface, which would be expected to increase the proportion of radical cations that combine to form a cyclic trimer (involving three radical cations) with respect to reaction with radical scavengers in the solvent or convective diffusion of a radical cation from the electrode to the bulk (both first order processes in radical cation). As with indole-5-carboxylic acid and 5-cyanoindole this film is electroactive, as demonstrated by cyclic voltammetry (CV) of the film in background electrolyte [Fig 1(b)]. The peak currents in the CV are proportional to the sweep rate in the range 1–100 mV s^{-1}, indicative of the rapid redox cycling of a surface-boun species. Integration of the peaks reveals that the redox reac tion involves about 0.14 of the charge passed in film forma tion. As with indole-5-carboxylic acid and 5-cyanoindole thi is consistent with the electropolymerisation involving the pro duction of a cyclic trimer on the electrode surface as an oxi dised species in approaching 100% yield. This work is i agreement with recent work by Kokkinidis and Kelaido polou,[6] who have also shown that 5-nitroindole forms electro active films on electroxidation on gold surfaces.

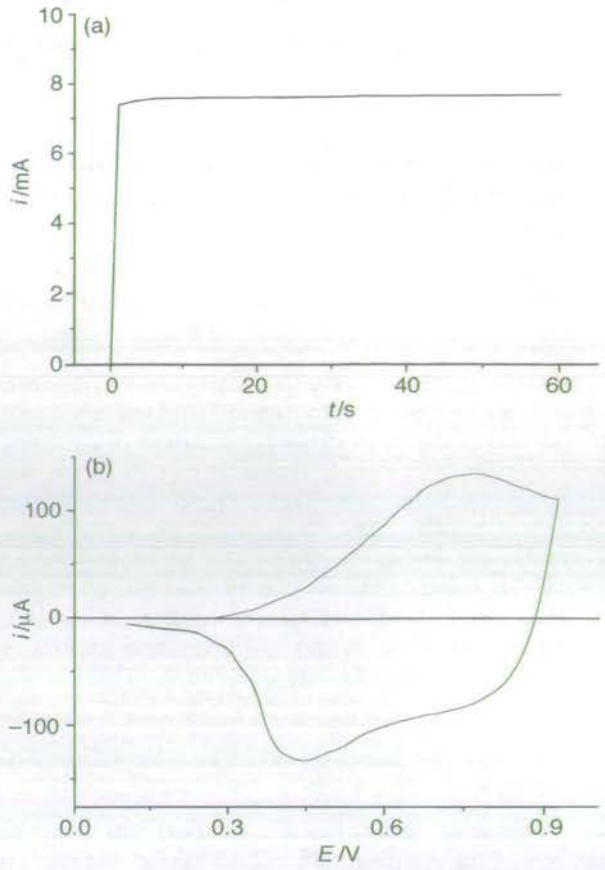

Fig. 1 (a) A typical chronoamperometric transient for the oxidatio of 50 mmol dm^{-3} 5-nitroindole at the Pt disc electrode. The oxidatio potential is +1.7 V applied at time (t) = 0 s and rotation spee (W) = 2 Hz. (b) Typical steady-state CV for the 5-nitroindole fil formed in (a) in background electrolyte, with sweep rate (v) = 10 mV s^{-1}.

Table 1 Data for the oxidation of the monomers

monomer	R	E_p[a]/V	E_o[b]/V
5-nitroindole	NO_2	+1.70	+1.70
5-cyanoindole	CN	+1.64	+1.64
indole-5-carboxylic acid	COOH	+1.46	+1.46
5-chloroindole	Cl	+1.30	+1.30
5-bromoindole	Br	+1.10	+1.10
indole	H	+1.10	+1.10
5-methylindole	Me	+0.94	+0.95
5-benzyloxyindole	$C_6H_5CH_2O$	+0.90	+0.90
5-methoxyindole	MeO	+0.83	+0.85
5-hydroxyindole	OH[c]	+0.74	+0.75
5-aminoindole	NH_2[c]	+0.56	+0.575

[a] Peak oxidation potential measured by LSV. [b] Oxidation potential used in chronoamperometry. [c] Data measured on predeposited poly(5-cyanoindole) film. Oxidation potentials on bare Pt are similar.

The electrooxidation of 0.1 mol dm^{-3} solutions of 5 methoxyindole, 5-chloroindole, 5-bromoindole, 5-methyl indole, indole and 5-benzyloxyindole showed simila behaviour, with an electroactive film being formed. Howeve each of these monomers showed a reduced steady-state elec trooxidation current (1.0–1.3 mA) once a film had forme under comparable conditions to 5-nitroindole (1.95 mA). A this relatively high bulk monomer concentration, although th reaction is first order with respect to monomer, the mas transport is relatively fast at all rotation speeds, the current i insensitive to changes in rotation speed and the observe current can be approximated to the mass transport indepen dent coupling current of the monomers on the electrod surface (i_∞, *vide infra*). These results therefore indicate tha 5-methoxyindole, 5-chloroindole, 5-bromoindole, 5-methy indole, indole and 5-benzyloxyindole all have reduced coup ling rates compared with 5-cyanoindole, 5-nitroindole an indole-5-carboxylic acid. Film growth occurred for indole, 5 chloroindole, 5-bromoindole, 5-methoxyindole and 5 methylindole, but only very slowly (over a timescale o

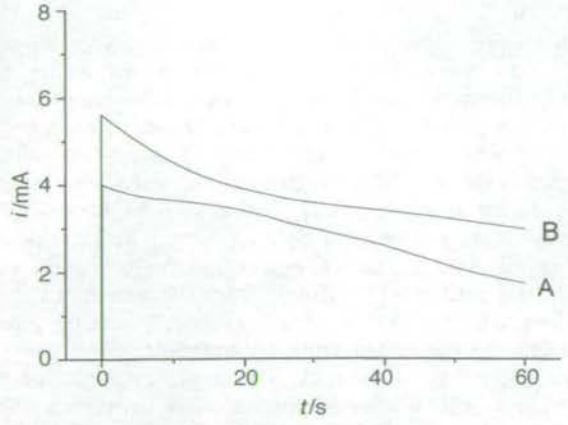

ig. 2 Typical chronoamperometric transients for the oxidation f: A, 50 mmol dm^{-3} 5-aminoindole; and B, 50 mmol dm^{-3} -hydroxyindole bulk concentration solutions on the Pt disc at +0.575 V (A) and +0.750 V (B), with $W = 2$ Hz

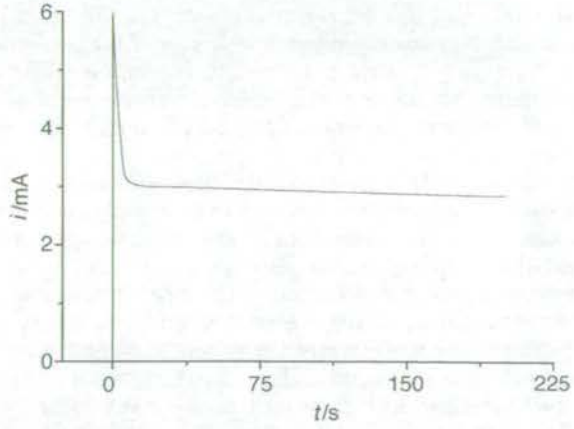

Fig. 3 Typical chronoamperometric transients for the oxidation of 50 mmol dm^{-3} 5-aminoindole on a predeposited poly(5-cyanoindole) film at +0.575 V with $W = 2$ Hz

inutes) at 2 Hz. Experiments performed with a stationary lectrode resulted in similar currents, due to the reaction rate eing insufficient to cause depletion of monomer at the elec- rode; however, for each monomer the solution near the elec- rode surface turned brown, indicating the formation of oluble product. The fraction of product deposited onto the lectrode for indole, 5-chloroindole, 5-bromoindole and 5- ethylindole also increased under these conditions, indicating hat as for 5-cyanoindole and indole-5-carboxylic acid initial lm formation is from product produced in the solution near he electrode, which is swept away under rotation. Hence, ncreased rotation speed hinders the initial deposition of an lectroactive film.

Electrooxidation of 5-aminoindole and 5-hydroxyindole nder comparable conditions to 5-nitroindole resulted in a apid decrease in the observed current with time and no film ormation (Fig. 2). Previous work[5] had shown that unlike the ther indoles studied the oxidation of 5-aminoindole involves he removal of one electron. This rapid decrease in current an therefore be attributed to adsorption of the monomer *via* he substituent and the preferential oxidation of the substit- ent of 5-aminoindole (and by inference 5-hydroxyindole) on Pt, which we have observed leads to an electroinactive roduct.

Polymerisation of 5-aminoindole and 5-hydroxyindole on preformed indole films

n order to avoid the adsorption of 5-aminoindole or 5- ydroxyindole on platinum (which inhibits film formation) nd to promote cyclic trimer formation *via* adsorption of the nonomer radical cation and cyclisation (the method by which he other indole layers grow) we have performed experiments n a preformed film of electrodeposited 5-cyanoindole and 5- itroindole. Fig. 3 shows a typical chronoamperometric esponse for 5-aminoindole on a predeposited layer of poly(5- yanoindole). (Please note that for simplicity throughout this aper, predeposited films will be referred to as polymers. It is mportant to remember that in reality these films contain a nixture of linked and unlinked trimers.) The potential chosen vas sufficient to oxidise the 5-aminoindole monomer, but nsufficient to link the 5-cyanoindole film further. It can learly be seen that, in contrast to bare platinum, after an nitial burst of current (due to oxidising the 5-cyanoindole edox centres in the layer) a nearly constant current is bserved. We have performed Koutecky–Levich analysis of he steady-state currents obtained on both 5-cyanoindole and 5-nitroindole films for 5-hydroxyindole and 5-aminoindole, examples of which are shown in Fig. 4. For both 5-aminoindole and 5-hydroxyindole, it can be seen that similar Koutecky–Levich plots are obtained on 5-cyanoindole and 5-nitroindole as the rotation speed (W/Hz) and the bulk monomer concentration (c_∞) are systematically varied; this is also true for films of varying thicknesses. This indicates that the coupling reaction is insensitive to the type of indole trimer in the preformed film. As for other 5-substituted indoles, the data show good straight lines, consistent with electrooxidation being first order with respect to monomer. Our previous work

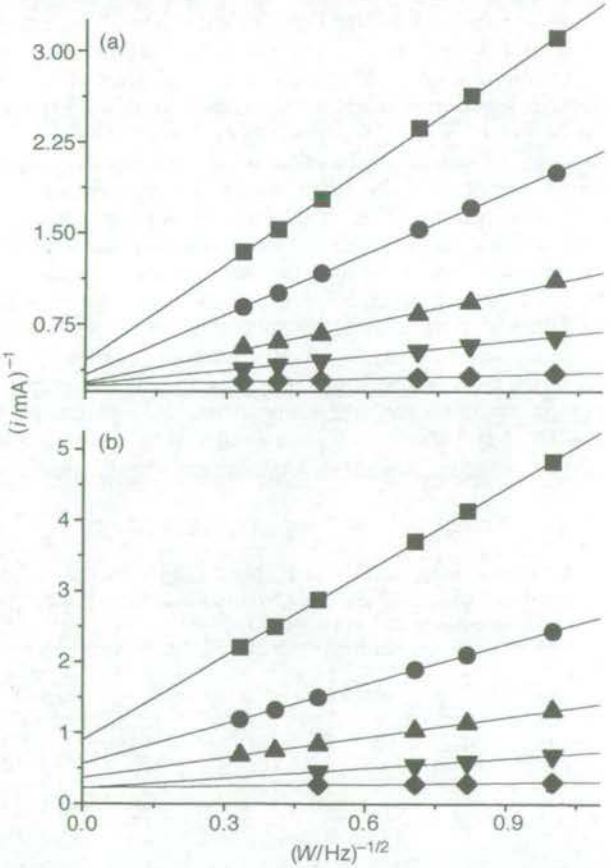

Fig. 4 Koutecky–Levich plots for the reciprocal of the steady-state currents (i^{-1}) *vs.* $W^{-1/2}$ for the electrooxidation of 5-aminoindole on (a) poly(5-cyanoindole) and (b) poly(5-nitroindole) films at +0.575 V. The data presented are for bulk monomer concentrations of 5-aminoindole of: ■, 2.5; ●, 5; ▲, 10; ▼, 20; and ◆, 50 mmol dm^{-3}.

has shown[1,7] that this behaviour is observed for indole-5-carboxylic acid, 5-cyanoindole and copolymers of the two monomers. We have published a detailed mathematical model for the coupling process on the surface,[7] where coupling of adsorbed monomer radical cations occurs on the electrode surface.

At the relatively high monomer concentrations used in these studies, the surface is expected to be completely covered with radical cations; these then couple in threes to form a trimer which can act as new sites for adsorption. Since the adsorption process is expected to be first order with respect to surface monomer concentration and the surface coupling rate will be insensitive to concentration under these conditions, we obtain first order kinetics.[7] These results therefore suggest that 5-aminoindole is coupling *via* a similar mechanism. From the Koutecky–Levich equation [eqn. (3)], $nD^{2/3}$ and i_∞ have been determined:

$$1/i = 1/i_\infty + 0.643v^{1/6}/(nFAD^{2/3}c_\infty W^{1/2}) \quad (3)$$

where i is the steady-state current, A is the electrode area, v is the kinematic viscosity of acetonitrile, F is the Faraday constant, D is the diffusion coefficient, n is the number of electrons and i_∞ is the current obtained as W tends to ∞, and the reaction rate is independent of mass transfer. Table 2 shows typical values of i_∞ and n calculated for 5-aminoindole from the plots in Fig. 4. These have been measured at each bulk concentration on 5-cyanoindole and 5-nitroindole preformed films, assuming that $D = 1.5 \times 10^{-5}$ cm^2 s^{-1}, similar to the values estimated for indole-5-carboxylic acid and 5-cyanoindole.[1,2] The linearity of the Koutecky–Levich plots indicates that the electrooxidation reaction is first order with respect to monomer. This is consistent with reaction occurring *via* oxidation and adsorption of monomer onto the electrode surface, on which further reaction occurs, as with our 5-cyanoindole and indole-5-carboxylic acid studies. However, it is clear that the values of n of around 1.2–1.8 found at bulk concentrations below 50 mmol dm^{-3} indicate that the product being formed is not a trimer, as n would be expected to be between 2.3 and 3.0 depending on the extent of linkage of the trimers formed or, in other words, the relative importance of eqn. (1) and (2). Furthermore, the dependence of i_∞ on the bulk concentration in this region indicates that reaction is not occurring *via* an adsorbed full monolayer of oxidised intermediates that covers the whole electrode surface, as is the case for the other indoles. This would mean that the probability of having three neighbouring monomer radical cations adsorbed on the electrode surface under these conditions would be very low, which may explain why trimerisation is not occurring to any significant extent. In contrast, at 50 mmol dm^{-3} and above, as for the electrooxidation studies for indole-5-carboxylic acid and 5-cyanoindole,[1,2] i_∞ does not vary with concentration and n is found to be constant at 2.3–2.8, the value expected for trimer formation. It is therefore most likely that under these conditions trimer formation is occurring from a monolayer of adsorbed intermediates and eqn. (1) and (2) accurately describe the reaction occurring. We have performed similar experiments studying the electropolymerisation of 5-hydroxyindole on poly(5-cyanoindole) and poly(5-nitroindole) films. Again, straight line plots are obtained using Koutecky–Levich analysis, with i_∞ increasing with concentration at bulk concentrations below 50 mmol dm^{-3}, and remaining constant above 50 mmol dm^{-3}. We therefore conclude that a similar reaction is occurring for 5-hydroxyindole compared with 5-aminoindole.

One interesting observation is that the gradients of these lines yield values of n for 5-aminoindole of between 5 and 7.5 electrons per monomer if D is assumed to be 1.5×10^{-5} cm^2 s^{-1}. Given that we expect the actual value of n to lie in the range $3.0 > n > 2.3$ these gradients are indicative of an anomalously high diffusion coefficient for 5-hydroxyindole when compared with the other indoles studied. This observation along with the anomalous half-wave potential ($E_{1/2}$) values observed for the 5-hydroxyindole monomer (*vide infra*) might indicate that 5-hydroxyindole is aggregating in solution (*vide infra*). For both 5-aminoindole and 5-hydroxyindole the values of i_∞ observed are much lower than those obtained for 5-cyanoindole, indole-5-carboxylic acid or 5-nitroindole. This is consistent with a slower surface coupling rate for the radical cation, because of the stabilising effect of the amino and hydroxy substituents, which would be expected to reduce the radical reactivity.

Table 2 Typical values of n and i_∞ for 5-aminoindole on a preformed poly(5-cyanoindole) and poly(5-nitroindole) film at +0.575 V, calculated from eqn. (3), and assuming that $D = 1.5 \times 10^{-5}$ cm^2 s^{-1}

monomer	c_∞ /mmol dm^{-3}	n	i_∞/mA
5-aminoindole on poly(5-nitroindole)	2.5	1.19 ± 0.02	1.20 ± 0.02
	5	1.22 ± 0.02	1.80 ± 0.03
	10	1.23 ± 0.02	2.70 ± 0.05
	20	1.20 ± 0.02	4.6 ± 0.1
	50	2.8 ± 0.5	4.5 ± 0.4
5-aminoindole on poly(5-cyanoindole)	2.5	1.78 ± 0.03	2.2 ± 0.2
	5	1.38 ± 0.04	2.7 ± 0.2
	10	1.39 ± 0.09	3.7 ± 0.3
	20	1.47 ± 0.03	3.9 ± 0.2
	50	2.3 ± 0.2	4.0 ± 0.1

Characterisation of the films formed from electrooxidation

We have performed laser-desorption laser-ionisation time-of-flight mass spectrometry (L^{2}TOF-MS) on the films produced by electrooxidation of these monomers.[6] As for indole-5-carboxylic acid and 5-cyanoindole,[1,2] the major constituent of the film for 5-chloroindole, 5-bromoindole, 5-methylindole, indole and 5-methoxyindole is a cyclic trimer, with a mass three times the mass of the monomer, less six protons due to the formation of six bonds in the trimer. Further characterisation has been by fluorescence spectroscopy of the layers in solution. Representative spectra are shown in Fig. 5. It can clearly be seen that the emission spectra of the film species are extremely similar and are very red-shifted in comparison to their monomer. Furthermore, the emission spectra are also extremly similar to those obtained for the asymmetric trimer produced during the electrooxidation of 5-cyanoindole[2] (Fig. 5A), indicating that the same chromophore is present in each case. 5-Nitroindole films do not fluoresce; this is often observed for nitro-subsituted aromatics, and is attributed to the accessibility of the $n \rightarrow \pi^*$ transitions. Also shown is the emission and excitation spectra obtained for 5-hydroxyindole solution after prolonged oxidation using a poly(5-nitroindole) modified electrode. It is clear that this product in solution is a similar species. For electropolymerised 5-aminoindole solutions, fluorescence is complicated by the aggregation of both 5-aminoindole monomer and products in solution. This can be overcome by adding 100% glacial acetic acid, which protonates the amino groups and prevents aggregation in ethanol. The resulting spectra, also presented in Fig. 5, show that the same chromophore is also present in these solutions. In addition, we have performed fluorescence measurements on solutions produced by dissolving the poly(5-nitroindole) film from the electrode in ethanol after electrooxidation. For both 5-aminoindole and 5-hydroxyindole we observed similar fluorescence spectra even after the film was washed with background electrolyte, indicating that a proportion of the 5-

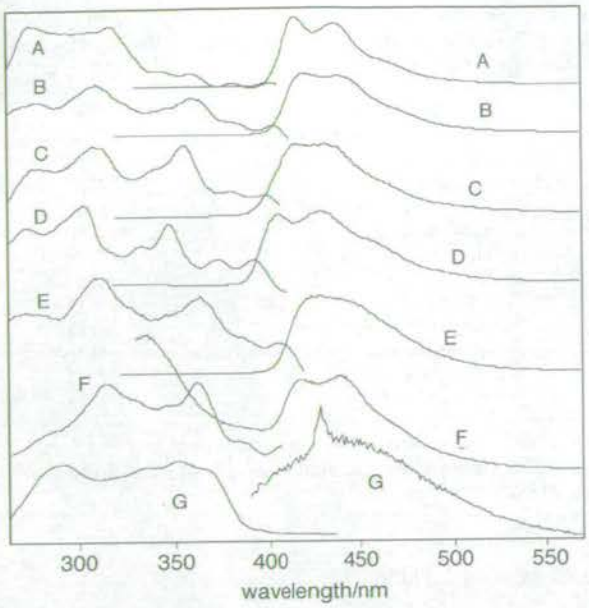

Fig. 5 Typical fluorescence spectra in MeOH obtained for the films produced by electrooxidation of 50 mmol dm^{-3} solutions of: A, 5-cyanoindole; B, 5-chloroindole; C, 5-bromoindole; D, indole; E, 5-methoxyindole; F, 5-hydroxyindole; and G, 5-aminoindole. For 5-aminoindole and 5-hydroxyindole the spectra obtained are for the soluble products of the electrooxidation reaction performed on the Pt disc electrode precoated with poly(5-nitroindole). For 5-aminoindole, the spectra have been acquired in the presence of 1% v/v glacial acetic acid. Emission spectra have been acquired using an excitation wavelength of between 310 and 320 nm. Excitation spectra are acquired at the maximum emission wavelength of the fluorescing species.

aminoindole and 5-hydroxyindole trimer produced remained on the film surface.

Characterisation of the electroactive products from electrooxidation by RRDE studies

We have used an RRDE downstream of the RDE at which monomer electrooxidation is occurring in order to probe the mechanism of reaction. For all these experiments we ensured that film formation occurred *via* adsorbed intermediates, this was done by ensuring that steady-state currents were passed and by using preformed 5-cyanoindole or 5-nitroindole films on the disc for 5-hydroxyindole and 5-aminoindole. Fig. 6 shows a typical ring voltammogram obtained during the oxidation of indole-5-carboxylic acid at the RDE. The large reduction wave seen at negative potentials is seen for all the

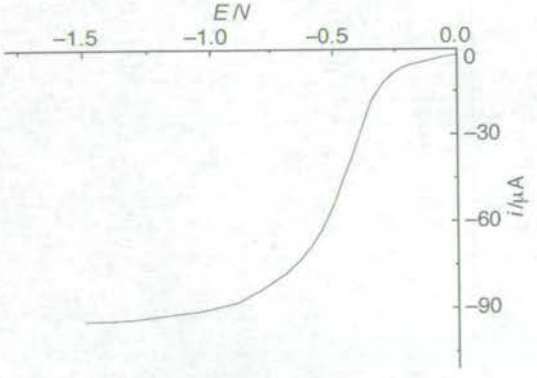

Fig. 6 A typical ring voltammogram of the products formed during the electrooxidation of 60 mmol dm^{-3} indole-5-carboxylic acid at the Pt RDE. The disc current is 0.500 mA, $W = 2$ Hz and $v = 10$ mV s^{-1}.

monomers and can be attributed to the one-electron reduction of protons liberated during the reaction, *i.e.*,

$$H^+ + e^- \rightarrow \tfrac{1}{2}H_2 \quad (4)$$

As expected, this wave shows variation in the measured $E_{1/2}$ value with the addition of trace amounts of water or the presence of a base (for example, the amino group of 5-aminoindole), as these stabilise the protons in acetonitrile. For each monomer, the mass transport limited current, i_L, for reaction (4), has been measured at a variety of disc currents, i, and the effective collection efficiency, N, calculated, where

$$N = |i_L|/i \quad (5)$$

A selection of these values is presented in Table 3. If the mechanism of film formation is the same as for indole-5-carboxylic acid [*i.e.*, eqn. (1) and (2)], there would be a predictable relationship between N and N_0, the collection efficiency of the RRDE. If eqn. (1) predominates and eqn. (2) is unimportant, then the film consists of free trimer units and the formation of a trimer unit involves the removal of seven electrons and the production of six protons. In this case, $N = \frac{6}{7}N_0$ or $N = 0.18$. If, however, the coat is of predominantly linked trimer [eqn. (2) goes to completion] then nine electrons will be removed and eight protons evolved to make each linked trimer and $N = \frac{8}{9}N_0$ or $N = 0.19$. With the exception of 5-cyanoindole, the values of N presented in Table 3 all lie within these two values indicating cyclic trimer formation. The value for 5-cyanoindole is equal to N_0, which suggests that the number of protons released is equal to the number of electrons removed. One possible explanation is that the cyclic trimer of 5-cyanoindole (CI) loses an extra proton when formed, giving a neutral oxidised species, *i.e.*,

$$3n\mathrm{CI(aq)} \rightarrow n(\mathrm{CI})_3(\mathrm{s}) + 7e^- + 7H^+ \quad (6)$$

However, during these experiments, the poly(5-cyanoindole) film was observed to deposit mainly on the outside of the disc. This means that further trimer formation would preferentially occur at the disc edges, which would lead to an increase in the collection efficiency of protons. We have therefore performed experiments measuring N for 5-cyanoindole on a preformed layer of poly(5-cyanoindole), which covers the whole of the disc (made by choosing $W < 2$ Hz). The measured value of N under these conditions (Table 3) clearly shows that the true value of N is similar to that obtained for indole-5-carboxylic acid, and the stoichiometry of the reaction is that given in eqn. (1) and not that in eqn. (6).

In addition to the observation of a proton wave, there is also another electroactive product observed as a wave at a more oxidising potential on the ring (Fig. 7). This wave is a reduction wave, due to an oxidised species. We attribute this wave as being due to oxidised cyclic trimer produced by the disc reaction. [In support of this, we have observed that the measured half-wave potentials of solutions prepared by preparing concentrated solutions of the deposited trimer films in *N*,*N*′-dimethylformamide (DMF), and then by adding these to

Table 3 Effective proton collection efficiencies for the electropolymerisation of 5-substituted indole monomers

indole monomer	N
indole	0.180 ± 0.005
5-cyanoindole	0.210 ± 0.005
indole-5-carboxylic acid	0.185 ± 0.005
5-nitroindole	0.175 ± 0.005
5-bromoindole	0.175 ± 0.005
5-cyanoindole[a]	0.185 ± 0.005

[a] Electropolymerisation on preformed poly(5-cyanoindole) film.

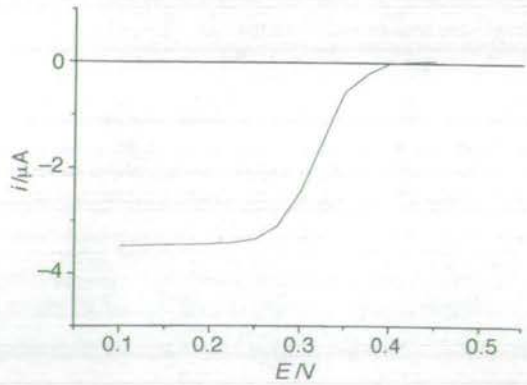

Fig. 7 A typical ring voltammogram for the reduction of the products seen for 100 mmol dm^{-3} indole at more oxidising potentials than Fig. 8. The disc current was 1.000 mA and all other conditions were as for Fig. 8.

Table 4 Typical values for the soluble fraction, x, of the trimer produced in the electropolymerisation reactions of the indole monome calculated from eqn. (8)

monomer	x
5-nitroindole	0.11
5-cyanoindole	0.05
indole-5-carboxylic acid	0.06
5-bromoindole	0.10
5-chloroindole	0.09
indole	0.25
5-methylindole	0.31
5-benzyloxyindole	0.17
5-methoxyindole	0.20
5-hydroxyindole[a]	0.21
5-aminoindole[a]	0.33

The solution concentration used was 50 mmol dm^{-3} in each case
[a] Electropolymerisation on a preformed poly(5-cyanoindole) film on the disc electrode.

background electrolyte, are generally within 50–100 mV of the measured half-wave potentials of these waves. The change in solvating species from acetonitrile to DMF can be expected to cause a shift in the measured $E_{1/2}$ value of this magnitude, and so it most likely that the electroactive species is the same in each case.] The fact that none of the trimer arriving at the ring is in its reduced form is further evidence that the cyclic trimer is formed on the disc surface, where it is then oxidised before dissolution. If appreciable amounts of trimer were formed by cyclisation of monomer radical cations or intermediates in the diffusion layer then the trimer would be formed away from the electrode in its reduced form

$$3n\ In^{+\cdot} \rightarrow n(In)_3(aq) + 6H^+$$

and a significant amount of reduced trimer would be detected at the ring as an oxidisable species. This is indeed what is seen as electrooxidation commences, or at low indole monomer concentrations, before a film has formed on the disc electrode. As the ring current is due to the reduction of the cyclic trimer produced at the disc electrode, *i.e.*,

$$(In)_3^+ + e^- \rightarrow (In)_3 \qquad (7)$$

in this case, assuming that free trimer is produced in the reaction, the apparent collection efficiency for this wave would be

$$N = \frac{x}{7} N_0 \qquad (8)$$

where x is the fraction of trimer formed at the disc that does not remain in the film, but rather dissolves into solution and is detected by the ring. Using eqn. (5) and (8) and the observed values of i_L and i, calculated values of x for the monomers under study are presented in Table 4. It is satisfying that for monomers such as 5-cyanoindole and indole-5-carboxylic acid, for which we have already shown that nearly all the cyclic trimers formed remain in the film, x is very low. However, for some of the other indoles x is not negligible. This is not entirely unexpected, as the presence of more solubilising substituents on the trimer would be expected to confer increased solubility on the $(In)_3^+$ species once formed.

A typical modified Tafel plot for these species is shown in Fig. 8. In all cases, the gradient of this Tafel plot is the same as that determined experimentally for the ferricinium ion, and the gradients are given by the expression for electrochemically reversible one-electron transfer with only a reducible species, $(In)_3^+$, present:

$$\ln[i_L/i - 1] = F/RT(E - E_{1/2}) \qquad (9)$$

where E is the electrode potential and $E_{1/2}$ is the half-wave potential, related to the standard potential, $E^\ominus$, for the reaction given in eqn. (7) by:

$$E_{1/2} = E^\ominus + RT/F \ln\{(D_R/D_O)^{2/3}\} \qquad (10)$$

and D_O and D_R are the diffusion coefficients of $(In)_3^+$ and $(In)_3$, respectively.

For these relatively large aromatic molecules, it is reasonable to assume that $D_O \approx D_R$, and hence, from eqn. (10), that $E_{1/2} \approx E^\ominus$. We have therefore measured values of $E_{1/2}$ for each of the trimers. Fig. 9(b) shows these values, plotted against the Hammett substituent constants σ^+ and σ^- [8] for each of the substituents R. These parameters are used to correlate the electron withdrawing (−) and donating (+) effect of the direct conjugation of the π-electron density of a *para*-substituent into the reactive centre of a delocalised system, such as a benzoic acid, on the equilibrium constant of the reaction. Also shown on this figure are data points for the trimers for which the full waves were difficult to observe experimentally by RRDE studies owing to the onset of the monomer oxidation wave at these potentials. The values of $E_{1/2}$ shown can be considered as a lower limit for the true value of $E_{1/2}$ in these cases.

With the exception of the oxy substituents (R = OX; X = H, CH_3, $C_6H_5CH_2$), it is clear from the Fig. 9(b) that the observed $E_{1/2}$ (and hence $E^\ominus$) values show close correlation with these parameters. This indicates that for all but the OX substituents, there is a great deal of π-electronic delocalisation between the redox centre (the delocalised π-system of the trimer) and the substituent. This trend is in good agreement with our observed variation of the peak monomer oxidation potential with σ^+ and σ^- [Fig. 9(a)], which indicates that similar conjugation is observed in the monomer, and that the difference in the behaviour of OX substituents is not solely

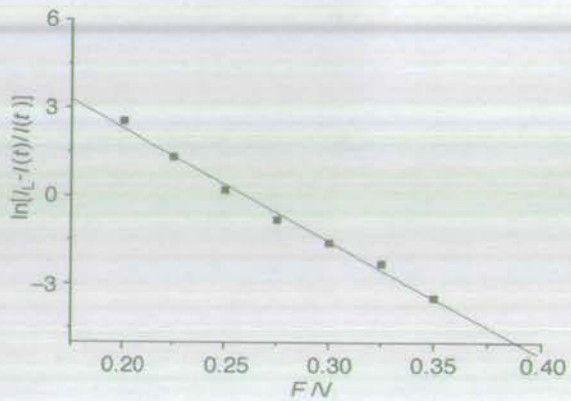

Fig. 8 Typical modified Tafel plot for the reduction wave at more positive potentials seen on the ring for 0.1 mol dm^{-3} 5-methylindole

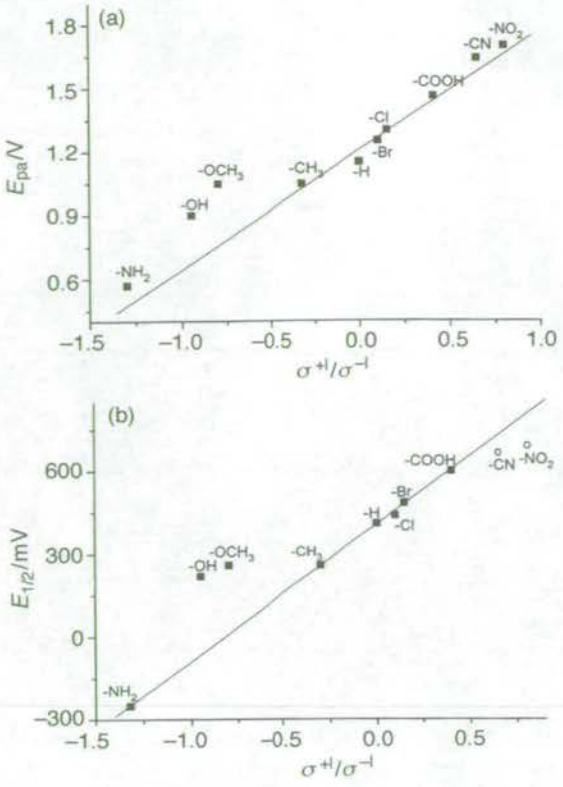

Fig. 9 (a) Observed oxidation peak potential for the monomer, E_{pa}, and (b) observed half-wave potential for the reduction wave at more positive potentials, $E_{1/2}$, *vs.* the Hammett substituent constant (σ^+/σ^- as appropriate[8]) for the 5-substituent, R, as shown. (The values for 5-nitroindole and 5-cyanoindole trimers shown (○) are lower limits for $E_{1/2}$, as the onset of the monomer oxidation wave overlaps with the trimer reduction wave.)

limited to the trimer. One possible explanation for this effect is that aggregation may be occurring between monomers (and also between trimers in solution). Hydrogen bonding between indole N—H and OX groups would lead to aggregation and would reduce the electron donating capacity of the OX group; this may also explain the anomalously high diffusion coefficients obtained for 5-hydroxyindole in the Koutecky–Levich experiments (*vide supra*) as aggregated molecules will have a combined solvation shell, which would mean that the solvation per monomer is reduced leading to a larger diffusion coefficient for the monomer. However, with these exceptions, it is clear from Fig. 9(b) that judicious choice of substituent allows for systematic variation in the observed redox potential of the trimer over a wide potential range.

Conclusions

In this paper, we have demonstrated that a wide variety of 5-substituted indoles form electroactive trimers which can further link to give polymers of linked trimers. Initial trimer formation occurs in the diffusion layer near the electrode, which results in the deposition of a film. This film then acts as a surface on which further oxidation and adsorption of monomer can occur, which is the mechanism by which the film grows. Contrary to previous work, all the monomers that we have studied electrooxidise to give redox active trimers; 5-aminoindole and 5-hydroxyindole do not form trimers on bare Pt, as oxidation occurs *via* the substituent. However, electrooxidation on a preformed indole film avoids this complication, and the electrooxidation reaction is similar to that observed for other indoles after initial film deposition, and results in trimer formation.

Once formed, the trimer can act as a surface on which further trimer can be produced, or it can dissolve from the surface and be detected in solution as soluble trimer. The amount of trimer which is soluble is clearly dependent on the solubilising nature of the substituents; for example for 5-aminoindole and 5-hydroxyindole, the lyophilic substituents confer an increased solubility on the trimer and increase the proportion of trimer in solution compared to other indoles. It is also clear that the redox potential of the trimers is dependent upon the nature of the substituent present. A more electron withdrawing substituent decreases the electron density of the aromatic system and leads to an increase in the redox potential for the trimer, whereas an electron donating substituent decreases the redox potential; this effect closely correlates with the Hammett constant for the substituent. This work therefore indicates that redox active trimers are relatively easily formed for a wide range of indoles, and that control of 5-substituent allows control of both the solubility and reactivity of these species.

We thank the EPSRC for their support. A.D.T. and P.J. thank the University of Edinburgh for financial support. Thanks also go to Dr Scott Wright for performing the L²TOF-MS experiments mentioned in this work.

References

1 J. G. Mackintosh and A. R. Mount, *J. Chem. Soc., Faraday Trans.*, 1994, **90**, 1121.
2 J. G. Mackintosh, C. R. Redpath, A. C. Jones, P. R. R. Langridge-Smith and A. R. Mount, *J. Electroanal. Chem.*, 1995, **388**, 179.
3 P. N. Bartlett and J. Farrington, *Bull. Electrochem.*, 1992, **8**, 208.
4 P. N. Bartlett and J. Farrington, *J. Electroanal. Chem.*, 1989, **261**, 471.
5 R. J. Waltman, A. F. Díaz and J. Bargon, *J. Phys. Chem.*, 1984, **88**, 4343.
6 G. Kokkinidis and A. Kelaidopolou, *J. Electroanal. Chem.*, 1996, **414**, 197.
7 J. G. Mackintosh, S. J. Wright, P. R. R. Langridge-Smith and A. R. Mount, *J. Chem. Soc., Faraday Trans.*, 1996, **92**, 4109.
8 O. Exner, in *Correlation Analysis in Chemistry: Recent Advances*, ed. N. B. Chapman and J. Shorter, Plenum, NY, 1978, ch. 10.

Paper 7/03128I; *Received* 7*th May*, 1997

Fluorescence properties of electropolymerised 5-substituted indoles in solution

Peter Jennings, Anita C. Jones* and Andrew R. Mount

Department of Chemistry, The University of Edinburgh, The Joseph Black Building, West Mains Road, Edinburgh, UK EH9 3JJ. E-mail: a.c.jones@ed.ac.uk

Received 27th August 1998, Accepted 16th October 1998

Electropolymerisation of the 5-substituted indole monomers, 5-cyanoindole, indole-5-carboxylic acid, 5-chloroindole, 5-bromoindole and 5-methoxyindole results in a redox-active film consisting of a cyclic trimer and chains of linked cyclic trimer (polymer). The monomer, trimer and polymer species are fluorescent and have been studied using steady state fluorescence spectroscopy in solution at room temperature. The excitation and emission spectra of the trimer species show a significant shift to longer wavelength compared to the monomer, consistent with the greater extent of electron delocalisation. The emission properties of the 5-substituted indole monomers are very dependent upon solvent polarity and the nature of the 5-substituent; in contrast, the trimer species show little dependence. Controlling the electrochemical conditions allows variation of the relative proportions of trimer and polymer species. The excitation and emission spectra of the polymer species are shifted to longer wavelength, are broader and are of lower intensity than those of the trimer.

Introduction

In previous papers[1–4] we showed that electropolymerisation of a range of 5-substituted indoles (**1**) involved the formation of a cyclic trimer, which was then deposited onto an electrode

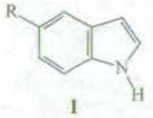

1

surface and linked to form a redox active polymer of linked trimers. Our previous chronamperometric studies[1] at a rotating disc electrode (RDE) showed that initial trimer formation occurs in the diffusion layer near the electrode, which results in the deposition of a film of an asymmetric cyclic trimer (**2**)

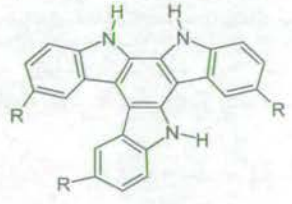

2

onto the electrode surface. This film then acts as a surface on which further adsorption and oxidation of monomer can occur, followed by radical cation linkage to form more cyclic trimer, which is the mechanism by which the film grows. Eqn. (1) shows the oxidation of monomer and eqn. (2) the subsequent linking to form polymer, where In is the 5-substituted indole monomer.

$$3n\mathrm{In} \rightarrow n(\mathrm{In})_{3(s)}^{+} + 7ne^{-} + 6n\mathrm{H}^{+} \quad (1)$$

$$n(\mathrm{In})_{3(s)}^{+} \rightarrow -[(\mathrm{In})_3^{+}]_n- + 2ne^{-} + 2n\mathrm{H}^{+} \quad (2)$$

Electropolymerisation results in a mixture of trimer and polymer species and the electrochemical conditions can be systematically controlled to vary the trimer to polymer ratio.

Polyindoles have been proposed as potential candidates for fast response potentiometric sensors[5] and for the direct oxidation and reduction of biomolecules;[6] however, they are also highly photoluminescent, presenting novel examples of photoluminescent conducting polymer systems. Similar systems such as poly(*p*-phenylene vinylene) have been studied in detail[7] with respect to their potential application as electroluminescent materials. Such materials are being used in the development of large area light emitting displays.[8] To date there have been no studies on the luminescence properties of polyindoles.

Previously, much interest has been directed towards the fluorescence properties of indole and its derivatives, as it is the fluorophore of the amino acid tryptophan, used extensively as a fluorescent probe in the studies of protein and enzyme structure.[9] The fluorescence properties of indoles are very sensitive to environmental conditions, as an unusually large Stokes shift is observed in polar media.[10] This shift arises from a bathochromic shift in the emission wavelength with increasing solvent polarity; the energy of the absorption band displays a much lower solvent dependence. The sensitivity of the indole emission is complex as it stems from the near degeneracy of two low lying electronic states, labelled ^1L_a and ^1L_b.[11] Various mechanisms have been proposed to account for this large Stokes shift such as ^1L_a–^1L_b level inversion,[12] formation of a solvent–solute exciplex[13,14] and relaxation of solvent dipoles about the increased dipole moment of the excited state, relative to that of the ground state.[15,16] It has been suggested that in non-polar solvents, emission arises from the ^1L_b state, which lies at lower energy than the ^1L_a state. However the ^1L_a state becomes the fluorescent state in polar media because it is more strongly stabilised by solvent–solute relaxation, due to a greater dipole moment than the ^1L_b state, resulting in ^1L_a–^1L_b level inversion. Photophysical studies have been carried out on indoles with a wide range of functional groups, including measurements on the 5-substituted indole monomers.[17–19] It has been observed that the presence of both electron withdrawing and electron donating groups

result in a bathochromic shift of the emission maxima relative to unsubstituted indole.

In this paper we report upon the solution phase fluorescence properties of the trimer and polymer species of 5-cyanoindole, indole-5-carboxylic acid, 5-chloroindole, 5-bromoindole and 5-methoxyindole, comparing them to the fluorescence properties of the monomers. We have carried out a systematic study of the effects of solvent polarity, nature of the 5-substituent and electrochemical preparation conditions on the fluorescence spectra. The results of picosecond time-resolved fluorescence measurements on these systems in solution and the solid state and *in situ* investigation of the fluorescence of polymer films on the working electrode will be reported in forthcoming publications.

Experimental

The indole monomers were purchased from Aldrich (99% purity). The solvents used were of spectrophotometric grade or equivalent. The indole monomers were recrystallised and dried in an oven at 130°C for several days prior to use. Fluorescence measurements were carried out on a Spex Fluoromax spectrofluorimeter using disposable PMMA cuvettes which have 100% transmission above 320 nm. Below 320 nm, spectra were corrected for the transmission function of the cuvette. All fluorescence spectra were collected using solution concentrations of 10^{-6} molar or lower to avoid inner filter, self absorption and dimerisation effects. Electrochemical control was by a 3-electrode potentiostat (Oxford Electrodes Ltd) with the data being collected on an *x–y–t* chart recorder (Bryans Instruments). A motor controller (Oxford Electrodes Ltd) was used to rotate the electrode. A 2 cm^2 platinum gauze was used as the counter electrode, whilst the working electrode was a Pt–Pt rotating disc electrode (Oxford Electrodes Ltd) disc area 0.387 cm^2 and measured collection efficiency, $N_0 = 0.21$, as measured by the ferrocene/ferrocinium couple. The reference electrode was made in house and consisted of a silver wire dipping into a solution of silver perchlorate (0.01 mol dm^{-3}) in background electrolyte solution of anhydrous lithium perchlorate in acetonitrile.

Results and discussion

Fluorescence of 5-substituted indole monomers

The fluorescence excitation and emission spectra of the indole monomers: 5-cyanoindole, indole-5-carboxylic acid, 5-bromoindole, 5-chloroindole and 5-methoxyindole in ethanol at room temperature are all broad and featureless. This is characteristic of indoles in polar solvents.[12] For example, the excitation and emission spectra of 5-bromoindole and indole-5-carboxylic acid are shown in Fig. 1. The excitation and emission maxima for the various 5-substituted monomers in ethanol at room temperature are presented in Table 1. The emission maximum of indole-5-carboxylic acid in ethanol is notable in being at considerably longer wavelength than the other indole monomers and showing a greater Stokes shift. This is likely to be due to hydrogen bonding interaction between the carboxylic acid group and the solvent, lowering the energy of the emitting excited state.

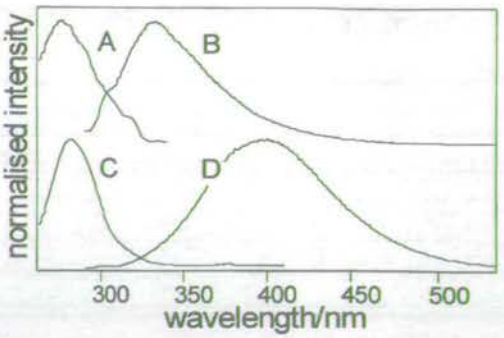

Fig. 1 Excitation and emission spectra of 5-bromoindole and indole-5-carboxylic acid monomers in ethanol at room temperature. 5-Bromoindole excitation spectrum (A) and emission spectrum (B). Indole-5-carboxylic acid excitation spectrum (C) and emission spectrum (D). For the excitation spectra, the emission wavelength was set at 350 nm, for the emission spectra an excitation wavelength of 280 nm was used. Intensities have been normalised to the maximum.

The solvent-dependence of the fluorescence of 5-cyanoindole was investigated in greater detail, as summarised in Table 2. To quantify the variation in solvent properties we have used the function $f(D, n)$:

$$f(D, n) = 2\left[\frac{D-1}{D-2} - \frac{n^2-1}{n^2+2}\right]$$

where D represents the static dielectric constant of the solvent and n the solvent refractive index. The function $f(D, n)$ has been used in previous models[10] to test the hypothesis attributing the anomalous Stokes shift of indoles to solvent dipole relaxation following excitation. Since $f(D, n)$ depends strongly on the dielectric properties of the solvent, it is a useful parameter when investigating the effect of solvent on the energy of the excited states. 5-Cyanoindole exhibits a considerable bathochromic shift in emission wavelength as the polarity of the solvent is increased, as shown in Fig. 2. The wavenumbers of the excitation and emission maxima, along with the Stokes shift are presented in Table 2. The Stokes shift was calculated as the difference in wavenumber between the excitation peak and emission peak. The shortest emission wavelength and narrowest emission spectrum is observed in isopentane. This is consistent with the emission in this non-polar solvent originating from the ^1L_b state. 5-Cyanoindole shows a bathochromic shift of the emission and an increase in the Stokes

Table 1 Excitation and emission data for 5-substituted indole monomers in ethanol solution at room temperature

Monomer	Excitation maximum /nm	Emission maximum /nm	Stokes shift, $\Delta\bar{\nu}/cm^{-1}$ [a]
Indole-5-carboxylic acid	282	397	10 300
5-Cyanoindole	283	364	7800
5-Bromoindole	275	338	6800
5-Chloroindole	275	328	5900
5-Methoxyindole	300	329	2900

[a] Calculated as the wavenumber difference between the excitation and emission maxima.

Table 2 Excitation and emission data for 5-cyanoindole (5-CI) in a variety of solvents

Solvent	$f(D, n)$[a]	Excitation maximum /cm^{-1}	Emission maximum /cm^{-1}	Stokes shift, $\Delta\bar{\nu}/cm^{-1}$ [b]
Isopentane	0.003	36 800	31 700	5100
DMSO	0.539	31 200	27 000	4200
Ether	0.619	34 400	29 300	5100
THF	0.885	34 000	28 600	5400
DMF	1.328	33 300	27 400	5900
EtOH	1.329	35 300	27 500	7800
MeOH	1.412	36 600	27 200	9400
MeCN	1.429	32 600	27 700	4900
H_2O	1.516	33 000	25 600	7400

[a] $f(D, n)$ is an expression of solvent polarity.[10] [b] Calculated as the wavenumber difference between the excitation and emission maxima.

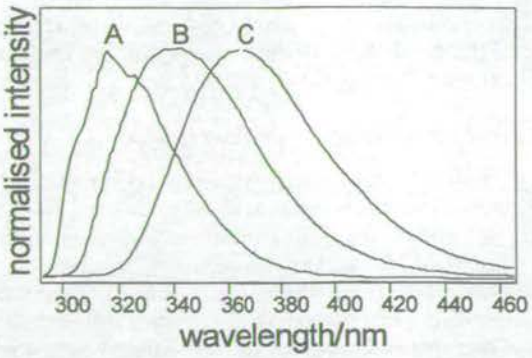

Fig. 2 Effect of solvents on the emission spectra at room temperature of 5-cyanoindole. Emission spectra of 5-cyanoindole in isopentane (A), ether (B), and DMF (C). An excitation wavelength of 280 nm was used. Intensities have been normalised to the maximum.

shift as the value of $f(D, n)$ increases due to a stabilisation of the excited state by solvent–solute relaxation. In similar work, the resulting emission has been attributed to both exciplex formation[13,14] and inversion of the two low lying excited states ^1L_a and ^1L_b.[13] In non-polar media, emission occurs from the ^1L_b state, which has been shown to have a lower dipole moment than the ^1L_a state,[11,20] and therefore is not affected by the presence of a polar solvent. Due to the near degeneracy of these two states, the presence of a polar solvent lowers the energy of the ^1L_a state below that of the ^1L_b state and the ^1L_a becomes the emitting state, resulting in the observed broadening and bathochromic shift of the emission spectrum.

Fluorescence properties of the trimer species

All of the above monomers can be electrooxidised at a platinum rotating disc electrode to form an electroactive film.[4] The composition and properties of the film can be altered by controlling the rotation speed of the electrode, time of polymerisation and concentration of monomer solution. Previous chronamperometric studies at a rotating disc electrode[1,3] for indole-5-carboxylic acid and 5-cyanoindole showed that initial formation of an asymmetric trimer, according to eqn. (1), in the diffusion layer is followed by deposition of a monolayer onto the electrode surface. This layer acts as a site for further electrooxidation and adsorption of the monomer radical cation, which gives further cyclic trimer formation on the electrode surface. During the initial surface layer growth phase, the current changes with time. Once the layer is formed a steady state current is observed, with the kinetics of deposition being first order in the monomer, since oxidation and adsorption of monomer controls the linking process. The deposited cyclic trimer can act as a site for further trimerisation, or the trimers can link to form polymers of linked trimers according to eqn. (2).

Eqn. (1) and (2) combined will dominate when the concentration of monomer at the surface falls, whereas eqn. (1) dominates when there is efficient supply of monomer to the surface for trimer formation. We have shown[1,3] that the former occurs when the bulk concentration of monomer is low (<20 mM) and/or the rotation speed is slow (0–2 Hz), whereas the latter occurs at high concentrations (>50 mM) and high rotation speeds (>5 Hz). Therefore at high rotation speed and high monomer concentration, a film rich in trimer species is formed. At low monomer concentration and slow rotation speeds a film rich in polymer is formed. For the following discussion of the unlinked trimer chromophore, typical film preparation conditions involved monomer concentrations higher than 50 mM, rotation speeds faster than 5 Hz and polymerisation times shorter than 10 s.

The trimer and polymer species can be separated chromatographically or on the basis of their differential solubility in DMF,[2,3] enabling characterisation of the pure trimer species. The mass spectra and NMR spectra of pure trimer species have been reported previously.[2,3] In practice, it is not necessary to separate the trimer and polymer species to investigate their fluorescence emission or excitation spectra because the different species can be excited or detected selectively, by judicious choice of excitation or emission wavelength.

Fig. 3 shows the excitation spectra (at an emission wavelength of 450 nm) and emission spectra (at an excitation wavelength of 320 nm) for trimers of indole-5-carboxylic acid, 5-bromoindole and 5-methoxyindole dissolved in ethanol. The wavelengths of peaks in the excitation and emission spectra are listed in Table 3. The fluorescence properties of the trimers are all very similar, but show a marked difference from the monomer species. A considerable bathochromic shift is seen between the spectra of the monomer and trimer species, accompanied by an increase in vibronic structure and a reduction in the Stokes shift. For example the excitation spectrum of 5-cyanoindole trimer in ethanol is shifted to lower energy by 10400 cm^{-1} with respect to the monomer. This reduction in excitation energy is consistent with an increase in

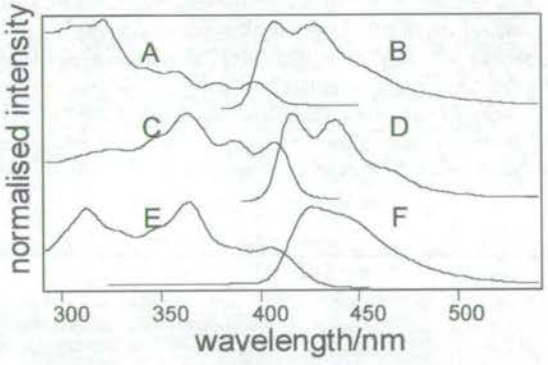

Fig. 3 Excitation and emission spectra of 5-substituted indole trimers in ethanol at room temperature. Indole-5-carboxylic acid, excitation spectrum (A), emission spectrum (B); 5-bromoindole, excitation spectrum (C), emission spectrum (D); 5-methoxyindole, excitation spectrum (E), emission spectrum. (F). Emission spectra were acquired using an excitation wavelength of 320 nm. Excitation spectra were acquired using an emission wavelength of 450 nm. Intensities have been normalised to the maximum.

Table 3 Excitation and emission data for 5-substituted indole trimers in ethanol at room temperature

Trimer	Excitation maxima/nm[a]	Emission maxima/nm	Stokes shift, $\Delta\bar{\nu}/cm^{-1}$ [b]
Indole-5-carboxylic acid	397/378/357/343/320	408/428	700
5-Cyanoindole	402/381/359/344/318	416/437	800
5-Chloroindole	402/381/360/344/311	420/439	1200
5-Methoxyindole	406/384/363/348/312	427/440	1200
5-Bromoindole	400/380/356/340/310	417/438	1000

[a] The origin bands of the S_1, S_2 and S_3 states in the excitation spectra are underlined. [b] Calculated as the wavenumber difference between the excitation (S_1) and emission origin bands.

the delocalisation of the π-molecular orbitals around the trimer unit. The S_1 excitation spectra of the trimers show vibronic structure that mirrors that of the emission spectra. Transitions to higher excited singlet states, S_2 and S_3, are also apparent, as indicated in Table 3. The reduced Stokes shift of the emission and the enhanced vibronic structure both imply that there is a weaker interaction with the solvent and suggest a relatively non-polar excited state, more similar to the ^1L_b state of the monomer than the ^1L_a state. The small Stokes shift implies that there is little change in polarity upon excitation.

There is a considerable difference in the effect of the 5-substituent on the fluorescence properties of the monomer and trimer species. The values of the Stokes shift of the monomers and trimers in ethanol are shown in Table 4. The excitation maxima are similar for all the monomers, indicating that their unrelaxed excited states are close in energy. However, the emission maxima vary considerably for the different substituents giving rise to a large variation in the values of $\Delta\bar{\nu}$. This suggests that the extent of solvent relaxation varies with substituent and implies that the substituent influences the change in polarity of the molecule on excitation. For the trimer species, it appears that the substituent has little effect on the solvent relaxation, with a much narrower range in the values of $\Delta\bar{\nu}$. This implies that the functional group has little effect on the polarity of the trimer excited state relative to the ground state.

As with the monomers, the effect of solvent on the emission properties of 5-cyanoindole trimer was studied. The results are summarised in Table 5. The excitation and emission wavenumbers are essentially independent of solvent polarity and there is a much smaller Stokes shift than was observed for the monomer. The contrast in the response of monomer and trimer species to solvent polarity indicates that the first excited singlet state of the trimer has a smaller dipole moment than in the monomer, hence it is less sensitive to solvent environment and experiences a reduced degree of solvent–solute relaxation in highly polar and protic solvents.

To obtain an estimate of the fluorescence quantum yield of the trimer species, the emission intensity of 5-cyanoindole trimer in ethanol solution was compared with that of unsubstituted indole monomer under identical experimental conditions, at an excitation wavelength of 280 nm. This indicated that the quantum efficiency of 5-cyanoindole trimer is about 1.3 times that of indole. The quantum efficiency of indole in ethanol is reported to be 0.4.[21]

Table 4 A comparison of the Stokes shift, $\Delta\bar{\nu}$, of the monomer and trimer species in ethanol solution

	Monomer Stokes shift, $\Delta\bar{\nu}/cm^{-1}$	Trimer Stokes shift, $\Delta\bar{\nu}/cm^{-1}$
Indole-5-carboxylic acid	10 300	700
5-Cyanoindole	7700	800
5-Bromoindole	6800	1000
5-Chloroindole	5900	1200
5-Methoxyindole	2900	1200

Fluorescence properties of the polymer species

In order to study the emission properties of the polymer species, electrochemical conditions were chosen to produce polymer-rich films. Typical conditions involved monomer solutions of 20 mM and less, a stationary working electrode and polymerisation times between one and five minutes. The more extensively polymerised films are less soluble than those rich in trimer (probably due to the presence of long chains of linked trimer units) and are therefore less amenable to study in the solution phase. The most soluble polymer is that of 5-bromoindole for which the fluorescence of both trimer and polymer species can be clearly observed in solution, as shown in Fig. 4. For samples produced at high rotation speeds and high monomer solution concentrations, an emission spectrum characteristic of the trimer chromophore, is seen. This is illustrated in Fig. 4B, for the case of a film grown from a 150 mM monomer solution at a rotation speed of 10 Hz. However, for samples produced at low rotation speeds and low monomer concentration, the spectrum is dominated by a broad, longer wavelength emission band. This is exemplified in Fig. 4D which shows the emission spectrum of a sample grown from a 10 mM monomer solution and with a stationary working electrode. The latter electrochemical conditions favour the formation of a film rich in polymer species. The presence of emission with a bathochromic shift relative to the trimer species is consistent with delocalisation of the excitation energy over several trimer units. The extent of this delocalisation, rather than the overall length of the polymer chains will determine the optical properties of the sample. The broadness of the emission suggests that the polymer chains comprise a distribution of local conformations, with each conformation exhibiting a different

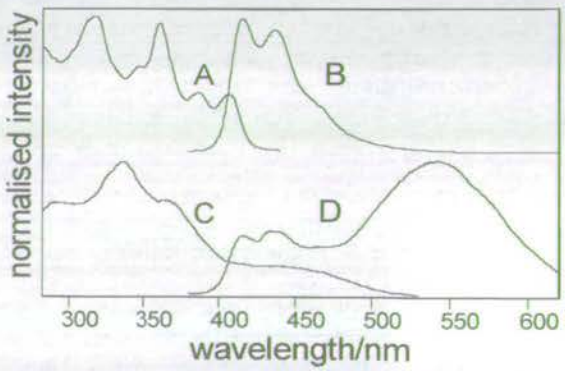

Fig. 4 Excitation spectrum (A) for 5-bromoindole trimer at an emission wavelength of 450 nm and emission spectrum (B) for 5-bromoindole trimer at an excitation wavelength of 335 nm. Excitation spectrum (C) for 5-bromoindole polymer at an emission wavelength of 550 nm and emission spectrum (D) for 5-bromoindole polymer and trimer at an excitation wavelength of 335 nm. Intensities have been normalised to the maximum.

Table 5 Excitation and emission data for 5-cyanoindole trimer in a variety of solvents

Solvent	Excitation maxima/cm^{-1} [a]	Emission maxima/cm^{-1}	Stokes shift, $\Delta\bar{\nu}/cm^{-1}$ [b]
DMSO	24 800/26 000/27 600/28 800/31 000	23 500/22 700	1300
Ether	25 000/26 400/21 800/31 800	24 400/23 200	600
DMF	24 800/26 100/27 800/31 500	23 600/22 600	1200
EtOH	24 900/26 200/27 900/29 100/31 400	24 000/22 900	900
MeOH	25 000/26 300/27 800/31 800	24 000/22 900	1000
MeCN	25 100/26500/28 000/31 700	24 000/23 100	1100

[a] The origin bands of the S_1, S_2 and S_3 states in the excitation spectra are underlined. [b] Calculated as the wavenumber difference between the excitation (S_1) and emission origin bands.

degree of delocalisation across the trimer units. Thus, there exists a multiplicity of emitting species, a phenomenon that has been studied in detail for other conjugated polymer systems such as poly(phenylene vinylene).[22]

The polymer emission has a characteristic, broad excitation spectrum that extends to lower excitation energies than the trimer spectrum, as shown in Fig. 4C. This confirms that the broad red-shifted emission is due to excitation of ground state polymer species and is not excimer emission from the trimer species. In Fig. 5 it can be seen that the polymer emission can be produced exclusively by exciting at longer wavelengths (between 420 and 500 nm), beyond the absorption band of the trimer species. This clearly illustrates that the trimer and polymer are distinct species which have their own characteristic absorption and emission spectra.

A study of 5-cyanoindole and indole-5-carboxylic acid films produced with electrochemical conditions tuned for high polymer yield has revealed similar emission properties as those seen for 5-bromoindole. However, the relative intensity of polymer to trimer emission is much lower than for 5-bromoindole. Since the peak of the polymer emission is in the same region as the tail of the trimer emission, it is hidden at all but the longest excitation wavelengths. The polymer emission can be revealed by exciting on the long wavelength edge of the excitation spectrum, as shown in Fig. 6 for indole-5-carboxylic acid. The polymer appears to have a lower fluorescence quantum yield than the trimer, which is consistent with the polymer possessing a greater number of non-radiative pathways for excited state decay. 5-Bromoindole polymer has a higher emission intensity relative to the trimer than the other 5-substituted indoles. The reduction in fluorescence intensity in 5-bromoindole trimer is attributed to the internal heavy atom effect. The presence of the heavy bromine atom enhances spin–orbit coupling and increases the rate of intersystem crossing to the triplet manifold. This provides an efficient non-radiative pathway for decay of the excited singlet state and accounts for the reduced fluorescence quantum yield. The high intensity of the 5-bromoindole polymer emission, relative to the trimer, implies that intersystem crossing is less favourable in the polymer species than in the trimer. This suggests that there is a closer coincidence of singlet and triplet states in the trimer than the polymer, allowing more efficient intersystem crossing in the trimer species.

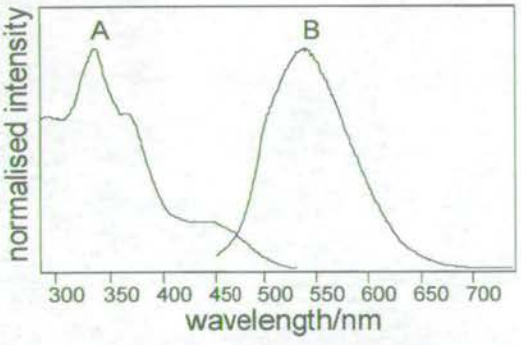

Fig. 5 Excitation (A) and emission (B) spectra for 5-bromoindole polymer in ethanol. Excitation spectrum obtained using an emission wavelength of 550 nm, emission spectrum obtained using an excitation wavelength of 440 nm. Intensities have been normalised to the maximum.

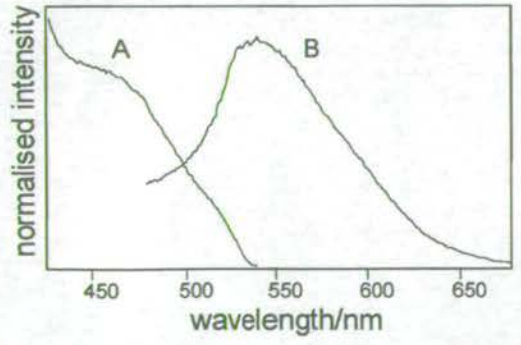

Fig. 6 Excitation (A) and emission (B) spectra for indole-5-carboxylic acid polymer in ethanol; emission wavelength 550 nm and excitation wavelength 440 nm, respectively. Intensities have been normalised to the maximum.

Conclusions

There is a considerable difference between the fluorescence properties of 5-substituted indole monomers and those of their electrochemically formed trimer and polymer species. The fluorescence properties of 5-substituted indole monomers are dependent upon the nature of the 5-substituent and the polarity of the solvating medium. In polar solvents there is a large Stokes shift (due to a considerable bathochromic shift in emission wavelength) which is attributed to the presence of a low-lying excited state that possesses a large dipole moment. The excitation and emission spectra of the trimer chromophore occur at longer wavelengths than those of the monomer, consistent with an increase in the delocalisation of the π-molecular orbitals around the trimer unit. The emission spectra of the trimers show little dependence on the polarity of the solvent or the nature of the 5-substituent. There is a much smaller Stokes shift and the spectra have resolvable vibronic structure. This indicates that there is less interaction of the excited state with the solvent, implying a lower excited state dipole moment than in the monomer and little change in polarity upon excitation. It is also apparent that the 5-substituent has little effect on solvent relaxation, indicating that the nature of the substituent has less effect on the polarity of the excited state, relative to the ground state, than for the monomer.

It was found that the 5-bromoindole trimer species has a much lower fluorescence quantum yield than the other 5-substituted trimer species. This is due to the presence of the heavy bromine atom which enhances spin–orbit coupling and leads to an increase in the efficiency of intersystem crossing to the triplet manifold. However, the fluorescence of the 5-bromoindole polymer species did not appear to be strongly quenched, implying that intersystem crossing is less favourable in the polymer species than in the trimer.

Control of the electrochemical conditions allows films rich in polymer species to be grown. The polymer fluorescence is observed as a broad emission band at longer wavelength than the trimer spectrum, with a corresponding bathochromically shifted excitation spectrum. This confirms the presence of extended chains of linked trimer units with energy delocalised along the polymer chain. The broadness of the emission suggests the presence of a broad distribution of local conformations, each with its own set of electronic states, in the polymer system. The polymer appears to have a lower fluorescence quantum yield than the trimer species. This is attributed to an increase in the number of available non-radiative decay pathways for the electronic excitation in the polymer system.

We have shown that 5-substituted indole electropolymers exhibit intense photoluminescence. These systems are new examples of organic polymer systems which combine electronic conductivity and efficient photoluminescence. This combination of properties means that these systems may be potential candidates for the development of new electroluminescent materials.

Acknowledgements

We gratefully acknowledge the financial support of the EPSRC in the form of a research grant (GR/K12625) and an earmarked PhD studentship.

References

1 J. G. Mackintosh and A. R. Mount, *J. Chem. Soc., Faraday Trans.*, 1994, **90**, 1121.
2 J. G. Mackintosh, C. R. Redpath, A. C. Jones, P. R. R. Langridge-Smith, D. R. Reed and A. R. Mount, *J. Electroanal. Chem.*, 1994, **375**, 163.
3 J. G. Mackintosh, C. R. Redapth, A. C. Jones, P. R. R. Langridge-Smith and A. R. Mount, *J. Electroanal. Chem.*, 1995, **388**, 179.
4 P. Jennings, A. C. Jones, A. R. Mount and A. D. Thomson, *J. Chem. Soc., Faraday Trans.*, 1997, **93**, 3791.
5 P. N. Bartlett and J. Farrington, *Bull. Electrochem.*, 1992, **8**, 208.
6 P. N. Bartlett and J. Farrington, *J. Electroanal. Chem.*, 1989, **261**, 471.
7 R. H. Friend, D. D. C. Bradley and P. D. Townsend, *J. Phys. D. Appl. Phys.*, 1987, **20**, 1367.
8 J. H. Burroughes, D. D. C. Bradley, A. R. Brown, R. N. Marks, K. Mackay, R. H. Friend, P. L. Burns and A. B. Holmes, *Nature (London)*, 1990, **347**, 539.
9 S. V. Konev, *Fluorescence and Phosphorescence of Proteins and Nucleic Acids*, Plenum, New York, 1967.
10 H. L. Lami and N. Glasser, *J. Chem. Phys.*, 1986, **84**, 597.
11 P. R. Callis, *J. Chem. Phys.*, 1991, **95**, 4230.
12 S. R. Meech, D. Phillips and A. G. Lee, *Chem. Phys.*, 1983, **80**, 317.
13 M. S. Walker, T. W. Bednar and R. L. Lumry, *J. Chem. Phys.*, 1966, **45**, 3455.
14 M. S. Walker, T. W. Bednar and R. L. Lumry, *J. Chem. Phys.*, 1967, **47**, 1020.
15 N. Mataga, Y. Kaifu and M. Koizum, *Bull. Chem. Soc. Jpn.*, 1956, **29**, 465.
16 N. Mataga, Y. Torihashi and K. Ezumi, *Theor. Chim. Acta*, 1964, **2**, 158.
17 J. J. Aaron, A. Tine, C. Villiers, C. Parkanyi and D. Bouin, *Croat. Chem. Acta.*, 1983, **56**(2), 157.
18 P. S. Song and W. E. Kurtin, *J. Am. Chem. Soc.*, 1969, **91**, 4892.
19 S. Arnold, L. Tong and M. Sulkes, *J. Phys. Chem.*, 1994, **98**, 2325.
20 D. K. Hahn and P. R. Callis, *J. Phys. Chem. A*, 1997, **101**, 2686.
21 I. B. Berlman, *Handbook of Fluorescence Spectra of Aromatic Molecules*, Academic Press, New York, 1971.
22 I. D. W. Samuel, B. Crystall, G. Rumbles, P. L. Burn, A. B. Holmes and R. H. Friend, *Chem. Phys. Lett.*, 1993, **213**, 472.

Paper 8/06721J